

University of Nottingham
UK | CHINA | MALAYSIA

Small molecule-based fluorescent probes as tool compounds for chemokine receptors CXCR4 and ACKR3

Sebastian Dekkers

Thesis submitted to the University of Nottingham for the degree of Doctor of Philosophy

October 2018

Declaration

This thesis is submitted to the University of Nottingham for the degree of Doctor of Philosophy. The work described in this thesis has been conducted by myself, unless stated otherwise.

The work presented in this thesis that was *not* conducted by myself is outlined below:

- Saturation binding experiments and competition binding experiments described in chapters 3.3.1.1 to 3.3.1.3 were carried out by fellow PhD student Birgit Caspar.
- Site-directed mutagenesis studies and homology model development in the ACKR3 chapter were carried out by collaborators of the VU University Amsterdam, as part of the Marie Curie training network ONCORNET.
- Single concentration binding experiments described in chapter 4.4.1 were carried out by research technician Jackie Glenn.



Sebastian Dekkers

Table of Contents

Declaration i

Abstract v

Acknowledgments viii

Abbreviations ix

1 Introduction 1

1.1 The chemokine system 1

1.1.1 CXCL12-CXCR4 signalling axis 3

1.1.2 CXCL12-ACKR3 signalling axis 4

1.2 Chemokine receptors and cancer 5

1.3 Drug design strategies currently targeting the CXCL12-CXCR4/ACKR3 axes 8

1.3.1 Small molecule inhibitors of CXCR4 10

1.3.2 Small molecule ligands of ACKR3 13

1.3.3 Peptide inhibitors of CXCR4 and ACKR3 13

1.3.4 Biologicals for CXCR4 and ACKR3 15

1.4 Fluorescent toolkit compounds for CXCR4 and ACKR3 15

2 Aims and objectives 21

3 Development of high affinity fluorescent CXCR4 receptor probes 23

3.1 Selection of appropriate pharmacophores 24

3.1.1 IT1t 24

3.1.2 AMD070 28

3.1.3 An isoquinoline scaffold 29

3.2 Synthesis of fluorescent conjugates 30

3.2.1 IT1t-based probes 30

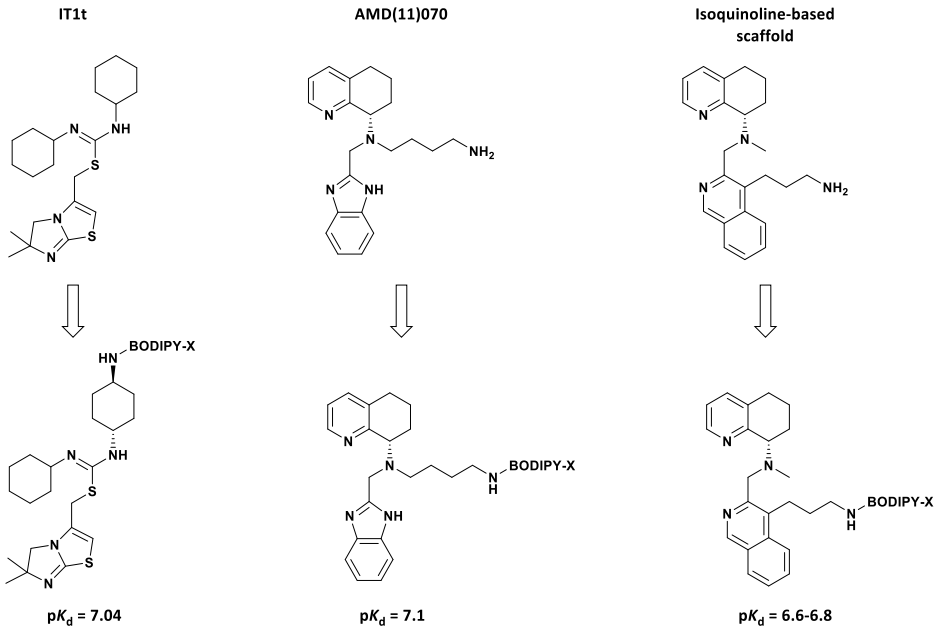
3.2.2 Isoquinoline-based probes 32
3.2.3 AMD070-based probes 35
3.3 Pharmacological characterisation 37
3.3.1 NanoBRET™ 37
3.3.2 GloSensor™ cAMP Assay 45
3.4 Confocal imaging 50
4 Development of high affinity fluorescent ACKR3 probes 56
4.1 VUF11207 as starting point for fluorescent ligand design 57
4.2 Docking of congeners of GD301 61
4.3 Synthesis of fluorescent conjugates 63
4.4 Pharmacological characterisation 66
4.4.1 Single concentration binding experiments 66
4.4.2 NanoBRET™ saturation binding experiments 68
4.4.3 NanoBRET™ competition binding experiments 78
4.5 Confocal imaging 80
5 Conclusions 85
5.1 Fluorescent CXCR4 receptor probes 85
5.2 Fluorescent ACKR3 receptor probes 86
6 Future work 89
6.1 Optimisation of the CXCR4 receptor probes 89
6.2 Optimise confocal imaging of the CXCR4 probes 90
6.3 Screening of different chemotypes using fluorescent ACKR3 probes 90
6.4 Functional screening of fluorescent ACKR3 probes 91
6.5 Future application of the probes described in this thesis 92
7 Experimental 94
7.1 Modelling 94

7.2 Materials and methods 94
7.2.1 Materials 94
7.2.2 Microwave-assisted synthesis 94
7.2.3 Liquid Chromatography Mass Spectrometry 94
7.2.4 High Performance Liquid Chromatography 95
7.2.5 High Resolution Mass Spectrometry 95
7.2.6 Nuclear Magnetic Resonance 95
7.3 Chemistry 96
7.3.1 Synthesis of fluorescent IT1t-based probes 96
7.3.2 Synthesis of fluorescent isoquinoline-based probes 101
7.3.3 Synthesis of fluorescent AMD070-based probes 109
7.3.4 Synthesis of fluorescent ACKR3 probes 114
7.4 Pharmacology 134
7.4.1 Cell culture 134
7.4.2 Membrane preparation 134
7.4.3 Transient transfection of HEK293 cells 134
7.4.4 NanoBRET™ saturation binding experiments using membranes ... 135
7.4.5 NanoBRET™ saturation binding experiments using whole cells..... 135
7.4.6 NanoBRET™ competition binding experiments using membranes 136
7.4.7 NanoBRET™ competition binding experiments using whole cells . 137
7.4.8 GloSensor™ cAMP assay 137
7.4.9 Confocal microscopy 138
7.5 Data analysis 140
8 References 142

Abstract

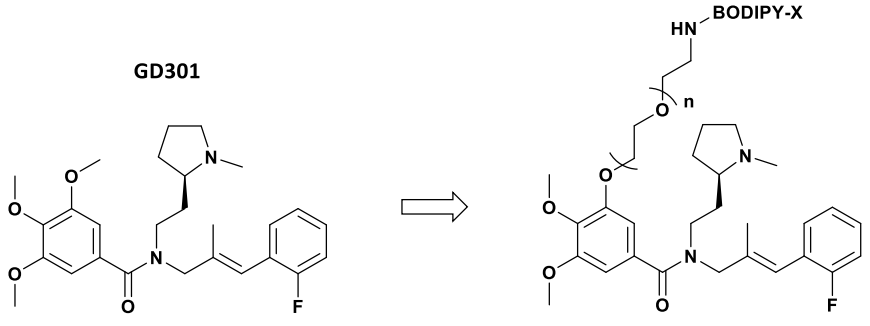
Chemokine receptors CXCR4 and ACKR3 form, together with their shared ligand CXCL12, a highly intricate signalling axis that recently has emerged as a promising target for the treatment of cancer. To further the understanding of how these receptors function, and how they are involved in the various processes of tumour development and metastasis, efforts were made to develop fluorescent tool compounds. In this thesis is described the design, synthesis, and biological characterisation of small molecule-based fluorescent probes for CXCR4 and ACKR3. It examines the use of these fluorescent probes as toolkit compounds for the study of ligand-receptor interactions and the characterisation of novel ligands. It furthermore shows their application in live cell microscopy.

A thorough evaluation of SAR of reported small molecule CXCR4 receptor inhibitors, in combination with *in silico* design, informed the synthetic strategy for linker and fluorophore conjugation. This project explored three chemical classes of CXCR4 receptor inhibitors, leading to the development of multiple high affinity probes that show specific binding in a novel fluorescence-based NanoBRET™ binding assay (pK_d values ranging 6.6-7.1). Using the same NanoBRET™ approach their utility in competition binding experiments was assessed, where they showed to be fully displaceable by established small molecule inhibitors. Additionally, the ability of



these fluorescent probes to affect CXCL12-mediated signalling of CXCR4 was assessed in a functional GloSensor™ cAMP assay. Here, the antagonist nature of the small molecules these probes were based on was found to be retained in the final probes. Finally, live cell confocal microscopy using selected compounds (6,6-dimethyl-5,6-dihydroimidazo[2,1-*b*]thiazol-3-yl)methyl(*E*)-*N*-cyclohexyl-*N*'-((1*r*,4*r*)-4-(6-(2-(4-((*E*)-2-(5,5-difluoro-7-(thiophen-2-yl)-5*H*-4λ^4,5λ^4-dipyrrolo[1,2-c:2',1'*f*][1,3,2]diazaborinin-3-yl)vinyl)phenoxy)acetamido)hexanamido)cyclohexyl)carbamimidothioate (**9**), (*S*,*E*)-6-(2-(4-(2-(5,5-difluoro-7-(thiophen-2-yl)-5*H*-4λ^4,5λ^4-dipyrrolo[1,2-*c*:2',1'-*f*][1,3,2]diazaborinin-3-yl)vinyl)phenoxy)acetamido)-*N*-(3-(3-((methyl(5,6,7,8-tetrahydroquinolin-8-yl)amino)methyl)isoquinolin-4-yl)propyl)hexanamide (**22**), and **(***S*,*E*)-*N*-(4-(((1*H*-benzo[*d*]imidazol-2-yl)methyl)(5,6,7,8-tetrahydroquinolin-8-yl)amino)butyl)-6-(2-(4-(2-(5,5-difluoro-7-(thiophen-2-yl)-5*H*-4λ^4,5λ^4-dipyrrolo[1,2-c:2',1'-*f*][1,3,2]diazaborinin-3-yl)vinyl)phenoxy)acetamido)hexanamide (**30**) showed clear localisation of the fluorescent ligands on the cell membrane, localising neatly at sites of high receptor expression.

Utilizing a similar approach high affinity fluorescent probes were developed for the atypical chemokine receptor ACKR3. An homology model of ACKR3 bound to small molecule agonist GD301 provided rational for the structural modification of this ligand and the incorporation of BODIPY dyes. A series of fluorescent derivatives were synthesised and assessed in a NanoBRET™ binding assay on whole cells. Nine fluorescent ligands were developed, of which six showed good affinity towards the receptor (pK_d values ranging 6.1-7.1). Competition binding experiments using the same NanoBRET™ approach revealed these fluorescent conjugates interact with the



pK_i = 7.1 **pK_d = 6.1 - 7.1**

receptor in a competitive manner, and suggests these probes are viable toolkit compounds in the characterisation of small molecule ligands. Finally, live cell confocal imaging with selected probe (*R*,*E*)-3-(2-(6-(3-(5,5-difluoro-7,9-dimethyl-5*H*-4λ^4,5λ^4-dipyrrolo[1,2-*c*:2',1'-*f*][1,3,2]diazaborinin-2-yl)propanamido)hexanamido)ethoxy)-*N*-(3-(2-fluorophenyl)-2-methylallyl)-4,5-dimethoxy-*N*-(2-(1-methylpyrrolidin-2-yl)ethyl)benzamide (**40a**) showed good localisation of the probe on the cell membrane. Upon binding to the receptor, the probe was furthermore able to induce internalisation over time, suggesting an agonist-like response. Treatment with a high concentration of competitive ligand resulted in complete dissipation of the fluorescent signal of the probe, revealing very low levels of nonspecific binding.

Overall, this project has led to the successful development of fluorescent probes for the chemokine receptors CXCR4 and ACKR3. With their high affinity for the receptor, alongside their excellent fluorescent properties, these compounds provide valuable means to study these receptors *in vitro*, and facilitate live imaging techniques such as confocal microscopy and flow cytometry.

Acknowledgments

I would like to sincerely give thanks to my supervisors Prof. Barrie Kellam and Dr. Michael Stocks, as well as co-supervisors Prof. Steve Hill and Dr. Steve Briddon, for their continued support and guidance throughout my PhD. I am thankful for the patience, scientific input, and banter I received over the years. The multidisciplinary skills I developed, and the successfulness of this project are a direct result of their involvement in this PhD.

I would like to give a special thanks to Birgit Caspar. Birgit and I both performed our PhD projects as part of the ONCORNET consortium, and has been an integral part of my research project. I thank her for her contribution in the pharmacological screening of my CXCR4 probes, and her willingness to train me to perform my own pharmacological experiments. I am also thankful for the fun times we had outside of work. I owe thanks to Marta Arimont of the VU University Amsterdam, for the ACKR3 homology model and important experimental data on the binding mode of GD301. I would like to thank Jackie Glenn, for her contribution in screening my ACKR3 probes and her help and guidance in pharmacology.

I also want to thank everyone in my lab C30, as well as all the other members of the C-floor. I am very grateful for their help and advice throughout the years, and I will miss all the fun we had together. I would also like to thank all members of the ONCORNET consortium. Besides the scientific input I received during the biyearly workshops and work meetings which aided my research, I thank them for all the fun times and lasting friendships.

Finally, this project has received funding from the European Research Council (ERC) under the European Union's Horizon 2020 research and innovation programme, under grant agreement No 641833. I thank the EU for the generous funding, and the opportunity to be involved in a multinational and multidisciplinary training network.

Abbreviations

9-BBN	9-Borabicyclo[3.3.1]nonane
ACKR3	Atypical chemokine receptor type 3
AcN	Acetonitrile
AcOH	Acetic acid
AIBN	Azobisisobutyronitrile
BODIPY	Boron dipyrromethene
BRET	Bioluminescence resonance energy transfer
BSA	Bovine serum albumin
CAFs	Carcinoma-associated fibroblasts
cAMP	Cyclic adenosine monophosphate
CCL2	C-C chemokine ligand type 2
CCL5	C-C chemokine ligand type 5
CCL19	C-C chemokine ligand type 19
CCL21	C-C chemokine ligand type 21
CCL27	C-C chemokine ligand type 27
CCR1	C-C chemokine receptor type 1
CCR3	C-C chemokine receptor type 3
CCR7	C-C chemokine receptor type 7
CCR10	C-C chemokine receptor type 10
cDNA	Complementary DNA
CGRP1	Calcitonin gene-related peptide 1
CXCL1	C-X-C chemokine ligand type 1
CXCL12	C-X-C chemokine ligand type 12
CXCL2	C-X-C chemokine ligand type 2
CXCL3	C-X-C chemokine ligand type 3
CXCL4	C-X-C chemokine ligand type 4
CXCR4	C-X-C chemokine receptor type 4
CXCR7	C-X-C chemokine receptor type 7
DAG	Diacylglycerol

DIPEA	Diisopropylethylamine
DMAP	4-dimethylaminopyridine
DMEM	Dulbecco's modified eagle's medium
DMP	Dess-Martin periodinane
ERK	Extra cellular-related kinases
FACS	Fluorescence activated cell sorting
FBS	Fetal bovine serum
FDA	Food and drugs administration
FITC	Fluorescein isothiocyanate
FRET	Fluorescence resonance energy transfer
FSK	Forskolin
GDP	Guanosine diphosphate
GPCR	G protein-coupled receptor
GTP	Guanosine triphosphate
HBSS	HEPES-buffered Hanks balanced salt solution
HEK293	Human embryonic kidney cells
HIV-1	Human immunodeficiency virus
HPLC	High performance liquid chromatography
HRMS	High resolution mass spectrometry
HSPC	Hematopoietic stem/progenitor cells
HSC	Hematopoietic stem cells
IP3	Inositol triphosphate
IPA	Isopropyl alcohol
JAK	Janus kinase
KI	Potassium iodide
KOH	Potassium hydroxide
LC/MS	Liquid chromatography / mass spectrometry
mAb	Monoclonal antibody
MAPK	Mitogen-activated protein kinases
$MgSO_4$	Magnesium sulfate
mRNA	Messenger ribonucleic acid

MSAP	Multifunctional single attachment point reagent
$NaBH(OAc)_3$	Sodium triacetoxy borohydride
$NaHCO_3$	Sodium bicarbonate
NaOH	Sodium hydroxide
Na_2SO_4	Sodium sulfate
$Na_2S_2O_3$	Sodium thiosulfate
NBS	*N*-Bromosuccinimide
NIS	*N*-Iodosuccinimide
NLuc	Nanoluciferase®
NMR	Nuclear magnetic resonance
PBS	Phosphate-buffered saline
PDB	Protein database
$Pd(dppf)Cl_2$	[1,1`-bis(diphenylphosphino)ferrocene]dichloropalladium(II)
$Pd(OAc)_2$	Palladium(II) Acetate
PEG	Polyethylene glycol
PET	Positron emission tomography
PF4	Platelet factor 4
PIP2	Phosphatidylinositol 4,5-biphosphate
PKC	Protein kinase C
pK_d	-log dissociation constant
PLC-β	Phospholipase C
PPh_3	Triphenylphosphine
PTK	Protein tyrosine kinase
QSAR	Quantitative structure–activity relationship
SAR	Structure-activity relationship
SDF-1	Stromal cell-derived factor 1
STAT	Signal transducer and activator of transcription proteins
TAMRA	Tetramethylrhodamine
TEA	Triethylamine
TFA	Trifluoroacetic acid
THF	Tetrahydrofuran

TLC	Thin layer chromatography
TOF ES+	Positive electrospray ionisation time-of-flight
VIP	Vasoactive intestinal peptide
WHIM	Warts, Hypogammaglobulinemia, Immunodeficiency, and Myelokathexis syndrome

1 Introduction

1.1 The chemokine system

The chemokine signalling system is the primary system controlling migration and positioning of immune cells in vertebrate tissues. The system is responsible for helping orchestrate a response against infection and inflammation, as well as release of innate immune cells from bone marrow during homeostasis[1]. It hosts a wide range of chemotactic cytokines; small proteins of about 8-10 kDa in size that promote increased motility and directional migration of hematopoietic cells when they bind to a chemokine receptor. Over the years about 50 different chemokines have been discovered[2]; the first discovery dating back to 1977 with the purification of secreted platelet factor 4 (PF4/CXCL4)[3]. Chemokines can be loosely classified into three functional groups: homeostatic, inflammatory, and dual inflammatory/homeostatic[4]. Homeostatic chemokines fulfil housekeeping functions and are used for immune system development and basal leukocyte trafficking, whereas inflammatory chemokines are used for emergency trafficking of leukocytes to sites of infection or tissue injury. Dual inflammatory/homeostatic chemokines provide both functions. Structurally, chemokines can be grouped based on the spacing of their highly conserved initial cysteine residues, resulting in four subgroups: XC, CC, CXC, and CX3C chemokines, with “C” denoting a cysteine residue and “X” denoting a non-cysteine residue[5]. Thus, XC chemokine ligands have one N-terminal cysteine residue, CC chemokines have two adjoining amino-terminal cysteine residues, CXC chemokines have two cysteine residues separated by one amino acid, and CX3C chemokines have three amino acids separating the two cysteines.

Chemokines fulfil their function by interacting with chemokine receptors; 7-transmembrane spanning receptors that belong to the class A (Rhodopsin-like) G protein-coupled receptor (GPCR) subfamily[6]. Chemokine receptors are mostly expressed on leukocytes and neuronal cells[1, 2, 7], but have also been found in over 23 different types of cancer[8]. About 20 different chemokine receptors have been identified[6] and their nomenclature is based on the type of chemokine they bind; CCR

chemokine receptors bind CC chemokines, whereas CXCR receptors bind CXC chemokines. Like chemokines, chemokine receptors too can loosely be classified as either being inflammatory or homeostatic. Chemokine receptors involved in inflammation tend to be promiscuous and are activated by numerous different chemokines, whereas homeostatic chemokine receptors are more conserved and bind far fewer ligands. For example, CCR1 is an inflammatory chemokine receptor and is known to have at least 8 chemokines that can bind to it with high affinity[9], in contrast to homeostatic chemokine receptor CXCR4 which is solely activated by CXCL12[6]. Like their receptors, inflammatory chemokines too are quite promiscuous and are found to activate several receptors. For example, chemokine CCL5 is able to bind to CCR1, CCR3, and CCR5, whereas homeostatic chemokine CXCL13 only binds to CXCR5.

Functionally, chemokine receptors are divided into two groups: G protein-signalling receptors and atypical chemokine receptors. G protein-coupled receptors account for most of the chemokine receptors and signal through G_i-type G proteins, causing cell proliferation and chemotaxis. Atypical chemokine receptors, of which only four

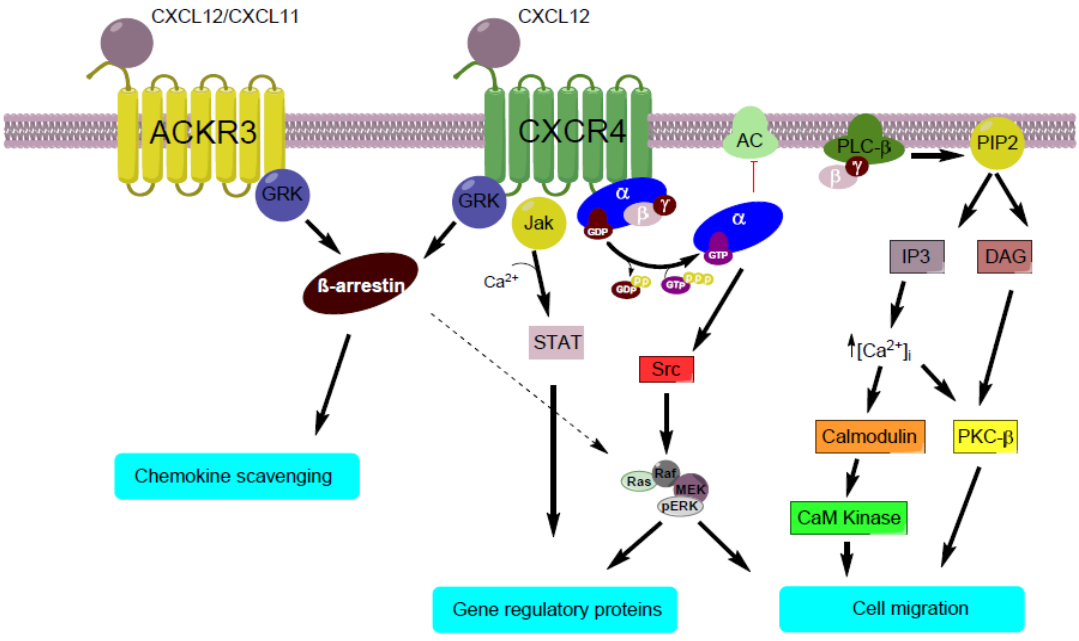


Figure 1. *Schematic representation of the signalling pathways induced by activation of atypical chemokine receptor ACRK3 and typical chemokine receptor CXCR4. GRK, G protein-coupled receptor kinase; AC, adenylate cyclase; PLC, phospholipase C; PIP2, phosphatidylinositol 4,5-biphosphate; Jak, Janus kinase; GDP, guanosine diphosphate; GTP, guanosine triphosphate; IP3, inositol 1,4,5-triphosphate; DAG, diacylglycerol; STAT, signal transducer and activator of transcription; Src, tyrosine-protein kinase; PKC, protein kinase C; Ras/Raf/MEK/pERK; mitogen-activated protein kinase cascade.*

have been reported[10], function G protein-independently and seem to shape chemokine gradients by scavenging the ligands from the microenvironment. The signalling pathways of ACKR3 and CXCR4, examples of an atypical chemokine receptor and a classic chemokine receptor respectively, are displayed in figure 1.

1.1.1 CXCL12-CXCR4 signalling axis

CXCR4 is, together with ACKR3, one of the most highly conserved chemokine receptors among vertebrates, showing 99% sequence homology between human and murine species[6, 11]. CXCR4 is essential for embryonic development, as it was shown in CXCR4-knockout mice that late gestational lethality occurred, as well as defects in B cell lymphopoiesis and bone marrow colonization[12-14]. CXCR4 is mainly expressed by neuronal cells and cells from hematopoietic origin, and it is the only known classically signalling GPCR that binds the chemotactic cytokine CXCL12. CXCL12 (C-X-C motif chemokine 12, also known as SDF-1) is a 10.6 kDa peptide secreted in various different organs, though it is most strongly expressed by bone marrow stromal cells. As CXCR4 is G_i-coupled, G-protein dependent signalling of CXCR4 leads to inhibition of adenylate cyclase, activation of the MAPK cascade, and Ca^{2+} efflux. Downstream signalling cascades result in cell migration, adhesion and transcriptional activation. G-protein independent activation of CXCR4 is thought to result in the stimulation of two pathways: 1) Tyrosine phosphorylation of CXCR4 results in the recruitment and activation of the JAK/STAT pathway, ultimately inducing transcription factors[14, 15]. 2) β-arrestins (arrestin-2 and arrestin-3) activate p38 and ERK following CXCR4 activation, regulating CXCR4/G_i interaction, internalisation and desensitisation of the receptor[14, 16, 17].

The CXCL12-CXCR4 axis induces migration of CXCR4-expressing cells along CXCL12 gradients, yet also plays a role in cell survival and cell proliferation[6, 18]. In pathophysiological conditions the CXCR4 receptor plays several roles. In the late 1990s CXCR4 expressing CD4+ T-cells were discovered to be involved in HIV infection[19]. After more research it was found that CXCR4 served as an important co-receptor in HIV-1 entry. WHIM syndrome (Warts, Hypogammaglobulinemia, Immunodeficiency, and Myelokathexis syndrome) is a rare congenital haematological immunodeficiency disorder in which matured neutrophils fail to

reach the blood stream, and for the most part is caused by a dysfunctional CXCR4/CXCL12 signalling axis[20]. Furthermore, the CXCR4 receptor is believed to be involved in conditions such as pulmonary fibrosis, ischemic injury and rheumatoid arthritis.

1.1.2 CXCL12-ACKR3 signalling axis

Atypical chemokine receptor 3, frequently also referred to as CXCR7, was first discovered in 1989 from a dog thyroid cDNA library[21], and initially thought to be an inactive member of the chemokine receptor family. ACKR3 is found on hematopoietic cells, mesenchymal cells, and neuronal tissue, and like CXCR4 is essential for gestational survival[22]. After its discovery ACKR3 was proposed to be a receptor for calcitonin gene-related peptide CGRP1[23] and vasoactive intestinal peptide VIP[24]. Subsequent studies have however disproven these findings[25, 26], and the receptor was officially deorphanised in 2005, when Balabanian *et al*.[27] revealed CXCL12 not only activates CXCR4 but also ACKR3. Shortly thereafter it was found that ACKR3 also binds CXCL11, albeit with a lower affinity compared to CXCL12[28]. Unlike typical chemokine receptors, ACKR3 does not signal through activation of heterotrimeric G proteins. Instead, receptor activation only results in the activation of the β-arrestin pathway, causing the receptor-ligand complex to be internalised. Since its activation only appears to lead to the internalisation of chemokines, for a long time this receptor was considered a 'decoy'-receptor[29]. It was found that ACKR3 continuously cycles between the plasma membrane and intracellular endosomal compartments, a process which appears to be ligand independent[30]. Chemokine binding does however seem to markedly enhance the cycling of ACKR3 between the cell surface and intracellular compartments[31], indicating an agonist-like response to ligand engagement. The enhanced trafficking of ACKR3 due both to CXCL12 and CXCL11 suggests a scavenging-type role of the receptor since this process leads to lysosomal degradation of the chemokines. Evidence for the importance of this scavenging role can be found *in vivo*. For example, the deletion of either CXCL12 or ACKR3 in zebrafish both resulted in disruption of the migration of lateral-line primordium[32]. A similar role can be found for mammalian ACKR3 which, for example, acts as a critical scavenger on brain microvessel endothelium. Under normal conditions the

perivascular of brain microvessel endothelium is exposed to a high concentration of CXCL12 which acts like molecular glue for leukocytes. During inflammation, proinflammatory interleukins IL-17-1 and IL-1 cause upregulation of ACKR3 expression, leading to a marked depletion of perivascular CXCL12 allowing leukocytes to enter the parenchyma[33, 34]. High expression levels of ACKR3 can also be found in ganglia of the central nervous system, where together with CXCR4 it mediates interneuron migration[35]. The importance of both these receptors in this process is shown by mutant cells lacking either CXCR4 or ACKR3, causing migration to be completely disrupted. It has been suggested that signalling of both receptors contributes to directed migration in distinct ways. Firstly, activation of CXCR4 causes G protein-mediated downstream signalling and ACKR3 has been suggested to activate MAPK pathways[35]; both resulting in cell migration. Alternatively, ACKR3 also modulates the concentration of CXCL12, shaping the microenvironment for optimal CXCR4-dependent migratory responses. If absent, excessive concentrations of CXCL12 causes downregulation of CXCR4 expression and ultimately to a defect in migration[36].

1.2 Chemokine receptors and cancer

Over the last 20 years increasing evidence has been found linking the chemokine system to proliferation, migration and invasion of various cancer types[11, 37, 38]. Chemokines of both inflammatory and homeostatic nature have been associated with various types of cancer, and can be found during all stages of tumour development[39]. For example, increased levels of inflammatory chemokine CCL2 can be found at pre-metastatic tumour sites in the bone marrow. Here, CCL2 has been found to attract myeloid-derived suppressor cells which are highly capable of suppressing an immune response by inactivating T cells, thus increasing tumour cell survival[40]. Angiogenesis has been found to be promoted by chemokines CXCL1, CXCL2, and CXCL3, through interaction with their cognate receptor CXCR2. For example, this was shown to be the case in melanoma. Transfecting murine melanocytes with these chemokines resulted in a phenotypic shift and the ability to form highly vascularized tumours *in vivo*[41]. The migration of cancer cells from the primary tumour to secondary tumour sites is thought to be a process largely due to

available gradients of chemokines and the expression of their cognate receptors. This would explain why different types of cancer show distinct tropism for secondary tumour sites. Evidence to support this idea has been found for the CCL19-CCL21/CCR7 and CCL27/CCR10 signalling axes which are linked to lymph node metastasis and skin metastasis, respectively[42]. Critically, CXCL12 and its receptors CXCR4 and ACKR3 have been linked to cancer progression and metastasis of multiple types of cancer. The remainder of this chapter will focus on the tangible role for the CXCL12-CXCR4/ACKR3 axis in various types and stages of cancer.

While expression of CXCR4 in healthy cells is mostly limited to neuronal cells and cells of hematopoietic origin, 23 different cancer types have been found to express this chemokine receptor[8]. The involvement of CXCL12 and CXCR4 in cancer was first suggested 1998 by Sehgal *et al*.[43], who found elevated levels of mRNA of the chemokine and its receptor CXCR4 in tumours. A few years later Koshiba *et al*.[44] found supporting evidence in pancreatic cancer cells and for the first time suggested a role for this signalling pair in cancer progression through tumour cell migration and angiogenesis; processes that were disrupted following administration of peptide-based CXCR4 antagonist T22. Years later we now have an abundance of evidence that the pattern of tumour migration is largely caused by available gradients of chemokines and the expression of their cognate receptors. For example, available gradients of CXCL12 are found to direct metastatic cells of primary breast carcinoma, which highly express CXCR4, to lung tissue, lymph nodes, liver, and bone marrow, all of which are known secondary tumour sites for primary breast carcinoma[45, 46] (figure 2). Critically, healthy breast tissue shows no expression of CXCR4 whatsoever so it appears that cancer cells specifically express this receptor for its protumorigenic effects. Metastatic cells of leukemia and multiple myeloma were found to home to the same bone marrow sites where hematopoietic stem cells and hematopoietic progenitor cells usually reside[47, 48], providing further evidence that CXCL12 directs CXCR4 expressing cancer cells to secondary sites.

The involvement of the CXCL12-CXCR4 signalling axis in cancer is not limited to only the metastatic stage. During the initial stages of tumour development stromal cells play a pivotal role in the creation of a favourable microenvironment for tumour

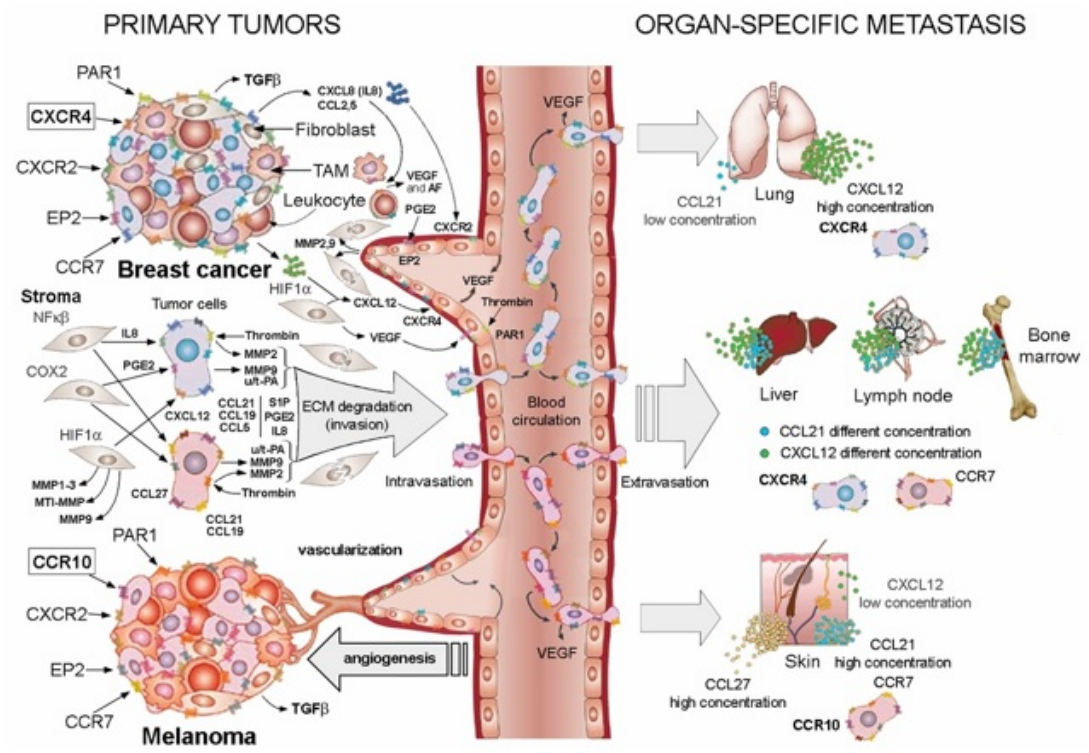


Figure 2. *Organ-specific metastasis is largely dependent on available chemokine gradients and the expression of their cognate receptor on tumour cells. Picture was adopted from Chemdiv, CXCR4-targeted library*[49].

growth. They do so by activating the CXCL12-CXCR4 axis, triggering the homing of a variety of protective cells to the tumour sites. Additionally, within the hypoxic areas of the tumour CXCL12 expression by carcinoma-associated fibroblasts (CAFs) and CXCR4 expression on cancer cells increases, stimulating tumour cell motility and invasiveness[50]. CXCL12 derived from CAFs also recruits endothelial progenitors, which allow for vascular growth[51], adding to the findings of Koshiba *et al*.[44] that CXCL12-CXCR4 is involved in tumour angiogenesis. Finally, CAF-derived CXCL12 stimulates *in vivo* growth of benign prostate hyperplasia by activating nearby CXCR4-positive epithelial cells[52].

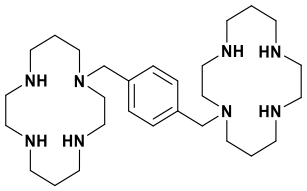
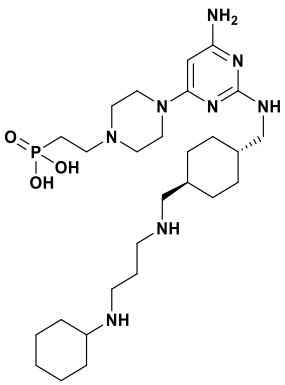
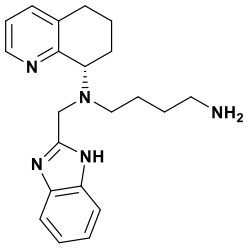
Considering the widespread involvement of the CXCL12-CXCR4 axis in various types of cancer, and the propensity for CXCL12 to engage with ACKR3, a role for this atypical chemokine receptor in cancer seems likely. Indeed, ACKR3 expression can be found on cancers of hematopoietic origin and of mesenchymal origin, such as lymphomas, prostate cancer, breast cancer, sarcomas and gliomas[53, 54]. The mechanisms involved that lead to expression of ACKR3 on these cells are not fully understood, nor are the mechanisms by which it promotes cancer progression and

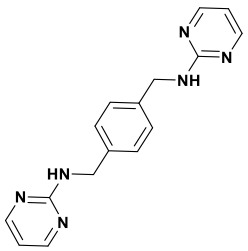
metastasis. Given the potential regulatory properties of ACKR3 as discussed earlier, it seems likely that ACKR3 is critical for shaping the CXCL12 concentration in the tumour microenvironment. This is supported by the evidence that CXCR4 is often co-expressed on tumour cells, and that a functional CXCL12-CXCR4 axis is critical for tumour growth, survival and metastasis[8]. Alternatively, investigations in which CXCR4 and ACKR3 were expressed ectopically have suggested a negative cooperative effect of ACKR3 on G protein-mediated signalling of CXCR4 and a shift towards β-arrestin recruitment, potentially through formation of heterodimers[55, 56]. However, since these investigations have relied on overexpression of both receptors it remains to be proven in the context of native cells. The therapeutic relevance of inhibition of ACKR3 has not been confirmed, though it could have several antitumorigenic effects. Firstly, inhibition of ACKR3 could result in lowering the metastatic burden due to local accumulation of CXCL12, leading to dimerization of the chemokine and thereby making it unable to activate CXCR4[57]. Increased local concentrations of CXCL12 could also trigger desensitisation and downregulation of CXCR4. Additionally, inhibition of ACKR3 could promote dissemination by disrupting adhesion-mediating effects caused by CXCL12/CXCR4 signalling.

1.3 Drug design strategies currently targeting the CXCL12-CXCR4/ACKR3 axes

CXCR4 has been a target for drug development efforts not only because of the relevant role it plays in cancer progression and cancer metastasis, but also due to its involvement in HIV-1 infection, rheumatoid arthritis, ischemic injury and WHIM syndrome[58, 59]. As a result, both the academic community and the pharmaceutical industry have strived to develop specific antagonists of this receptor, resulting in the discovery of well over 20 different chemical classes of small molecule antagonists, and numerous peptides and biologicals that inhibit CXCR4. Furthermore, this has led to the clinical approval of Plerixafor, a small molecule-bicyclam used for the mobilization of hematopoietic stem cells[60]. Besides Plerixafor, several other inhibitors of CXCR4 have advanced to the clinical trial phase of drug development, an overview of which can be found in table 1. Endeavours to develop ligands that act on

Table 1. Current list of pharmaceutical entities that target CXCR4 and are under investigation in clinical trials.

Drug Name	**Type**	**Structure**	**Phase study**	**Indication**
Plerixafor	Small molecule		FDA approved	Hematopoietic stem cell mobilization
BKT-140	Peptide		3	Multiple myeloma[61], non-Hodgkin lymphoma[62]
CTCE-9908	Peptide		1,2	Advanced solid tumors[63, 64]
TG-0054	Small molecule		1,2	Multiple myeloma, non-Hodgkin lymphoma[65]
POL6326	Peptide		1,2	Metastatic breast carcinoma, hematologic malignancies[66]
AMD070	Small molecule		1,2	Human immune-deficiency virus[58, 59]

MSX-122	Small molecule		1	Refractory metastatic or locally advanced solid tumours[67]
MDX-1338	Antibody		1	Acute myeloid leukaemia[68]
ALX-0651	Nanobody		1	Stem cell mobilization[59]
LY2510924	Peptide		1	Advanced stage cancer[59]

the CXCL12-ACKR3 axis only began to emerge recently. Due to the novelty of the target, and the still developing understanding of its role in pathological conditions, only a few different classes of ACKR3 ligands have been reported[69], none of which have yet made it to the clinical phase. Overall, exogenous ligands that affect CXCL12 and its receptors can be classified into three categories; small molecules, peptides/peptidomimetics, and biologicals. A brief overview will be given of efforts in drug design strategies targeting the CXCL12-CXCR4/ACKR3 axes. Because the development of CXCR4 inhibitors has already been reviewed extensively[70-73], only the most important and the most recent developments will be highlighted.

1.3.1 Small molecule inhibitors of CXCR4

Plerixafor, also referred to as AMD3100, is the only clinically approved inhibitor of the CXCR4 receptor to date. Although it is used to mobilize hematopoietic stem cells from the bone marrow in patients with non-Hodgkin lymphoma and multiple myeloma, it was initially assessed for its ability to block HIV-1 entry. Structurally, AMD3100 consists of two 14-member tetra-aza macrocyclic (cyclam) rings linked by an aromatic bridge (see figure 3), and engages with the receptor *via* electrostatic interactions between the positively charged nitrogens of the cyclam rings and carboxylate residues of the receptor. Because of the organisation and flexibility of its macrocyclic structure, AMD3100 has been used to incorporate metal ions to form highly stable complexes. These metal-coordinating AMD3100 derivatives displayed

improved affinity towards the CXCR4 receptor[74], and allowed for the development of radiotracers by incorporation of ^{62}Zn, ^{64}Cu, ^{67}Ga, and ^{99}mTc ions. [^{64}Cu]-AMD3100 was the first radiotracer to be studied *in vivo*, where it was demonstrated to selectively accumulate in CXCR4 expression tissues, such as bone marrow and lymph nodes[75].

TG-0054, which is also known as Burixafor, is orally bioavailable and has shown to rapidly mobilize blood stem cells and progenitor cells from the bone marrow. It is currently in a phase IIa clinical trial to investigate its use in treating multiple myeloma, non-Hodgkin lymphoma and Hodgkin disease[65]. Structurally, the triaminopyrimidine-based compound incorporates several basic nitrogens and a phosphonic acid to increase solubility and bioavailability.

AMD070, or AMD11070, is another small molecule inhibitor of CXCR4 that was originally developed for its ability to block HIV-1 entry. The molecule is highly potent towards CXCR4 (IC_{50} = 12.5 nM)[76] and does not interact with ACKR3. It has shown to be efficacious in inhibiting T-tropic HIV-1 entry and oral administration was generally well tolerated in clinical studies[77]. *In vitro* and *in vivo* studies have shown that AMD070 is capable of inhibiting cancer metastasis and progression[78, 79], but its development was put on hold by the FDA due to alterations of liver histology. The high specificity of AMD070 shown for CXCR4 is explained by its interactions in the allosteric binding pocket of the receptor. The basic nitrogens that the structure incorporates engage in ionic interactions particularly with residues Glu288 and Asp97 of the receptor[80, 81]. Furthermore, nitrogens of the tetrahydroquinoline - and benzimidazole moieties form a so-called “basic nitrogen triad”, a common structural feature of many CXCR4 inhibitors[70].

MSX-122 is a highly potent CXCR4 receptor antagonist that can be synthesised from a single reductive amination step[82]. It is a non-competitive receptor antagonist and displays an IC_{50} value of 10nM at the human CXCR4 receptor.

IT1t is a unique compound in that it bears no structural resemblance to most small molecule antagonists of CXCR4 (see figure 3). This isothiourea-based ligand was developed by Novartis and showed good specificity and a high affinity for CXCR4 (IC_{50}

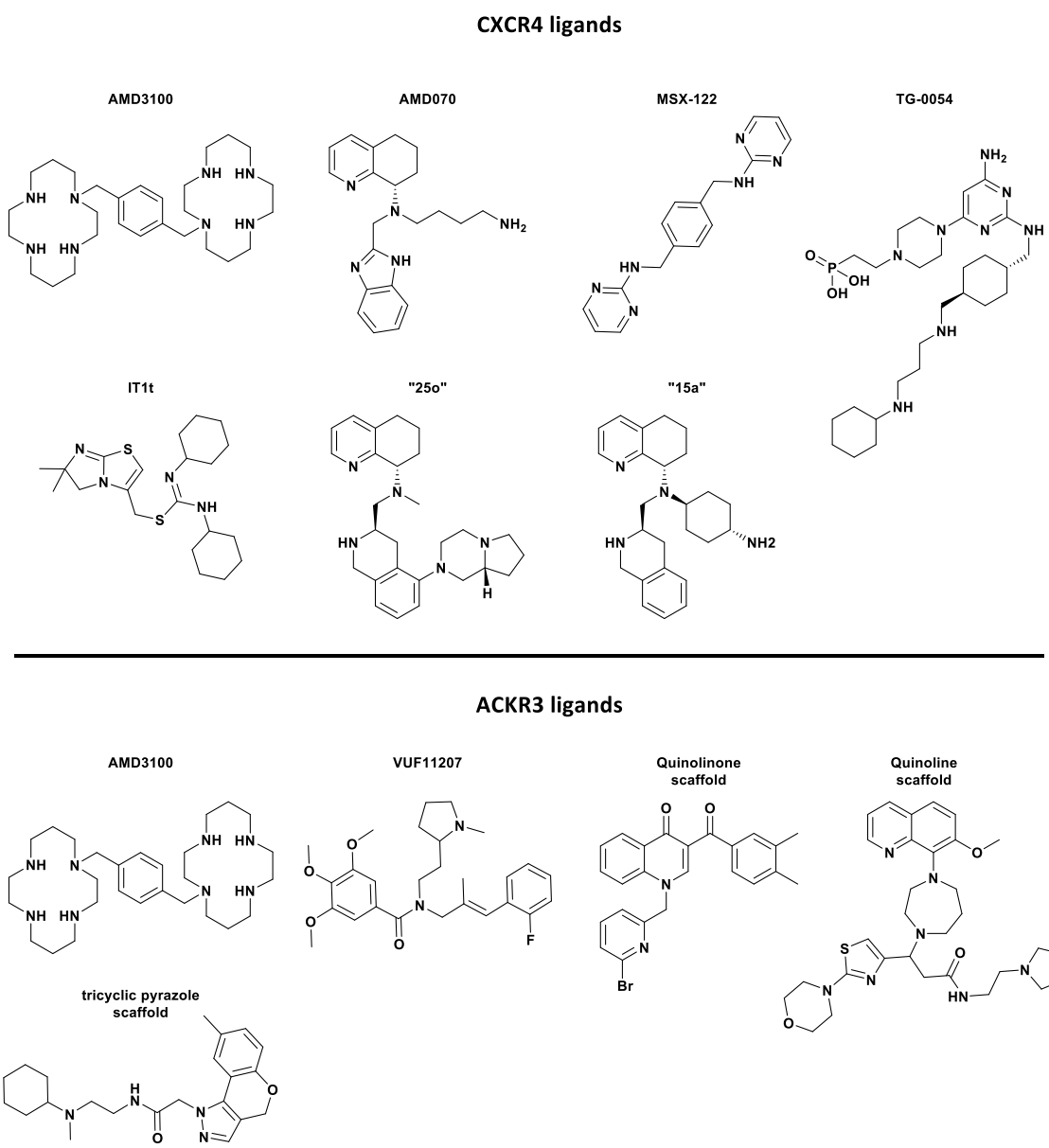


Figure 3. *Chemical structures of selected small molecule ligands of CXCR4 and ACKR3.*

= 8.0 nM)[83]. Despite good oral rat bioavailability there have been no reports showing its entry into clinical trials. Although this small molecule never progressed to the clinical stage, its use as a tool compound was shown when the crystal structure of the CXCR4 receptor was resolved with IT1t bound to the allosteric binding site[84] (picture is shown in chapter 3.1.1). Like AMD070, IT1t binds to the receptor through salt bridges with residues Glu288 and Asp97 in the allosteric binding pocket.

Compounds ***25o*** *and* ***15a*** were developed by Nguyen *et al.*[85] and Jecs *et al.*[86], respectively, and represent the very latest efforts in the development of potent and

orally bioavailable small molecule receptor antagonists. As can be seen in figure 3, structurally they are both similar to AMD070 and incorporate the same "nitrogen triad". Their improved ADME properties come through functionalization of either the side chain or the tetrahydroquinoline moiety.

1.3.2 Small molecule ligands of ACKR3

AMD3100, a potent inhibitor of the CXCR4 receptor (IC_{50} = 5.3 nM)[87], is also a ligand for ACKR3, albeit with a significantly lower affinity for the receptor (EC_{50} = 46 μM)[88]. While it blocks G protein-mediated signalling of CXCR4, it was found AMD3100 produces an agonist-like response on ACKR3 by stimulating β-arrestin recruitment and subsequent internalisation of the ligand-receptor complex.

VUF11207 is part of a family of styrene-amide compounds reported by Wijtmans *et al*.[89] and is a potent agonist of ACKR3. It was reported to have a pK_i of 8.1 in a radiolabelled competition binding assay and a pEC_{50} of 8.8 in a β-arrestin2 recruitment assay. SAR studies were supported by computational 3D QSAR and helped to obtain important descriptors for the SAR of this styrene scaffold, resulting in two findings: 1) an H-bond acceptor interaction site at the left-hand side of the ligand and 2) the molecular shape of the right-hand side of the molecule.

Since 2009 several patents have been filed by ChemoCentryx, Inc. describing a variety of small molecule ligands for ACKR3[90-92]. Among these were small molecules based on quinolinone, quinoline, and tricyclic pyrazole-based scaffolds (see figure 3). CCX771, a selective ACKR3 agonist patented by ChemoCentryx whose chemical structure has not been disclosed, is presumably based on one of these scaffolds. CCX771 is a prominent tool compound to study ACKR3 and showed an ability to block CXCL12-mediated activation of ACKR3 with an IC_{50} of 4.1 nM and an ability to induce β-arrestin2 recruitment upon binding (EC_{50} = 2.8 nM)[93]. Recently, *in vitro* and *in vivo* studies showed that CCX771 was able to inhibit tumour growth and tumour angiogenesis, further establishing ACKR3 as a critical mediator in cancer[94].

1.3.3 Peptide inhibitors of CXCR4 and ACKR3

BKT-140 is the serum stable version of T140, a 14-amino acid cyclic peptide whose structure itself is based on a horseshoe crab self-defence peptide that has

antagonistic activity on CXCR4[95]. BKT-140 is a highly potent inhibitor of CXCR4 (IC_{50} = 0.65 nM)[96]. In December 2015 BioLineRx Ltd., a clinical-stage biopharmaceutical company developing the drug, announced that phase II studies have shown positive results in the treatment of relapsed or refractory acute myeloid leukemia[97], greenlighting phase III clinical trials.

CTCE-9908 is a 17-amino acid peptide derived from the *N*-terminus of CXCL12. Although derived from the endogenous ligand of CXCR4, it has strong antagonistic effects on the receptor[98]. It has been shown to be an effective antimetastatic agent, independently whether tumour cells were injected, implanted or naturally occurring. Phase I studies demonstrated its safety in humans, and phase II studies are currently ongoing.

POL6326 is a second-generation cyclic peptidomimetic molecule capable of rapidly mobilizing hematopoietic stem/progenitor cells (HSPCs) from the bone marrow[99]. Its structure mimics that of secondary structure motifs involved in protein-protein interactions. A phase II trial showed POL6326 is well tolerated and efficacious in the recruitment of HSPC in healthy volunteers.

LY2510924 was developed by Peng *et al.*[100] and is a cyclic peptide that incorporates non-natural amino acids to increase stability. It has a high affinity for CXCR4 and *in vivo* studies showed that the peptide is effective in reducing tumour size and metastasis[101]. Phase I studies have been carried out in patients with advanced solid tumours where it showed a dose-dependent increase in mobilization of CD34+ cells with a tolerable safety profile.

TC14012, like BKT-140, is a peptide derived from T140 and has been shown to be a potent ligand for both CXCR4 and ACKR3. On CXCR4, TC14012 displays inverse agonist properties (IC_{50} = 19 nM), while on ACKR3 it acts as an agonist by stimulating β-arrestin2 recruitment (EC_{50} = 350 nM)[102, 103].

FC313 is an ACKR3 selective cyclic pentapeptide that was developed through SAR studies of the CXCR4 receptor ligand FC131[104]. Substitution of a glycine residue with L-proline resulted in a selectivity switch from CXCR4 to ACKR3. FC313 blocks CXCL12

association with ACKR3 (IC_{50} = 1.5 μM) and induces β-arrestin2 mediated internalisation (EC_{50} = 2.4 μM).

1.3.4 Biologicals for CXCR4 and ACKR3

Biologicals, and in particular antibodies, represent a class of molecules known for their high specificity towards their target, and a long serum half-life. Therapeutic antibodies act not only by binding to their target interrupting their function, but also through subsequent recruitment of cytotoxic monocytes. Biologicals acting on CXCR4 and ACKR3 therefore provide potentially valuable tools for the treatment of cancer.

12G5 was the first anti-human CXCR4 monoclonal antibody (mAb) and is widely used in *in vitro* experiments[73].

MDX-1338, or Ulocuplumab, is a fully human mAb that blocks CXCR4-mediated cell migration. It is currently undergoing phase I clinical trials for the treatment of acute myeloid leukaemia[68] (see table 1).

ALX-0651 is a nanobody; a single-domain antigen-binding fragment that is derived from the variable regions of heavy-chain antibodies produced by camelids. Nanobodies are smaller than antibodies, allowing them to cross tissue barriers more easily and possess greater stability and solubility. ALX-0651 showed mobilization of HSCs in a cynomolgus monkey and is currently undergoing phase I clinical trials[59, 105].

Efforts to develop biologicals that target ACKR3 resulted in the discovery of a group of camelid-derived nanobodies[106]. These nanobodies inhibit CXCL12-mediated β-arrestin2 recruitment *in vitro* and showed inhibition of tumour growth in a patient-derived, CXCR7-expressing, head and neck cancer xenograft model implanted in mice.

1.4 Fluorescent toolkit compounds for CXCR4 and ACKR3

Despite the continuous development of new drug candidates and the immense variety of small-molecule based ligands that have been described, little work has been performed on developing toolkit compounds that target the CXCL12-CXCR4/ACKR3 signalling axes. Fluorescent molecules in particular are valuable compounds that provide a potentially new way to further interrogate these biological

systems in the context of cancer and aid the development of novel ligands targeting these receptors. Fluorescently conjugated ligands (i.e. fluorescent molecules) have gained attention over the last years as reliable and more versatile alternatives to the traditional radiolabelled ligands in their use of interrogating ligand-receptor pharmacology[107]. Practically, the use of fluorescent ligands rather than radiolabelled ligands circumvent the increasing difficulties and expense in disposing of radioactive waste material. Additionally, and with respect to CXCR4, binding assays using [^{125}I]CXCL12 are known to be quite arduous[108], and thus fluorescently labelled ligands should provide a more convenient alternative. Besides practical considerations, there are a number of scientific reasons that underlie the potential for the use of fluorescent ligands. Firstly, G protein-coupled receptors such as CXCR4 and ACKR3 exist on the cell membrane within highly ordered domains, in conjunction with many signalling proteins (associated or not). As these highly ordered domains can vary per cell type, and even within the same cell, it is important to be able to study receptor pharmacology at the single cell or sub-cellular level. Evidence has emerged indicating that GPCR-mediated activation of G proteins occurs not only from the membrane, but also from endosomes. β-Arrestin associated signalling was furthermore found to be transduced from the plasma membrane by β-arrestin trafficking to clathrin-coated pits, after dissociation from an activated GPCR[109]. These findings further stimulate the need for tools that allow the study of GPCR function at the sub-cellular level. Fluorophores, in conjunction with highly sensitive detection techniques are perfect candidates for doing so. Secondly, fluorophores are much more versatile in their use than their radioactive counterparts, as they can be used in a wide range of different experiments. For example, optical imaging techniques such as fluorescence microscopy are highly sensitive techniques that often use fluorescent ligands for visualising ligand-receptor complexes in real time, with detection sensitivity in the pico- or even femtomolar concentration range[110]. Another advanced use of fluorescent probes is the application of cell sorting assays such as flow cytometry and fluorescence-activated cell sorting (FACS). With appropriate fluorophores these techniques allow for rapid discrimination of cell types based on receptor expression and can potentially be used for the detection of cancer cells in *ex vivo* patient material[111]. More fundamentally, fluorescent probes perform just as well as

radiolabelled ligands, if not better, in the characterisation of novel ligands using cell-based assays[107]. Though cellular uptake and increased non-specific binding are sometimes associated limitations of fluorescent ligands, these can be overcome by the application of proximity assays, such as bioluminescence resonance energy transfer (BRET). Recently, the development of the ultra-small Nanoluc®[112] has allowed for the engineering of Nanoluc®-tagged GPCRs, providing quantitative study of ligand-receptor pharmacology in living cells in real time[113].

Although reports on (fluorescent) imaging agents that specifically target CXCR4 or ACKR3 are scarce, there have been some developments. Ac-TZ14011, a cyclic peptide-based fluorescent probe, displayed an ability to inhibit CXCR4 function with an IC_{50} of 1.2 nM in a CXCL12 binding assay, and 2.6 nM in a Ca^{2+} mobilization assay[114]. Utilizing the D-lysine of this peptide, Nomura *et al*.[115] introduced TAMRA- and fluorescein dyes with the resulting fluorescent probes displaying IC_{50} values of 14 nM and 11 nM respectively, in a competitive binding assay. Use of Ac-TZ14011 in development of CXCR4 targeting probes was further exploited by Kuil *et al.*[116], who labelled the peptide with a multifunctional single attachment point reagent (MSAP) containing a DTPA chelate and a fluorescent dye (MSAP-Ac-TZ14011, figure 4). Although a decrease in binding affinity was observed (K_d = 177.1 ± 37.2 nM for the conjugate, K_d = 8.61 ± 1.42 nM for the unlabelled peptide), the probe was successfully used to image CXCR4 expressing cells both *in vitro* and *in vivo*. A different fluorescent peptide was developed by Yang *et al*.[108], consisting of a fluorescein isothiocyanate (FITC) conjugated to DV1. DV1 is an all D-amino acid analog of V1; a synthetic peptide derived from the *N*-terminus of viral macrophage protein (vMIP)-II[117]. This fluorescent conjugate showed binding affinity for the CXCR4 receptor in the micromolar range and was competitively displaced by small molecules AMD3100 and IT1t, as well as parent peptide DV1.

The majority of the small molecule-based tool compounds that have been reported are direct derivatives of AMD3100. As mentioned earlier, the structural characteristics of AMD3100 allows for the chelation of various metal ions. This makes AMD3100 an ideal tool for the development of PET tracers. An early study showed that metalation of AMD3100 using Zn^{II}, Ni^{II}, and Cu^{II} ions yielded highly stable metal

complexes and even increased the affinity towards the CXCR4 receptor[74]. This discovery allowed for the further development of radiotracers, as ^{62}Zn, ^{64}Cu, ^{67}Ga, and ^{99m}Tc ions were efficiently incorporated[74]. [^{64}Cu]-AMD3100 was the first radiotracer to be studied *in vivo*, where it demonstrated to selectively accumulate in CXCR4 expressing tissues such as bone marrow and lymph nodes[75]. Subsequent

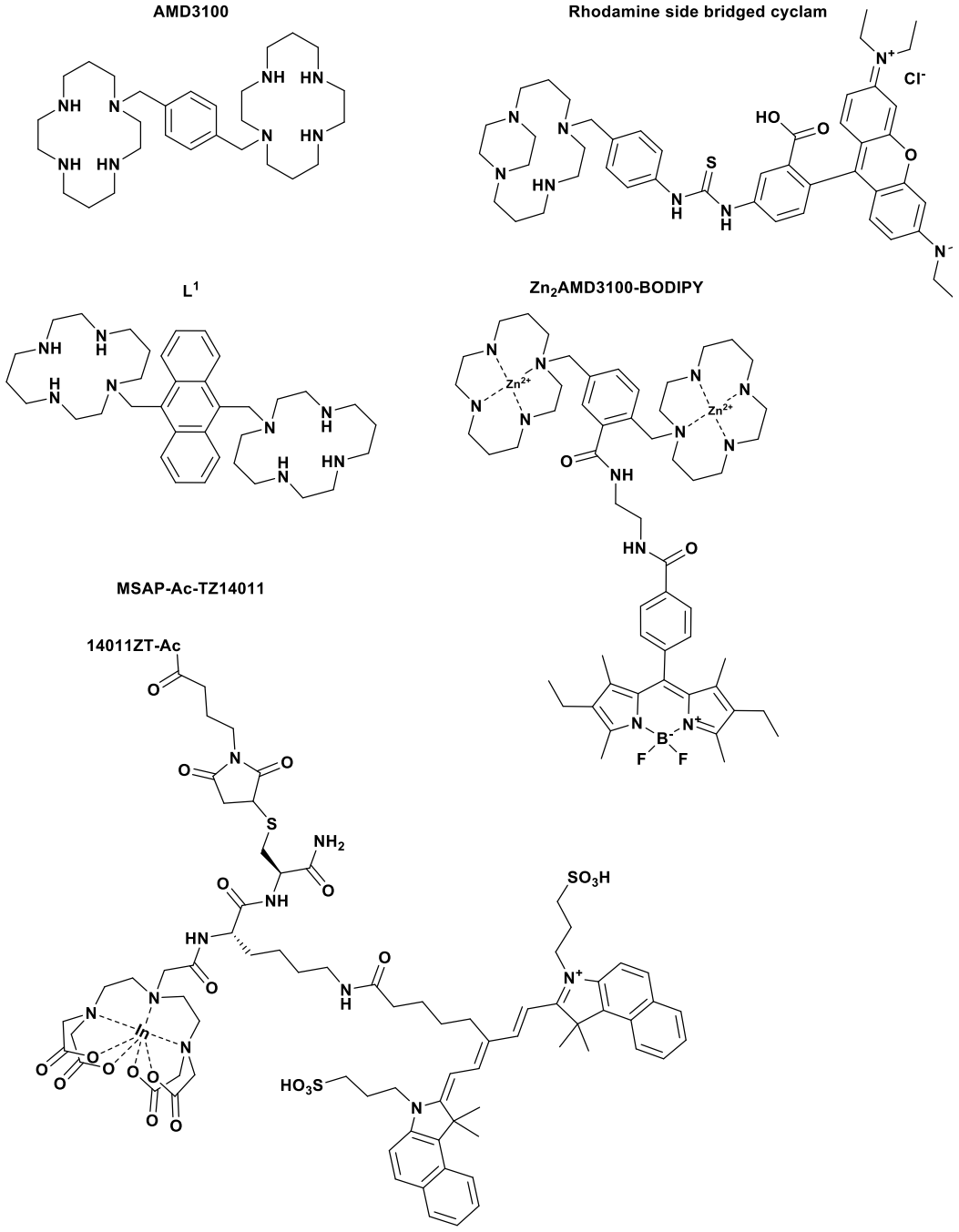


Figure 4. *Chemical structures of some reported fluorescent probes for CXCR4.*

studies using mice models revealed CXCR4 receptor-selective uptake in tumours, although accumulation was found highest in the liver[118]. In an attempt to decrease liver uptake of this family of PET tracers, Poty *et al*.[119] introduced a PEG_3 chain linked to a phenyl-NODAGA moiety. Chelating with non-radioactive gallium yielded ^{nat}Ga-AMD3100 p-NCS-Benzyl-NODAGA, whose IC_{50} value for CXCR4 receptor was found to be 121 nM. Although the binding affinity is lower than that of AMD3100 (44 nM, red.), it was high enough to use in PET studies where ^{68}Ga was used instead of ^{nat}Ga. Unfortunately, this radiotracer showed only mild improvements in terms of distribution and CXCR4-specific uptake in tumours compared to its predecessors.

The first small molecule-based fluorescent probe that targets the CXCR4 receptor was developed in 2007 by Khan *et al*.[120] and besides metal ion chelation, incorporated a rhodamine isothiocyanate moiety for visualisation (see figure 4, rhodamine side bridged cyclam). Binding properties of this fluorophore were not reported, however in flow cytometry studies it was shown that the copper-complexed probe actively competes with CXCR4-specific antibodies. In line with previous findings, the un-complexed fluorophore displayed no CXCR4-specific binding indicating that metal ions are necessary for receptor-binding by conformational restriction of the cyclam. Another direct derivative of AMD3100 is L^1 and uses an anthracene moiety that links the two cyclam rings[121]. Interestingly, it was found that the free anthracenyl ligand L^1 displayed a 6-fold increase in affinity versus its Zn^{2+} complex (IC_{50} of 0.6 µM and 3.4 µM, respectively). Finally, further exploration of the AMD3100 scaffold led to the discovery of a new, BODIPY-labelled, CXCR4 receptor antagonist (AMD3100-BODIPY, figure 4)[122]. The use of a BODIPY as fluorescent imaging component is well documented and has several advantages. They are known to be highly stable, have sharp emission bands, and are quite versatile when it comes to emission wavelengths and physical properties such as solubility and reactivity[123]. Unfortunately, the incorporation of the BODIPY tag resulted in binding properties much lower than AMD3100. While AMD3100 showed an EC_{50} of 11 nM in an anti-HIV assay using MT-4 cell lines, the most potent AMD3100-BODIPY conjugate showed an EC_{50} of only 0.8 µM. Furthermore, this

fluorescent conjugate was not found to directly compete with SDF-1α in a calcium flux competition assay.

Overall these reported toolkit compounds displayed disappointing pharmacological properties for the CXCR4 receptor, showing a significant attenuation of affinity compared to their parent AMD3100. Surprisingly, peptide-based probes too lack high affinity for the receptor. Moreover, the use of small molecules as the parent ligand in the development of novel imaging agents offer advantages over peptide-based probes as the former tend to be more stable, and usually can be produced in more convenient synthetic approaches. Unfortunately, AMD3100 has showed to be an unfulfilling parent ligand. The required incorporation of metal ions has proved to be a challenging process and may complicate ligand binding assays. Also, the incorporation of a BODIPY tag lead to 77-fold decrease in potency[122]. An explanation for this drop off in potency might be found by looking at PET tracer ^{nat}Ga-AMD3100 p-NCS-Benzyl-NODAGA[119]. This compound, compared to the AMD3100-BODIPY, incorporates a much longer linker. Since both compounds utilize the same conjugation strategy to AMD3100, the drop off in potency of the BODIPY compound can be explained by the linker length. In other words, an increase in potency might be observed of the AMD3100-BODIPY compound by increasing the length of the linker.

Considering the potential value of fluorescent probes in studying the pharmacology of chemokine receptors, and their use in further unravelling the involvement of these GPCRs in cancer, there is a distinct need for high affinity fluorescent probes. So far there have been a few reported efforts in developing fluorescent probes for the CXCR4 receptor, however none resulted in highly applicable probes. Additionally, there have been no reported efforts in developing fluorescent probes for the atypical chemokine receptor ACKR3. Collectively, high affinity fluorescent probes for both CXCR4 and ACKR3 would present a unique way of studying these receptors. With selective and versatile probes, these receptors can be studied either individually or in the presence of each other. This thesis will therefore discuss efforts in developing novel high affinity small molecule-based fluorescent probes.

2 Aims and objectives

The aim of this thesis was to develop novel small molecule-based fluorescent probes as toolkit compounds for chemokine receptors CXCR4 and ACKR3. Fluorescence-based techniques have evolved over the last few decades into reliable and ultrasensitive methods for the study of biological systems. When combined with fluorescent probes they provide a unique opportunity to study the interactions of drug molecules with their target and to study receptor pharmacology in real-time, at the single molecule level. Despite overwhelming evidence for the involvement of the CXCL12-CXCR4/ACKR3 signalling axes in cancer progression and cancer metastasis, little is understood about their intricate interactions on cancer cells. The development of highly specific fluorescent probes, and their application in fluorescence-based techniques, will afford a unique insight on how these two signalling axes interact with each other. By providing selective and high affinity fluorescent probes, I hope to elucidate the mechanisms that underlie the signalling of these chemokine receptors, and ultimately aid the development of novel therapeutics for the treatment of cancer.

A classic medicinal chemistry approach will be used for the development of CXCR4 specific fluorescent probes. Evaluation of the extensive structure-activity relationships (SAR) of reported CXCR4 receptor antagonists, as well as *in silico* design through the use the ligand-bound CXCR4 protein crystal structure, will inform the synthetic strategy to conjugate fluorescent dyes to previously reported CXCR4 receptor inhibitors.

Despite the lack of a crystal structure of ACKR3, or extensive SAR of ACKR3 ligands, a similar medicinal chemistry approach will be used for the development of ACKR3 specific fluorescent probes. Identification of an appropriate parent ligand will be based on SAR of a reported class of ACKR3 ligands. Rational for ligand modification and subsequent conjugation to fluorescent dyes will be obtained through the use of an homology model of ACKR3, and supported by site-directed mutagenesis studies.

Despite being derived from already established ligands full pharmacological characterisation of the synthesised fluorescent ligands is imperative, before

application of these probes in advanced fluorescence-based experiments. This is mostly due to the fact that the addition of a large fluorophore is likely to have a major impact on the pharmacological profile of the final conjugate. Affinity for their respective targets will be assessed in a novel cell-based NanoBRET™ proximity assay[113]. Their use as tool compounds will be assessed in competition binding experiments using the same NanoBRET™ technique. Where possible, functional experiments will be performed to investigate their mode of action on their receptors. Finally, successful fluorescent probes will be used to visualise ligand-receptor interactions in confocal microscopy experiments.

3 Development of high affinity fluorescent CXCR4 receptor probes

The aim for this part of the project was to develop small molecule-based fluorescent probes that, with good affinity and high specificity, bind to the chemokine receptor CXCR4. Fluorescent probes generally consist of three distinct but interdependent parts: 1) the parent ligand, or pharmacophore, 2) the fluorescent tag, or fluorophore, and 3) the linker that separates these two components (figure 5). For the development of such a successful probe all three elements require careful consideration, as each part can exert an influence on the pharmacological profile of

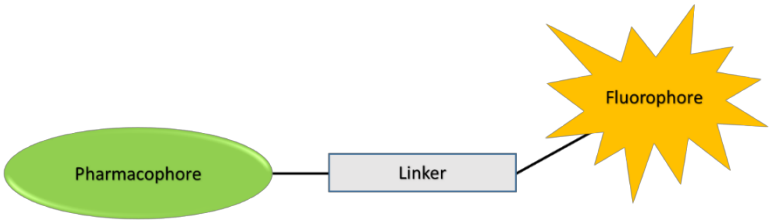


Figure 5. *Schematic representation of a fluorescent probe.*

the final conjugate. Design considerations include structure-activity relationships (SAR) of the pharmacophoric element, length and chemical composition of the linker and the type and size of the fluorophore. Naturally, for the development of small molecule-based probes the choice of the pharmacophore, and its SAR with the receptor, is an important one. A ligand must be chosen that displays high affinity towards the receptor, and its SAR must provide insight on where to attach a linker/fluorophore combination. Most commercial fluorescent dyes are large molecules (400-1000 Da), and conjugation to a receptor ligand is thus likely to double the overall weight and size of the final probe. The part of the pharmacophore that is used as a conjugation point must therefore be tolerant towards substitution. To investigate whether reported CXCR4 receptor antagonists fit the requirements necessary for the development of such probes I looked to use the reported crystal structure and available structure-activity relationships.

3.1 Selection of appropriate pharmacophores

3.1.1 IT1t

In 2010 Wu *et al*.[84] successfully resolved the crystal structure of the chemokine receptor CXCR4. Crystal structures were obtained in complex with two inhibitors: small molecule antagonist IT1t (2.5 Å, see figure 6A), and cyclic peptide inhibitor CVX15 (2.9 Å, see figure 6B). IT1t is part of a class of isothioureas originally described by Thoma *et al*.[83] that were found to have excellent bioavailability and *in vivo* activity. Furthermore, IT1t was shown to be highly potent towards CXCR4 with a reported IC_{50} value of 8.0 nM in a binding assay, and 1.1 nM in Ca^{2+} mobilization assays. As figure 6A displays, IT1t binds to the receptor in a region situated close to the extracellular surface of the receptor, a feature which is common for chemokine receptors but unusual for most other class A GPCRs[81, 124]. Since the natural ligand CXCL12 binds to the *N*-terminus and the outer regions of the receptor[125], this shallow binding pocket is considered an allosteric binding site. The position of this allosteric binding pocket relative to the extracellular environment is convenient for the development of fluorescent probes. With easy access to the extracellular environment, the fluorophore is less likely to interfere with ligand-binding. Furthermore, the chemical spacer between the pharmacophore and fluorophore can remain relatively short, benefiting the overall properties of the conjugate. Key interactions between CXCR4 and small molecule IT1t are displayed in figure 6C. The aliphatic cyclohexane moieties interact with several amino acid residues through hydrophobic interactions, whereas the nitrogen atoms from the isothiourea moiety form salt bridges with residues Asp97 and Glu288. The importance of the interactions of these nitrogen atoms with residues Asp97 and Glu288 is demonstrated by reduction in binding affinity of ~100-fold upon methylation[83]. Overall, the crystal structure of CXCR4 complexed with IT1t shows that the allosteric binding pocket is conveniently located for the development of small molecule-based fluorescent probes, and that a spacer separating the pharmacophore and fluorophore does not require to be exceptionally long.

Besides giving insight on the nature of the allosteric binding pocket, IT1t itself might be considered as a pharmacophore for the development of fluorescent probes. Considering the importance of the interaction of the thiourea moieties with residues

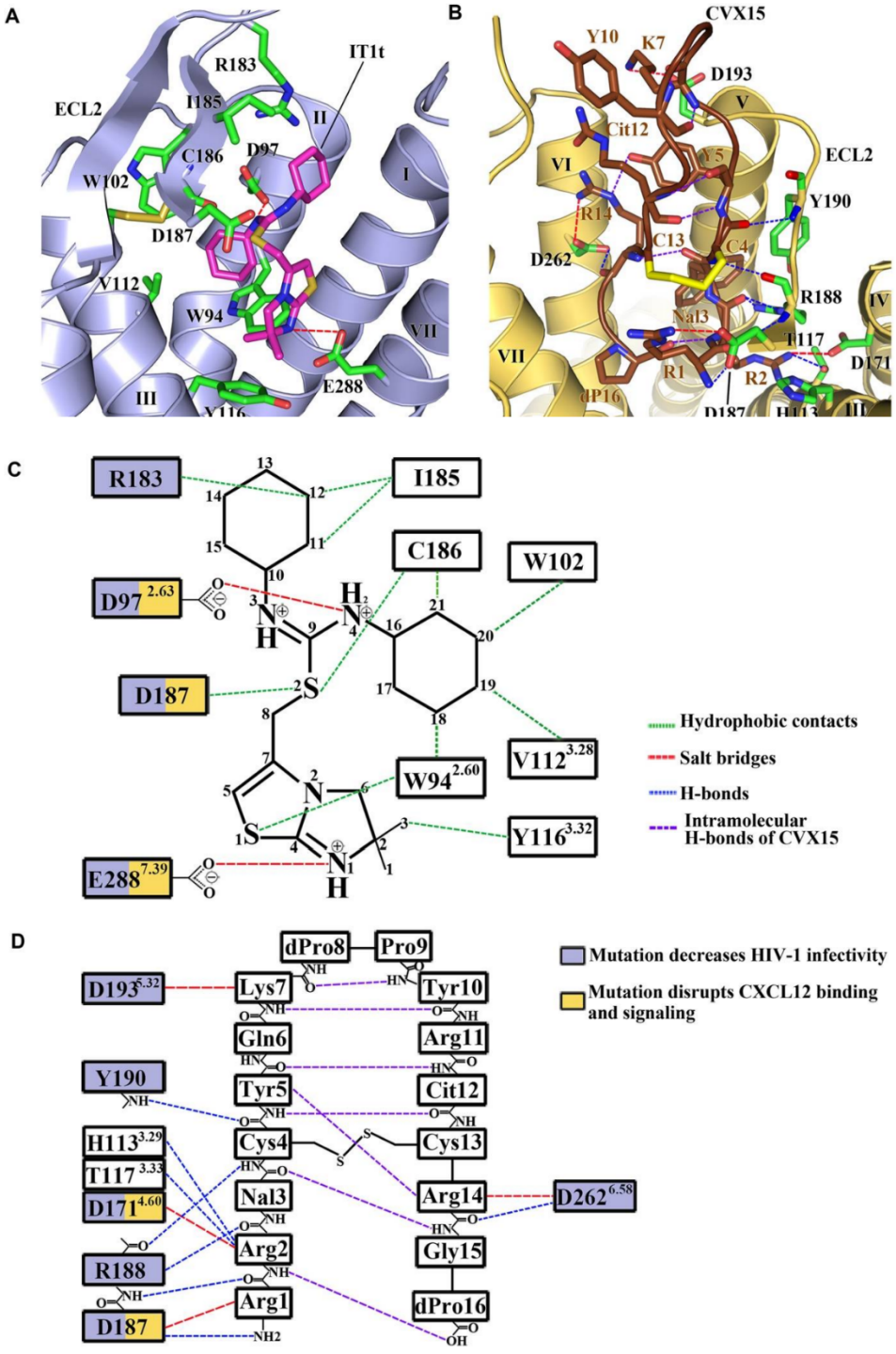


Figure 6. *Crystal structures of chemokine receptor CXCR4 containing small molecule IT1t and cyclic peptide CXV15. (A) Binding mode of small molecule IT1t. (B) Binding mode of cyclic peptide CVX15. (C) Schematic representation of the interactions between IT1t and residues within the binding pocket of CXCR4. (D) Schematic representation of the interactions between peptide CXV15 and residues within the binding pocket of CXCR4. Picture adopted from Wu et al.*[84]

Asp97 and Glu288, conjugation to the heterocycle part of IT1t should be avoided, as that may affect ligand binding. The structure also shows one of the cyclohexane moieties pointing up, towards the extracellular surface. Closer inspection of the binding pocket confirmed that the cyclohexane moiety is relatively unrestricted and that indeed it may be an appropriate site for conjugating to a fluorescent tag. Using one of the cyclohexane moieties as a linkage point will require chemical modification, which can be achieved in a number of ways. A convenient way of doing so is by the introduction of a free amine group which allows for single step coupling to amine-reactive fluorophores, which are widely commercially available. I therefore envisioned I could develop IT1t into fluorescent probes by modifying one of the cyclohexane rings to a piperidine ring and using the basic nitrogen to conjugate a linker/fluorophore. A binding pose was generated of a piperidine-substituted IT1t derivative by docking the ligand in the crystal structure, which suggests that positioning a nitrogen on the *meta*-position allows for the least hindered conjugation approach (figure 7).

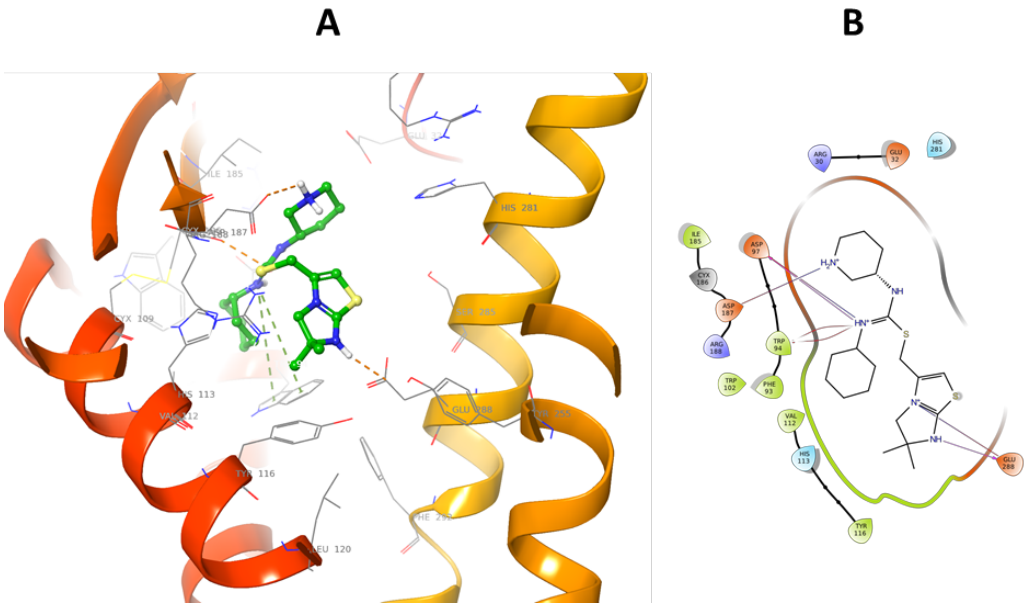


Figure 7. *Docking of a piperidine-substituted IT1t derivative. (A) Binding pose of the IT1t derivative within the receptor. (B) 2D representation of the interactions between the ligand and key residues of the receptor.*

A patent search revealed that the IT1t structure has also been used in combination with peptidomimetic- and glycomimetic structures to generate new potent and selective CXCR4 receptor inhibitors[126], of which two are depicted in figure 8.

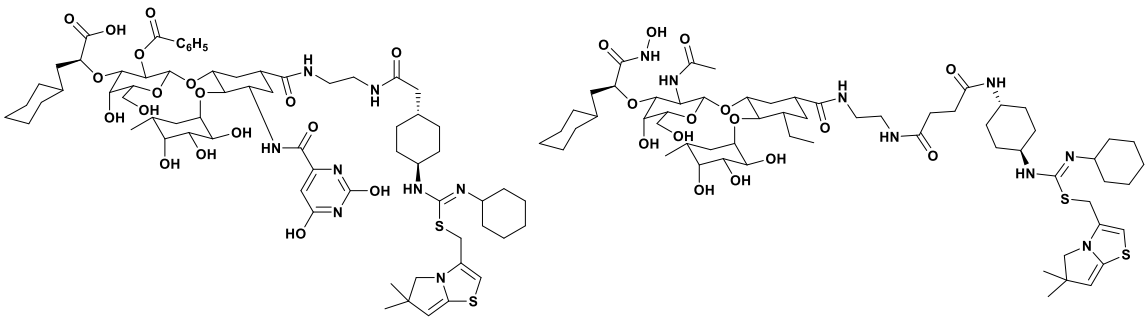


Figure 8. *Examples of glycomimetic structures as CXCR4 inhibitors that were described in a patent*[126].

Although these structures are not suited as ligands for fluorescent conjugates themselves due to their large size, they show a similar conjugation strategy of functionalisation of one of the cyclohexane moieties of IT1t. Rather than inserting a nitrogen in the 3' position of the cyclohexane ring however, the nitrogen was attached outside the ring on the 4' position, allowing conjugation to the glycomimetic through peptide coupling. I anticipated that placing the point of conjugation outside the ring would also be a good strategy, since it preserves the symmetry and flexibility of the parent ligand. Cognisant of the above I generated a binding pose for the *trans*-aminocyclohexane derivative of IT1t (figure 9). As can be seen from the figure, this derivative adopts a binding pose similar to the 3'-piperidine substituted IT1t

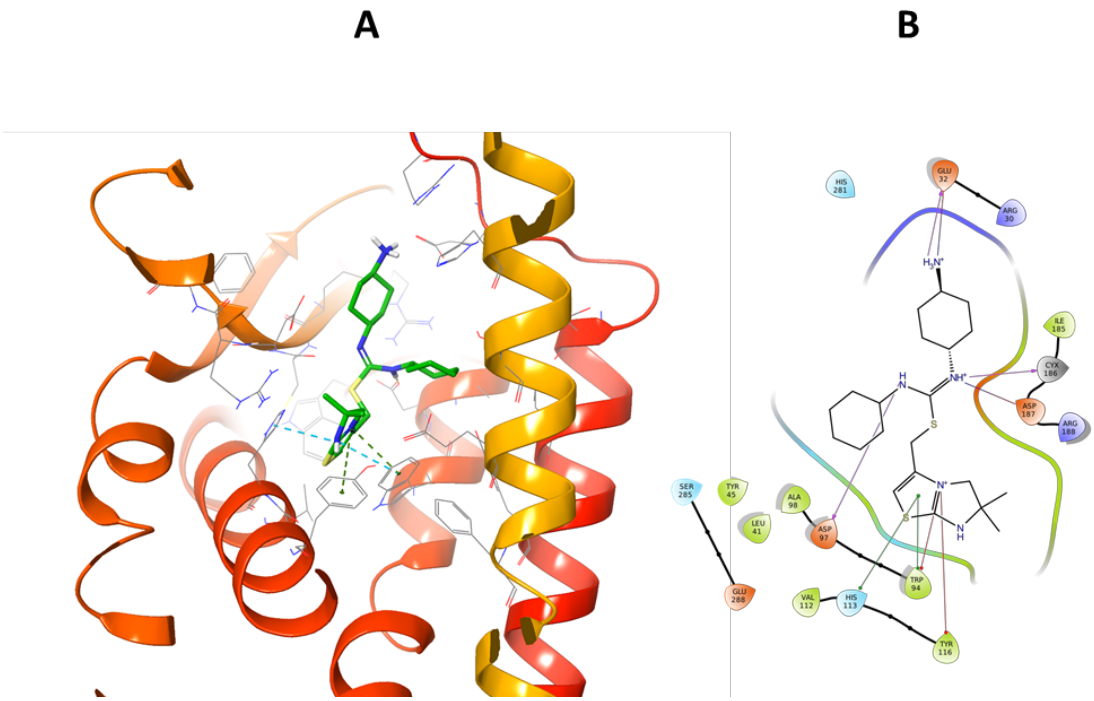


Figure 9. *Docking of a trans-aminocyclohexane substituted IT1t derivative. (A) Binding pose of the IT1t derivative within the receptor. (B) 2D representation of the interactions between the ligand and key residues of the receptor.*

derivative. Furthermore, the amine that will be used as point of linkage is situated near the top of the receptor and is easily accessible. This provides good rational for the development of small molecule-based fluorescent probes based on the IT1t scaffold.

3.1.2 AMD070

When evaluating structure-activity relationships of other reported classes of CXCR4 receptor inhibitors it is evident most scaffolds bear little resemblance to IT1t. In general, most CXCR4 inhibitors are small, flat, incorporate multiple aromatic heterocycles, and contain basic nitrogen atoms that form a so-called "nitrogen triad"[70]. Many of these compounds also include a short aliphatic chain and a distal amine which is positively charged at physiological pH; AMD(11)070 is perhaps the best example of this class of compound. This highly potent antagonist is currently under clinical evaluation for its use in the treatment of HIV infection, and several studies have supported its use in cancer[78, 79]. This tetrahydroquinoline-based structure incorporates multiple basic nitrogen atoms of which three form a triad. Recent docking studies performed on AMD070 have revealed this triad forms crucial interactions with residues Glu288 and Asp187 with the crystal structure, and hydrophobic interactions are formed between the aromatic heterocycles of AMD070

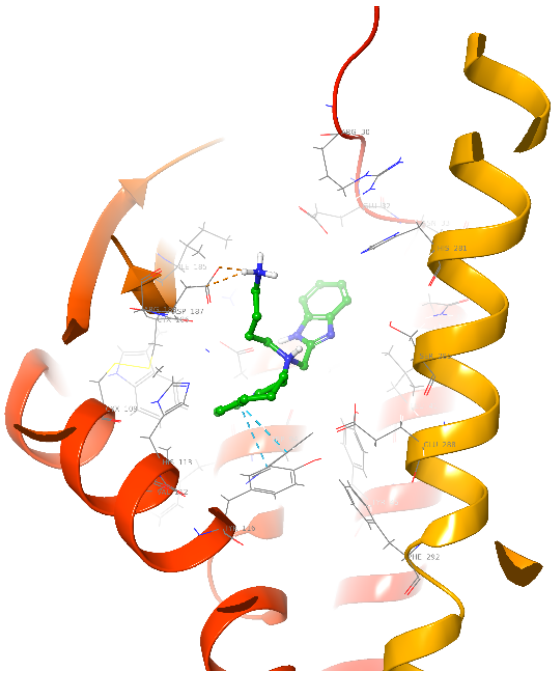


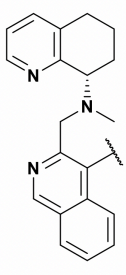
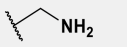
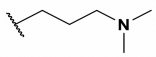
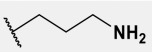
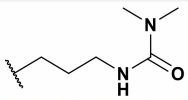
Figure 10. *Binding pose of small molecule AMD070 in the CXCR4 crystal structure.*

and residues His294, Ile265, and Ser295. Critically, a salt bridge is formed between the distal amine of the molecule and residue Asp97[127]. Residue Asp97 is part of transmembrane helix II and is located relatively close to the extracellular surface and, similarly to the piperidine-substituted IT1t derivative, causes the distal amine of the ligand to angle upwards towards to solvent. To confirm this binding mode the ligand was docked into the crystal structure using Glide[128] (Figure 10). It appears that this amine is unhindered and might provide a useful conjugation point for the development of fluorescent probes. Though conjugation directly onto this amine removes its basic nature and potentially attenuates its ability to interact with Asp97, it remains the least hindered and most flexible part of the molecule and therefore should allow for facile conjugation.

3.1.3 An isoquinoline scaffold

Further exploration of the SAR around AMD070 shows a shift of the distal amine from the central nitrogen atom to the benzimidazole ring[129, 130]. Furthermore, it revealed that the use of an isoquinoline core instead of a benzimidazole core increased potency and improved ADME properties[131]. Additionally, it was found that changing the length of the side-chain and functionalising the primary amine did not affect binding properties markedly (see table 2). Interestingly, increasing the chain length from a methyl- to a propylamine led to an increase in affinity from 27 ± 11 nM to 12 ± 2.0 nM. Methylation of the primary amine to form dimethylpropylamine further increased binding affinity to 5.0 ± 2.0 nM. These findings suggest that this flexible part of the molecule is highly tolerant towards substitution, and is therefore

***Table 2**: A series of isoquinoline-based compounds showed high potency for the CXCR4, even with the introduction of bulky side-chains.*

Isoquinoline scaffold	Side-chain	Reported IC_{50}
		27 ± 11 nM
		5 ± 2 nM
		12 ± 2 nM
		38 ± 12 nM

positioned in such a way it could allow conjugation to a linker/fluorophore combination.

After careful consideration of the shape and size of the allosteric binding pocket, and a thorough evaluation of the structure-activity relationships of different small molecule inhibitors, three different scaffolds were selected for development into corresponding fluorescent ligands (figure 11). Functionalisation of one of the cyclohexane moieties of IT1t will involve incorporation of an amine, either incorporated into the ring or placed outside the ring. This amine will serve as a linkage point for the conjugation to a linker/fluorophore. By making use of the flexible aliphatic amines of the AMD070 scaffold and the isoquinoline scaffold I looked to directly couple these ligands to a linker/fluorophore combination.

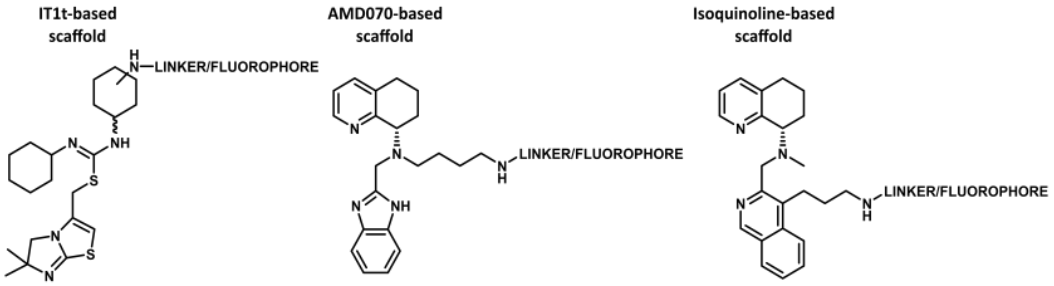


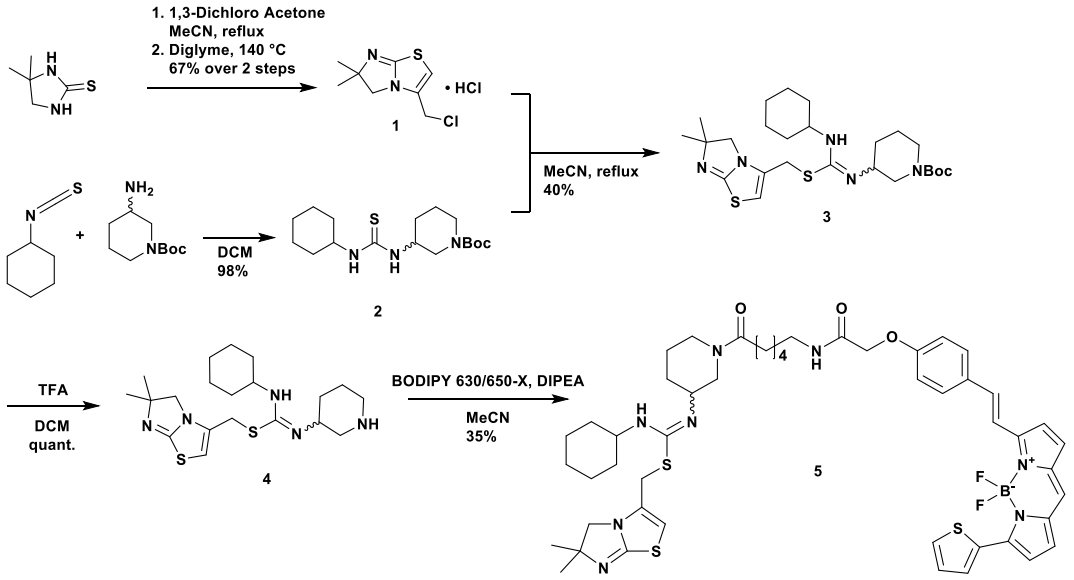
Figure 11. *Fluorescent ligands will be synthesised based on three different scaffolds: IT1t-based (left), AMD070-based (middle), and isoquinoline-based (right).*

3.2 Synthesis of fluorescent conjugates

3.2.1 IT1t-based probes

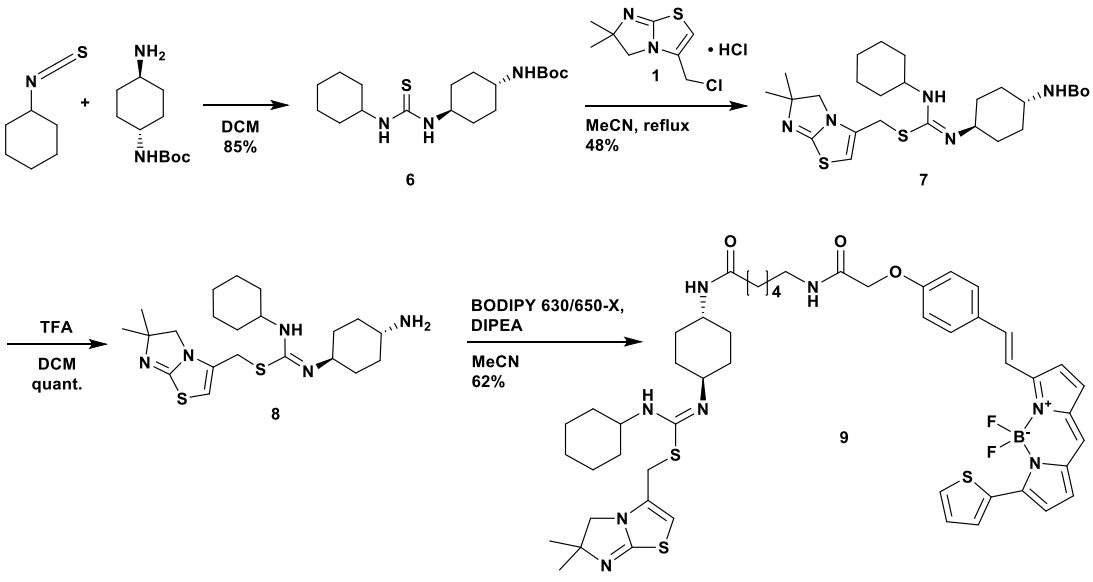
The development of IT1t-based fluorescent probes commenced with the synthesis of a piperidine-substituted IT1t derivative (scheme 1). From commercially available 4,4-dimethyl-2-imidazolidinethione, and following the original procedure published by Thoma et al.[83], a two-step reaction with dichloroacetone allowed for the conversion of the thiourea into isothiourea **1**. Separately, *N*-alkylation of cyclohexyl isothiocyanate with racemic 1-Boc-3-aminopiperidine afforded key intermediate **2** in excellent yield, and provided the necessary amine for conjugation to a linker/fluorophore combination. Subsequent alkylation between key intermediates **1** and **2** was achieved under reflux conditions, affording the desired pharmacophore

Scheme 1. *Synthesis of a fluorescent piperidine-based IT1t derivative.*



3, which after treatment with trifluoroacetic acid to remove the Boc group was ready for the final conjugation step. With the pharmacophoric element of the probe in hand, I proceeded with the conjugation of a linker/fluorophore combination. Here, I chose to incorporate a boron-dipyrromethene-based dye, or BODIPY. Specifically the BODIPY 630/650-X which, for convenience, already incorporates a seven-atom aminohexanoyl spacer. This BODIPY dye is available through commercial sources and comes as an amine-reactive, succinimidyl ester–protected dye, allowing us to couple

Scheme 2. *Synthesis of a para-substituted fluorescent IT1t derivative.*

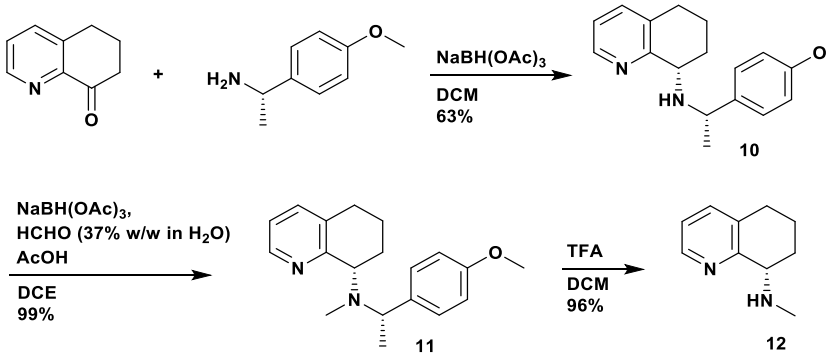


this pharmacophore in a single step. In the presence of Hünig's base this coupling as achieved under stirring conditions, and the final conjugate fluorophore **5** was purified by preparative reversed-phase high pressure liquid chromatography (RP-HPLC). With the successful synthesis of the first IT1t-based fluorescent conjugate, focus shifted towards synthesising a *4*-substituted IT1t derivative (scheme 2). Following the same synthetic strategy, starting from an *N*-Boc protected *trans*-cyclohexanediamine thiourea **6** was formed in good yields. Similar to the synthesis of the first fluorophore, this intermediate was then reacted with isothiourea **1**, and after removal of the Boc group, the congener was ready for linkage to a linker/fluorophore combination. Again the use of the succinimidyl ester-protected BODIPY 630/650-X dye allowed for single-step conjugation, and the final fluorescent conjugate **9** was purified by preparative reversed-phase HPLC.

3.2.2 Isoquinoline-based probes

Having successfully synthesised two fluorescent probes based on the IT1t scaffold, focus was again shifted; this time towards developing isoquinoline-based probes. An important feature of this CXCR4 receptor antagonist chemotype is the chiral centre at the tetrahydroquinoline moiety (see figure 11). Literature has shown that the *S*-isomer of the chiral amine significantly improves binding to CXCR4 compared to the *R*-isomer[129-131]. I therefore felt it was necessary to synthesise the desired fluorescent probes enantiomerically pure. To do so, I first synthesised key fragment **12** (scheme 3). Several ways have been developed for the synthesis of these types of chiral amines. Chiral auxiliaries, for example, provide an excellent way of controlling the stereochemistry outcome of reactions[132]. I was able to obtain the desired enantiomer by reductive amination of a tetrahydroquinolinone using the chiral auxiliary (*S*)-1-(4-methoxyphenyl)ethanamine. Here, the stereochemistry of the product is controlled by steric hindrance at the face of the auxiliary and therefore reduction of the imine by sodium triacetoxyborohydride proceeds only from the opposite face. NMR studies of intermediate **10** showed no presence of a mixture of diastereomers and therefore it was assumed only the desired (*S*)-*N*-((*S*)-1-(4-methoxyphenyl)ethyl)-5,6,7,8-tetrahydroquinolin-8-amine was isolated. A kilogram-scale synthesis of the same intermediate was published by Boggs *et al*.[133] and reported a 9:1 diastereoselectivity

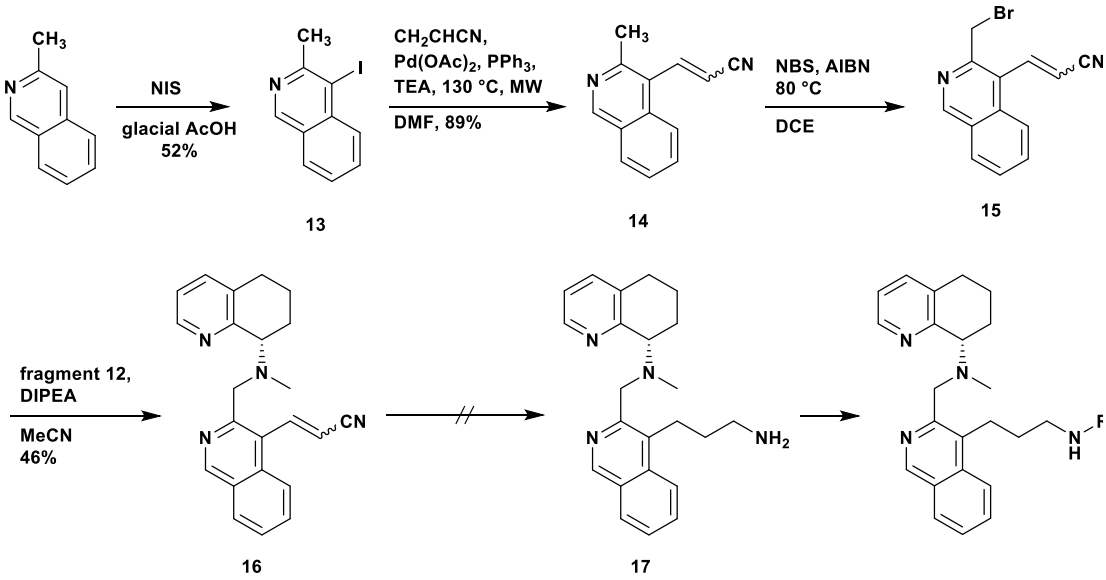
Scheme 3. *Synthesis of the chiral fragment.*



of the desired product, further supporting the assumption I had isolated the desired enantiomer. Next, to avoid possible di-substitution of the final fragment I installed a methyl group on the central nitrogen of intermediate **10**, before removing the auxiliary. Methylation of the amine was achieved *via* reductive amination using a solution of formaldehyde in water (37% w/w). Subsequent treatment of the intermediate with trifluoroacetic acid removed the auxiliary and finally afforded key fragment **12**. It was observed that the freebase of this compound was prone to decomposition over time, so for storage purposes the compound was kept as an HCl salt.

With this fragment in hand I proceeded with the synthesis towards *ortho*-substituted methylisoquinolines. Starting from 3-methylisoquinoline, and following the procedures reported by Miller *et al*.[131], electrophilic iodination with *N*-iodosuccinimide (NIS) afforded only the *ortho*-substituted product (**13**, scheme 4). This iodine intermediate was then subjected to Heck coupling with acrylonitrile, in the presence of triethylamine and palladium catalyst, affording *ortho*-substituted 3-methylisoquinoline **14** in excellent yields. Radical bromination using azobisisobutyronitrile (AIBN) as initiator and *N*-bromosuccinimide as source of bromine efficiently installed the bromine on the methyl group. The reaction proceeded in an apparent good yield, however after workup and purification by flash column chromatography only starting material was recovered. Decomposition of the product back to the starting material is most likely due to the weakness of the alkyl-halide bond, and the relative stability of the carbon cation that is formed upon decomposition. During the work-up and purification stages this cation is likely to be

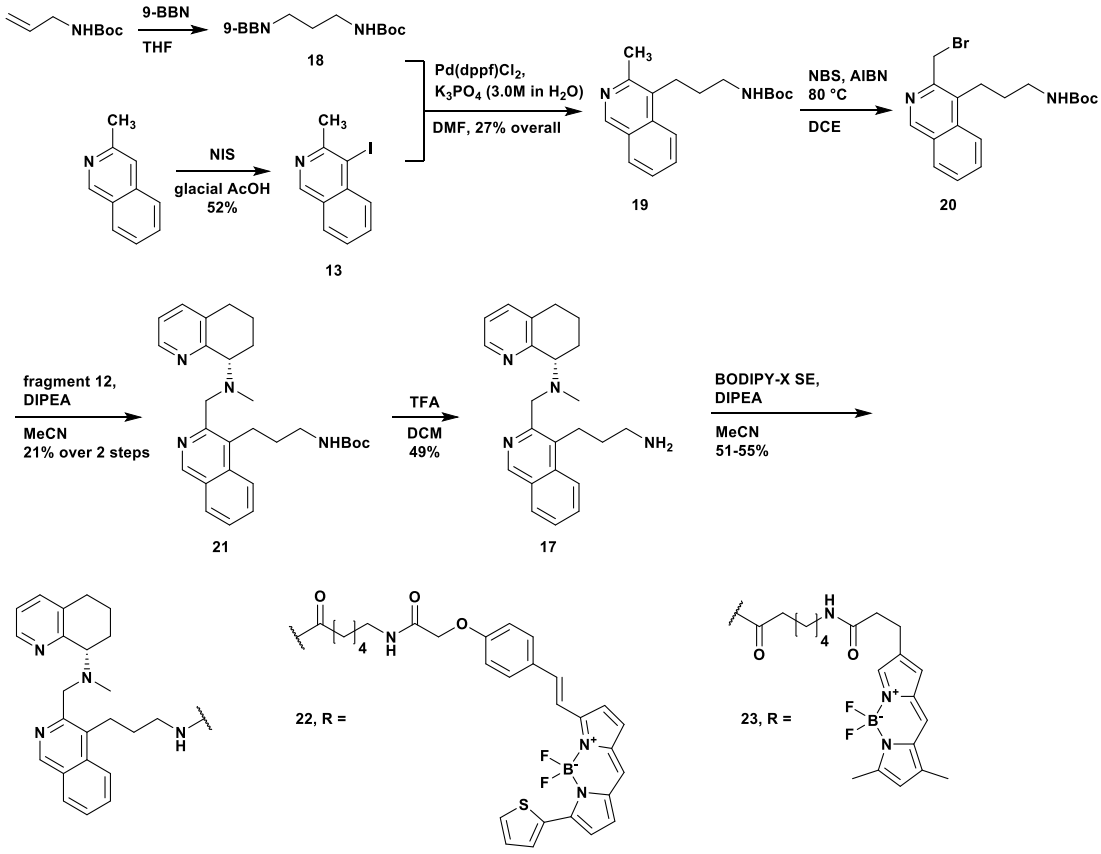
Scheme 4. *Synthesis of isoquinoline-based fluorescent probes.*



quenched resulting in reformation of starting material. To avoid this issue the reaction was carried out again and, upon completion, was concentrated *in vacuo* and added immediately to a stirring solution of fragment **12** in acetonitrile. In the presence of Hünig's base this successfully resulted in the alkylated product (**16**, scheme 4). Unfortunately, hydrogenation of the olefin and reduction of the nitrile using Raney nickel and ammonia under a hydrogen atmosphere was unsuccessful, as were other hydrogenation conditions.

Due to the conjugated nature of the olefin I decided to avoid Heck coupling and introduce the distal amine in a different fashion. Hydroboration-Suzuki coupling is a well-known procedure that allows synthesis of functionalised alkenes, arenes and cycloalkenes[134]. Hydroborating a terminal alkene efficiently reduces the double bond and forms an organoborate capable of undergoing Suzuki-Miyaura coupling. In my synthesis I found by using a solution a solution of 9-BBN in THF I was able to hydroborate *tert*-butyl *N*-allylcarbamate using the conditions reported by Miyaura *et al*.[134] (scheme 5). The crude organoborate was then allowed to react with the iodinated methylisoquinoline under standard Suzuki-Miyaura cross coupling conditions. With the distal amine successfully introduced, synthesis was continued as I had set out. Bromomethyl intermediate **20** was prepared by radical bromination and in a one-pot fashion was alkylated with chiral amine **12**. Finally, after removal of

Scheme 5. *Alternative synthesis route towards isoquinoline-based fluorescent probes.*



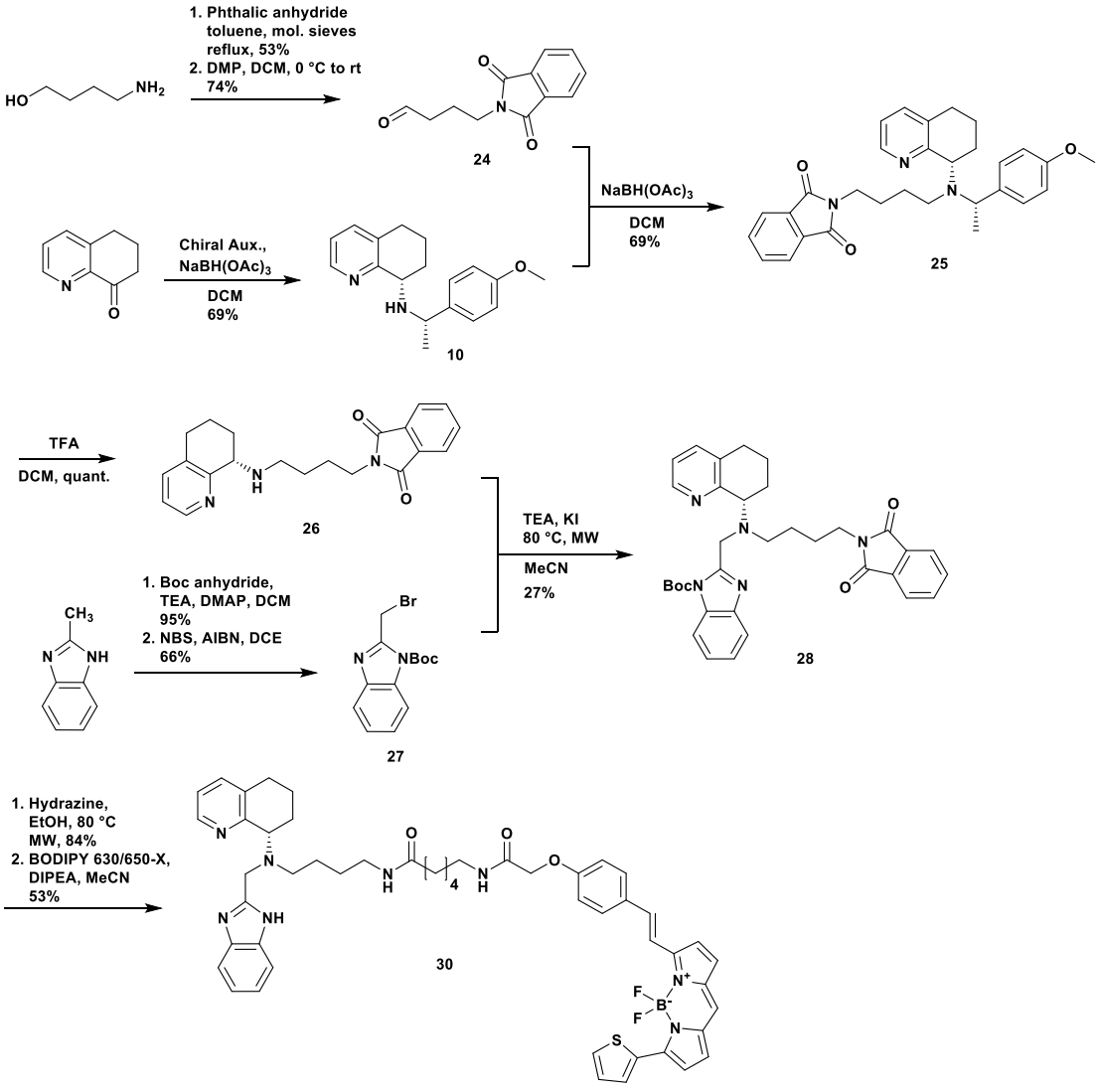
the *N*-Boc in the presence of TFA I was finally able to obtain the desired congener. To determine whether this scaffold lends itself for the development of potent fluorescent probes it was decided to couple BODIPY dyes directly to the distal amine of this scaffold. Additional to the introduction of the BODIPY 630/650-X dye (**22**, scheme 5) I also decided to introduce the green fluorophore BODIPY FL-X (**23**, scheme 5). Introducing this smaller, green fluorescent dye will allow us to investigate the effect of fluorophore size on ligand-binding. Furthermore, this bright green fluorescent dye can be used in experiments where red-labelled probes are incompatible, further expanding the available toolkit for studying the CXCR4 receptor.

3.2.3 AMD070-based probes

Finally, the development of fluorescent derivatives of the AMD070 scaffold was pursued. Largely following the procedure reported by Crawford *et al.*[135], I started synthesis with a phthalimide protection of 4-amino-1-butanol (scheme 6) which

subsequently allowed me to oxidize the alcohol to aldehyde **24** with Dess-Martin Periodinane (DMP). Similar to the preparation of fragment **12**, I installed the critical chiral amine *via* reductive amination with a chiral auxiliary. Again, to avoid unwanted di-substitution of this chiral amine I proceeded with reductive amination of aldehyde **24** by intermediate **10** before removing the auxiliary. Separately, *N*-Boc protection and subsequent radical bromination of 2-methylbenzimidazole afforded intermediate **27** in good yield. *N*-alkylation of this alkyl-bromide intermediate by secondary amine **26** finally assembled the scaffold. Heating of this compound in the presence of hydrazine simultaneously removed the phthalimide and Boc protecting groups, after which I could couple this congener to a BODIPY 630/650-X dye.

Scheme 6. *Synthesis of an AMD070-based fluorescent probe.*



All fluorescent ligands synthesised from these three scaffolds have been purified and isolated by preparative reverse-phased HPLC, and their purities were confirmed to be >95%. Furthermore, their identity was confirmed using high resolution mass spectrometry (HRMS TOF ES+).

3.3 Pharmacological characterisation

With the successful development of small molecule-based fluorescent probes based on three distinct chemotypes, I proceeded with their pharmacological characterisation. To test the affinity of these compounds towards the chemokine receptor CXCR4 I looked to use a novel BRET-based ligand-binding assay. Using the same assay, I also investigated their ability to compete with CXCL12 and unlabelled small molecules. Finally, using a functional assay I investigated their ability to affect CXCL12-induced inhibition of cAMP production.

3.3.1 NanoBRET™

Bioluminescence Resonance Energy Transfer (BRET) is a technique that allows for the real time monitoring of protein-protein and ligand-protein interactions[136]. The technique relies on the dipole-dipole transfer of energy from a donor enzyme to an acceptor fluorophore upon oxidation of a substrate (illustrated in figure 12). This transfer of energy can result in excitation of the acceptor fluorophore when its

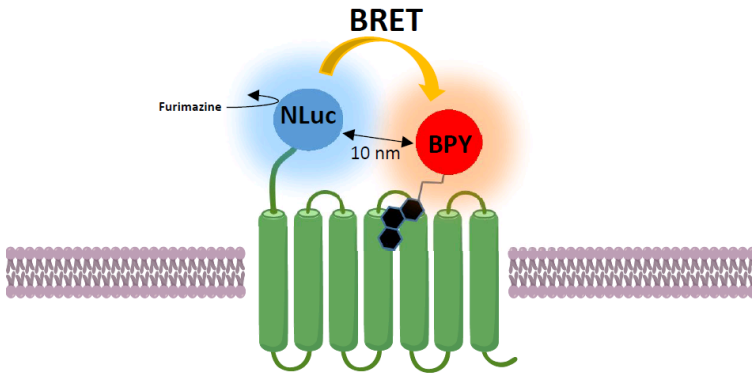


Figure 12. *Schematic illustration of the use of BRET to study ligand-receptor interactions. A bioluminescent signal, originating from the enzymolysis of furimazine by Nanoluciferase®, can excite a fluorophore in close proximity. Upon excitation, this fluorophore will then emit a distinct fluorescent signal at a longer wavelength. The ratio of emitted luminescence and fluorescence therefore can be used as a measure of ligand-binding.*

excitation spectrum overlaps with the emission spectrum of the donor, resulting in fluorescence of the fluorophore at a longer wavelength than the donor light emission. The efficiency of this energy transfer is inversely proportional to the sixth power of the distance between the two dipoles, meaning that the distance between the donor enzyme and acceptor fluorophore has to be within 10 nm in order for the energy transfer to occur. Selection and placement of the enzyme that produces the donor signal is crucial for accurate ligand-binding experiments. A range of luciferase enzymes have been developed and utilised as donors in experiments studying protein-protein interactions[137], most of which are based on firefly luciferase and Renilla luciferase. For use in the study of ligand-receptor interactions however these enzymes are sub-optimal, as their large size (61 and 38 kDa, respectively) makes them difficult to express on receptors, and is also likely to interfere with ligand binding. Fortunately, recent reverse engineering of a luciferase variant of deep sea shrimp has led to the development of Nanoluc®: a much smaller (19 kDa) and much brighter bioluminescent enzyme[138]. When used in conjunction with the substrate furimazine, a small molecule engineered from coelenterazine, it produces a luminescent signal that is approximately 30 times brighter than that of other luciferase enzymes[113]. The first step in developing a NanoBRET™ assay to evaluate fluorescent ligands at the CXCR4 receptor is the labelling of the receptor at the *N*-terminus with Nanoluciferase®. To this end, an in-house cell line of HEK293 cells stably expressing NLuc-CXCR4 had already been developed. These cells were cultured in 500 cm^2 trays after which they were collected, lysed, and their membranes isolated. After quantification of the protein content of the membranes using a BCA protein assay, the membranes were ready to be used.

3.3.1.1 Validation of the NanoBRET™ assay

To determine whether the NanoBRET™ approach will give a reliable and accurate measurement of the pharmacological properties of the fluorescent probes, the assay was first validated for the CXCR4 receptor. This was done by performing saturation binding experiments and competition binding experiments using fluorescently labelled CXCL12. Alexa Fluor® 647-labelled CXCL12 is available for research use through commercial sources (Almac group, UK), and was used to this end. For

saturation binding experiments, isolated membranes were added to 96-well plates and suspended in assay medium. To this were added increasing concentrations of $CXCL12^{AF\text{-}647}$ in the presence and absence of AMD3100 (10 µmol/L, equal to 100x K_d). AMD3100 is a small molecule inhibitor of the CXCR4 receptor and is used in these experiments to determine the level of nonspecific binding. After an incubation period of 1 hour at 37 °C the Nanoluc® substrate furimazine was added and the BRET ratio was immediately measured on a PHERAstar FS plate reader. For competition binding experiments, isolated membranes were added to 96-well plates and suspended in assay medium, to which were added a fixed concentration of $CXCL12^{AF\text{-}647}$ and increasing concentrations of CXCL12 and small molecules AMD3100 and IT1t. After an incubation period of 2 hours at 37 °C the Nanoluc® substrate furimazine was added and the BRET ratio was measured on a PHERAstar FS plate reader. The results of these experiments are shown in figure 13 and table 3. For saturation binding of $CXCL12^{AF\text{-}647}$, shown in figure 13A, a concentration-dependent ligand-binding BRET ratio could be observed, which reaches saturation at concentrations >100 nM. Minimal nonspecific BRET was furthermore observed, as indicated by the very low signal of the nonspecific binding (black line). That indicates the fluorescent compounds can be tested with good signal over noise and that AMD3100 is a good ligand to determine nonspecific binding. From these experiments the affinity of

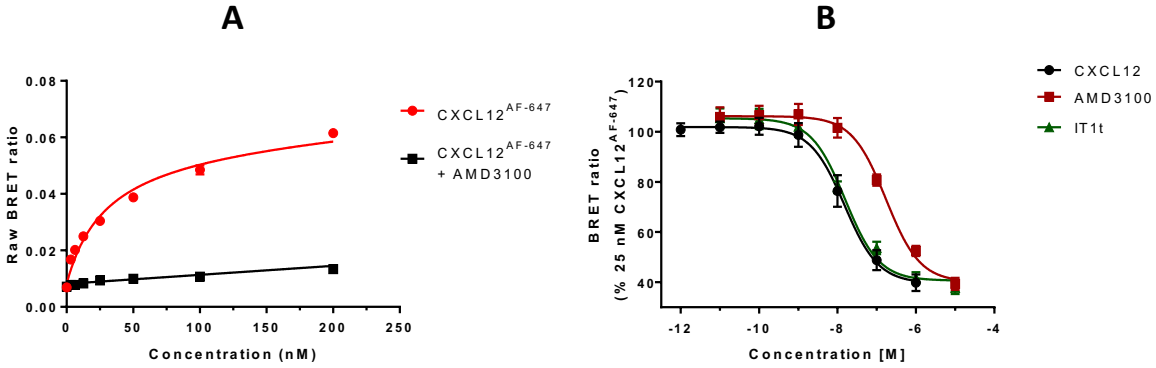


Figure 13. *Validation of the NanoBRET™ system for the characterisation CXCR4 receptor ligands. Figure* ***A*** *shows a saturation binding curve obtained for* $CXCL12^{AF\text{-}647}$ *using the NanoBRET™ system. HEK293 cell membranes expressing NLuc-CXCR4 were incubated with increasing concentrations of* $CXCL12^{AF\text{-}647}$*, in or without the presence of 10 µmol/L AMD3100. Raw BRET ratio is determined as the ratio of fluorescence/luminescence. Data points represent mean ± SEM of triplicate determinations of a single experiment. These single experiments are representative of five separate experiments. Figure* ***B*** *shows binding of CXCL12 and small molecules AMD3100 and IT1t, in the presence of 25 nM* $CXCL12^{AF\text{-}647}$*. Here, BRET ratio was determined as the ratio of fluorescence/luminescence and subsequently normalised to the maximum response to* $CXCL12^{AF\text{-}647}$*. Data points represent the combined mean ± SEM of five separate experiment performed in triplicate.*

Table 3. *Binding affinities of CXCL12, AMD3100, and IT1t as calculated from the competition NanoBRET™ assay.[a]*

	CXCL12		**AMD3100**		**IT1t**	
	pK_i	*n*	pK_i	*n*	pK_i	*n*
CXCL12^{AF-647}	8.00 ± 0.07	5	7.00 ± 0.04	5	8.00 ± 0.01	5

[a]Values show mean ± SEM. In each individual experiment triplicate determinations were made for each experimental condition. pK_i values were calculated from IC_{50} values using the Cheng-Prusoff equation.

CXCL12^{AF-647} was determined to be 27 ± 7 nM (K_d ± SEM, n = 5). This K_d value of CXCL12^{AF-647} was subsequently used for the competition binding experiments, where NLuc-CXCR4 cell membranes were incubated with CXCL12^{AF-647} at 25 nM in addition to increasing concentrations of CXCL12, AMD3100, and IT1t. The results, shown in figure 13B, show full concentration-dependent displacement of CXCL12^{AF-647} by unlabelled CXCL12, AMD3100, and IT1t. Affinities of these compounds were calculated, and reported as pK_i values in table 3. Overall, these experiments show that the NanoBRET™ system can reliably be used for the assessment of my fluorescent conjugates, and that it allows for the effective screening of unlabelled ligands.

3.3.1.2 NanoBRET™ Saturation Binding

To determine the affinity of my fluorescent conjugates I looked to apply saturation binding experiments. Isolated membranes expressing NLuc-CXCR4 were added to a 96-well plate at a concentration of 10 000 ng protein per well, and to it increasing concentrations of the fluorescent ligands were added. As validated in the previous experiments, a high concentration of unlabelled AMD3100 (10 µmol/L) was used to determine nonspecific binding. After an incubation period of 1 hour at 37 °C the Nanoluc® substrate furimazine was added and the BRET was immediately measured on a PHERAstar FS plate reader. I observed a concentration-dependent increase in BRET ratio that reached saturation at the higher concentrations for most of the synthesised compounds (figure 14). Of the five synthesised probes only compound **5** appeared to be a very weak binder for CXCR4. Figure 14A shows an essentially linear increase in BRET ratio over a 0-1000 nmol/L concentration range, consistent with very low affinity. Because the observed total binding shows a higher BRET ratio than the nonspecific binding, there does seem to be some binding. Interestingly,

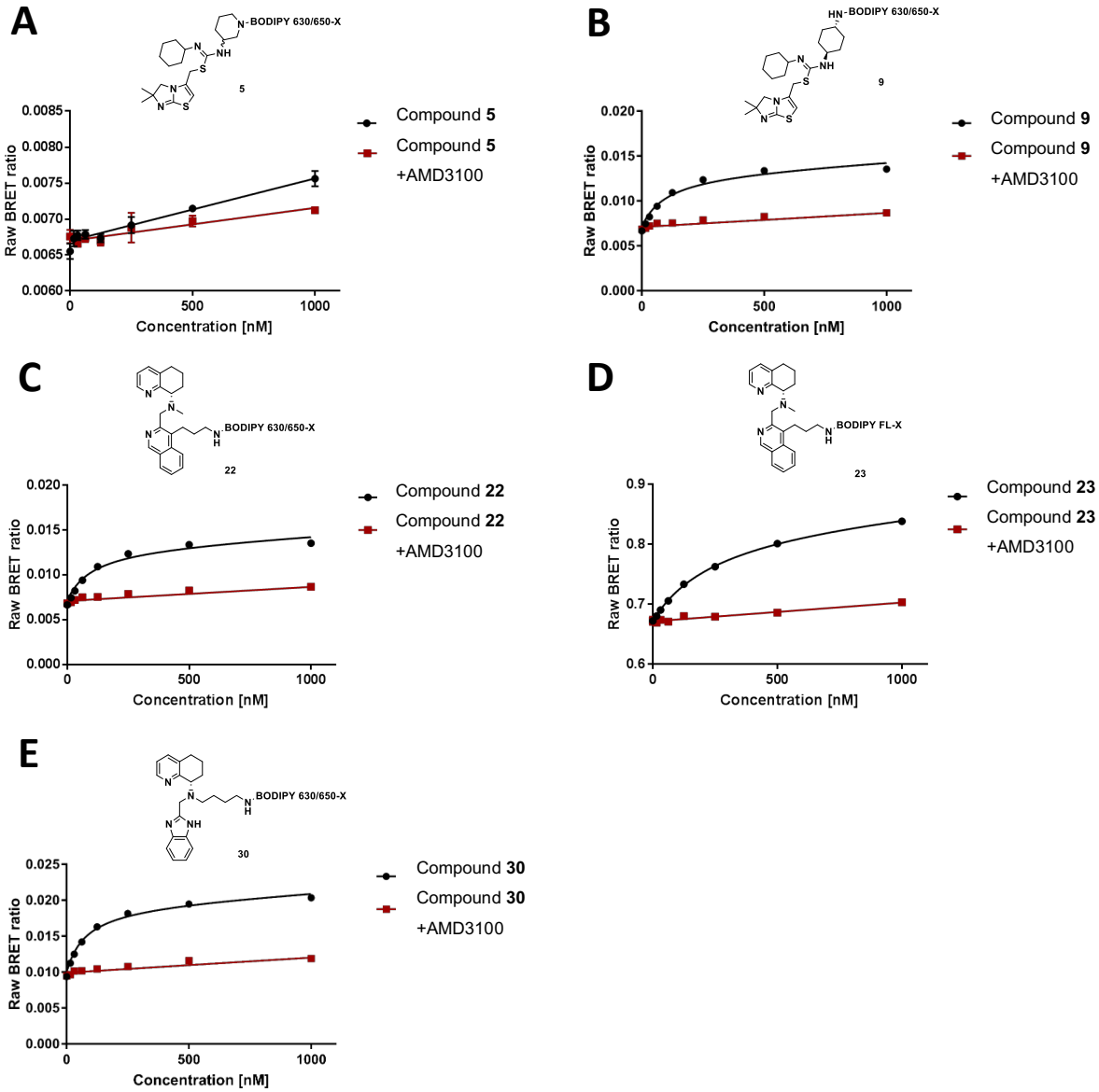


Figure 14. *NanoBRET™ signal obtained from HEK293 NLuc-CXCR4 cell membranes incubated with increasing concentrations of the synthesised compounds. Raw BRET ratio is determined as the ratio of fluorescence/luminescence. Non-specific binding was determined in the presence of 10 µmol/L AMD3100. Data points represent mean ± SEM of triplicate determinations of a single experiment. These single experiments are representative of four separate experiments. Where not seen, error bars are within the symbol.*

compound **9** (figure 14B) shows increase in BRET ratio much more indicative of specific ligand-receptor binding. A marked increase in BRET signal is observed over lower concentrations and reaching saturation at about 0.5µM. This suggests that positioning of the linker/fluorophore combination is crucial for IT1t-based probes. It appears that the flexibility and symmetry of the cyclohexane moieties play an important role in the affinity of the compound for the receptor. The two fluorescent probes based on the isoquinoline scaffold were both able to produce a

concentration-dependent BRET signal, with compound **22** reaching saturation at 0.5 µM and compound **23** reaching saturation above 1 µM (figures 14C and 14D, respectively). Interestingly, BODIPY FL-X-labelled compound **23** produces a significantly larger BRET window than the BODIPY 630/650-X-labelled **22**. This is likely due to the spectral overlap between Nanoluciferase® emission and the excitation and emission wavelengths of the BODIPY FL-X dye[113]. Because of the spectral overlap it is possible that the emitted light of the NLuc is also recorded in the acceptor emission channel, adding background noise. For the red fluorescent BODIPY 630/650-X dye there is greater separation between its excitation and emission wavelengths and NLuc emission wavelengths, contributing to lower background noise[113]. Lastly, the fluorescent AMD070 derivative **30** also displays an good concentration-dependent BRET signal and reaches saturation at 0.5 µM. Affinity values of the compounds towards CXCR4 are displayed in table 4. Of the four fluorescent probes that show specific binding towards NLuc-CXCR4, compounds **9** and **30** have the highest affinity, with excellent K_d values of 92 nM and 84 nM, respectively (pK_d of 7.0 and 7.1). Although isoquinoline-based probe **22** and AMD070-based probe **30** are based on similar chemotypes, there is a two-fold difference in affinity. Despite the relatively small difference in affinity, it is quite possible that the AMD070-based probe binds to the receptor more easily due to the more preferred position of the distal amine, and its more flexible nature. Overall, these experiments have shown that all three

Table 4. *Affinities of the fluorescent probes towards NL-CXCR4.* [a]

Compound	K_d (nM)	pK_d
6	-	-
9	92.3 ± 5	7.04 ± 0.03
22	162.3 ± 33	6.82 ± 0.09
23	240.6 ± 27	6.62 ± 0.08
30	84.3 ± 4	7.07 ± 0.03

[a] *The K_d and pK_d values were obtained from saturation-binding experiments. Data shown are means ± SEM of four separate experiments.*

scaffolds allow the development of high affinity fluorescent ligands, with pK_d values ranging 7.07-6.62. The next step in the characterisation of these fluorescent ligands is their behaviour in competition binding experiments. This will verify whether these types of probes are competitive binders, and thus useful tool compounds in the screening of unlabelled ligands.

3.3.1.3 NanoBRET™ competition binding

Using the same NanoBRET™ assay, I attempted to displace the synthesised fluorescent compounds with increasing concentrations of the endogenous ligand CXCL12 and established small molecules AMD3100 and IT1t. To represent the scaffolds I chose to use high affinity compound **9** and the BODIPY FL-X-labelled compound **23** as the labelled ligands, and pre-incubated NLuc-CXCR4 cell membranes with these compounds at either 100nM for compound **9** or 250 nM for compound **23**; approximating their K_d values. After an incubation period of 2 hours the Nanoluc® substrate furimazine was added and the BRET ratio was measured (figure 15). The affinities of CXCL12, AMD3100, and IT1t, as determined in these experiments are given in table 5. From figures 15A and 15B it can be observed that small molecules AMD3100 and IT1t displace the two fluorescent compounds in a concentration-dependent manner. At first glance, it might appear that the small molecules are unable to fully displace green fluorophore **23**, as even at the higher concentrations a BRET signal can be observed. As these ligands both displace the probe to the same level, it would however suggest full displacement. It is more likely that the increased background noise that is often observed with BODIPY FL-X dyes plays a role here. Both small molecules are also able to competitively displace compound **9** in a concentration-dependent manner, showing that this compound also can be used to screen unlabelled small molecules. For both fluorescent compounds, it appears that the endogenous ligand CXCL12 only partly displaces these probes, at best. Although unexpected, an explanation can be found when considering the binding mechanism of CXCL12 to the CXCR4 receptor. It is well known that CXCL12 first engages with the CXCR4 receptor by interacting with the *N*-terminus of the receptor, after which it folds itself into the receptor[81, 139]. It is plausible that the *N*-terminal tail of the

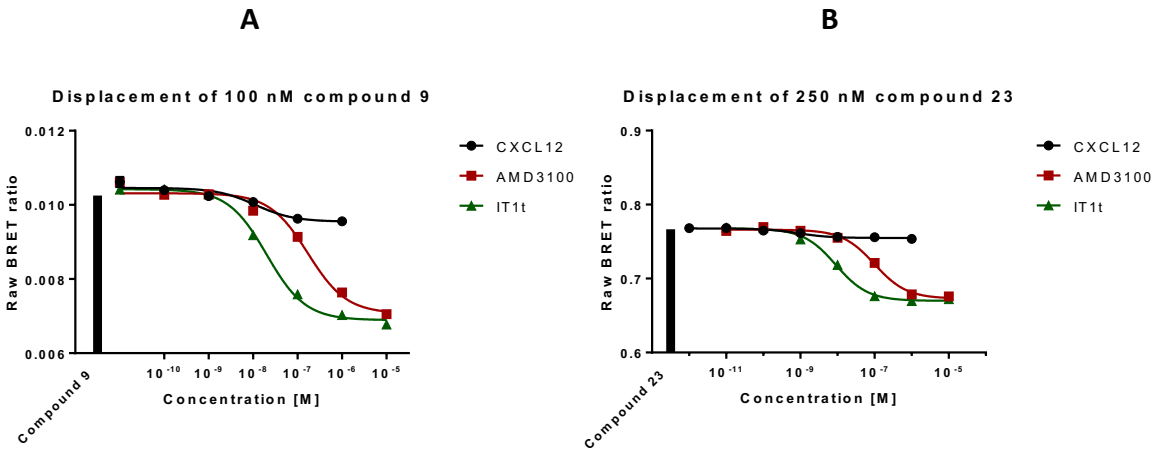


Figure 15. *NanoBRET signal from NLuc-CXCR4 cell membranes treated with (A) 100 nmol/L compound **9**, (B) 250 nmol/L compound **23**, and increasing concentrations of CXCL12, AMD3100, and IT1t. Raw BRET ratio is determined as the ratio of fluorescence/luminescence. Data points represent mean ± SEM of each separate experiment performed in triplicate.*

Table 5. *Binding affinities of CXCL12, AMD3100, and IT1t as calculated from the competition BRET assay.[a]*

	CXCL12		**AMD3100**		**IT1t**	
	pK_i	*n*	pK_i	*n*	pK_i	*n*
Compound 9	8.42 ± 1.09	4	7.00 ± 0.07	4	8.03 ± 0.11	4
Compound 23	ND	4	7.29 ± 0.06	4	8.52 ± 0.05	4
Reference (CXCL12^{AF-647})	7.97 ± 0.07	5	7.00 ± 0.04	5	8.04 ± 0.01	5

[a]Values show mean ± SEM. In each individual experiment triplicate determinations were made for each experimental condition. pK_i values were calculated from IC_{50} values using the Cheng-Prusoff equation.

receptor is interacting with the fluorophore of the conjugates and is therefore unable to interact with incoming CXCL12. Alternatively, a more simple explanation could be the fact these probes do not compete for the same binding pocket as CXCL12, and therefore are non-competitive. The pK_i values obtained for small molecules AMD3100 and IT1t from both experiments closely represent affinities obtained in the validation experiments, using CXCL12^{AF-647} as the "hot" ligand. This confirms that these small molecule-based probes, in combination with the Nanoluc®-BRET assay, indeed provide excellent means to study CXCR4 receptor pharmacology and characterise novel small molecules.

3.3.2 GloSensor™ cAMP Assay

So far, I have shown that these fluorescent probes have good affinity towards the CXCR4 receptor and are competitively displaced by small molecule ligands. To provide more insight on the nature of the fluorescent ligands I felt it was important to study their activity on the receptor. Despite the fact that these fluorescent probes are based on small-molecule inhibitors of CXCR4, it should not be assumed that they retain the same activity. The incorporation of a linker/fluorophore combination may well affect their mode of action on the receptor. To this end I looked to use a functional assay to further characterise these ligands.

The GloSensor™ cAMP assay is an extremely sensitive assay that allows for the interrogation of overexpressed or endogenous GPCRs whose activation causes changes in the intracellular concentration of cAMP. The assay relies on a genetically encoded biosensor that is comprised of cAMP binding domains fused to mutant forms of *Photinus pyralis* luciferase[140]. Upon binding to cAMP, conformational changes occur that results in large increases in light output (figure 16). Because this conformational change only occurs upon binding of cAMP, the emitted light is a direct measure of the concentration of cellular cAMP, and thus a measure for receptor activity. As CXCR4 is a G_i-coupled receptor, activation leads to inhibition of adenylate cyclase activity, resulting in a cellular decrease of cAMP (see chapter 1.1.1). Therefore in order to accurately measure CXCR4 receptor activation, Forskolin must be added to stimulate adenylate cyclase and raise levels of cAMP.

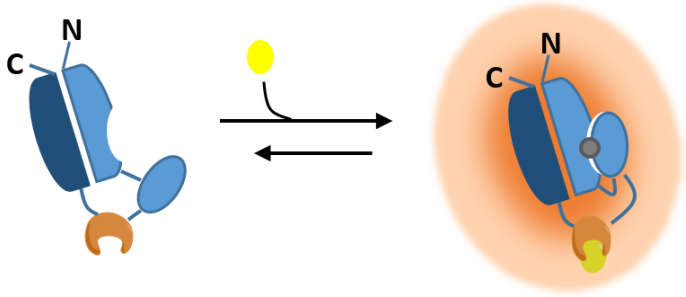


Figure 16. *Schematic illustration of the Glosensor assay biosensor. In the presence of luciferase substrate, and upon binding to cAMP, a conformational change occurs that results in the emission of light.*

A HEK 293 Glosensor™ cell line stably expressing CXCR4 containing an *N*-terminal SNAP-tag was created in-house (HEK293_SNAP-CXCR4). These cells were plated on clear-bottomed, poly-D-lysine treated 96-well plates and grown to confluency. The assay was performed by treating the cells with GloSensor™ cAMP reagent, leaving them to incubate for 2 hours at 37 °C. After one hour of the incubation period the fluorescent compounds were added reaching a final concentration of 1 µM, and were left to equilibrate. Cellular luminescence was read on a PHERAstar FS plate reader immediately following the addition of forskolin (final concentration 30 µM) and varying concentrations of CXCL12. The results of this functional assay are presented in figure 17. Here, CXCL12 elicited a concentration-dependent inhibition of Forskolin-mediated luminescence with a pEC_{50} of 9.98 ± 0.12 (*n* = 8). The three fluorescent probes used in this assay all displayed an ability to affect CXCL12-induced activation of CXCR4, as can be seen in the right-ward shift of the concentration response curve (*n* = 7 for compound **9**, *n* = 5 for compounds **22** and **30**). Of the three different compounds, compound **22** elicits the most clear antagonist response, by shifting the EC_{50} curve of the agonist to the right without significantly affecting the maximum response. This ability to shift the concentration-response curve of the agonist can be quantified and is a measure of the affinity of the antagonist. In this functional assay, where CXCL12-mediated signalling is blocked by a competitive antagonist, the equilibrium dissociation constant is expressed as pK_b. For compound **22**, the pK_b is

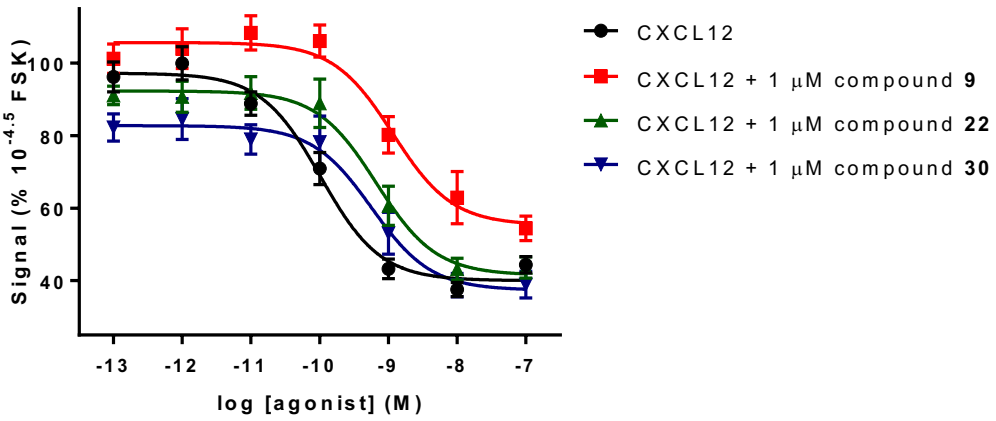


Figure 8. *Concentration response curves for CXCL12 (n = 8), and CXCL12 in the presence of 1µM compound **9** (n = 7), 1µM compound **22** (n = 5), and 1µM compound **30** (n = 5). CXCR4 activation is measured as percent inhibition of Forskolin stimulated cAMP. Data points are represented as mean ± SEM of combined experiments, each performed in triplicate.*

found to be 6.4 ± 0.28 (n = 4). Interestingly, besides shifting the dose response curve to the right, fluorescent compounds **9** and **30** appear to have additional, but distinct, effects on CXCL12-CXCR4 binding. IT1t-based compound **9** appears to shift the dose response curve upwards, and at very low concentrations of CXCL12 seems to increase Forskolin-mediated luminescence. This could suggest compound **9** has some inverse agonist-like properties, as inverse agonism of CXCR4 would lower the baseline activity of the receptor, leading to an increase of cellular cAMP. Fluorescent AMD070 derivative compound **30** also induces a slight right-ward shift of the EC_{50} curve, but more interestingly it shows a significant decrease in forskolin-mediated luminescence in the presence of low concentrations of agonist. At first glance this could suggest that compound **30** is in fact a positive allosteric modulator, or PAM, as positive allosteric modulation of CXCR4 would amplify the decrease in cAMP. However as this effect disappears at higher concentrations of CXCL12, it seems unlikely it is actually a PAM as there is no cooperative effect. Due to the vertical shift of the EC_{50} curves of CXCL12 in the presence of compounds **9** and **30**, pK_b values of these compounds cannot accurately be obtained from this data. To adjust for this shift, experiments would have to be repeated where several fixed concentrations of the antagonists are used. This allows for a full Schild analysis of the antagonists, of which pA_2 values can be determined. The pA_2 is a value representing the -Log[antagonist] needed to shift the EC_{50} curve of the agonist by a factor of 2, and is a measure of the potency of the antagonist.

To provide further insight into the nature of these fluorescent ligands, the functional experiments were repeated but instead of using the fluorescent ligands as antagonists, I looked whether they could elicit an agonist-like response in the absence of CXCL12. The results of these experiments are presented in figure 18A. As can be seen from this figure, none of the fluorescent ligands are capable of inducing an agonist-like response. Only at a concentration of 10^{-5} M do the ligands start to show inhibition of forskolin-mediated luminescence, however at this concentration the compounds are likely interfering with the assay or causing cell toxicity. Interestingly, in this experiment compound **9** again appears to increase forskolin-mediated luminescence, at up to a concentration of 10^{-7} M. When the curves of

CXCL12 and compound **9** are isolated, and the values at 10^{-5} M are excluded, a slight inverse agonist response can be observed (figure 18B and 18C). Though this response might not appear to be significant, support for inverse agonism of this compound is found in literature[141]. Here, certain IT1t derivatives have shown to be inverse agonists in both $G\alpha_i$ and β-arrestin assays, performed on HEK293 cells expressing a constitutively active mutant of the CXCR4 receptor (CXCR4-N119S). Despite the current findings however, further experimental work is necessary to properly classify compound **9**. Compound **30** still causes a significant decrease in luminescence and appears to do so in a concentration-independent manner, which could mean compound **30** is somehow interfering with the assay.

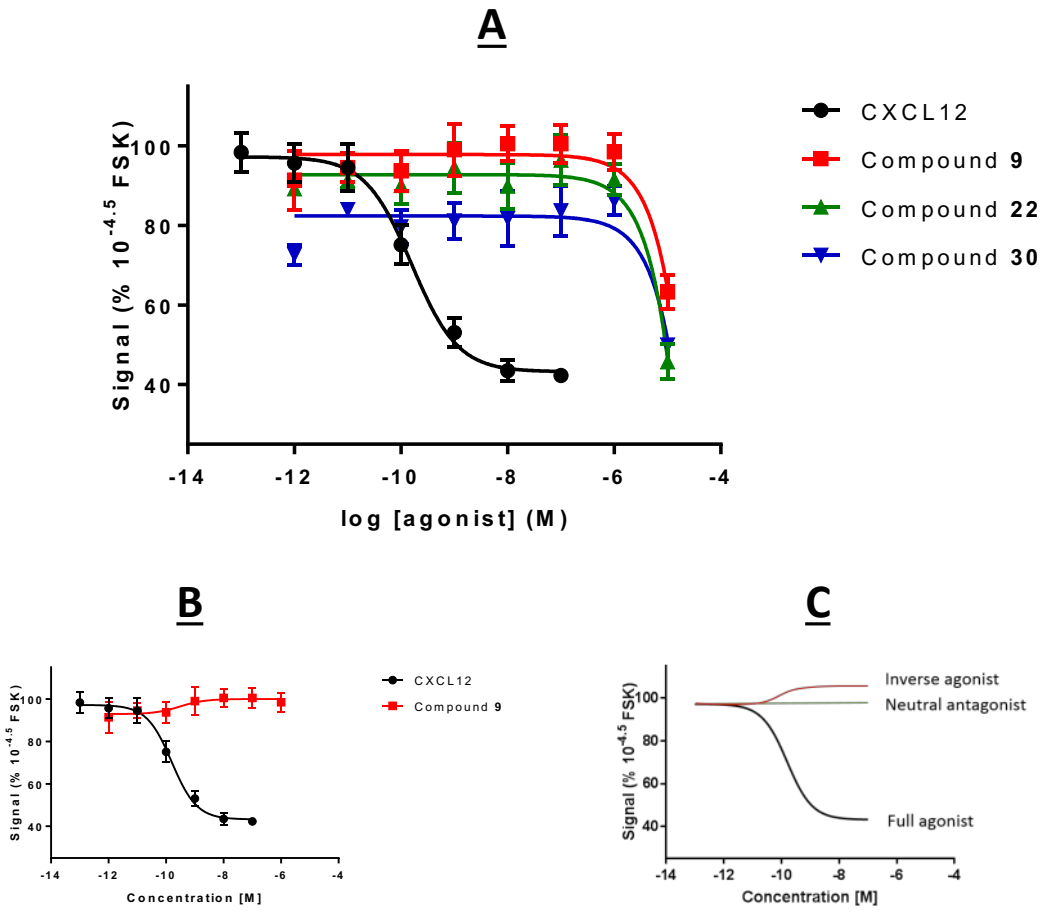


Figure 18. *(A) Concentration response curves for CXCL12 (n = 4), compound **9** (n = 4), compound **22** (n = 4), and compound **30** (n = 4). (B) Isolated concentration-response curves of CXCL12 and compound 9. (C) Schematic representation of the classification of ligands interacting with G_i-coupled GPCRs. CXCR4 activation is measured as percent inhibition of Forskolin stimulated cAMP. Data points are represented as mean ± SEM of combined experiments, each performed in triplicate.*

It is possible that the fluorescent dyes incorporated in the probes have an effect on the assay. Though it seems unlikely that the photochemical properties of the dyes interfere with the assay, since there is no spectral overlap between luciferase emission and BODIPY 630/650-X excitation and emission wavelengths. Furthermore, BRET seems unlikely to take place since the probes engage with the receptor on the extracellular surface of the cell whereas the biosensor is located in the cytosol. It is, however, possible that the fluorescent dye prevents CXCL12 from competing with the probes for the CXCR4 receptor. As observed in the competition binding experiments CXCL12 indeed is unable to displace the fluorescent probes (chapter 3.3.1.2 figure 15). To study the effect of the addition of a linker/fluorophore combination in a functional assay I compared fluorescent compound **22** with its unconjugated version (compound **17**), the results of which are displayed in figure 19. Here, the maximum response of Forskolin-mediated luminescence for both compounds is around 100 percent, showing that for this scaffold the incorporation of a linker/fluorophore combination does not interfere with the assay. Interestingly, Compound **17**, the isoquinoline-based compound without a fluorophore attached, is able to shift the EC_{50} curve more towards the right than the fluorescent conjugate, showing that it is more potent towards CXCR4 with a pK_b value of 7.7 ± 0.17 versus 6.4 ± 0.28 for compound **22** (*n* = 4 for both).

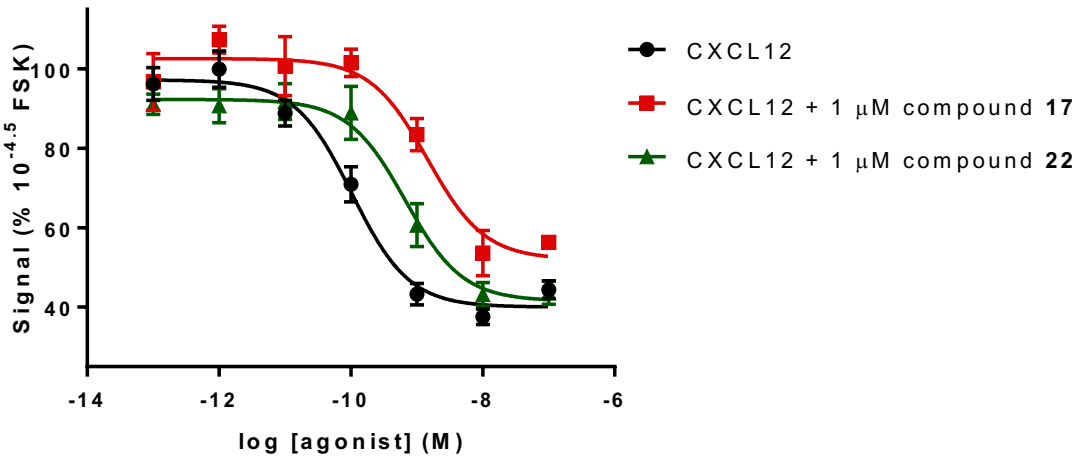


Figure 9. *Effect of introducing a linker/fluorophore combination on the ability to antagonise CXCR4. Concentration-response curves for CXCL12 (n = 8), and CXCL12 in the presence of 1μM compound **17** (n = 5), and 1μM compound **22** (n = 5).CXCR4 activation is measured as percent inhibition of Forskolin stimulated cAMP. Data points are represented as mean ± SEM of combined experiments, each performed in triplicate.*

Overall, these experiments show that the fluorescent probes are functionally competitive antagonists and are capable of shifting the CXCL12 concentration-response curve. Of the three compounds tested, compound **22** displayed characteristics of neutral competitive antagonism by shifting the EC_{50} curve without affecting basal levels of luminescence and max response to CXCL12, and a pK_b value was obtained of 6.4 ± 0.28 (n = 4). Compounds **9** appears to induce a inverse agonist-like response, by concentration-dependently increasing luminescence. Though the data might not be significant, evidence for inverse agonism of the IT1t scaffold is found in literature[141]. Compound **30** showed to decrease Forskolin-mediated luminescence in a concentration-independent manner, both in competition with CXCL12 and without CXCL12. A possible reason for this could be that this scaffold interferes with the assay in some way. The addition of a BODIPY to small molecule AMD070 is unlikely to be the cause of this, as experiments with compounds **17** and **22** showed no significant effect of the incorporation of the BODIPY.

3.4 Confocal imaging

One of the key applications of fluorescent probes is the direct visualisation of ligand-receptor interactions. Fluorescent probes, in conjunction with optical imaging techniques, furthermore can give insight in the real-time localisation of the receptor and its spatial-temporal distribution across the cell[142]. For the visualisation of membrane-bound receptors, such as GPCRs, the choice of fluorophore is an important one. In this project I chose to incorporate BODIPY dyes to small-molecule ligands. BODIPY dyes offer a number of advantages over other commercially available fluorophores, including high fluorescence quantum yields, high chemical- and photo stability and good solubility in various solvents. One of the key advantages of the BODIPY dyes used in this project however, especially in their application in imaging techniques, is their non-fluorescent behaviour in aqueous environments. This non-emissive behaviour, or “quenching”, in an aqueous environment is attributed to the energetically accessible intersection between the ground state and the lowest energy state of the excited fluorophore[143]. In lipophilic environments this intersection is not accessible, causing relaxation of the excited fluorophore to the ground state to occur through emission of fluorescence. When using BODIPY-labelled

probes to visualise GPCR function, the only fluorescence will therefore originate from ligand bound on the cell surface or in lipid domains within the cell. This characteristic thus avoids having to pre-treat cells with the fluorescent ligand followed by fixation- and several washing steps. Instead, ligand engagement with the receptor can be followed in real-time, on living cells.

Confocal laser scanning microscopy, or confocal imaging, is such a technique that allows the real-time visualisation of biological processes. This highly sensitive technique uses a laser beam to excite a fluorescent biological sample. The resulting mixture of reflected light and fluorescence is captured by the objective and sent to a dichroic mirror, where the fluorescence is separated from the reflected light and passed through a pinhole to reduce 'out of focus' light. The captured fluorescence is then passed through an emission filter and amplified using a photomuliplier, enabling detection up to the picomolar concentration range[110].

Having established that the fluorescent probes have a high affinity towards the receptor and competitively antagonise CXCL12-mediated signalling, I was interested in using these probes to visualise ligand-receptor binding on live cells. Using the same HEK293_SNAP-CXCR4 cell line used for the GloSensor™ assay, cells were seeded on poly-D-lysine-treated Nunc™ Lab-tek™ 8 well chambered cover glasses and labelled with SNAP-Surface Alexa Fluor 488 dye to visualise receptor distribution. Confocal experiments were performed using a Zeiss 710 confocal microscope. Upon addition of three of my BODIPY 630/650-X-labelled probes at a final concentration of 100 nM, and an incubation period of 30 minutes at 37 °C prior to imaging, I was able to detect localised membrane fluorescence (figure 20). All three compounds showed localised fluorescence at sites with high receptor expression and furthermore show very little intracellular fluorescence of the probe, indicating an inability of the probes to enter the cell.

As mentioned earlier, the fluorescent signal from the BODIPY dye relies on its ability to incorporate into the lipid environment of the cell membrane. It is possible, therefore, that some of the fluorescent signal detected in figure 20 was due to nonspecific interactions of the probes with the cell membrane. To investigate this, cells were imaged under the same conditions, but after a 30 minute incubation of the

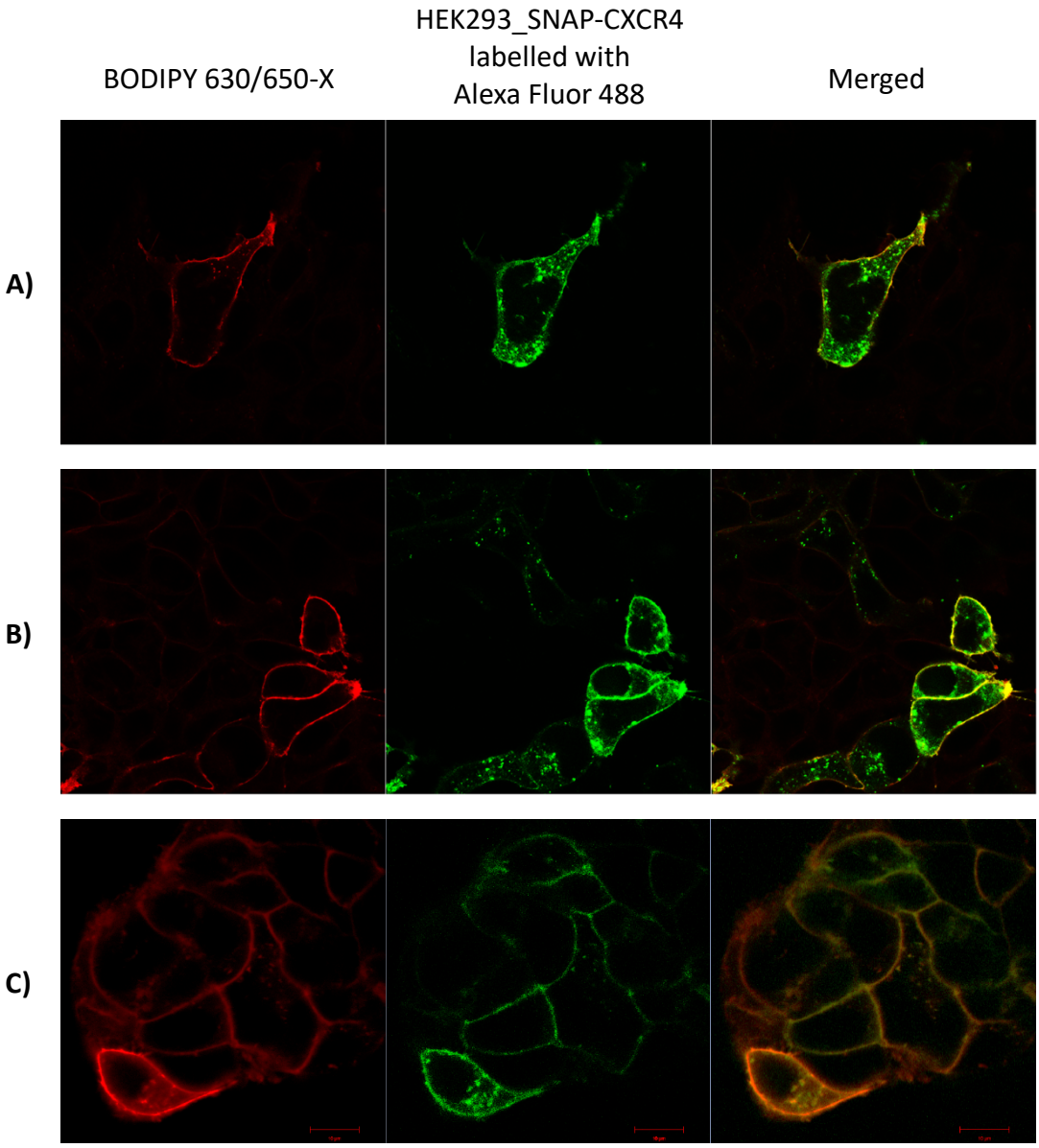


Figure 20. *Visualisation of binding of the fluorescent probes to CXCR4 on HEK293 cells stably expressing SNAP-CXCR4. Images on the left-hand side show the fluorescent signal obtained from the BODIPY 630/650-X dye (compound **9** for (A), compound **22** for (B), and compound **30** for (C). The centre images show receptor expression through labelling with Snap-Surface Alexa fluor 488. Images on the right represent the merge of the two channels. Cells were incubated for 30 min at 37 °C with 100 nM of fluorescent ligands, after which single equatorial confocal slices were obtained. These images are representative of three separate experiments.*

cells with the fluorescent ligands at 37 °C, a high concentration (10 µmol/L) of competitive displacer was added. After leaving this to equilibrate for another 30 minutes images were obtained, which are displayed in figure 21. Although a slight decrease in fluorescent signal was observed upon treatment of the cells with 10 µM AMD3100, as can be seen in the bottom row images of figures 21A and 21B, there is still a substantial amount of residual fluorescence. It was anticipated that the high

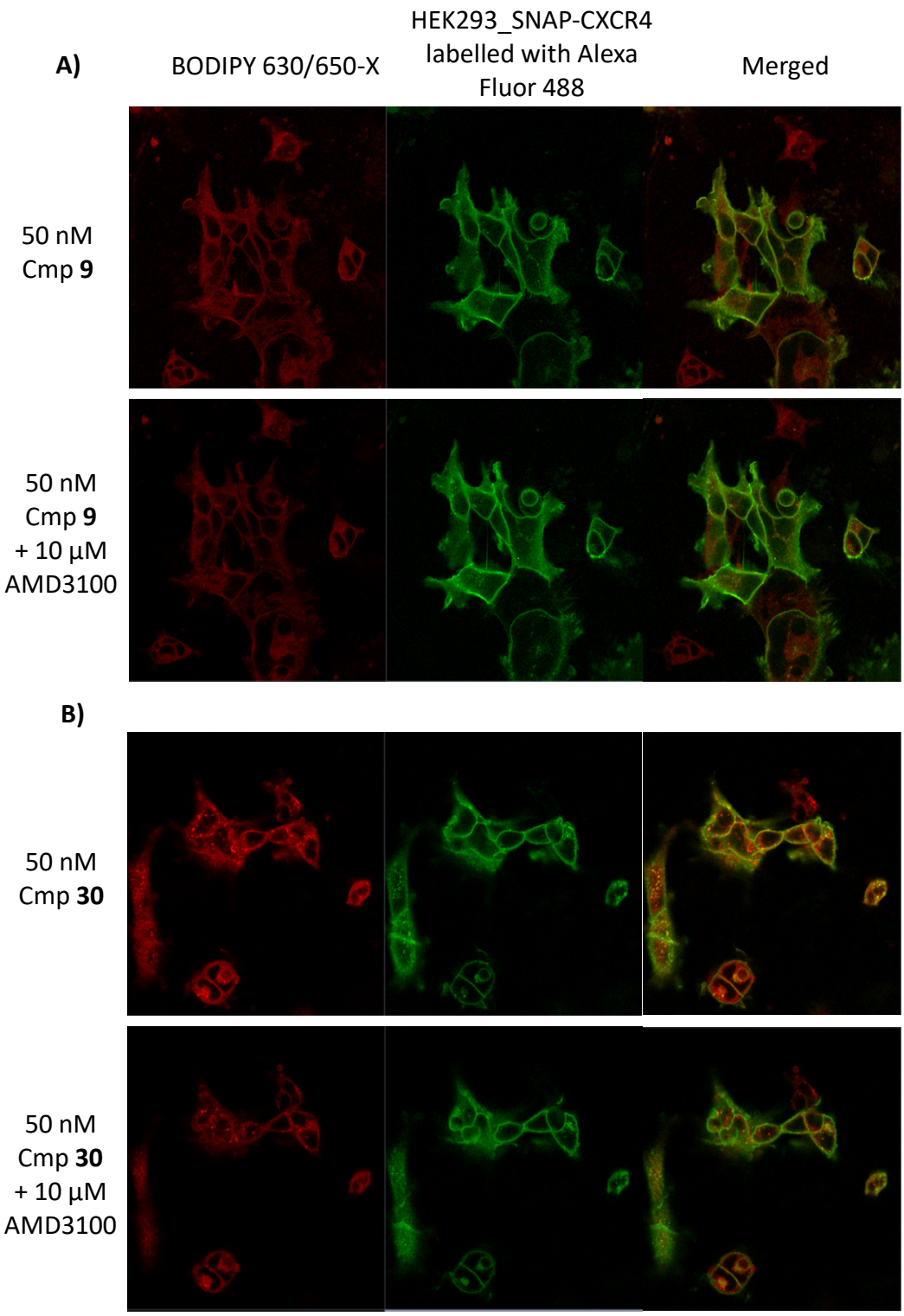


Figure 21. *Visualisation of the binding of A) compound **9**, and B) compound **30** to CXCR4 in absence and presence of 10 µmol/L AMD3100. For both compounds HEK293 cells stably expressing SNAP-CXCR4 were incubated for 30 min at 37 °C with 50 nM of fluorescent ligand, as shown in the upper row images, and 50 nM of fluorescent ligand + 10 µmol/L AMD3100, as shown in the lower row images. The left-hand side images show the fluorescent signal obtained from the BODIPY 630/650-X dye, while the centre images show receptor expression through labelling with Snap-Surface Alexa fluor 488. Images on the right represent the merge of the two channels. Single equatorial confocal slices were obtained. In each case, images were obtained using identical settings for laser power and detector offset and gain. These images are representative of two separate experiments.*

concentration of AMD3100 would displace the fluorescent ligands, resulting in a marked reduction in fluorescence observed in the red channel. It is possible that the fluorescent ligands have very slow off rates (K_{off}), making it hard for AMD3100 to displace them. Alternatively, the obtained images could indicate that there is a relative high amount of nonspecific engagement into the cell membrane by fluorescent compounds **9** and **30**. If indeed there is a substantial amount of nonspecific interaction with the cell membrane, a possible cause could be the highly lipophilic nature of both the pharmacophores and the BODIPY 630/650-X dye. The cLogP values of the fluorescent conjugates indeed indicate that these molecules are highly lipophilic (cLogP = 9.9, 9.0, and 8.8 for compounds **9**, **22**, and **30**, respectively, as calculated using Chemdraw). Reduction of nonspecific binding to the lipid bilayer might therefore be achieved by reducing the lipophilicity of the conjugates. Modifying the pharmacophore-part of the conjugates to incorporate polar groups is likely to affect the overall affinity towards the receptor, and therefore should be done with great care. Rather than changing the pharmacophore-part of the conjugate, a better approach might by modifying the linker-part of the conjugates. The probes developed in this project make use of a relatively liphophilic hexanoyl spacer to separate the pharmacophore from the BODIPY dye. Instead of this hexanoyl spacer, a peptide-based linker may provide better physiochemical properties. The use of peptide-based linkers for fluorescent ligand design is well established[144], and has led to the development of highly potent fluorescent probes that show very low levels of nonspecific interactions. The decreased lipophilicity of these linkers is likely to reduce the nonspecific interactions of the CXCR4 probes, and might potentially even increase their affinity. The use of peptide-based linkers in these CXCR4 probes is further encouraged by the availability of a crystal structure of CXCR4, allowing for a rational approach towards their design.

To summarise, in this project is described the successful development of several high affinity fluorescent probes for the chemokine receptor CXCR4. By utilizing available SAR and *in silico* design, three different scaffolds of small molecule inhibitors were selected and developed into fluorescent conjugates. Five compounds were tested in a novel fluorescence-based NanoBRET™ assay, which revealed four probes to

actively bind to CXCR4. The NanoBRET™ assay was furthermore showed their use as tool compounds in the screening of small molecules. Further evaluation of the fluorescent probes in a functional GloSenor™ cAMP assay revealed that the ligands competitively inhibited CXCL12-induced $G_{\alpha i}$ protein activation. Finally, receptor-ligand interactions were visualised using confocal microscopy. Though optimisation of the probes would be required for their use in studying CXCR4 signalling in the context of cancer, I was able to show that these are robust tool compounds and a valuable addition to the CXCR4 receptor toolkit.

4 Development of high affinity fluorescent ACKR3 probes

This part of the thesis focuses on the development of high affinity fluorescent probes for the atypical chemokine receptor ACKR3. As discussed in the introduction section of this thesis, ACKR3 is a relatively novel drug target and therapeutic strategies that act on its signalling axis are still in its infancy. What makes ACKR3 a particularly difficult receptor to target is the fact that, not only is its function under normal physiological conditions poorly understood, its relevance in disease is also still unclear[69]. There does nonetheless seem to be a strong connection between various types of cancer and increased expression levels of ACKR3 and CXCR4 on these cells. For example, it is well established that increased expression of these receptors leads to metastasis and tumour growth[53]. This seems contradictory, as activation of CXCR4 by CXCL12 leads to G protein-mediated signalling, ultimately causing cell migration and tumour growth, whereas activation of ACKR3 by CXCL12 only causes internalisation of the ligand-receptor complex, essentially having opposite effects. One of the proposed roles for ACKR3 on these cancer cells is that it reduces the local concentration of CXCL12, preventing desensitisation of CXCR4 and shaping the chemokine gradient, therefor having pro-metastatic and pro-tumorigenic effects[145], though this is still under debate.

Due to the novelty of the target and lack of full understanding of its function, efforts to develop synthetic ligands have only recently begun to emerge[89-92]. Unsurprisingly, tool compounds to study the function of this receptor and to characterise novel ligands are practically non-existing. Currently, the most widely used compound to study ACKR3 function is the endogenous ligand CXCL12. Though human CXCL12 and its radiolabelled- and fluorescently labelled versions are available through commercial sources, their arduous synthesis make them very expensive tool compounds. Antibodies and nanobodies have also emerged as highly selective tools to study ACKR3[106, 146], but similar to CXCL12, the development of ACKR3-specific antibodies and nanobodies is difficult and time consuming, making them also very expensive. Small molecule ligands that target ACKR3 are sparse, but can offer several advantages over chemokines and antibodies as tool compounds. Though their development may be challenging, they're less expensive to synthesis, they are more

stable and generally more versatile. For ACKR3, only two small molecule ligands have seen frequent use as tool compounds: VUF11207[89] and CCX771[94, 147, 148] (see also chapter 1.3.2).

Fluorescent probes can be of high value in the interrogation of ACKR3 in (patho)-physiological conditions and can provide a unique insight on the signalling pathways induced by activation of the receptor, especially in the context of cancer. Due to the limited availability of tool compounds to study this receptor there is therefore a clear need for the development of such probes. Using a similar strategy employed for the development of CXCR4-specific fluorescent probes, high affinity small molecule-based probes will look to be developed that target the atypical chemokine receptor ACKR3.

4.1 VUF11207 as starting point for fluorescent ligand design

The development of small molecule-based fluorescent probes for the chemokine receptor ACKR3 is challenging due to the limited availability of small molecule ligands. One of the few active series of compounds was reported in 2012 by Wijtmans *et al.*[89], who described a series of styrene-amides as potent full agonists of the ACKR3 receptor based on structures disclosed by Chemocentryx. Among this series of compounds Wijtmans *et al*. described VUF11207, a receptor agonist of ACKR3 with a reported pIC_{50} of 8.1 ± 0.1 (see figure 22). The ligand furthermore showed an ability to reduce cell surface expression of ACKR3 with a reported EC_{50} of 14.1 nM, indicating activation of the β-arrestin pathway. As can be observed from figure 22 VUF11207 exists as a mixture of diastereomers, containing a chiral centre in the pyrrolidine ring. Chiral separation of the racemate was performed by collaborators of this project working at the VU University of Amsterdam, who found the *R*-isomer to be significantly more active than the *S*-isomer (pIC_{50} = 8.3 ± 0.1 and 7.7 ± 0.1,

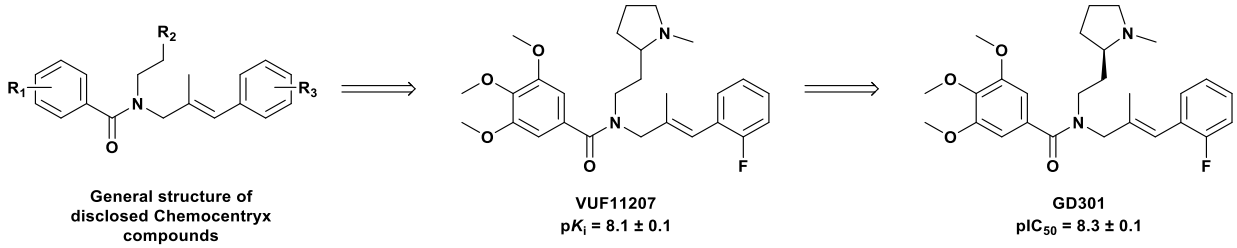


Figure 22. *ACKR3 receptor agonist VUF11207 was developed based on disclosed Chemocentryx structures*

respectively). Though both ligands are full agonists of ACKR3, activation of the receptor by these ligands inhibits the cellular uptake of CXCL12 and thus their potency is reported as pIC_{50} values and not pEC_{50} values (figure 22). The *R*-isomer of VUF11207 was given the name GD301.

SAR studies based on the compounds published by Wijtmans *et al.*, revealed several key indicators for affinity, which are summarised in figure 23. On the left-hand side of the molecule, the *para*-methoxy group provides an essential hydrogen-bond acceptor, and removal of this group results in a significant decrease in affinity. Substituents on the *meta*-positions are allowed and provide bulkiness but contribute less to the overall affinity profile. On the right-hand side of the molecule, the fluorine

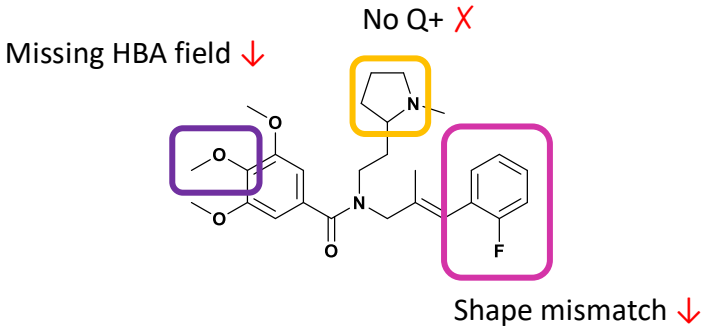


Figure 23. *Summary of the SAR for styrene-amide-based ligands for chemokine receptor ACKR3*

on the *ortho*-position helps to shape the overall structure, potentially filling a sub-pocket of the receptor. Additional substituents on this benzyl group, or moving the fluorine to other positions has a negative impact on affinity. Finally, the tertiary amine of the pyrrolidine provides a hydrogen-bond site essential for affinity. Quaternisation of this amine resulted in complete disruption of the binding to ACKR3. To identify the binding mode of GD310 to ACKR3, the collaborators at the VU University of Amsterdam developed a homology model of ACKR3 based on the crystal structures of CXCR4, US28 and CCR5. An initial binding pose was generated using this model, which is depicted in figure 24. Several receptor residues were identified as potential key residues for ligand-receptor interactions. To confirm this binding pose and the importance of these receptor residues for ligand-binding, the collaborators performed site-directed mutagenesis studies (see figure 25). These studies identified

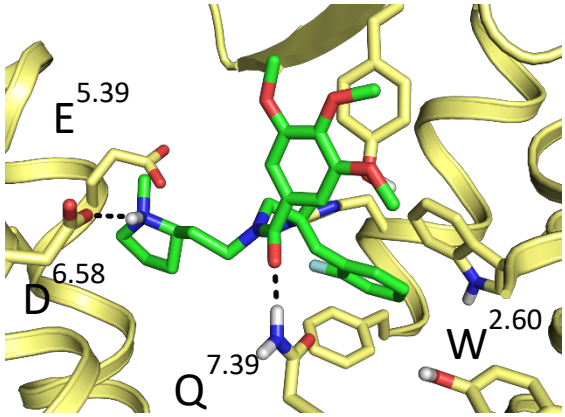


Figure 24. *Binding pose for GD301 in a homology model of ACKR3. This figure was generated by collaborators of the VU University Amsterdam.*

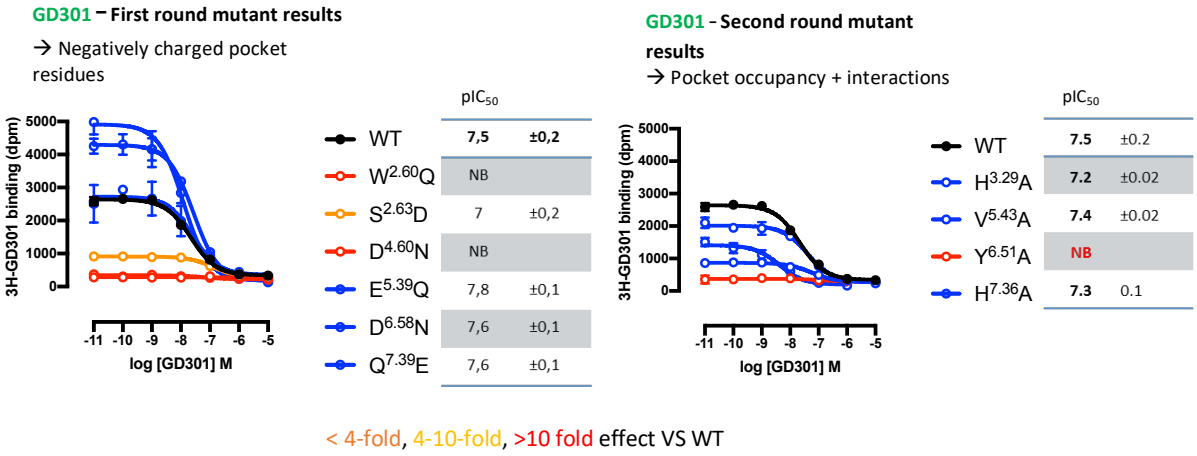


Figure 25. *Site-directed mutagenesis studies were performed by collaborators of the VU University Amsterdam, identifying key residues for ligand-receptor interactions.*

residues $D^{4.60}$, $W^{2.60}$, and $Y^{6.51}$ as being the most important for binding of GD301, as mutating these residues resulted in a marked decrease in its binding. Aspartate $D^{4.60}$ is a residue that is well known for being important for ligand binding, as binding of CXCL12 as well as cyclic peptide TC14012 is also disrupted upon mutation of this residue[149], whereas residues $W^{2.60}$ and $Y^{6.51}$ appear to be ligand specific. Ultimately, these studies allowed for a more accurate binding mode prediction, which is depicted in figure 26.

When combining the information obtained from the SAR, docking studies, and site-directed mutagenesis studies, it was possible to create a rational plan for the development of small molecule-based probes. As identified by the SAR of these styrene-amides, chemical modification of the 2'-fluorobenzyl group is not

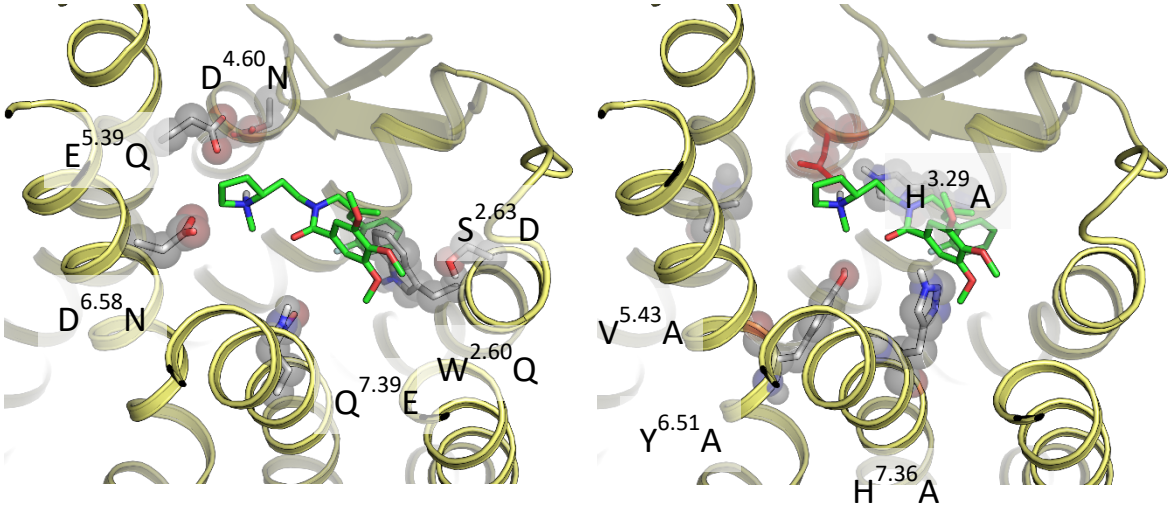


Figure 26. *The final binding mode of GD301 was generated after identifying key residues (highlighted). The two figures represent the same binding mode, highlighting different residues. This figure was generated by collaborators of the VU University Amsterdam.*

encouraged, as it is likely to disrupt ligand binding. Based on both the SAR and the final binding mode, using the 2-(1-methylpyrrolidin-2-yl) ethyl side chain as an anchor point for linker/fluorophore conjugation is also not encouraged. This side chain appears to be imbedded deeper in the binding pocket of ACKR3, making it not accessible for conjugating to a linker/fluorophore combination. Furthermore, *N*-acetylation of the amine would remove its ability to act as a hydrogen-bond donor and thus is likely to disrupt overall binding. It might, however, be feasible to use the trimethoxybenzyl-moiety of the molecule to conjugate to linker/fluorophore combination. Based on the final binding mode of GD301 and the available SAR, this part of the molecule is least restricted and might allow chemical modification. Though conjugating to the 4'-methoxy substituent is likely to cause disruption of binding, as is indicated by the SAR, the 3'-position is much less restricted. This is mostly supported by the binding pose of GD301, which shows this ring pointing up towards the extracellular environment, and with the 3'-position being most accessible.

To incorporate a linker/fluorophore combination it will be necessary to modify this 3'-methoxy substituent. To give insights on how this trimethoxybenzyl ring can be modified to facilitate conjugation to a fluorophore I proceeded with docking several ligands into the homology model that was developed by collaborators in Amsterdam.

4.2 Docking of congeners of GD301

The homology model used to perform the docking studies in this part of the chapter was the final frame of a molecular dynamics (MD) simulation. The MD simulation was biased, meaning GD301 was encouraged to interact with the key residues that were revealed by site-directed mutagenesis studies. Using this model I looked at possible conjugation strategies for incorporating a fluorophore to GD301, and to evaluate the length of the linker needed. First, looking at the binding mode of GD301 I saw that indeed the trimethoxybenzyl-group offered the best location for the incorporation of a linker/dye (figure 27B). It also appeared that the small-molecule binding pocket is situated a little deeper in the receptor than that of chemokine receptor CXCR4 (figure 27A). The use of just the aminohexanoyl spacer that is included in the BODIPY-X dyes may therefore not be enough. I felt it was necessary to generate binding modes of congeners based on GD301 that include additional spacers. To maintain the same level of flexibility that the aminohexanoyl offers, but without adding unnecessary lipophilicity, I chose to use polyethylene glycol-like (PEG) chains of varying lengths. This also allowed the linker to interact with residues of the receptor through hydrogen bonding, potentially aiding the overall affinity profile of the probe. To this end I docked a small series of compounds based on the structure of GD301, where PEG-like linkers were introduced at the 3'-position of

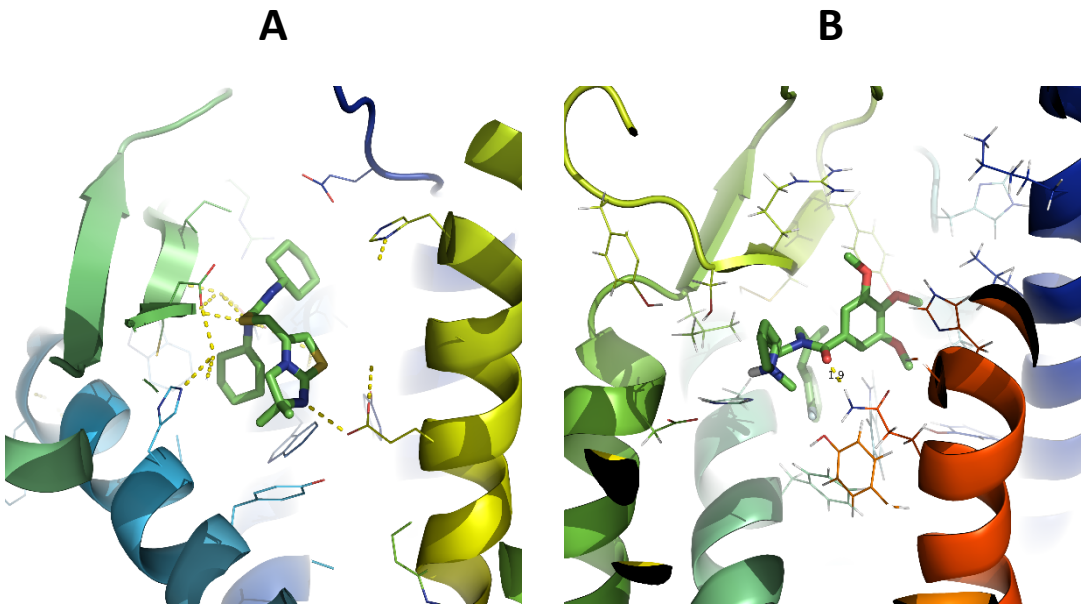


Figure 27. *Side-to-side comparison of the ligand binding sites of CXCR4 (A) and ACKR3 (B).*

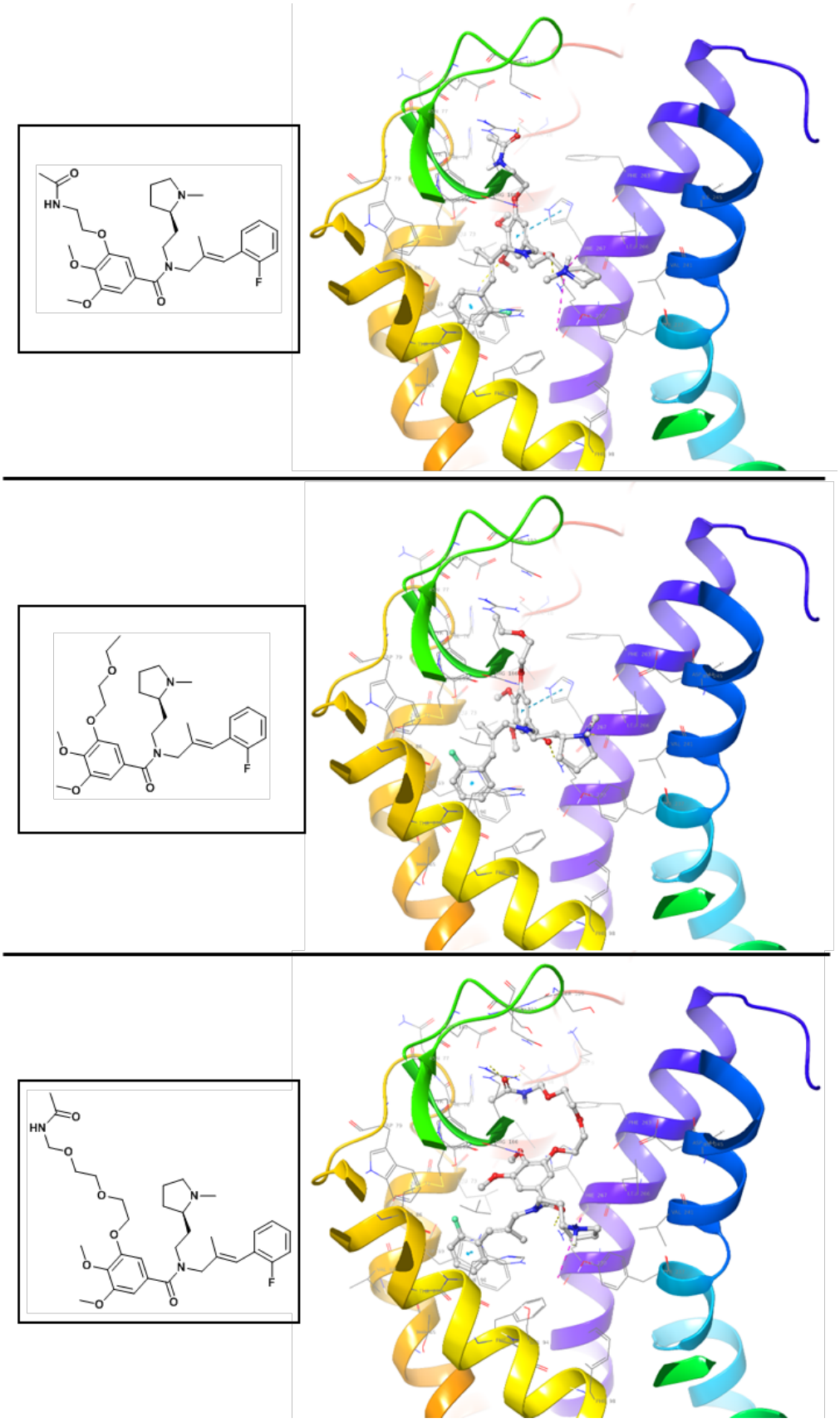


Figure 28. *Docking studies were performed of congeners based on GD301 using a homology model of ACKR3. Binding poses were generated of congeners containing either one, two or three PEG units (top image, middle image, and bottom image, respectively). Top and bottom images furthermore show the incorporation of a methylamide.*

the trimethoxybenzyl group (displayed in figure 28). As can be seen from the figure, binding poses were generated of GD301 congeners containing either one, two or three PEG units (top image, middle image, and bottom image, respectively). For the congeners containing one and three PEG units a methylamide was used to cap off the linker. This allowed us to evaluate whether the same conjugation strategy could be employed as was used in the CXCR4 project (coupling the congeners to amine-reactive succinimidyl-protected BODIPY dyes). Docking of these congeners resulted in binding poses that are quite consistent, showing a similar orientation of the GD301 scaffold and linkers that point toward the extracellular environment.

Based on SAR, data obtained from collaborators of this project, and these docking studies, I felt confident to develop fluorescent derivatives of GD301. To allow the fluorophore-part of the probe to exit the receptor I looked to introduce PEG-like chains of varying lengths and containing a terminal amine, which will serve as an anchor point for fluorophore conjugation. The proposed scaffold will therefore look as follows:

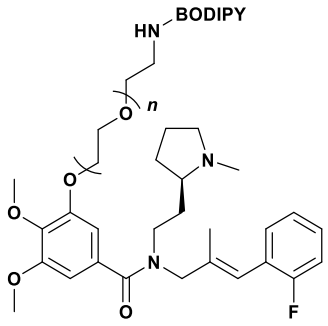
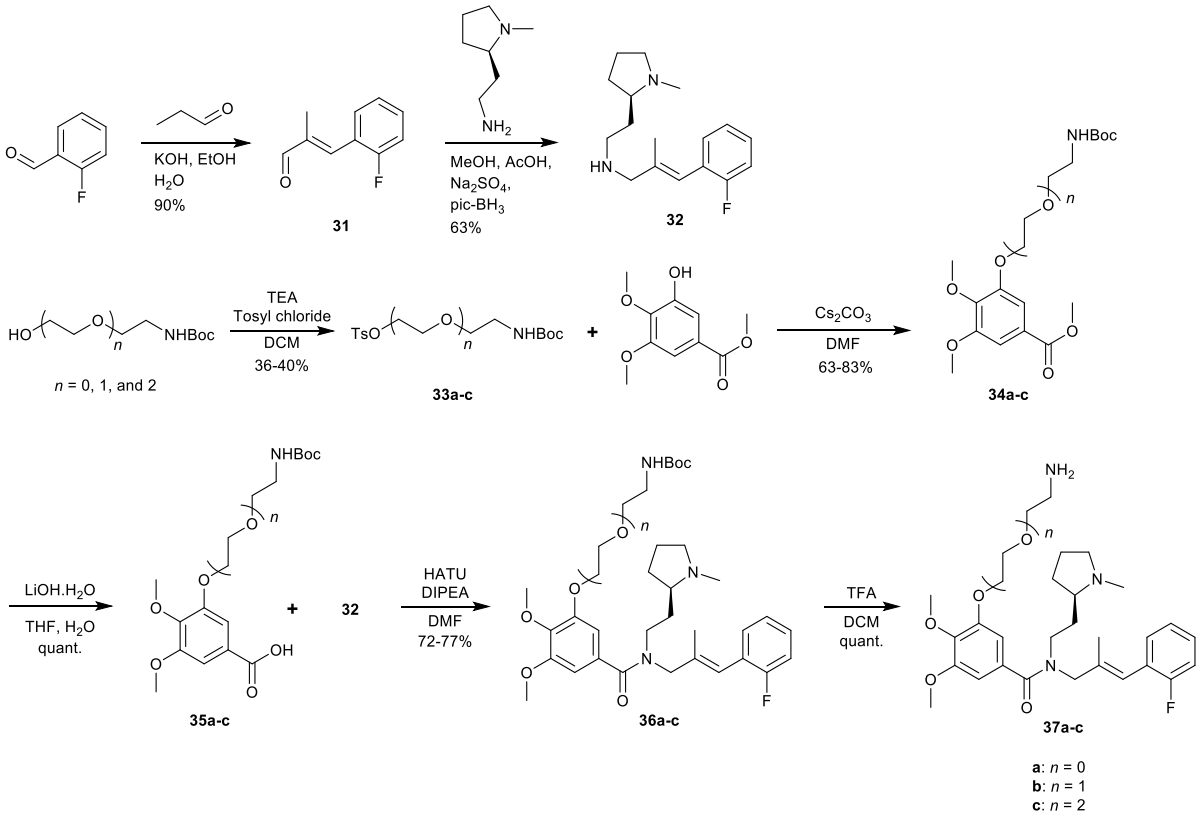


Figure 29. *Proposed scaffold of GD301-based fluorescent probes.*

4.3 Synthesis of fluorescent conjugates

The synthesis of fluorescent derivatives of GD301 was based on procedures that were described by Wijtmans *et al.*[89] in the development of VUF11207. Synthesis started with an aldol reaction between 2-fluorobenzaldehyde and propionaldehyde, which under basic conditions provided (*E*)-3-(2-fluorophenyl)-2-methylacrylaldehyde in excellent yield (**31**, scheme 7). I then sought to use reductive amination to install the 2-(1-methylpyrrolidin-2-yl) ethyl side chain. Fortunately, (*R*)-2-(1-methylpyrrolidin-2-

Scheme 7. *Synthesis towards GD301-based congeners.*

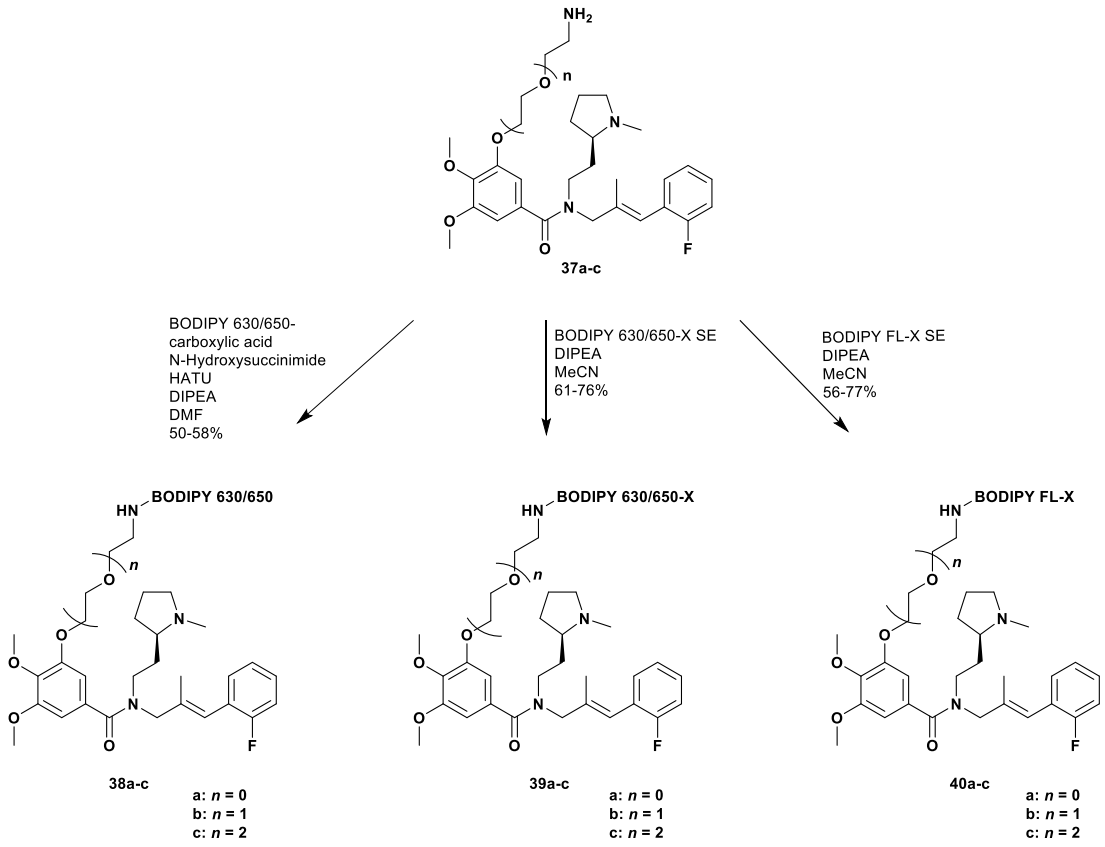


yl)ethanamine was available through commercial sources, which allowed for convenient chirally pure synthesis of these GD301 derivatives. Due to the precious nature of this fragment, I was concerned standard reductive amination conditions would result in the disubstitution of the amine; as the secondary amine of the initial product (compound **32**, scheme 7) is more nucleophilic than the primary amine of the starting material. To avoid this potential issue reducing agent α-picoline-borane was used, a highly stable and water soluble reductive reagent known to yield secondary amines in good fashion[150]. In acidic conditions, and using methanol as solvent, I was able to successfully convert methylacrylaldehyde **31** into key fragment **32** in good yields (63%). Both TLC and NMR analyses provided evidence this intermediate existed as a single isomer. Having generated the aldol product using the same synthetic procedure, original authors Wijtman *et al.*[89] performed 1D-NOESY experiments and verified existence of only the *E*-configuration. Here, a signal was obtained between the *ortho*-proton and the allylic CH_3, whereas lack of this signal was observed between the *ortho*-proton and the allylic CH_2 group. I felt this provided strong evidence I had synthesised only the desired *E*-product. With this fragment in

hand I set out to synthesise the various linkers. Here, I chose to develop linkers of three different lengths, with PEG chains ranging from zero to two. Commercially available alcohol-carbamates were first converted into tosylates using tosyl chloride (compounds **33a-c**, scheme 7). *O*-alkylation of these tosylates using methyl 3-hydroxy-4,5-dimethoxybenzoate efficiently installed the linkers on the 3'-position. Hydrolysis of the methyl ester to benzoic acids **35a-c** using lithium hydroxide proceeded with quantitative yields, allowing subsequent peptide coupling with key intermediate **32** to assemble the scaffold. After *N*-Boc deprotection the congeners were ready for conjugation to BODIPY dyes.

The final conjugation of these GD301 congeners to a range of fluorescent dyes is depicted in scheme 8. Besides conjugation to the standard BODIPY 630/650-X dye and BODIPY FL-X dyes (compounds **39a-c** and **40a-c**, respectively), I also decided to introduce the BODIPY 630/650 dye without the aminohexanoyl spacer (compounds **38a-c**). This fluorophore was previously synthesised in-house, and allows for the evaluation of the relative effect of hexanoyl linker on the pharmacological profile of

Scheme 8. *Final conjugation of GD301-based congeners to BODIPY dyes.*



these conjugates. As this fluorophore comes as a carboxylic acid, I used peptide-coupling conditions to generate the final conjugates **38a-c**.

Similar to the fluorescent probes developed for the chemokine receptor CXCR4, all fluorescent ligands that were synthesised from this scaffold have been isolated and purified by preparative reverse-phased HPLC, and their purities confirmed to be >95%. Furthermore, their identity was confirmed using high resolution mass spectrometry (HRMS TOF ES+).

4.4 Pharmacological characterisation

4.4.1 Single concentration binding experiments

Having synthesised several fluorescent probes based on small molecule agonist GD301, I proceeded with the pharmacological characterisation of the ligands. To quickly determine whether the strategy of using the trimethoxybenzyl-moiety to incorporate a linker/fluorophore combination allowed for the development of active probes I decided to initially screen these ligands at a single concentration. For this I again looked to use the novel NanoBRET^{TM} approach and investigated the ability of the probes to produce a BRET response at a 1 μM concentration. Using this convenient and fast approach I was also interested in screening the previously synthesised CXCR4 probes against ACKR3 to assess their selectivity for CXCR4 over ACKR3. To determine the nonspecific binding in this assay I decided to use the parent ligand GD301, which I synthesised in-house using the same synthetic approach outlined in scheme 7, and using commercially available methyl 3,4,5-trimethoxybenzoate as a key starting material. As this ligand was synthesised in-house, it was given the experimental compound code SD02-17-1 and will henceforth be referred to as this.

Using a stable cell line previously developed in-house of HEK293 cells expressing N-terminally tagged NLuc-ACKR3, cells were plated on 96-well, clear-bottomed plates. Following an incubation period of 1 hour at 37 °C with 1 μM ligand in the presence or absence of 10 μM SD02-17-1, the NLuc substrate furimazine was added and the plates were read on a PHERAstar FS plate reader. As shown in figure 30, all ACKR3 probes show an increase of BRET signal compared to the nonspecific binding.

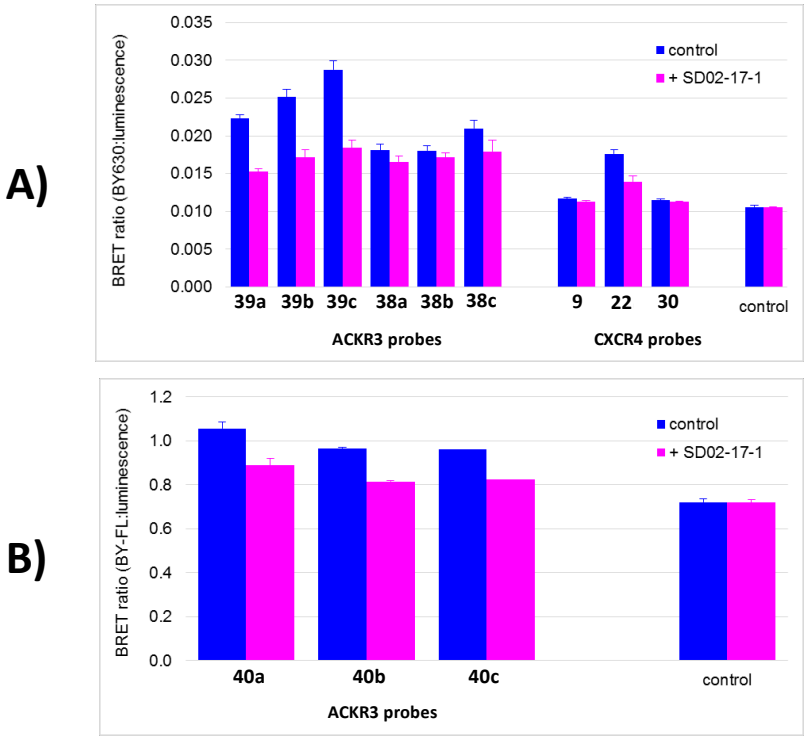


Figure 30. *NanoBRET signals obtained from single concentration binding experiments using HEK293 NLuc-ACKR3 cells and the BODIPY 630/650-labelled compounds (**A**) and the BODIPY FL-X labelled compounds (**B**). BRET ratio is determined as the ratio of fluorescence/luminescence. Non-specific binding was determined in the presence of 10 µmol/L SD02-17-1, and the control was determined as the BRET obtained in the absence of ligand. Data points represent mean ± SEM of three separate experiments performed in triplicate. Where not seen, error bars are within the columns.*

Interestingly, compounds **39a-c**, which contain the BODIPY 630/650-X fluorophore, show a much larger difference in total binding *vs.* nonspecific binding than compounds **38a-c**, which lack the aminohexanoyl spacer. Though I expected that the difference in chemical composition of the linkers would affect ligand binding (PEG-based for **38a-c** versus PEG + hexanoyl-based for **39a-c**), I expected that this effect would be much smaller than the effect of the full length of the conjugates on ligand binding. Instead, there does not seem to be a difference between the BRET windows of compounds **39a**, **39b**, and **39c**, indicating that for these compounds length of the conjugates does not affect ligand binding. The total BRET ratio does seem to increase as the lengths of these compounds increase, however since the BRET ratio for the nonspecific binding similarly increased it does not appear to be caused by specific interactions of the compounds with the receptor. Interestingly, of the BODIPY FL-X labelled probes the shortest probe, compound **40a**, appears to produce the best BRET window. This further shows that the length of these probes is less important for ligand binding than originally assumed. The red fluorescing CXCR4 probes were

also screened against the ACKR3 receptor and it appears that isoquinoline-based probe **22** has some specific binding at the receptor, whereas IT1t-based probe **9** and AMD070-based probe **30** both fail to produce a ligand specific BRET signal. The specific binding of **22** with the ACKR3 is rather surprising, but potentially very interesting as it would be a completely novel chemotype for this receptor.

4.4.2 NanoBRET™ saturation binding experiments

*4.4.2.1 NanoBRET™ saturation binding of compounds **38a-c** and **39a-c** on membranes*

As all ACKR3 probes were capable of producing a BRET window at 1 µM I felt encouraged to continue the characterisation of all nine compounds, as well as CXCR4 probe **22**. To determine the affinity of these compounds I therefore performed saturation binding experiments. Initially it was decided to use isolated membranes of HEK-NLuc-ACKR3 cells, as this method gave us robust results in the characterisation of the CXCR4 probes. HEK-NLuc-ACKR3 cells were therefore cultured on 500 cm^2 trays after which they were collected, lysed, and their membranes isolated. After quantification of the protein content of the membranes using a BCA protein assay, the membranes were added to 96-well plates and suspended in assay media. After addition of increasing concentrations of the ligands with and without the presence of 10 µmol/L SD02-17-1, and an incubation period of 1 hour at 37 °C furimazine was added and the BRET was immediately measured on a PHERAstar FS plate reader.

Out of convenience, I first screened the BODIPY 630/650 labelled ACKR3 probes **38a-c** and **39a-c**. As figure 31 shows, there does not appear to be much specific binding for any of these probes. In fact, for the series **38a-c** only linear increases of BRET ratio were observed, identical to the BRET ratio of the nonspecific binding, indicating an almost complete lack of specific binding over the concentration range tested. Even though only a small BRET window was obtained for these compounds in the single concentration experiments, I was not expecting these ligands to be inactive. For the compounds **39a-c** a larger difference can be observed between total binding *versus* nonspecific binding, which is in accordance with the single concentration experiments. Interestingly, for compounds **39a** and **39b** again linear increases in BRET signal were observed, indicating very low affinity compounds. The only

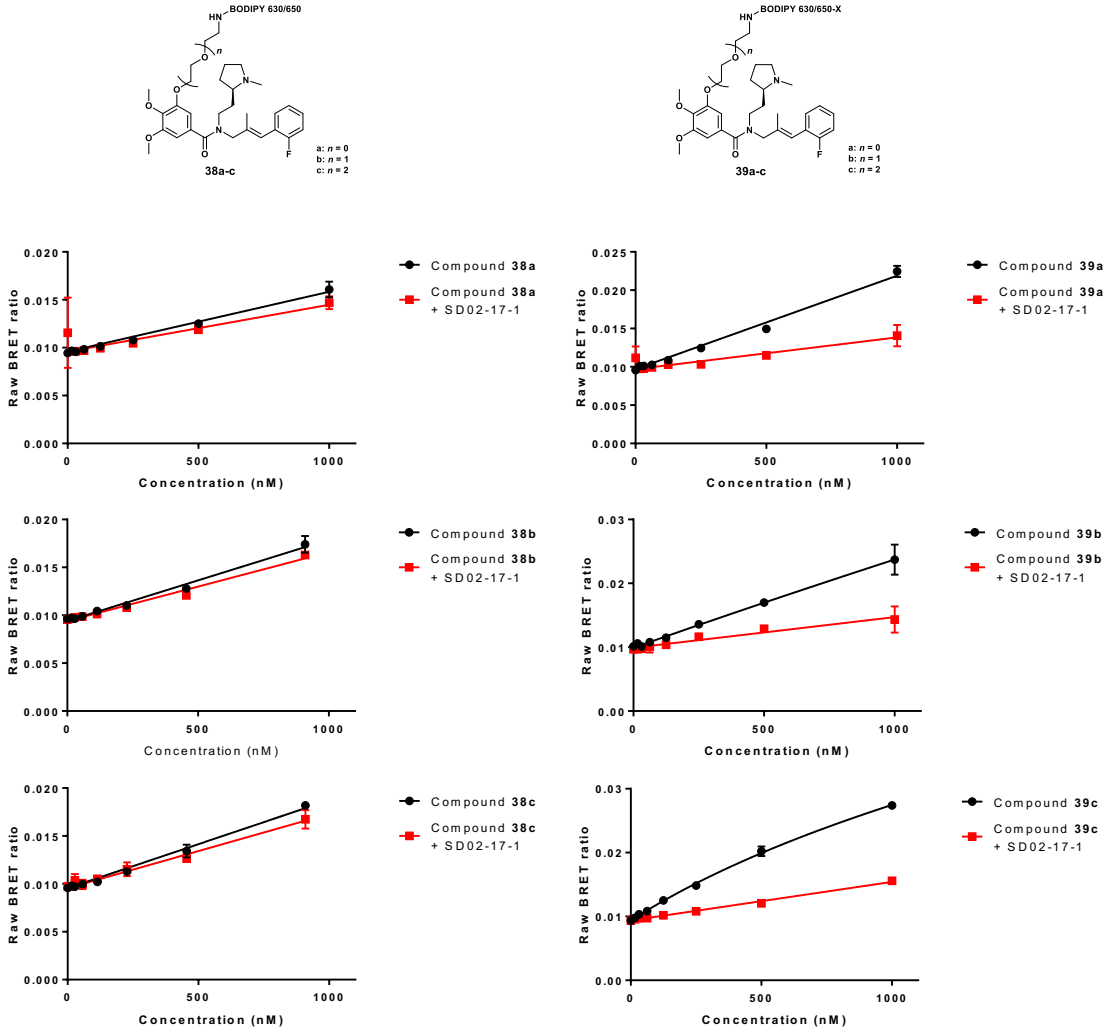


Figure 31. *NanoBRET signal obtained from HEK293 NLuc-ACKR3 cell membranes incubated with increasing concentrations of compounds* ***38a-c*** *and* ***39a-c****. Raw BRET ratio is determined as the ratio of fluorescence/luminescence. Non-specific binding was determined in the presence of 10 µmol/L SD02-17-1. Data points represent mean ± SEM of triplicate determinations of a single experiment. These single experiments are representative of two separate experiments. Where not seen, error bars are within the symbol.*

compound that shows signs of affinity, though very weak, is compound **39c**. Saturation was not achieved over the concentration range tested, so a K_d value could not be determined.

Confocal imaging had indicated that much of the receptor is found internalised even in the absence of natural ligand[30], and lysing the cells to harvest the membranes could therefore have resulted in a significant loss of receptor expression. This in turn might explain the surprising lack of activity of these red fluorescing compounds. To see if lysing the cells and using only the membranes to characterise my compounds is the problem, I repeated the experiments on whole cells.

*4.4.2.2 NanoBRET™ saturation binding of compounds **38a-c** and **39a-c** on whole cells*

HEK293 cells stably expressing NLuc-ACKR3 were seeded on poly-D-lysine-coated 96-well plates at a 10 000 cells per well and were left to grow. After two days the cells achieved ~90% confluence and were ready to be used in the assay. The growth medium was replaced with assay medium, and after addition of increasing concentrations of the ligands with and without the presence of 10 µmol/L SD02-17-1, and an incubation period of 1 hour at 37 °C, furimazine was added and the BRET was immediately measured on a PHERAstar FS plate reader. In figure 32 it can indeed be observed that using whole cells for the characterisation of these compounds yields better results than using isolated membranes. Though compound series **38a-c**

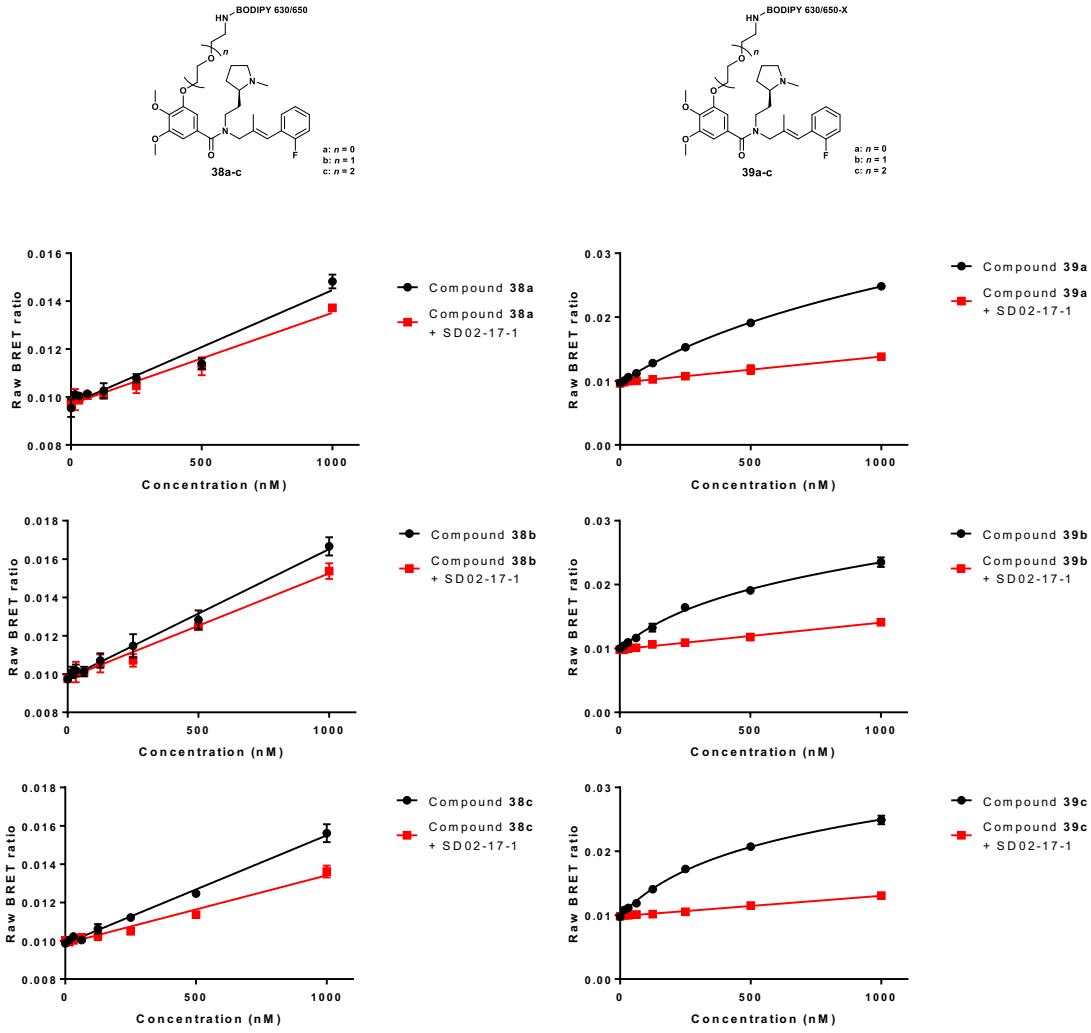


***Figure 32.** NanoBRET signal obtained from HEK293 NLuc-ACKR3 cells incubated with increasing concentrations of compounds **38a-c** and **39a-c**. Raw BRET ratio is determined as the ratio of fluorescence/luminescence. Non-specific binding was determined in the presence of 10 µmol/L SD02-17-1. Data points represent mean ± SEM of triplicate determinations of a single experiment. These single experiments are representative of n=2 for **38a-c**, n=8 for **39a**, and n=5 for **39b-c**. Where not seen, error bars are within the symbol.*

still show very weak specific binding towards NLuc-ACKR3 over a concentration range of 0-1000 nmol/L, a much better signal is obtained for compound series **39a-c**, with BRET ratios for all three compounds showing a concentration-dependent increase which likely to reach saturation at higher concentrations (>1 µM). From these saturation curves I was able to obtain affinities, which range from 6.1 ± 0.05 for **39a** to 6.16 ± 0.09 for **39c** (as pK_d values, see table 6). Quite surprising is the fact that all three compounds from series **38** show little activity. Structurally, the only difference between them and compound series **39** is that they lack the aminohexanoyl spacer, making them overall a little shorter. The importance of this spacer was already suggested with the single concentration-binding experiments, however it being the only distinguishing feature between high affinity probes and very weak probes is surprising. In an attempt to rationalise the difference in activity of these probes a number of physiochemical properties have been calculated and outlined in table 7. Here, affinities of the compounds are compared to the total length of the linker, total polar surface area (tPSA) and lipophilicity (ClogP). In this case the length of the linkers

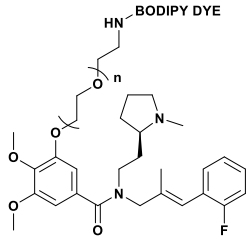


Table 6. *Overview of affinities obtained for compounds **38a-c** and **39a-c**. For compounds 38a-c no specific binding was detected up to 1 µmol/L.*

Compound	PEG length	BODIPY	Affinity (pK_d ± SEM)	*n*
38a	0	630/650	ND	*2*
38b	1	630/650	ND	*2*
38c	2	630/650	ND	*2*
39a	0	630/650-X	6.10 ± 0.05	*8*
39b	1	630/650-X	6.13 ± 0.10	*5*
39c	2	630/650-X	6.16 ± 0.10	*5*

is defined as the number of chemical bonds separating the pharmacophore and fluorophore. As table 7 shows, the high affinity compounds **39a-c** indeed have a longer overall linker, suggesting length plays a key role in the activity of these probes. Interestingly, even with the inclusion of a lipophilic alkyl chain, an increase in total polar surface area is observed. The aminohexanoyl spacer of the BODIPY dye consistently adds 29 $Å^2$ to the overall total polar surface area, while each PEG unit adds 9 $Å^2$. Interesting also is that the lipophilicity of the conjugates decreases slightly, as their size increases. The inclusion of the aminohexanoyl spacer yields two additional amide bonds, which explain for the increase in tPSA and a slight reduction in clogP. The difference in tPSA and clogP values between these compounds is relatively small however, and is therefore unlikely to be the reason why compounds **39a**, **39b**, and **39c** have measurable affinity, and compounds **38a-c** do not.

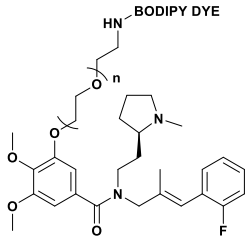


Table 7. *Overview of key physiochemical properties of compounds* ***38a-c*** *and* ***39a-c****. tPSA and clogP values were calculated using Chemdraw.*

Compound	Affinity (pK_d)	Length of linker (number of atoms)	tPSA ($Å^2$)	clogP
38a	ND	6	96	10.5
38b	ND	9	105	10.5
38c	ND	12	114	10.4
39a	6.10	13	125	10.3
39b	6.13	16	134	10.4
39c	6.16	19	143	10.2

4.4.2.3 NanoBRET™ saturation binding of BODIPY FL-X labelled compounds ***40a-c***

Having identified red fluorescent probes **39a-c** as active binders with decent affinity towards NLuc-ACKR3, I moved to the characterisation of the green fluorescing probes **40a-c**. As whole cells provided much better results in previous saturation-binding experiments with NLuc-ACKR3, I looked to again use this same method. HEK293 cells stably expressing NLuc-ACKR3 were therefore seeded on poly-D-lysine-coated 96-well plates at a 10 000 cells per well and were left to grow. After two days the cells achieved ~90% confluence and were ready to be used in the assay. The growth medium was replaced with assay medium, and after addition of increasing

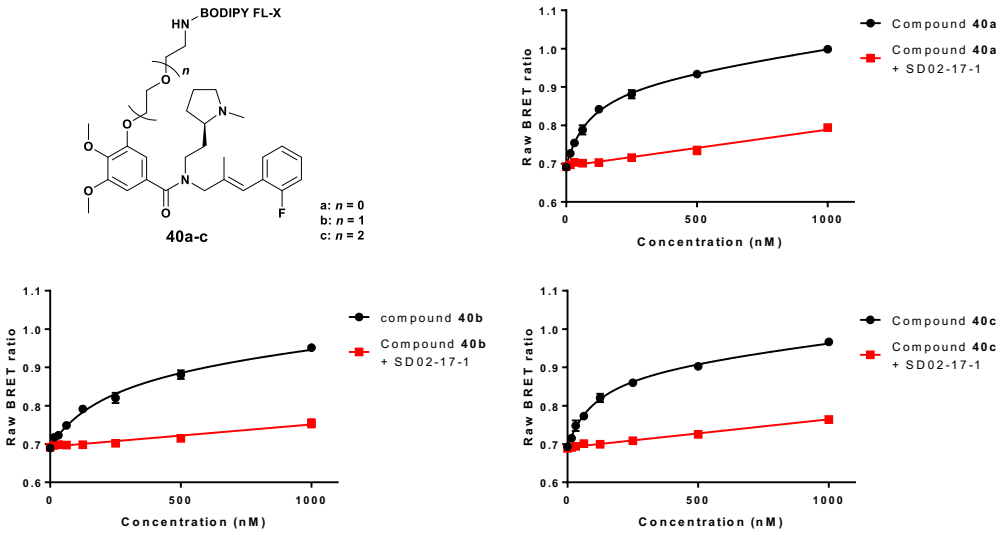


Figure 33. *NanoBRET saturation-binding experiments for BODIPY FL-X labelled compounds* ***40a-c****. Raw BRET ratio is determined as the ratio of fluorescence/luminescence. Non-specific binding was determined in the presence of 10 µmol/L SD02-17-1. Data points represent mean ± SEM of triplicate determinations of a single experiment. These single experiments are representative of n=5 for all three compounds. Where not seen, error bars are within the symbol.*

Table 8. *Overview of affinities obtained for compounds* ***40a-c****.*

Compound	PEG length	BODIPY	Affinity (pK_d ± SEM)	*n*
40a	0	FL-X	7.05 ± 0.06	*5*
40b	1	FL-X	6.65 ± 0.04	*5*
40c	2	FL-X	6.84 ± 0.06	*5*

concentrations of the ligands with and without the presence of 10 µmol/L SD02-17-1, and an incubation period of 1 hour at 37 °C, furimazine was added and the BRET was immediately measured on a PHERAstar FS plate reader. The results of these experiments are displayed in figure 33. All three green fluorescing compounds show much better binding to NLuc-ACKR3 than the red fluorescing compounds **38a-c** and **39a-c**, with BRET ratios showing a concentration-dependent increase and reaching saturation at concentrations above 500 nanomolar. The affinities obtained from these experiments are displayed in table 8. Unsurprisingly, these compounds show much higher affinities towards NLuc-ACKR3 compared to the red fluorescing compounds. Interestingly, however, for this series of compounds the smallest conjugate, compound **40a**, has the highest affinity with a pK_d of 7.05 ± 0.06, or roughly 90 nM. At first glance this would suggest that in fact the length of the conjugate does *not* play a significant role in the activity of these compounds, contradicting the findings from the series of red fluorescent of compounds. However when the number of chemical bonds of compound **40a** that separate the pharmacophore from the fluorophore is considered, a trend can be observed. Below, table 9 outlines the same physiochemical properties as outlined earlier, but for all ACKR3 compounds synthesised. Indeed, the number of chemical bonds that separate the pharmacophore and the fluorophore for compound **40a** is the same as for compound **39a**, and greater than 12, which appears to be crucial. The affinity does not further improve as the length of the linker increases. This raises the believe that for activity a minimal linker length is required, but that above that length linker size is irrelevant for increasing affinity. Though for compound series **39a-c** affinity increases with the size of the linker, this difference is considered insignificant. From table 9 it can also be observed that there is a ~10-fold difference in affinity of the green fluorescing ligands compared to the red fluorescing ligands. A possible explanation for this could simply be the size of the fluorophore. The BODIPY FL-X is much smaller fluorophore than the 630/650 dye, and as an interdependent part of the conjugate, it might be hindering ligand binding less than its larger counterpart. Alternatively, lipophilicity of the fluorescent conjugates might offer an explanation too. A significant drop in lipophilicity can be observed when conjugating to a BODIPY FL-X dye rather than the 630/650 dye, as is shown by a decrease in clogP values from

~10.5 to ~6.5 (table 9). Lipophilicity is an important physiochemical property that affects the solubility and permeability of molecules. In drug discovery it is a crucial predictor for ADMET properties and the overall suitability of a drug candidate[151]. For fluorescent probes this too is an important property that is likely to affect affinity and applicability. BODIPY-labelled probes with clogP values too low are likely to be inactive as the BODIPY dye needs to incorporate into the lipid bilayer of the cell to fluoresce. Inversely, probes with clogP values too high will yield a high degree of nonspecific binding, which is what was observed with CXCR4 targeting probes. Compounds **40a-c** show much improved clogP values of around 6.5, which is likely to contribute to their high affinity, and hopefully excellent applicability.

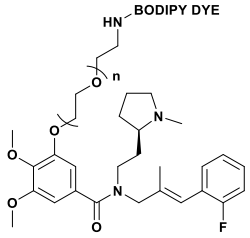


Table 9. *Overview of key physiochemical properties of compounds* ***38a-c****,* ***39a-c*** *and* ***40a-c****.*

Compound	Affinity (pK_d)	Length of linker (number of atoms)	tPSA (Å^2)	clogP
38a	ND	6	96	10.5
38b	ND	9	105	10.5
38c	ND	12	114	10.4
39a	6.1	13	125	10.3
39b	6.13	16	134	10.4
39c	6.16	19	143	10.2
40a	7.05	13	115	6.5
40b	6.65	16	125	6.6
40c	6.84	19	134	6.4

*4.4.4.4 NanoBRET™ saturation binding of CXCR4 probe **22** against NLuc-ACKR3*

With the characterisation of the ACKR3 targeting probes finished, I continued with the evaluation of CXCR4 probe **22** as a possible new chemotype for the ACKR3 receptor. Compound **22** was identified as a possible binder to the ACKR3 receptor following single-concentration binding experiments of the CXCR4 probes against the ACKR3 receptor (see figure 30). Following the same method that was used for the characterisation of the ACKR3 probes, saturation-binding experiments were performed on whole cells expressing NLuc-ACKR3. As can be seen in figure 34, compound **22** unfortunately shows no specific interactions with NLuc-ACKR3, as a linear increase in BRET was observed similar to the nonspecific binding in two separate experiments.

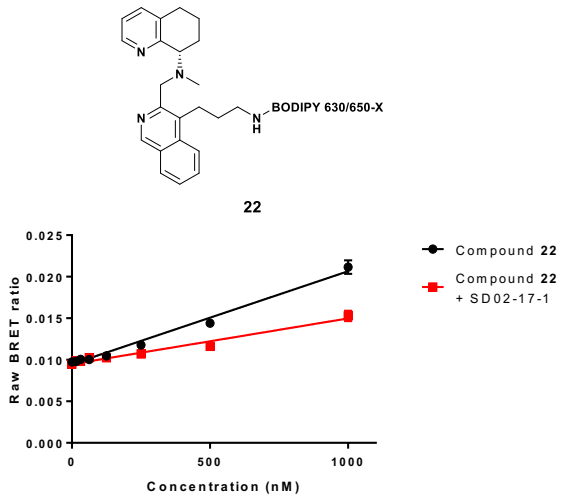


Figure 34. *NanoBRET signal obtained from HEK293 NLuc-ACKR3 cells incubated with increasing concentrations of compound **22**. Raw BRET ratio is determined as the ratio of fluorescence/luminescence. Non-specific binding was determined in the presence of 10 µmol/L SD02-17-1. Data points represent mean ± SEM of triplicate determinations of a single experiment. This single experiment is representative of two separate experiments. Where not seen, error bars are within the symbol.*

To summarise, with these experiments I was able to show that of the nine GD301-based fluorescent probes, six have been identified as binders to the ACKR3 receptor possessing good affinity. Of these, three red fluorescing probes show affinities ranging 0.75 - 0.84 µM, while three green fluorescing probes show affinities ranging 0.09 - 0.23 µM. I furthermore showed that the previously synthesised CXCR4 probes show no specific binding to ACKR3 over the concentration range tested. An overview of the compounds and their affinity towards the ACKR3 receptor is given in table 10, along with their structural features.

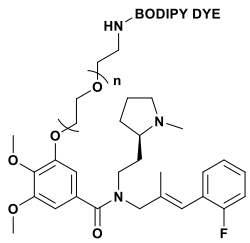


Table 10. *Overview of the fluorescent probes tested against NLuc-ACKR3 in Nano-BRET saturation binding experiments.*

Compound	PEG length	BODIPY	Affinity (pK_d ± SEM)	*n*
22	-	630/650-X	ND	*2*
38a	0	630/650	ND	*2*
38b	1	630/650	ND	*2*
38c	2	630/650	ND	*2*
39a	0	630/650-X	6.10 ± 0.05	*8*
39b	1	630/650-X	6.13 ± 0.10	*5*
39c	2	630/650-X	6.16 ± 0.10	*5*
40a	0	FL-X	7.05 ± 0.06	*5*
40b	1	FL-X	6.65 ± 0.04	*5*
40c	2	FL-X	6.84 ± 0.06	*5*

4.4.3 NanoBRET™ competition binding experiments

Having identified six novel probes that, with medium to high affinity, interact with NLuc-ACKR3, I wanted to assess their behaviour in a competitive setting. Similar to the approach in performing competition binding experiments using CXCR4 probes, I looked to displace two of the ACKR3 probes with competing ligands. Since the ACKR3 receptor is quite a novel target, the commercial availability of small molecule ligands is severely limited. The availability of ligands I can use in this assay is therefore limited to just the endogenous ligand CXCL12 and the small molecule ligand SD02-17-1. Nevertheless I was interested in assessing whether the fluorescent probes are competitive ligands, and if they could be used in the characterisation of novel small molecule ligands. For these competition binding experiments I chose to use a red fluorescent probe, compound **39c**, and a green fluorescent probe, compound **40a**. Pre-incubating HEK293 NLuc-ACKR3 cells for 1 hour at 37 °C with these compounds at concentrations similar to their K_d value, varying concentrations of human CXCL12 and small molecule SD02-17-1 were added. After a final incubation period of 1 hour at 37 °C the Nanoluc® substrate furimazine was added and the BRET was measured. The results of these experiment are shown in figure 35. As can be seen in these results, CXCL12 is much better able to compete for the NLuc-ACKR3 receptor with these probes than for the CXCR4 receptor with the CXCR4 targeting probes. While in the competition binding experiments with the CXCR4 probes CXCL12 was unable to displace the probes, here it is able to reach 52% ± 3 displacement of compound **39c**

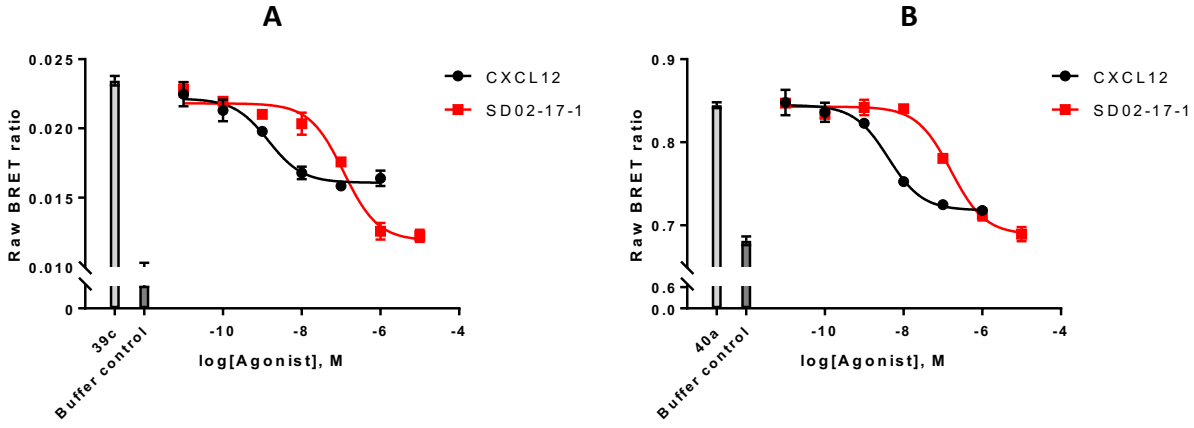


Figure 35. *NanoBRET signal from NLuc-ACKR3 cells treated with (**A**) 750 nmol/L compound **39c**, (**B**) 100 nmol/L compound **40a**, and increasing concentrations of CXCL12 and SD02-17-1. Raw BRET ratio is determined as the ratio of fluorescence/luminescence. Data points represent mean ± SEM of triplicate values of four separate experiments.*

Table 11. *Binding affinities of CXCL12 and SD02-17-1 as calculated from the competition BRET assay.*[a]

	CXCL12		**SD02-17-1**	
	pK_i ± SEM	*n*	pK_i ± SEM	*n*
Compound **39c**	8.85 ± 0.14	*4*	7.00 ± 0.11	*4*
Compound **40a**	8.60 ± 0.07	*4*	7.10 ± 0.17	*4*

[a]*Values show mean ± SEM. In each individual experiment triplicate determinations were made for each experimental condition. pK_i values were calculated from IC_{50} values using the Cheng-Prusoff equation.*

(As mean ± SEM, *n* = 3, see figure 35A), and 78% ± 2 displacement of compound **40a** (As mean ± SEM, *n* = 3, figure 35B). The observed difference in the ability of CXCL12 to displace compounds **39c** and **40a** is likely attributed to the size difference of the probes, and perhaps also their difference in overall lipophilicity. The in-house synthesised GD301 ligand SD02-17-1 is able to fully displace both probes, in a concentration-dependent matter. This shows that the fluorescent probes are competitively displaced, and could potentially be used as "hot" ligands in the characterisation of novel chemotypes. Of course without the availability of more diverse ligands this remains to be further investigated. From these competition binding experiments affinities were obtained for both CXCL12 and SD02-17-1, which are shown in table 11. The obtained pK_i values for both these ligands are very similar in both experimental setups, showing that both probes yield robust results. Interestingly, a smaller difference was observed in the affinity of CXCL12 for the ACKR3 receptor versus the CXCR4 receptor, than is found in literature. It is reported that CXCL12 has a ~10-fold higher affinity for the ACKR3 receptor than for the CXCR4 receptor, with a K_d of 0.4 nM for ACKR3 versus a K_d of 3.6nM for CXCR4[27, 152]. In these experiments a difference of only ~5-fold is observed, although pK_i values obtained in the CXCR4 experiments might not be very reliable as CXCL12 was unable to displace the CXCR4 probes. The affinity of SD02-17-1 was determined to be around 100nM, or -7.0 in log units. This is about ~5-fold lower than the pK_i reported for GD301 by my collaborators, which was found to be 7.56 ± 0.1 as determined in a radioligand competition binding assay using ^{125}I-CXCL12. Several factors can contribute to this difference in affinity. Firstly, quite often the use of different types of assays can yield different results, so comparing radioligand-based assays with BRET-based assays

should be done carefully[153]. Secondly, the cell type used, as well as the expression level of the receptor can influence the observed affinity of ligands. In my competition binding experiments a cell line was used of HEK293 cells stably expressing NLuc-ACKR3. Stable cell lines often have lower receptor expression levels than overexpressing cells, which for example were used in the β-arrestin recruitment assay used for the characterisation of VUF11207[89]. Finally, the amount of "hot" ligand used in the competition binding experiments plays a large factor as well. As compounds **40a**, and especially compound **39c**, are relatively low affinity ligands, a high concentration of ligand is required to occupy the receptors. This is likely to interfere with the ability of the "cold" ligands to occupy the receptor. Overall, with these experiments I was able to show that these fluorescent ACKR3 probes are competitive ligands, and that they show to be robust pharmacological tool compounds.

4.5 Confocal imaging

With the successful identification of some high affinity fluorescent probes for the ACKR3 receptor, I next looked to visualise ligand-receptor interactions using live cell confocal microscopy. For this I chose to use the probe with the highest affinity towards the receptor, namely the green fluorescing compound **40a**. Its high affinity towards the receptor allows for the experiments to be conducted at a lower concentration of ligand, thereby reducing the level of nonspecific binding and background fluorescence. Additionally, this compound has more favourable physiochemical properties compared to the red fluorescent compounds. Particularly the level of lipophilicity is more favourable, as the estimated ClogP of **40a** is 6.5 while for compounds **39a-c** ClogP values range 10-10.5. I expect this further reduces the level of nonspecific fluorescence, as the BODIPY dye of any unbound ligand will be less likely to incorporate into the lipid bilayer of the cell.

To visualise receptor expression I was interested in using a HEK293 cell line expressing a SNAP-receptor construct similar to what was used for the CXCR4 experiments. A SNAP-tag consists of a self-labelling protein of 19.4 kDa in size that, when fused to a protein of interest, allows for direct visualisation of the protein via coupling to fluorescent dyes containing an O^6-benzylguanine group[154].

Unfortunately, a stable cell line expressing SNAP-ACKR3 was not available in-house and I therefore looked to transfect HEK293 cells with cDNA encoding SNAP-ACKR3. I was fortunate to have collaborators in this project who shared cDNA of wild-type ACKR3, which was successfully tagged with the SNAP protein on the N-terminus of the receptor by colleagues. This meant that for this project ready-made cDNA encoding SNAP-ACKR3 could be used, conveniently allowing transient transfection of HEK293 cells. Rather than creating a stable HEK293 cell line expressing SNAP-ACKR3 I chose to perform a transient transfection, resulting in the overexpression of the receptor. The obvious advantage of overexpression of the receptor is the increased presence of the protein of interest on the cells, allowing for better interrogation of ligand-receptor interactions. A downside of this method is that the cDNA is not permanently incorporated into the cellular genome, resulting in the loss of expression after only a few cell cycles[155]. For these confocal microscopy experiments however, it is not essential to have a stable cell line.

For the transient transfection, HEK293 cells were plated on poly-D-lysine-treated Nunc™ Lab-tek™ cover slips and cultured until 50% confluent. A 3:1 ratio mixture was prepared in OptiMEM of cDNA and FuGENE®HD, respectively, and left to incubate for 20 minutes at room temperature. This was then added to the cells, after which the next day the cells were ready for imaging. To visualise receptor expression the cells were tagged with SNAP-Surface Alexa Fluor 647 dye before imaging. Confocal experiments were performed using a Zeiss 710 confocal microscope, where the stage was warmed to 37 °C. After clusters of cells were found with reasonable levels of receptor expression, compound **40a** was added to achieve a final concentration of 50 nM. Single equatorial confocal slices were obtained over the course of the experiment, which are displayed in figure 36.

The first thing that can be seen from figure 36 is that the transfection of the HEK293 cells was not highly successful. While the transmitted light (bottom row images) reveal a good number of viable cells in the field of view, only a few cells were successfully labelled with the red Alexa Fluor dye (middle row images), indicating a low transfection efficiency. Several factors could have contributed to the poor

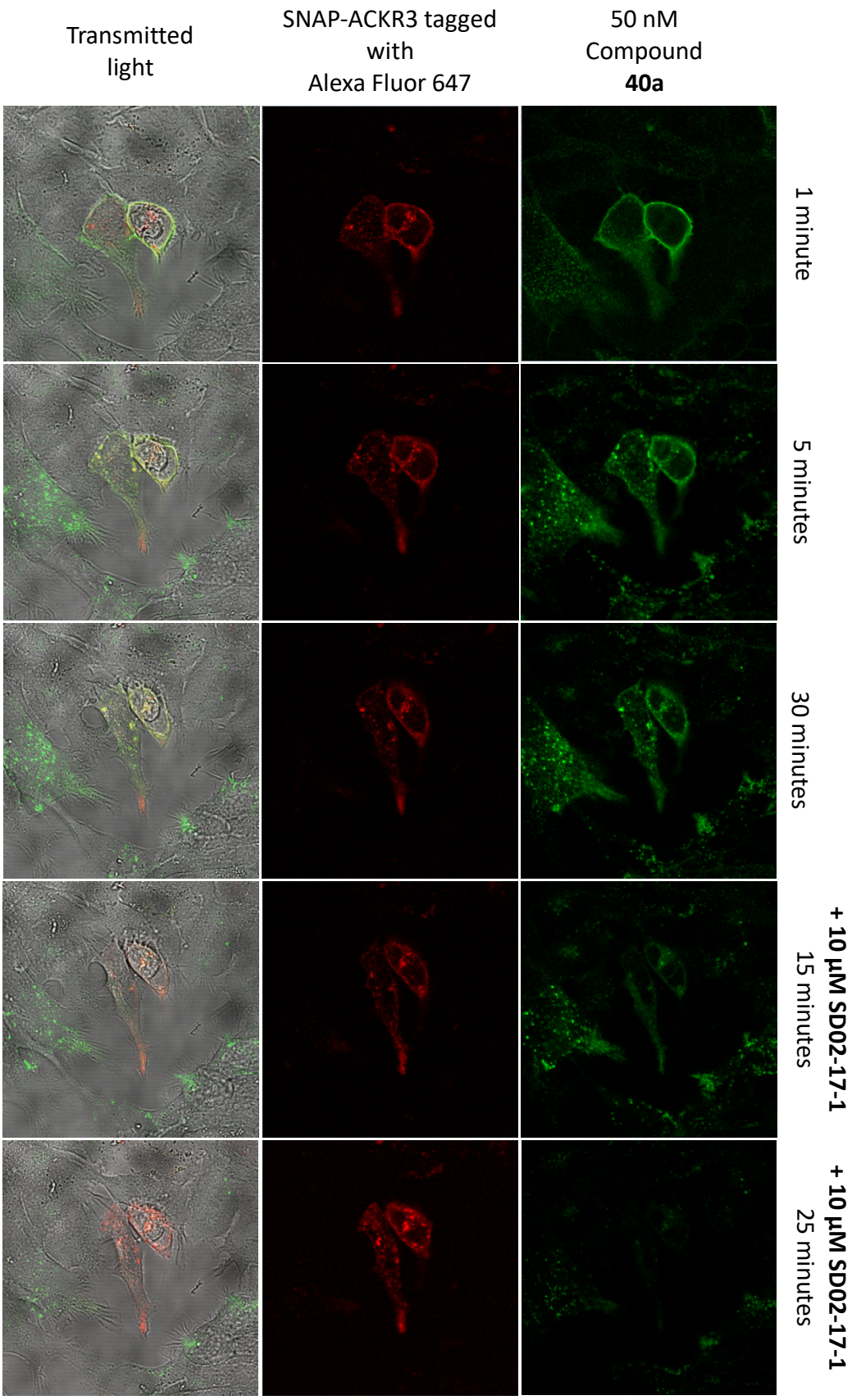


Figure 36. *Visualisation of binding of compound* ***40a*** *to HEK 293 cells transiently expressing SNAP-ACKR3. Single equatorial confocal slices were obtained following addition of 50 nM* ***40a*** *at 1 minute, 5 minutes, and 30 minutes. Following subsequent addition of 10 µmol/L SD02-17-1 single equatorial confocal slices were obtained after 15 minutes and 25 minutes. All images were obtained within one experiment and taken with identical microscope settings.*

transfection efficiency, such as confluency of the cells, growth medium, cDNA used, or type of transfection method. In spite of the low transfection efficiency however, a couple of cells were successfully transfected and allowed for the investigation of ligand-receptor engagement.

Immediately after treating the cells with 50 nM of compound **40a** the first confocal images were obtained (first column of images). I can be observed that already after 1 minute the compound localises neatly on the cell surface, and is brightest on the cells that were labelled with the Alexa Fluor dye. Over the course of 30 minutes the compound was allowed to interact with the cells and snapshots were obtained after 5 minutes and 30 minutes. From these snapshots it can be seen that over the course of the experiment the compound interacts with the receptor and, as a result, causes internalisation of the ligand-receptor complex. As GD301 is reported as a full agonist, I anticipated that the fluorescent probes - which are derived from its structure - would retain this agonist function. This was supported by the observation that the ligand-receptor complex was internalised, providing evidence on the agonist nature of these fluorescent ligands. Upon subsequent addition of 10 µmol/L of SD02-17-1 an almost complete dissipation of the fluorescent signal of the probe can be observed. This further shows the competitive nature of the fluorescent ligands, and also shows there is very little nonspecific interaction with the cell membrane. The low nonspecific binding is likely due to the high affinity and more favourable physiochemical properties of compound **40a**. Its relative low lipophilicity prevents any unbound ligand to incorporate into the cell membrane, which is what was observed with the highly lipophilic CXCR4 probes. Interestingly, the confocal images also show clustering and internalisation of the fluorescent probe on cells that have not been labelled with the Alexa Fluor dye. As this clustering appears to be highly localised, and is suppressed after addition of SD02-17-1, it can be assumed that this due to ACKR3-mediated signalling. This could therefore mean that the transfection was more successful than originally thought, and that in fact the labelling of the receptor with the Alexa Fluor dye was inadequate. Perhaps a reason the labelling was inadequate was, due to the continuous and ligand independent uptake of the receptor by the cell[30], much of the receptor was inaccessible for the probe. As a cell

impermeable SNAP-Surface® Alexa Fluor® dye was used, it makes sense that not all receptor was successfully labelled. Irrespective of the poor transfection efficiency, or the inadequate labelling of the receptor, these experiments clearly allowed visualisation of ligand-receptor interactions. They show that the ligand engages with the receptor and causes internalisation of the ligand-receptor complex. Upon treatment of the cells with a high concentration of competitive ligand, the fluorescent signal of the probe is completely suppressed, proving competitive displacement of the probe. It furthermore shows fluorescent probe **40a** has very little nonspecific binding.

To summarise, in this chapter I decribe the successful development of high affinity fluorescent probes for the atypical chemokine receptor ACKR3. By using key structural and functional information of the VUF11207 scaffold, I designed and synthesised nine fluorescent probes. I was able to show the affinity and competitive nature of these fluorescent probes in a novel NanoBRET™ assay. Confocal imaging using fluorescent probe **40a** showed it neatly localises with ACKR3, with low levels of nonspecific binding. The resulting ligand-receptor complex was internalised, indicating an agonist-like response, and was fully disrupted after treatment with a high concentration of competing ligand. Overall, these fluorescent probes will provide valuable tools in the study of ACKR3 signalling and the involvement of this receptor in disease states. Particularly the series of BODIPY FL-X-labelled probes (**40a-c**) possess excellent affinity and physiochemical properties, allowing them to be used in a range of fluorescence-based experiments such as FACS, FCS, and BRET-based experiments.

5 Conclusions

The study of cancer, and the development of novel therapeutics for the treatment this disease, is of great value to society. To provide further insight on how the chemokine receptors CXCR4 and ACKR3 are involved in cancer, and to provide tool compounds that will aid the development of novel therapeutics targeting these receptors, I set out to develop small molecule-based fluorescent probes.

5.1 Fluorescent CXCR4 receptor probes

Fluorescent probes for the chemokine receptor CXCR4 were developed based on SAR and *in silico* drug design of several small molecule inhibitors. Ultimately, synthesis efforts yielded five fluorescent conjugates, which were based on three different scaffolds (figure 37). Pharmacological characterisation using a novel NanoBRET™ assay identified four high affinity probes and one very weak probe. IT1t-based compound **5** shows very weak affinity for CXCR4, indicating that the flexibility and symmetry of the cyclohexane-ring must be preserved. This is supported by high affinity compound **9** (pK_d = 7.0), which incorporates a *trans*-aminocyclohexane

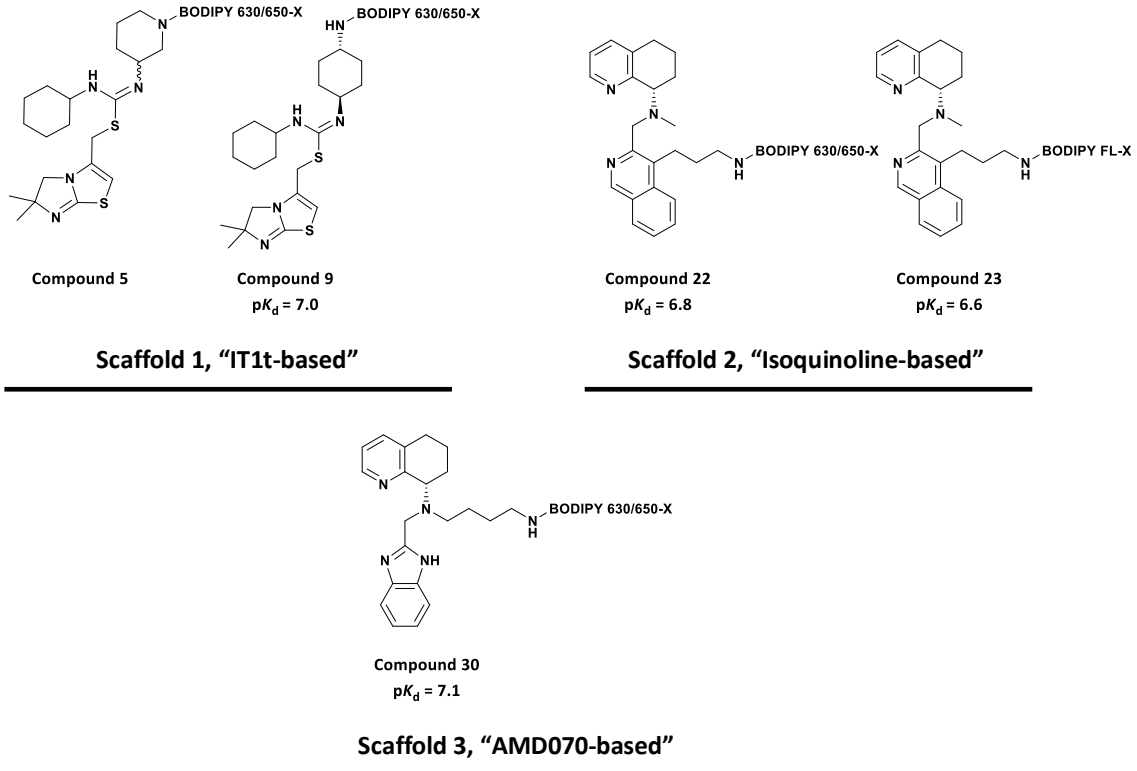


Figure 37. *Five different fluorescent probes were synthesised for the CXCR4 receptor, based on three unique scaffolds of small molecule ligands.*

moiety for the conjugation to the fluorophore. Compounds **22**, **23** and **30** furthermore show high affinity towards CXCR4, with pK_d values ranging 6.6 – 7.1. Using the same NanoBRET™ approach I was also able to show these compounds are competitive binders and robust toolkit compounds in the characterisation of small molecule ligands. A separate, functional, assay showed their ability to affect CXCL12-mediated signalling of CXCR4 and provided evidence of their antagonistic character. Finally, live cell confocal microscopy was performed with three selected probes and showed these ligands localise on the cell membrane, at sites with high receptor expression. Upon subsequent treatment of the cells with a high concentration of competitive ligand the fluorescent signal of the probes was not fully suppressed. There are several factors could be causing this. As the competitive ligand was added after treating the cells with the fluorescent probes, it is possible that the binding kinetics of the probes prevent the competitive ligand from displacing them. Alternatively, it could indicate that these probes have a high degree of nonspecific binding to the cell membrane, potentially limiting the applicability of these probes. The high lipophilic nature of these probes, and the di-basic nature of the congeners they incorporate, could stimulate these probes to engage with the lipid bilayer. Further optimisation of these probes will therefore be required to enable their use in studying receptor expression with techniques such as FACS and confocal microscopy.

Overall, this project has yielded the first high affinity small molecule-based fluorescent probes for the chemokine receptor CXCR4. Though further optimisation is required to reduce the level of lipophilicity of these probes, I was able to show their robust use in the characterisation of small molecule ligands in conjunction with the NanoBRET™ system. These probes have the potential to be used in a wide range of fluorescence-based experiments, and will hopefully help to further the understanding of the involvement of CXCR4 in cancer.

5.2 Fluorescent ACKR3 receptor probes

The development of fluorescent probes targeting the atypical chemokine receptor ACKR3 started from a collaboration with researchers at the VU University of Amsterdam. Using an enantiomerically pure version of the reported small molecule

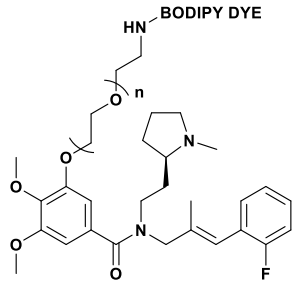


Figure 38. *General structure of the fluorescent probes developed for the ACKR3 receptor.*

VUF11207 as a starting point, fluorescent derivatives were designed with the support of a homology model of ACKR3 and site-directed mutagenesis studies. Synthesis efforts yielded nine fluorescent conjugates, of which the general structures are outlined in figure 38. Similar to the fluorescent probes developed for the CXCR4 receptor, these probes have been characterised in a novel NanoBRET^{TM} -based assay. All nine probes were shown to specifically interact with the receptor, with six compounds possessing good affinity, ranging 6.1 – 7.1 (as pK_d values). These experiments also revealed that length of the linker, lipophilicity and size of the fluorophore have a large impact on affinity of these compounds. Compounds possessing only a few PEG units as linkers performed far less than compounds that include an additional hexanoyl spacer. For the synthesised compounds that include both PEG units and the hexanoyl spacer, overall linker length did not seem to correlate to increased affinity. In fact, the most potent compound (compound **40a**, pK_d = 7.1) represents the smallest fluorescent conjugate, both in molecular weight and linker length. An explanation for its high affinity might instead be the relatively small size of the fluorophore used (BODIPY FL-X) and the overall lipophilicity of the conjugate. Critically, compared to the probes incorporating the BODIPY 630/650-X dye (which show clogP values of around 10.5), the probes incorporating the BODIPY FL-X dye show much lower clogP values of only around 6.5. Besides driving the affinity of these probes toward their target, this favourable physiochemical property might also result in the application of these probes in more diverse *in vitro* experiments and perhaps even in *in vivo* experiments. It is likely to result in good solubility in physiological conditions and reduce nonspecific binding. Overall, these findings further emphasise that fluorophores have a large impact on the overall

pharmacological profile of the conjugate. Every fluorescent conjugate therefore needs to be evaluated as a completely new compound. Compound **40a** was selected for confocal microscopy experiments to visualise ligand-receptor interactions. These experiments showed excellent localisation of the probe on the cell surface, and provided evidence of ligand-induced internalisation of the ligand-receptor complex. It furthermore confirmed the hypothesis that, due to its physiochemical properties, compound **40a** has very little nonspecific binding. Overall, this project has led to the successful development of the first small molecule-based fluorescent probes for the atypical chemokine receptor ACKR3. The high affinity and favourable physiochemical properties of compound **40a** will allow its use in various fluorescence-based experiments, such as FACS and confocal microscopy, and could potentially even see application in *in vivo* experiments.

I believe that the probes described in this thesis will be valuable toolkit compounds in studying the pharmacology of CXCR4 and ACKR3, and the characterisation of ligands that act on their signalling axes.

6 Future work

The aim of the current project was to develop high affinity fluorescent probes for the chemokine receptors CXCR4 and ACKR3. This thesis describes the successful synthesis and biological characterisation of several high affinity probes, and provides evidence for their robust use in the characterisation of small molecule ligands with the NanoBRET™ system. There are, however, several experiments that could be performed to further corroborate these findings, and add to the overall impact of the current work.

6.1 Optimisation of the CXCR4 receptor probes

As discussed in chapter 3, a potential issue with the CXCR4 receptor probes could be the level of lipophilicity they possess. Confocal microscopy experiments appeared to reveal a high level of nonspecific binding for the three probes that were used; possibly caused by nonspecific interaction with the cell membrane. Though it is possible that the binding kinetics of the probes prevent the competitive ligand from displacing them, and therefore the level of nonspecific binding is overestimated, reducing their lipophilicity could substantially improve their applicability. In this thesis it was reasoned that changing either the pharmacophore- or the fluorophore component is ill-advised, as this is likely to disrupt overall affinity towards the target or affect the photochemical properties of the probe. Instead, a change to the linker-region of the conjugates could be considered. Functionalisation of the linker through incorporation of amino acids is well established, and has led to the development of some highly potent fluorescent probes that show very low levels of nonspecific interactions[144, 156]. By introducing a peptide chain as a linker to separate the pharmacophore and fluorophore, lipophilicity could be decreased and perhaps even lead to an increase in affinity and receptor selectivity. An example of how such a CXCR4 receptor probe would look is illustrated in figure 39, where exchange of the hexanoyl spacer of compound **9** for a Gly-Ser-Ser peptide linker of similar length is proposed. The choice of amino acids, their order, and the length of the linker can furthermore be rationalised with *in silico* guidance using the available crystal structure of CXCR4.

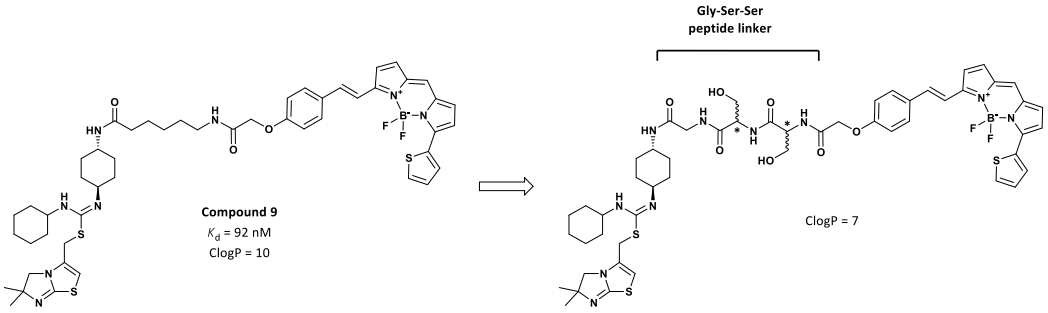


Figure 39. *Example of the incorporation of a peptide-based linker to significantly reduce the overall lipophilicity of the conjugate.*

6.2 Optimise confocal imaging of the CXCR4 probes

Besides optimisation of the fluorescent probes to reduce lipophilicity and thereby reduce nonspecific interactions of the probes with the cell membrane, the conditions under which these ligands have been visualised can also be optimised. In my confocal microscopy experiments, I allowed the fluorescent probes to bind to the receptor before attempting to displace them with a competing ligand. A more common practise, however, is to pre-incubate the cells with the competing ligand before adding the fluorescent probe[156-158]. Though the approach used in this thesis allows the direct visualisation of the competitive displacement of the fluorescent probes, there are some pitfalls to this method. Most importantly, this method does not allow for the fair assessment of nonspecific binding. To visualise the nonspecific binding it is important to pre-occupy all of the available receptor with a competing ligand, which is only achieved by pre-incubation of the cells with the competing ligand. When all of the available receptor is occupied by the competing ligand, any fluorescence observed therefore has to be nonspecific. In the case of my experimental setup, it is possible that not all of the fluorescent probe was displaced by the competing ligand, even at a concentration of 10 µM. Investigating the binding kinetics of the fluorescent probes using NanoBRET™ will also help to design the confocal imaging experiments properly.

6.3 Screening of different chemotypes using fluorescent ACKR3 probes

One of the main goals set out for this project was to provide robust tool compounds that would allow for fast, cheap, safe, and accurate screening of novel ligands. Combined with the novel NanoBRET™ system, the fluorescent probes described in

this thesis have accomplished exactly that. While I was able to provide sufficient evidence that the CXCR4 probes can be displaced by various (chemotypically diverse) small ligands, and that the affinity of these ligands can accurately be measured, I was only able to show this for my ACKR3 probes with one compound. The challenge I faced when working on this project was the unavailability of any additional ligands. To provide unequivocal evidence that these ACKR3 probes too are robust tool compounds for the screening of novel small molecules, different ligands will have to be tested. Fortunately, collaborators at the VU University of Amsterdam have recently developed a small library of novel, chemically diverse ACKR3 ligands. The screening of these ligands in the NanoBRET™ assay using the probes I developed, will further validate the probes as robust tool compounds.

6.4 Functional screening of fluorescent ACKR3 probes

In chapter 3.3.2 I was able to provide experimental data on functional nature of the CXCR4 probes. As the CXCR4 probes were based on small molecule inhibitors of the CXCR4 receptor, I felt it was necessary to validate that the fluorescent derivatives thereof retain their functionality. Similarly, I am interested in the functional screening of the ACKR3 receptor probes, which are based on small molecule agonist GD301. Though I was able to provide evidence supporting their agonist-like behaviour in confocal imaging, I was unable to quantify any pharmacological parameters. The issue of working on the atypical chemokine receptor ACKR3 is that it does not seem to signal through G-proteins, and the majority of functional assays to study GPCRs are based on downstream signalling of G-proteins[159, 160] (such as the GloSensor™ cAMP assay used in chapter 3.3.2). Functional assays that investigate activation of β-Arrestin pathways primarily make use of fluorescent- or luminescent biosensors, resulting in either FRET or BRET based assays[89, 161, 162]. As the probes are fluorescent themselves, they are likely to interfere with the readout of the assay. This was particularly the case for the series of green-fluorescing compounds **40a-c**. Currently, screening of the non-fluorescing GD301-based congeners (compounds **37a-c**, scheme 7) is being performed by a fellow ONCORNET PhD student in Würzburg, Germany. The FRET-based assay that is being used for this screening makes use of FlAsH dye, which shows great spectral overlap with the BODIPY FL dye,

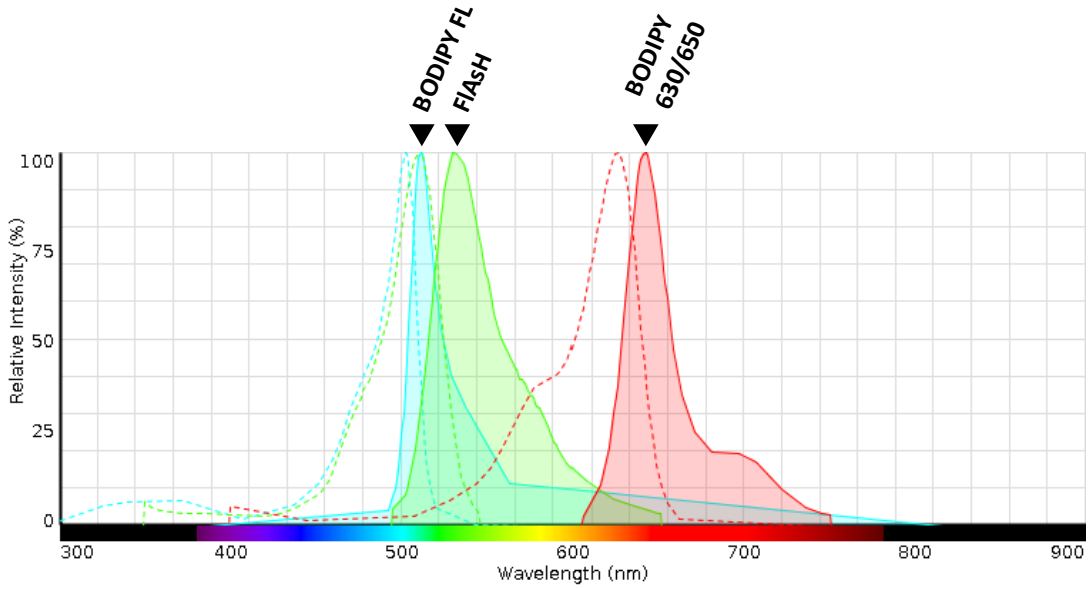


Figure 40. *Excitation and emission spectra of fluorescent dyes BODIPY FL, FlAsH and BODIPY 630/650. Excitation spectra is represented by the dotted lines.*

and even to some extend with the BODIPY 630/650 dye (figure 40). As the data generated for the congeners cannot be extrapolated to full fluorescent conjugates, a different experimental setup would therefore need to be developed for the functional characterisation of these fluorescent ligands.

6.5 Future application of the probes described in this thesis

The fluorescent probes described in this thesis have the potential to be of great value in studying the involvement of these chemokine receptors in cancer. One of the key applications where these compounds could serve a purpose, is in flow cytometry. This technique allows the detection and measurement of physical and chemical characteristics of a population of cells or particles[163, 164]. A specialised type of flow cytometry, FACS, can be used in conjunction with the fluorescent probes for the identification and sorting of cell types that express either CXCR4 or ACKR3 from a complex mixture. A specific example would be the sorting of cells derived from *ex vivo* patient samples, using FACS. Potentially, this would allow for the identification of CXCR4- or ACKR3 expressing cell types, and perhaps even the identification of metastatic cancer cells. Validation for the application of this technique in the identification of metastatic tumour cells was given by Leers *et al.*[165], who successfully detected micrometastatic tumour cells in the sentinel lymph node of patients with

breast cancer. Currently, these type of experiments are conducted mostly using fluorescently labelled antibodies. Though antibodies can be developed to be highly selective, they are expensive and time consuming to produce. Additionally, often these experiments require the use of two types of antibodies: the antibody that binds to the biological target that is being investigated, and a secondary antibody containing the fluorescent tag[108]. The fluorescent probes developed in the current project could provide a much cheaper and reliable alternative. Tandem application of an optimised red-fluorescing probe for CXCR4 and a green-fluorescing probe for ACKR3 could also allow for the study of these receptors at the same time. Tandem application of these probes could furthermore allow for the investigation of (hetero-) dimer formation, and may yield insight in the relative differences in function of hetero-dimers *versus* homo-dimers and monomers of CXCR4 and ACKR3.

7 Experimental

7.1 Modelling

ChemDraw from the ChemOffice 2015 software suite was used to generate 2D molecular structure .sdf files. For the docking studies Schrödinger Suite Glide was used. The crystal structure of CXCR4 (PDB code 3ODU) was imported into the software and the receptor was prepared by the protein preparation wizard. The receptor grid was generated using the grid preparation tool, and the 2D molecular structures of the ligands were converted to 3D structures using the LigPrep tool. Compounds were docked using the glide docking tool with standard settings and enhanced planarity and Epik calculated protonation states at pH 6.8. Binding poses were generated, visually inspected, and ranked according to their GlideScore. Only docking poses with GlideScores lower than -7 were considered. The final poses were then exported as images using either the Schrödinger Suite or PyMOL Molecular Graphics System.

7.2 Materials and methods

7.2.1 Materials

HPLC grade chemicals and solvents were purchased from the standard suppliers and were used without further purification. BODIPY fluorophores were obtained from Fischer Scientific, U.K. High grade silica, 60 Å, 230-400 mesh, for flash chromatography was supplied by Sigma Aldrich, and deuterated solvents (Chloroform-d, Methanol-d_4, DMSO-d_6) were purchased from Sigma Aldrich.

7.2.2 Microwave-assisted synthesis

For reactions requiring elevated pressure and temperatures, 10 mL or 35 mL reaction vessels were loaded into a Discover® SP microwave (CEM, USA). The required duration and temperatures of the reactions were programmed using the software Synergy, which calculated the amount of power that was needed to perform the reaction.

7.2.3 Liquid Chromatography Mass Spectrometry

For the analysis of reaction mixtures and isolated compounds a Shimadzu UFLCXR HPLC was used, equipped with a Biosystems MDS SCIEX API2000 ESI+ MS. The column

was a Gemini 3 µm C18 110 Å, LC column 50 x 2 nm. As eluent a mixture was used of MeCN and H_2O, containing 0.1% formic acid. Samples were run using a gradient of 1:19 v/v to 19:1 v/v over either 5 or 15 minutes, with a flowrate of 0.5 mL/min. UV absorption was detected at 254 nm and 220 nm.

7.2.4 High Performance Liquid Chromatography

Preparative RP-HPLC was performed on a Waters 2767 sample manager coupled to Waters 2525 binary-gradient module and a Waters 2457 dual-wavelength absorbance detector. The column used was a Phenomenex Gemini-NX (5 µm, 110 Å, C18, 150 × 21 mm) at ambient temperature. The flow rate was 25 mL/min, and UV detection was at 254 nm. Mobile phases were solvent A, 0.1% TFA in water, and solvent B, acetonitrile, degassed by helium bubble and sonication, respectively.

7.2.5 High Resolution Mass Spectrometry

HRMS was done on a Bruker microTOF II mass spectrometer using electrospray ionization (ESI-TOF) operating in the positive mode. Adducts within errors of ±10 ppm were reported.

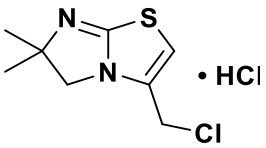
7.2.6 Nuclear Magnetic Resonance

NMR spectra were recorded with a Bruker AV(III) 400 NMR spectrometer. ^{1}H NMR was recorded at 400.13 MHz, and ^{13}C NMR was recorded at 101.6 MHz. Deuterated solvents used for the preparation of NMR samples were $CDCl_3$, MeOD-d_4, or DMSO-d_6. Chemical shifts (δ) are recorded in ppm with reference to the chemical shift of the deuterated solvent. Coupling constants (J) are recorded in hertz, and the signal multiplicities are described by the following: s, singlet; d, doublet; t, triplet; q, quartet; br s, broad singlet; m, multiplet; dd, doublet of doublets; ddd, double doublet of doublets; dt, doublet of triplets; p, pentet. NMR data was processed using MestReNova version 10.0.2.

7.3 Chemistry

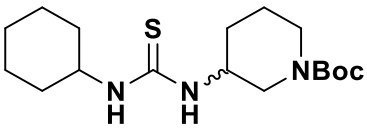
7.3.1 Synthesis of fluorescent IT1t-based probes

3-(chloromethyl)-6,6-dimethyl-5,6-dihydroimidazo[2,1-*b*] thiazole (1):



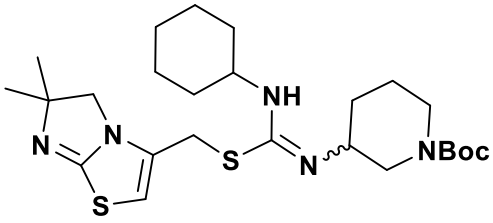
4,4-dimethylimidazolidine-2-thione (500 mg, 3.84 mmol) was dissolved in 12 mL DCM, and to it was added 1 equivalent of 1,3-dichloroacetone. This mixture was left to reflux for 2 hours, after which the reaction was concentrated *in vacuo* and the intermediate was crashed out by triturating with diethylether. This intermediate was filtered off, washed with diethylether and suspended in 3.5 mL of diglyme. This mixture was then heated at 140 °C for 2 hours, solids were filtered off and washed with diethylether to give compound **1** as an HCl salt (615 mg, 67% yield). ^{1}H NMR (400 MHz, DMSO-d_6): δ 10.94 (s, NH, 1H), 7.07 (s, CH, 1H), 4.86 (s, CH_2Cl, 2H), 4.22 (s, CH_2, 2H), 1.50 (s, $2CH_3$, 6H). ^{13}C NMR (101 MHz, DMSO-d_6): δ 168.36, 133.17, 111.08, 69.48, 57.84, 35.90, 27.44.

***Tert*-butyl 3-(3-cyclohexylthioureido)piperidine-1-carboxylate (2):**



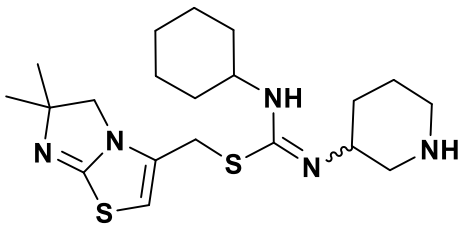
Tert-butyl 3- aminopiperidine-1-carboxylate (232 mg, 1.16 mmol) was dissolved in 15 mL DCM, to which was added cyclohexyl isothiocyanate (329 µL, 2 eq.). This mixture was left to stir at room temperature until completion. Solvents were evaporated and the crude was purified by column chromatography using a gradient of 0-10% MeOH in DCM as eluent, affording the product as a colourless oil. Yield: 388 mg (1.15 mmol, 98%). ^{1}H NMR (400 MHz, $CDCl_3$): δ 6.10 (br s, NH, 1H), 4.14 (s, NH, 1H), 3.77 (br s, CH, 1H), 3.61 (br s, CH, 1H), 3.33 (s, CH_2, 3H), 2.01-1.95 (m, CH_2, 2H), 1.83 (br s, CH_2, 1H), 1.72-1.69 (m, CH_2, 2H), 1.61-1.49 (m, CH_2, 4H), 1.44 (s, Boc, 9H), 1.39-1.28 (m, CH_2, 4H), 1.19 (dd, *J* = 12 Hz, *J* = 10.4 Hz, CH_2, 2H).

***tert*-butyl 3-(((cyclohexylamino)(((6,6-dimethyl-5,6-dihydroimidazo[2,1-*b*]thiazol-3-yl)methyl)thio)methylene)amino)piperidine-1-carboxylate (3):**



Thiourea **2** (130 mg, 0.38 mmol) was dissolved in 5 mL acetonitrile and to it was added halide **1** (109 mg, 1.2 eq.). This mixture was left to stir at 90 °C for 2 hours after which thiourea **2** was fully consumed (confirmed by LCMS). Solvents were evaporated and the crude was purified by column chromatography using 1-2.5% MeOH in DCM as eluent, affording the product as a colourless oil. Yield: 77 mg (0.15 mmol, 40%). LC-MS; *m*/*z*: 508.3 $[M+H]^+$. ^{1}H NMR (400 MHz, MeOD-d_4): δ 6.93 (br s, CH, 1H), 4.32 (s, CH_2, 2H), 4.04-3.79 (m, 2CH_2, 4H), 3.75 (s, CH_2, 2H), 3.47-3.39 (m, CH, 1H), 2.93-2.87 (m, CH, 1H), 2.17-1.69 (m, 4CH_2, 8H), 1.60 (s, 2CH_3, 6H), 1.48-1.40 (m, 3CH_2+Boc, 15H). ^{13}C NMR (101 MHz, $CDCl_3$) δ 179.92, 155.50, 154.83, 103.43, 80.29, 55.82, 53.54, 52.82, 50.80, 49.90, 48.71, 34.90, 32.92, 32.87, 32.84, 29.79, 29.58, 28.54, 28.51, 25.50, 24.78, 24.72, 22.69.

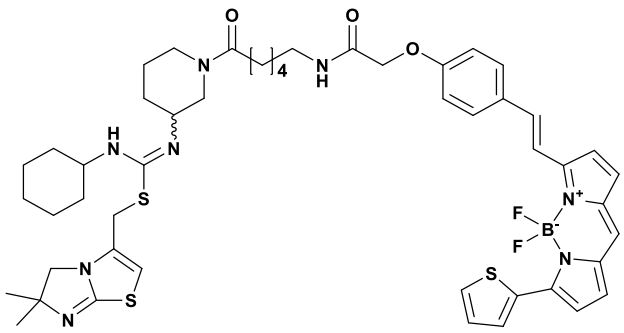
(6,6-dimethyl-5,6-dihydroimidazo[2,1-*b*]thiazol-3-yl)methyl *N*-cyclohexyl-*N*'-(piperidin-3-yl)carbamimidothioate (4):



Isothiourea intermediate **3** (120 mg, 0.24 mmol) of stirred in a 10 mL solution of DCM and TFA (4:1) at room temperature. After 3.5 hours complete consumption of starting material was observed by TLC. Solvents were evaporated *in vacuo* and residual TFA was removed under high vacuum. The product was purified by column chromatography using 0-10% 7N NH_3 in MeOH in DCM as eluent. Product was isolated as a colourless oil. Yield: 96 mg (0.24 mmol, quant.). LC-MS; *m*/*z* 408.2 $[M+H]^+$. ^{1}H NMR (400 MHz, MeOD-d_4) δ 6.94 (s, CH, 1H), 4.56 (s, CH, 1H), 4.31 (s, CH_2, 2H), 3.58 (dd, *J* = 11.8, 4.3 Hz, CH_2, 1H), 3.39 (d, *J* = 12.2 Hz, CH_2, 1H), 3.09 (t, *J* = 12.0 Hz, CH, 1H), 2.90 – 2.80 (m, CH, 1H), 2.20 – 2.02 (m,

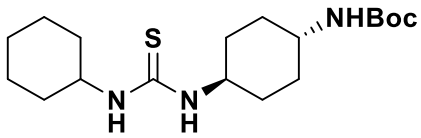
CH_2, 2H), 1.99 – 1.77 (m, CH_2, 6H), 1.74 – 1.65 (m, CH_2, 1H), 1.61 (s, $2CH_3$, 6H), 1.59 – 1.52 (m, CH_2, 1H), 1.50 – 1.29 (m, CH_2, 5H), 1.28 – 1.16 (m, CH_2, 1H). ^{13}C NMR (101 MHz, MeOD-d_4) δ 170.52, 162.30, 161.95, 111.62, 71.30, 66.89, 64.53, 62.53, 58.98, 46.58, 44.60, 44.42, 28.70, 28.04, 28.00, 27.51, 26.79, 25.88, 22.24.

(6,6-dimethyl-5,6-dihydroimidazo[2,1-*b*]thiazol-3-yl)methyl *N*-cyclohexyl-*N*'-(1-(6-(2-(4-((*E*)-2-(5,5-difluoro-7-(thiophen-2-yl)-5*H*-4λ^4,5λ^4-dipyrrolo[1,2-c:2',1'-f][1,3,2]diaza-borinin-3-yl)vinyl)phenoxy)acetamido)hexanoyl)piperidin-3-yl)carbamimidothioate (5):



1.0 mg (1.5 pmol) BODIPY 630/650-X succinimidyl ester was dissolved in 1 mL acetonitrile. To this solution was added 2 µL DIPEA (4 eq.) and 2.0 mg of compound **4**. This mixture was stirred overnight, in an amber coloured flask. LC-MS showed complete conversion of the BODIPY to the product (m/z: 954.06; $[M+H]^+$) so the mixture was concentrated *in vacuo* and purified by preparative RP-HPLC (5-95% solvent B, 30 min). Yield: 0.5 mg (35%). Purity of the compound was confirmed to be >95% by LC-MS using a long method run. HRMS calculated for $C_{49}H_{59}B_1F_2N_8O_3S_3$: 953.4011 found: 953.4054 $[M + H]^+$.

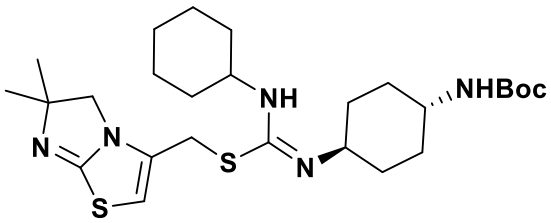
***Tert*-butyl ((1*r*,4*r*)-4-(3-cyclohexylthioureido)cyclohexyl) carbamate (6):**



Tert-butyl((1r,4r)-4-aminocyclohexyl)-carbamate (0.429 g, 2.0 mmol) and cyclohexyl isothiocyanate (0.567 mL, 2 eq.) were taken up in 10 mL DCM, and the reaction mixture was left to stir at room temperature for 20 hours. Note: the *trans*-cyclohexanediamide

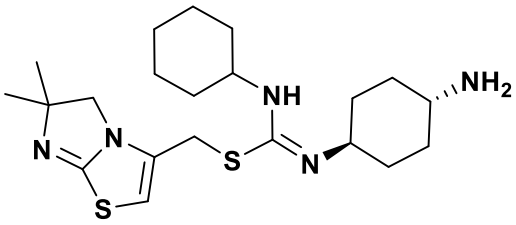
did not dissolve in DCM and therefore the mixture was stirred as a suspension. After 20 hours the mixture was concentrated *in vacuo* and purified by column chromatography using 2% MeOH in DCM as eluent. The product was isolated as a brownish oil. Yield: 0.603 g (1.7 mmol, 85%). ^{1}H NMR (400 MHz, $CDCl_3$): δ 5.74 (s, NH, 1H), 5.49 (s, NH, 1H), 4.46 – 4.39 (m, CH, 1H), 4.03 (s, NH, 1H), 3.73 (s, CH, 1H), 3.55 – 3.28 (m, CH, 1H), 2.14 (s, CH_2, 2H), 2.07 – 1.91 (m, $2CH_2$, 4H), 1.76 – 1.67 (m, $2CH_2$, 2H), 1.65 – 1.57 (m, CH_2, 1H), 1.42 (s, Boc, 9H), 1.40 – 1.31 (m, CH_2, 2H), 1.33 – 1.14 (m, $4CH_2$, 8H).

***Tert*-butyl ((1*r*,4*r*)-4-(((*E*)-(cyclohexylamino)(((6,6-dimethyl-5,6-dihydroimidazo [2,1-*b*]thiazol-3-yl)methyl)thio)methylene)amino)cyclohexyl)carbamate (7):**



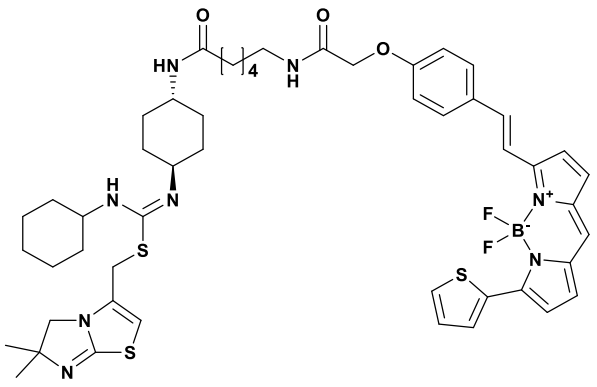
Isothiourea-based intermediate **1** (100 mg, 0.42 mmol) was dissolved in 1.5 mL acetonitrile and to it was added intermediate **6** (178 mg, 1.2 eq.). This mixture was left to reflux for 16 hours, after which TLC and LCMS showed complete conversion to the product (mass found: 522.5; M+H). Solvents were evaporated *in vacuo* and the crude was purified by column chromatography (0-5% 7N NH_3 in MeOH in DCM), affording the desired product as a white solid. Yield: 104 mg (0.2 mmol, 48%). LC-MS; *m*/*z*: 522.3 $[M+H]^+$. ^{1}H NMR (400 MHz, $CDCl_3$ + MeOD-d_4) δ 6.78 (s, CH, 1H), 4.53 (s, CH_2, 2H), 4.39 – 4.24 (m, CH, 1H), 4.18 (s, CH_2, 2H), 3.16-3.10 (m, CH, 1H), 2.14 – 1.57 (m, CH_2, 12H), 1.53 (s, $2CH_3$, 6H), 1.51 – 1.45 (m, CH_2, 1H), 1.37 (s, Boc, 9H), 1.32 – 1.01 (m, CH_2, 6H).

(6,6-dimethyl-5,6-dihydroimidazo[2,1-*b*]thiazol-3-yl)methyl (*E*)-*N*'-((1*r*,4*r*)-4-aminocyclo-hexyl)-*N*-cyclohexylcarbamimidothioate (8):



104 mg of carbamate **7** was stirred in a 10 mL solution of DCM and TFA (4:1) at room temperature. After TLC and LCMS showed complete deprotection of the primary amine (mass found: 422.4; M+H), the solvents were removed *in vacuo* and the TFA was removed under high vacuum. The crude was purified by column chromatography using 0-10% 7N NH_3 in MeOH in DCM as eluent, affording the desired product as a colourless oil. Yield: 84 mg (0.19 mmol, quant.). LC-MS; *m*/*z*: 422.4 $[M+H]^+$. ^1H NMR (400 MHz, MeOD-d_4) δ 6.93 (s, CH, 1H), 4.58 (s, CH_2, 2H), 4.33 (s, CH_2, 2H), 3.95-3.82 (m, CH, 1H), 3.18-3.15 (m, 2CH, 2H), 2.25-2.08 (m, CH_2, 7H), 2.03-1.80 (m, CH_2, 8H), 1.60-1.57 (m, CH_3, 3H), 1.49 (s, CH_3, 3H), 1.44-1.37 (m, CH_2, 3H). ^{13}C NMR (101 MHz, MeOD-d_4) δ 170.51, 162.87, 162.52, 111.40, 71.26, 66.87, 64.51, 59.43, 58.96, 30.26, 30.15, 29.98, 29.88, 29.61, 28.02, 27.49, 26.76, 25.85.

(6,6-dimethyl-5,6-dihydroimidazo[2,1-*b*]thiazol-3-yl)methyl (*E*)-*N*-cyclohexyl-*N*'-((1*r*,4*r*)-4-(6-(2-(4-((*E*)-2-(5,5-difluoro-7-(thiophen-2-yl)-5*H*-4λ^4,5λ^4-dipyrrolo[1,2-c:2',1'-*f*][1,3,2]diazaborinin-3-yl)vinyl)phenoxy)acetamido)hexanamido)cyclo-hexyl)carbamimidothioate (9):

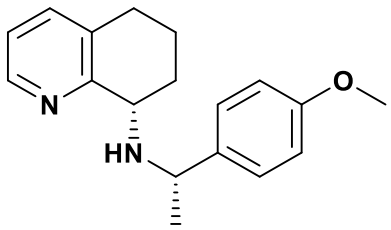


BODIPY 630/650-X succinimidyl ester (1 mg, 1.5 pmol) was dissolved in 1 mL acetonitrile, and to it were added DIPEA (2 µL, 4 eq.) and compound **8** (2.0 mg, 3 eq.). The reaction mixture was left to stir overnight in an amber coloured flask. After 16 hours LCMS showed complete conversion of the BODIPY into the fluorescent conjugate

(mass found: 968.2; M+H), so solvents were evaporated and the crude mixture was purified by preparative RP-HPLC (5-95% solvent B, 30 min). Yield: 0.9 mg (62%). Purity of the compound was confirmed to be >95% by LC-MS using a long method run. HRMS calculated for $C_{50}H_{61}B_1F_2N_8O_3S_3$: 967.4168 found: 967.4238 $[M+H]^+$.

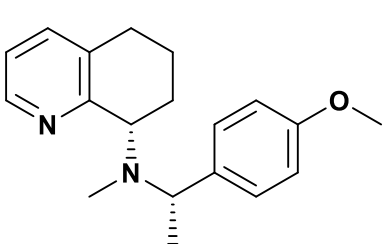
7.3.2 Synthesis of fluorescent isoquinoline-based probes

(*S*)-*N*-((*S*)-1-(4-methoxyphenyl)ethyl)-5,6,7,8-tetrahydroquinolin-8-amine (10):



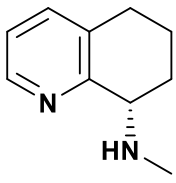
6,7-dihydroquinolin-8(5*H*)-one (1.0 g, 6.79 mmol) was dissolved in 40 mL DCM. To this solution was added $NaBH(OAc)_3$ (2.88 g, 2 eq.) and (*S*)-1-(4-methoxyphenyl)ethan-1-amine (1.0 mL, 1 eq.), and the reaction was left to stir under a N_2 atmosphere for 20 hours. Upon completion (TLC) the reaction was quenched with 1M NaOH, and the pH was adjusted to 8.0. The layers where separated and the organic layer was washed with 1M NaOH, adjusting the pH to 11.0. The product was extracted with DCM (3 x 60 mL) after which the organic layers were combined, dried and concentrated *in vacuo*. Column purification was performed using 1-2% 7N NH_3 in MeOH in DCM as eluent, affording the desired fragment as a colourless solid. Yield: 1.21 g (63%). LCMS: 583.2 [M+H]. ^{1}H NMR (400 MHz, $CDCl_3$): δ 8.1 (d, *J* = 4 Hz, CH_{Ar}, 1H), 7.40 – 7.30 (m, CH_{Ar}, 3H), 7.06 (dd, *J* = 7.7 Hz, *J* = 4.7 Hz, CH_{Ar}, 1H), 6.90 – 6.81 (d, *J* = 8.0 Hz, CH_{Ar}, 2H), 4.05 (q, *J* = 6.6 Hz, **CH**CH_3, 1H), 3.83 (dd, *J* = 7.7 Hz, *J* = 5.3 Hz, CH, 1H), 3.80 (s, CH_3, 3H), 2.81 – 2.60 (m, CH_2, 2H), 1.91 – 1.78 (m, CH_2, 1H), 1.78-1.70 (m, CH_2, 1H), 1.63 – 1.48 (m, CH_2, 2H), 1.45 (d, *J* = 8.0 Hz, CH_3, 3H).

(*S*)-*N*-((*S*)-1-(4-methoxyphenyl)ethyl)-*N*-methyl-5,6,7,8-tetrahydroquinolin-8-amine (11):



Intermediate **10** (1.6 g, 5.67 mmol) of was dissolved in 40 mL DCE, and to it were added $NaBH(OAc)_3$ (2.4 g, 2 eq.), formaldehyde (0.85 mL, 1.5 eq., 37% wt in H_2O), and glacial AcOH (0.5 mL, 1.5 eq.). This slurry was left to stir under a N_2 atmosphere for 16 hours. Upon completion the reaction mixture was diluted with 50 mL DCM and quenched with 60 mL saturated $NaHCO_3$. This was stirred vigorously for 30 minutes. The layers were separated and the aqueous was extracted with DCM (2 x 50 mL). The combined organic layers were washed with brine (2 x 100 mL), dried over $MgSO_4$ and evaporated to dryness *in vacuo*. No further purification was required, and the desired product was yielded as brownish solids. Yield: 1.77 g (quant.). LC-MS; *m/z*: 297.2 $[M+H]^+$. ^1H NMR (400 MHz, $CDCl_3$): δ 8.48 (d, *J* = 4.6 Hz, CH_{Ar}, 1H), 7.47 – 7.39 (m, CH_{Ar}, 2H), 7.30 (ddt, *J* = 7.7 Hz, *J* = 1.9 Hz, *J* = 0.9 Hz, CH_{Ar}, 1H), 7.01 (ddd, *J* = 7.6 Hz, *J* = 4.7 Hz, *J* = 0.6 Hz, CH_{Ar}, 1H), 6.90 – 6.81 (m, CH_{Ar}, 2H), 4.44 (q, *J* = 6.7 Hz, **CH**CH_3, 1H), 4.01 (dd, *J* = 8.2 Hz, *J* = 6.2 Hz, CH, 1H), 3.79 (s, CH_3, 3H), 2.87 – 2.74 (m, CH_2, 1H), 2.62 (dt, *J* = 16.9 Hz, *J* = 4.9 Hz, CH_2, 1H), 2.03 (s, CH_3, 3H), 2.00 – 1.83 (m, CH_2, 2H), 1.64 – 1.51 (m, CH_2, 1H), 1.39 (d, *J* = 6.7 Hz, CH_3, 3H). ^{13}C NMR (101 MHz) δ 159.01, 158.20, 146.61, 138.56, 136.24, 134.12, 129.04, 128.69, 128.23, 125.31, 121.09, 113.47, 77.38, 77.27, 77.06, 76.75, 60.85, 59.69, 55.22, 34.01, 29.19, 27.62, 21.48, 21.09, 20.13.

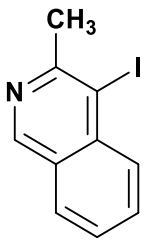
(*S*)-*N*-methyl-5,6,7,8-tetrahydroquinolin-8-amine (12):



Intermediate **11** (1.77 g, 5.97 mmol) was taken up in 30 mL solution of DCM and TFA (4:1) and left to stir at room temperature for 1.5 hours. Over the course of the reaction the colour of the solution went from a transparent colour to dark purple. The solvents were removed *in vacuo*, and the purple oil was partitioned between 0.5N HCl and EtOAc. The layers were separated and the aqueous was washed 3x with

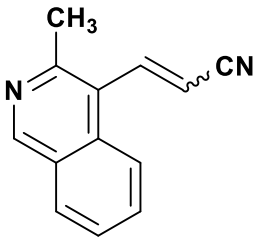
EtOAc. The organic layers were discarded and the pH of the aqueous layer was adjusted to 12.0 using concentrated NaOH. The product was extracted using DCM (5 x 100 mL) and the combined organics were dried over $MgSO_4$ and evaporated until dryness. The freebase product proved to be unstable so for storage purposes this was kept as an HCl salt. This was afforded by stirring the freebase in a 4N solution of HCl in dioxane. The product was then crashed out by triturating with diethylether, affording brown solids. Yield: 1.18 g (96%). ^{1}H NMR (400 MHz, DMSO-d_6) δ 8.49 (dd, *J* = 4.8, *J* = 1.5 Hz, CH_{Ar}, 1H), 7.67 (dd, *J* = 7.8 Hz, *J* = 1.6 Hz, CH_{Ar}, 1H), 7.37 (dd, *J* = 7.8 Hz, *J* = 4.7 Hz, CH_{Ar}, 1H), 4.37 (dd, *J* = 9.7 Hz, *J* = 5.6 Hz, CH, 1H), 2.81 (dd, *J* = 7.6 Hz, *J* = 4.9 Hz, CH_2, 2H), 2.63 (s, CH_3, 3H), 2.31 (ddt, *J* = 11.8 Hz, *J* = 6.1 Hz, *J* = 3.1 Hz, CH_2, 1H), 2.08 – 1.93 (m, CH_2, 1H), 1.91 – 1.67 (m, CH_2, 2H). ^{13}C NMR (101 MHz) δ 150.37, 146.44, 139.25, 134.50, 124.44, 56.99, 40.62, 40.41, 40.20, 39.99, 39.78, 39.57, 39.37, 30.69, 27.60, 24.55, 19.41.

4-iodo-3-methylisoquinoline (13):



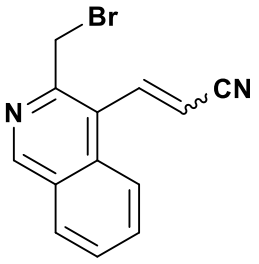
To a roundbottom flask containing 10 mL glacial acetic acid was added 3-methylisoquinoline (285 mg, 2.0 mmol) and *N*-iodosuccinimide (495 mg, 1.1 eq.), and the reaction was stirred at 80 °C for 16 hours. Upon completion (TLC) the reaction mixture was quenched with saturated $NaHCO_3$ while keeping the roundbottom flask on ice. The product was extracted from the aqueous by DCM (3 x 100 mL), washed with brine, and dried over $MgSO_4$. Column chromatography using 5% EtOAc in DCM as eluent yielded the title compound as a light yellow crystalline solid. Yield: 0.278 g (1 mmol, 51.6%). LC-MS; *m*/*z*: 270.1 $[M+H]^+$. ^{1}H NMR (400 MHz, $CDCl_3$) δ 9.03 (s, CH_{Ar}, 1H), 8.08 (dd, *J* = 8.6 Hz, *J* = 1.1 Hz, CH_{Ar}, 1H), 7.87 (d, J = 8.1 Hz, CH_{Ar}, 1H), 7.75 (ddd, J = 8.4 Hz, *J* = 6.9 Hz, *J* = 1.3 Hz, CH_{Ar}, 1H), 7.59 (ddd, J = 8.0 Hz, *J* = 6.9 Hz, *J* = 1.0 Hz, CH_{Ar}, 1H), 2.99 (s, CH_3, 3H).

3-(3-methylisoquinolin-4-yl)acrylonitrile (14):



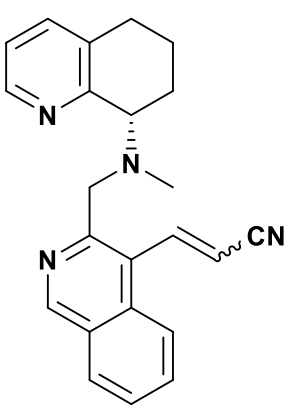
To a microwave vessel were added 4-iodo-3-methylisoquinoline intermediate **13** (0.457 g, 1.7 mmol), acrylonitrile (1.5 eq.), and 4 mL DMF. The microwave vessel was capped and flushed with nitrogen before were added $Pd(OAc)_2$ (5 mol%), triphenylphosphine (10 mol%), and TEA (3 eq.). The reaction was carried out in a microwave at 130 °C for 3 hours. Upon completion of the reaction (TLC), solvents were removed under high vacuum and the crude was purified by column chromatography using a gradient of 5% EtOAc in DCM to 5% MeOH in DCM, yielding a mixture of E/Z and brownish solids. Yield: 0.298 g (1.5 mmol, 89%). LC-MS; *m*/*z*: 195.1 $[M+H]^+$. ^1H NMR (400 MHz, $CDCl_3$) δ 9.15 (s, CH_{Ar}, 1H), 7.96 (d, *J* = 8.2 Hz, CH_{Ar}, 1H), 7.91- 7.83 (m, CH_{Ar}, 1H), 7.75-7.45 (m, CH_{Ar}, CH, 3H), 5.90 (dd, *J* = 11.52 Hz, *J* = 16 Hz, CH, 1H), 2.71 (s, CH_3, 3H).

3-(3-(bromomethyl)isoquinolin-4-yl)acrylonitrile (15):



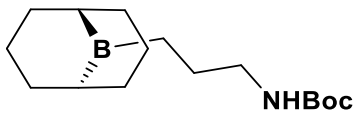
Isoquinoline **14** (48.5 mg, 0.25 mmol) was dissolved in 7 mL DCE, and to it were added AIBN (10 mg, 20 mol%), and NBS (70 mg, 1.3 eq.) This solution was stirred at 80 °C and after 4 hours LC-MS showed complete conversion of starting material to the product (*m*/*z*: 274.8; $[M+H]^+$). Due to observed decomposition of the product, the reaction mixture was concentrated *in vacuo* and directly used in the next step without any purification.

(*S*)-3-(3-((methyl(5,6,7,8-tetrahydroquinolin-8-yl)amino)methyl)isoquinolin-4-yl)acrylonitrile (16):



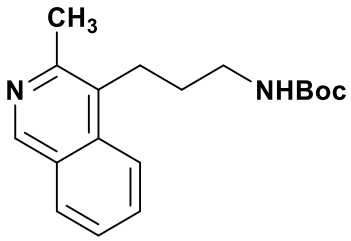
100 mg of crude **15** was dissolved in 10 mL acetonitrile and to it were added DIPEA (3 eq.) and amine fragment **12** (75 mg, 0.38 mmol. Under a N_2 atmosphere this mixture was stirred at room temperature for 20 hours. Upon completion (TLC) the mixture was concentrated *in vacuo* and purified by column chromatography using a gradient of 1-5% 7N NH_3 in MeOH in DCM as eluent. The product was isolated as a brown oil. Yield: 62 mg (0.17 mmol, 46%). LC-MS; *m*/*z*: 355.3 $[M+H]^+$. ^1H NMR (400 MHz, $CDCl_3$) δ 9.16 (s, CH_{Ar}, 1H), 8.58 (dd, *J* = 4.7 Hz, 1.7 Hz, CH_{Ar}, 1H), 8.34 (d, *J* = 16.8 Hz, CH_{Ar}, 1H), 7.99 (ddt, *J* = 17.8 Hz, *J* = 8.0 Hz, *J* = 0.9 Hz, CH_{Ar}, 2H), 7.73 (ddd, *J* = 8.5 Hz, *J* = 6.9 Hz, *J* = 1.4 Hz, CH_{Ar}, 1H), 7.60 (ddd, *J* = 8.0 Hz, *J* = 6.9 Hz, *J* = 1.1 Hz, CH_{Ar}, 1H), 7.37 (d, *J* = 7.7 Hz, CH, 1H), 7.07 (dd, *J* = 7.7 Hz, *J* = 4.7 Hz, CH_{Ar}, 1H), 6.39 (d, *J* = 16.8 Hz, CH, 1H), 4.15 – 3.93 (m, CH_2, CH, 3H), 2.92 – 2.79 (m, CH, 1H), 2.72 (s, 3H), 2.20 (s, CH_2, 2H), 2.15 – 1.99 (m, CH_2, 2H), 1.83 – 1.63 (m, CH_2, 1H).

***Tert*-butyl (3-((1*r*,5*r*)-9-borabicyclo[3.3.1]nonan-9-yl)propyl)carbamate (18):**



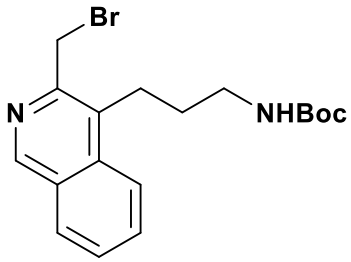
A roundbottom flask containing 7 mL of a 0.5M solution of 9-BBN in THF was cooled to 0°C and to it was added t*ert*-butyl *N*-allylcarbamate (20 mg, 3.2 mmol). This mixture was stirred at 0°C for 1.5 hours, after which the reaction mixture was allowed to warm to room temperature and stirred for another 1.5 hours. The hydroborated product was directly used in the next step without isolation of the intermediate.

***Tert*-butyl (3-(3-methylisoquinolin-4-yl)propyl)carbamate (19):**



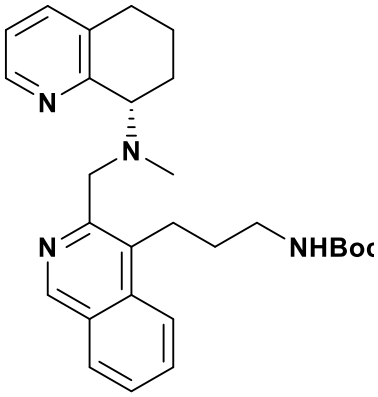
The reaction mixture from the previous step, containing the hydroborated allyl carbamate **18**, was transferred into a microwave vessel and to it were added isoquinoline **13** (0.69 g, 0.8 eq.), 1M KOH in H_2O (2.5 mL), and $Pd(PPh_3)_4$ (10 mol%). The reaction was conducted *via* microwave assistance, at 80 °C for 1 hour. The reaction mixture was poured onto brine and extracted with EtOAc (2 x 50 mL). The organics were combined, dried over $MgSO_4$ and concentrated *in vacuo*. The product was purified by column chromatography using 20-100% EtOAc in Pet, yielding a light yellow oil. Yield: 209 mg (0.7 mmol, 27% over 2 steps). LC-MS; *m*/*z*: 301.3 $[M+H]^+$. ^{1}H NMR (400 MHz, $CDCl_3$) δ 9.05 (s, CH_{Ar}, 1H), 7.93 (td, *J* = 8.6 Hz, *J* = 7.9 Hz, *J* = 1.0 Hz, CH_{Ar}, 2H), 7.68 (ddd, *J* = 8.5 Hz, *J* = 6.8 Hz, *J* = 1.4 Hz, CH_{Ar}, 1H), 7.51 (ddd, *J* = 8.0 Hz, *J* = 6.8 Hz, *J* = 1.1 Hz, CH_{Ar}, 1H), 4.81 (s, NH, 1H), 3.33 – 3.23 (m, CH_2, 2H), 3.13 – 2.99 (m, CH_2, 2H), 2.71 (s, CH_3, 3H), 1.95 – 1.76 (m, CH_2, 2H), 1.46 (s, Boc, 9H). ^{13}C NMR (101 MHz, $CDCl_3$) δ 156.07, 150.07, 148.97, 135.03, 130.29, 128.28, 127.58, 127.31, 125.75, 122.40, 40.77, 32.87, 30.25, 28.42, 25.41, 22.16.

***Tert*-butyl (3-(3-(bromomethyl)isoquinolin-4-yl)propyl)carbamate (20):**



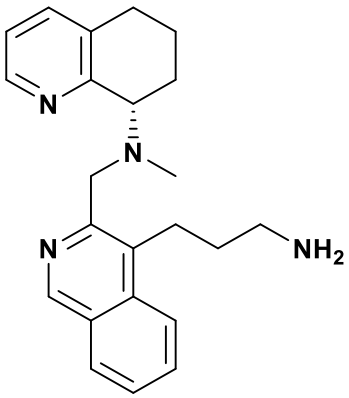
A roundbottom flask containing 10 mL DCE was charged with methylisoquinoline **19** (0.209g, 0.7 mmol), NBS (0.173g, 1.3 eq.), and AIBN (0.023g, 20 mol%). Under a N_2 atmosphere, the reaction was carried out at 80 °C for 3 hours. When LCMS showed ~70% conversion of the starting material to the product, the solvents were removed *in vacuo* and the crude product was carried over to the next step without further purification due to the instability of the product.

***Tert*-butyl (*S*)-(3-(3-((methyl(5,6,7,8-tetrahydroquinolin-8-yl)amino)methyl)isoquinolin-4-yl)propyl)carbamate (21):**



The concentrated crude from the previous step was redissolved in 10 mL MeCN. To it were added amine fragment **12** (97 mg, 0.8 eq.) and DIPEA (0.5 mL, 4 eq.), and the reaction was stirred at room temperature overnight. Upon completion (TLC) the solvents were evaporated and the product was purified by column chromatography using a system of EtOAc in Pet (1:1) as eluent, followed by 2-5% 7N NH_3 in MeOH in DCM. The product was isolated as a brown solid. Yield: 55 mg (0.12 mmol, 21% over 2 steps). LC-MS; *m*/*z*: 461.3 $[M+H]^+$. ^1H NMR (400 MHz, $CDCl_3$) δ 9.07 (s, CH_{Ar}, 1H), 8.55 (dd, *J* = 4.8 Hz, *J* = 1.7 Hz, CH_{Ar}, 1H), 7.99 (dt, *J* = 8.6 Hz, *J* = 0.9 Hz, CH_{Ar}, 1H), 7.92 (dt, *J* = 8.1 Hz, *J* = 1.0 Hz, CH_{Ar}, 1H), 7.67 (ddd, *J* = 8.5 Hz, *J* = 6.8 Hz, *J* = 1.4 Hz, CH_{Ar}, 1H), 7.53 (ddd, *J* = 7.9 Hz, *J* = 6.8 Hz, *J* = 1.0 Hz, CH_{Ar}, 1H), 7.36 (ddt, *J* = 7.8 Hz, *J* = 1.9 Hz, *J* = 1.0 Hz, CH_{Ar}, 1H), 7.06 (ddd, *J* = 7.7 Hz, *J* = 4.7 Hz, *J* = 0.6 Hz, CH_{Ar}, 1H), 4.86 (s, NH, 1H), 4.16 – 4.00 (m, CH_2, CH, 3H), 3.26 (t, *J* = 8.0 Hz, CH_2, 2H), 2.93 – 2.62 (m, CH_2, 4H), 2.27 (s, CH_3, 3H), 2.12 (dtd, *J* = 8.8 Hz, *J* = 5.5 Hz, *J* = 2.6 Hz, CH_2, 2H), 2.08 – 1.98 (m, CH_2, 1H), 1.95 – 1.75 (m, CH_2, 2H), 1.68 (tdd, *J* = 13.4 Hz, *J* = 9.9 Hz, *J* = 5.2 Hz, CH_2, 1H), 1.47 (s, Boc, 9H).

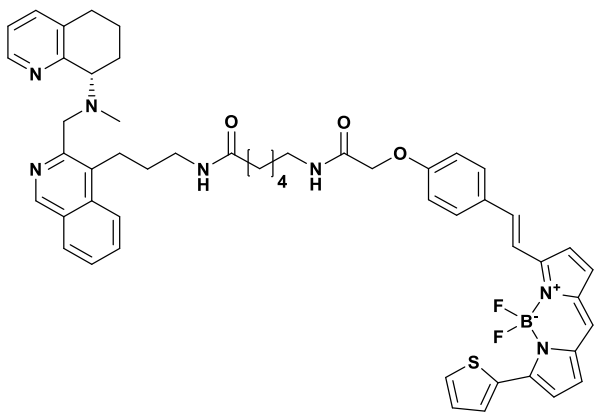
(*S*)-*N*-((4-(3-aminopropyl)isoquinolin-3-yl)methyl)-*N*-methyl-5,6,7,8-tetrahydroquinolin-8-amine (17):



Compound **21** was taken up in a 4:1 solution of DCM and TFA, and was stirred for 1 hour at room temperature. Upon completion (TLC), the reaction mixture was concentrated *in vacuo* and residual TFA was removed under high vacuum. Column chromatography using 5% 7N NH_3 in MeOH in DCM afforded the congener as a colourless oil. Yield: 21

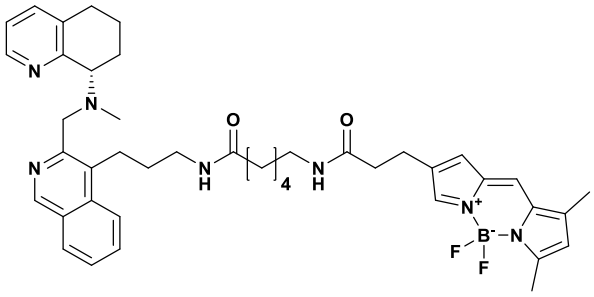
mg (0.06 mmol, 49%). LC-MS; *m*/*z*: 361.4 $[M+H]^+$. ^{1}H NMR (400 MHz, MeOD-d_4) δ 9.02 (s, CH_{Ar}, 1H), 8.44 (dd, *J* = 4.8 Hz, *J* = 1.6 Hz, CH_{Ar}, 1H), 8.13 (dd, *J* = 8.7 Hz, *J* = 1.0 Hz, CH_{Ar}, 1H), 8.05 (dt, *J* = 8.1 Hz, *J* = 1.0 Hz, CH_{Ar}, 1H), 7.79 (ddd, *J* = 8.4 Hz, *J* = 6.8 Hz, *J* = 1.3 Hz, CH_{Ar}, 1H), 7.64 (ddd, *J* = 8.0 Hz, *J* = 6.8 Hz, *J* = 1.0 Hz, CH_{Ar}, 1H), 7.55 (ddd, *J* = 7.8 Hz, *J* = 1.8 Hz, *J* = 0.9 Hz, CH_{Ar}, 1H), 7.22 (dd, *J* = 7.7 Hz, *J* = 4.8 Hz, CH_{Ar}, 1H), 4.08 – 3.90 (m, CH_2, CH, 3H), 3.29 – 3.15 (m, CH_2, 2H), 2.90 (ddd, *J* = 15.4, 9.5, 5.3 Hz, CH_2, 1H), 2.82 – 2.67 (m, CH_2, 3H), 2.29 – 1.96 (m, CH_3, CH_2, 5H), 1.96 – 1.52 (m, CH_2, 2H). ^{13}C NMR (101 MHz, MeOD-d_4) δ 158.02, 150.56, 149.88, 147.40, 138.87, 136.79, 136.45, 133.04, 132.07, 129.48, 128.21, 124.37, 123.58, 64.89, 58.93, 41.88, 38.64, 33.20, 29.87, 25.37, 23.96, 21.79.

(*S*,*E*)-6-(2-(4-(2-(5,5-difluoro-7-(thiophen-2-yl)-5*H*-4λ^4,5λ^4-dipyrrolo[1,2-*c*:2',1'-*f*][1,3,2]diazaborinin-3-yl)vinyl)phenoxy)acetamido)-*N*-(3-(3-((methyl(5,6,7,8-tetrahydroquinolin-8-yl)amino)methyl)isoquinolin-4-yl)propyl)hexanamide (22):



BODIPY 630/650-X succinimide ester (1.0 mg, 1.5 pmol) was dissolved in 1 mL MeCN, and to it were added compound **21** (1.0 mg, 1.9 eq.) and DIPEA (2 µL, 4 eq.). This mixture was left to stir in an amber vial for 4 hours. LCMS showed complete consumption of the BODIPY dye, so solvents were evaporated *in vacuo* after which the crude was purified by preparative RP-HPLC (5-95% solvent B, 30 min). Yield: 1.3 mg (51%). Purity of the compound was confirmed to be >95% by LC-MS using a long method run. HRMS calculated for $C_{52}H_{55}BF_2N_7O_3S$: 906.4143 found: 906.4190 $[M+H]^+$.

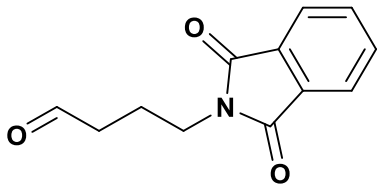
(*S*)-6-(3-(5,5-difluoro-7,9-dimethyl-5*H*-4λ^4,5λ^4-dipyrrolo[1,2-*c*:2',1'-*f*][1,3,2]diazaborinin-2-yl)propanamido)-*N*-(3-(3-((methyl(5,6,7,8-tetrahydroquinolin-8-yl)amino)methyl)isoquinolin-4-yl)propyl)hexanamide (23):



BODIPY FL-X succinimidyl ester (1.2 mg, 3 pmol) was dissolved in 1 mL acetonitrile. To it were added compound **21** (1.0 mg, 2.8 pmol) and DIPEA (2 µL, 4 eq.), and the reaction was stirred in an amber vial for 72 hours. The solvents were removed *in vacuo* and the crude product was purified by preparative RP-HPLC (5-95% solvent B, 30 min). Yield: 1.0 mg (55%). Purity of the compound was confirmed to be >95% by LC-MS using a long method run. HRMS calculated for $C_{43}H_{53}BF_2N_7O_2$: 748.4316 found: 748.4322 $[M+H]^+$.

7.3.3 Synthesis of fluorescent AMD070-based probes

4-(1,3-dioxoisoindolin-2-yl)butanal (24):

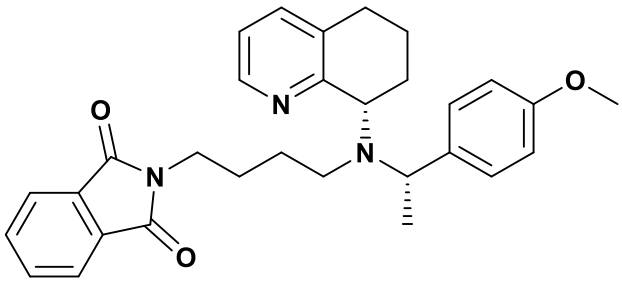


This fragment was synthesised in two steps. Step one: 4-amino-1-butanol (0.2 mL, 2.2 mmol) was taken up in 25 mL toluene. To this were added phthalic anhydride (0.321 g, 1 eq.) and molecular sieves (4 Å), and the mixture was maintained at refluxing temperatures for 3 hours. Upon completion (TLC) the solvents were removed and the crude was purified by column chromatography using 0-2% MeOH in $CHCl_3$ as eluent. Yield: 0.26 g (1.2 mmol, 53%). ^{1}H NMR (400 MHz, $CDCl_3$) δ 7.80 (dd, *J* = 5.2 Hz, *J* = 2.5 Hz, CH_{Ar}, 2H), 7.68 (dd, *J* = 5.5 Hz, *J* = 3.1 Hz, CH_{Ar}, 2H), 3.67 (dt, *J* = 15.6 Hz, *J* = 6.9 Hz, CH_2, 4H), 2.26 – 2.14 (m, OH, 1H), 1.84 – 1.68 (m, CH_2, 2H), 1.66 – 1.52 (m, CH_2, 2H).

Step two: 0.196g (0.9 mmol) of the intermediate phthalimide was dissolved in 5 mL DCM and was dropwise added to a stirring solution of DMP (0.569g, 1.5 eq.) in 15 mL which was being maintained at 0 °C. After dropwise addition the mixture was slowly

allowed to warm to room temperature, at which it was maintained for 1.5 hours. Upon completion of the reaction, the reaction mixture was concentrated to 1/3rd of its original volume and diethylether was added. This was then washed with saturated solutions of $Na_2S_2O_3$ and $NaHCO_3$. The organic solvent was dried over $MgSO_4$ and finally removed *in vacuo*, affording the desired aldehyde as a colourless oil. Yield: 0.143g (0.66 mmol, 74%). LC-MS; *m*/*z*: 218.1 $[M+H]^+$. ^{1}H NMR (400 MHz, $CDCl_3$) δ 9.77 (d, *J* = 1.2 Hz, CHO, 1H), 7.84 (dd, *J* = 5.4 Hz, *J* = 3.1 Hz, CH_{Ar}, 2H), 7.72 (dd, *J* = 5.4 Hz, *J* = 3.1 Hz, CH_{Ar}, 2H), 3.74 (t, *J* = 6.8 Hz, CH_2, 2H), 2.54 (t, *J* = 7.3 Hz, CH_2, 2H), 2.02 (p, *J* = 7.0 Hz, CH_2, 2H). ^{13}C NMR (101 MHz, $CDCl_3$) δ 200.97, 168.50, 134.16, 132.13, 123.42, 41.23, 37.26, 21.31.

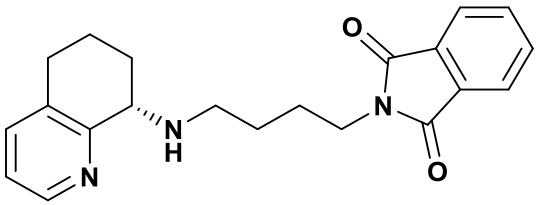
2-(4-(((*S*)-1-(4-methoxyphenyl)ethyl)((*S*)-5,6,7,8-tetrahydroquinolin-8-yl)amino)butyl)iso-indoline-1,3-dione (25):



$NaBH(OAc)_3$ (0.156g, 2 eq.) was stirred in 15 mL DCM and to it were added aldehyde **24** (80mg, 0.37 mmol), and chiral amine **10** (0.104g, 1 eq.), and the reaction was stirred under a N_2 atmosphere overnight. Upon completion of the reaction (TLC), the reaction mixture was diluted with DCM and added to a vigorously stirring solution of saturated aqueous $NaHCO_3$. After 15 minutes the layers were separated, the aqueous washed with DCM, and the combined organics washed with brine. After drying over $MgSO_4$, the solvents were evaporated and the crude was purified by column chromatography using 2-10% MeOH in DCM as eluent. The product was isolated as a white solid. Yield: 0.123g (0.25 mmol, 69%). LC-MS; *m*/*z*: 484.3 $[M+H]^+$. ^{1}H NMR (400 MHz, $CDCl_3$) δ 8.37 (s, CH_{Ar}, 1H), 7.80 (dt, *J* = 5.6 Hz, *J* = 2.9 Hz, CH_{Ar}, 2H), 7.70 (dq, *J* = 7.1 Hz, *J* = 4.2 Hz, CH_{Ar}, 2H), 7.39 (s, CH_{Ar}, 2H), 7.16 (d, *J* = 7.6 Hz, CH_{Ar}, 1H), 6.94-6.80 (m, CH_{Ar}, 3H), 4.48 (br s, CH, 1H) 3.95 (br s, CH, 1H), 3.77 (s, CH_3, 3H), 3.48-3.42 (m, CH_2, CH, 3H), 2.91 – 2.70 (m, CH, 1H), 2.61 (dt, *J* = 16.8 Hz, *J* = 5.1 Hz, CH_2, 1H), 2.57-2.38 (m, CH_2, 2H), 2.17 – 1.70 (m, CH_2, 4H), 1.64-1.51 (m, CH_2, 1H), 1.45-1.25 (m, CH_2, CH_3, 5H), 1.01-

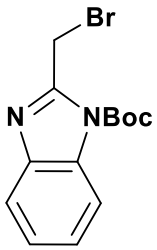
0.91 (m, CH_2, 1H). ^{13}C NMR (101 MHz, $CDCl_3$) δ 168.24, 146.73, 146.37, 133.81, 132.14, 128.78, 123.09, 121.24, 118.08, 113.28, 60.16, 55.20, 47.14, 37.94, 29.50, 29.24, 28.84, 26.32, 20.57, 18.87.

(*S*)-2-(4-((5,6,7,8-tetrahydroquinolin-8-yl)amino)butyl)isoindoline-1,3-dione (26):



To a roundbottom flask containing a 20 mL solution of DCM and TFA (1:1) was added compound **25** (0.115g, 0.24 mmol). This was stirred at room temperature for 30 minutes, after which LCMS showed complete conversion to the product (mass found: 350.1; M+H). The reaction mixture was concentrated *in vacuo* and residual TFA was removed under high vacuum. For storage purposes the product was kept as an oxalate salt. This was done by dissolving the product in 10 mL IPA and adding oxalic acid (32 mg, 1.3 eq.), after which it was stirred for 10 minutes and subsequent evaporation of the solvents, yielding a colourless oil. Yield: 0.105 g (0.24 mmol, quant.). LC-MS; *m*/*z*: 350.1 $[M+H]^+$. ^1H NMR (400 MHz, DMSO-d_6) δ 8.87 (s, NH_2^+, 2H), 8.48 (d, *J* = 4.7 Hz, CH_{Ar}, 1H), 7.94 – 7.79 (m, CH_{Ar}, 4H), 7.66 (d, *J* = 7.8 Hz, CH_{Ar}, 1H), 7.37 (dd, *J* = 7.8 Hz, *J* = 4.7 Hz, CH_{Ar}, 1H), 3.73 – 3.65 (m, CH, 1H), 3.61 (t, *J* = 4.0 Hz *J* = 8.0 Hz, CH_2, 2H), 3.02-2.04 (m, CH_2, 2H), 2.81-2.78 (m, CH_2, 2H), 2.32 (dd, *J* = 11.4 Hz, *J* = 4.9 Hz, CH_2, 1H), 1.98 (dd, *J* = 11.3 Hz, *J* = 5.4 Hz, CH_2, 1H), 1.90 – 1.58 (m, CH_2, 6H). ^{13}C NMR (101 MHz, DMSO-d_6) δ 168.46, 161.44, 158.78, 158.43, 151.10, 147.15, 138.31, 134.94, 133.93, 132.07, 124.15, 123.53, 62.49, 56.38, 44.17, 37.32, 27.60, 25.95, 25.63, 25.13, 23.59, 19.83.

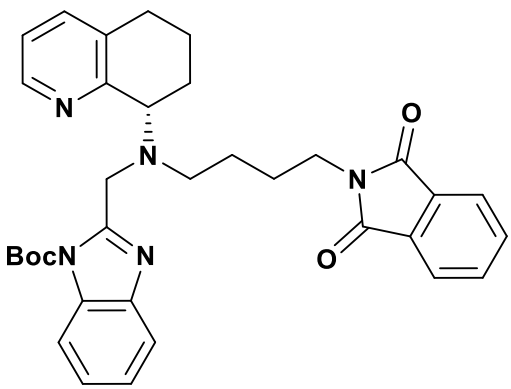
***Tert*-butyl 2-(bromomethyl)-1*H*-benzo[*d*]imidazole-1-carboxylate (27):**



This fragment was synthesised in two steps. Step one: 2-methylbenzimidazole (1.0g, 0.76 mmol) was added to a roundbottom flask containing 25 mL DCM and to it were added TEA (1.1 mL, 1.05 eq.), DMAP (46 mg, 5 mol%), and Boc anhydride (2.5g, 2 eq.). The reaction was stirred at room temperature for 5 minutes, before being concentrated *in vacuo*. The residue was taken up in 20 mL H_2O and stirred for 15 minutes. The solids were filtered off, washed, dissolved in DCM and the organics were dried over $MgSO_4$, after which the DCM was removed. Yield: 1.66 g (7.2 mmol, 95%). ^{1}H NMR (400 MHz, $CDCl_3$) δ 7.95 – 7.84 (m, CH_{Ar}, 1H), 7.67 – 7.58 (m, CH_{Ar}, 1H), 7.38 – 7.20 (m, CH_{Ar}, 2H), 2.80 (s, CH_3, 3H), 1.69 (s, Boc, 9H).

Step two: 1.6g, 7.2 mmol, of the Boc-protected imidazole intermediate was dissolved in 35 mL DCE and to it were added NBS (1.4g, 1.1 eq.), and AIBN (0.3g, 25 mol%) and the reaction was heated at 95 °C for 6 hours. The reaction mixture was then concentrated *in vacuo* and purified by column chromatography using 5-10% EtOAc in Pet as eluent, isolating the desired product as a white solid. Yield: 1.47g (4.7 mmol, 66%). ^{1}H NMR (400 MHz, $CDCl_3$) δ 8.04 – 7.93 (m, CH_{Ar}, 1H), 7.80 – 7.68 (m, CH_{Ar}, 1H), 7.45 – 7.31 (m, CH_{Ar}, 2H), 5.07 (s, CH_2Br, 0.5H), 4.96 (s, CH_2Br, 1.5H), 1.74 (s, Boc, 9H). ^{13}C NMR (101 MHz, $CDCl_3$) δ 150.55, 141.91, 133.49, 125.87, 125.83, 124.81, 124.77, 120.62, 120.55, 115.31, 115.26, 86.65, 28.10, 25.31, 23.60.

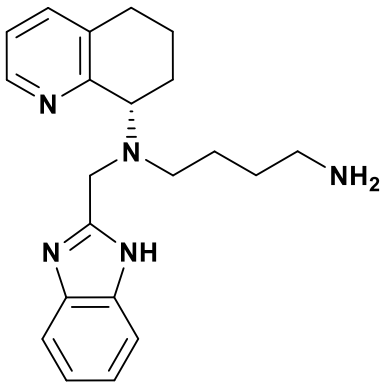
***Tert*-butyl (*S*)-2-(((4-(1,3-dioxoisoindolin-2-yl)butyl)(5,6,7,8-tetrahydroquinolin-8-yl)amino)methyl)-1*H*-benzo[*d*]imidazole-1-carboxylate (28):**



To a microwave vessel were added amine fragment **26** (0.075g, 0.17 mmol), **27** (0.05g, 0.16 mmol), TEA (0.1 mL, 3 eq.), KI (5 mg, 20 mol%), and 3 mL MeCN. This mixture was heated in a microwave for 1 hour at 80 °C. Upon completion, the mixture was dryloaded

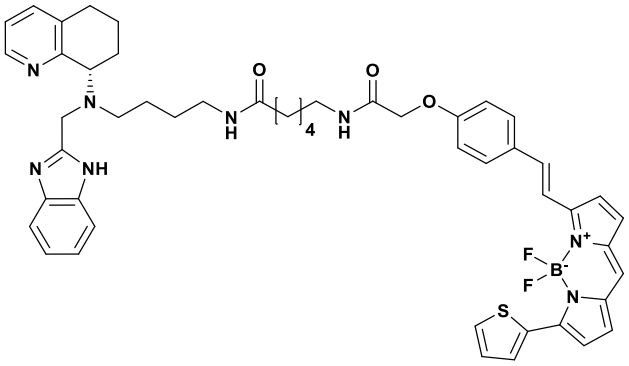
onto a column of silica and purified using 0-10% MeOH in DCM as eluent. The product was isolated as a brownish oil. Yield: 25 mg (0.04 mmol, 27%). LC-MS; *m*/*z*: 580.3 $[M+H]^+$. ^{1}H NMR (400 MHz, $CDCl_3$) δ 8.58 (d, *J* = 4.8 Hz, *J* = 1.6 Hz, CH_{Ar}, 1H), 7.75 (dd, *J* = 5.5 Hz, *J* = 3.1 Hz, CH_{Ar}, 2H), 7.65 (dd, *J* = 5.4 Hz, *J* = 3.1 Hz, CH_{Ar}, 2H), 7.63 – 7.54 (m, CH_{Ar}, 2H), 7.39 (d, *J* = 7.7 Hz, CH_{Ar}, 1H), 7.18 (dd, *J* = 6.0 Hz, *J* = 3.1 Hz, CH_{Ar}, 2H), 7.12 (dd, *J* = 7.7 Hz, *J* = 4.7 Hz, CH_{Ar}, 1H), 4.15 – 3.96 (m, CH_2, CH, 3H), 3.52 (t, *J* = 7.1 Hz, CH_2, 2H), 2.83 (ddt, *J* = 14.7 Hz, *J* = 8.8, *J* = 4.6 Hz, CH_2, 1H), 2.78 – 2.65 (m, CH_2, 2H), 2.65 – 2.53 (m, CH_2, 1H), 2.29 – 2.14 (m, CH_2, 1H), 2.09 – 1.97 (m, CH_2, 1H), 1.96 – 1.85 (m, CH_2, 1H), 1.72 (s, Boc, 9H), 1.70 – 1.52 (m, CH_2, 3H), 1.52 – 1.32 (m, CH_2, 2H). ^{13}C NMR (101 MHz, $CDCl_3$) δ 168.48, 157.59, 156.55, 146.87, 137.34, 134.61, 133.90, 132.14, 123.22, 122.25, 121.61, 61.63, 49.90, 49.75, 37.68, 29.33, 28.21, 26.09, 25.77, 23.69, 21.59.

(*S*)-*N*^{1}-((1*H*-benzo[*d*]imidazol-2-yl)methyl)-*N*^{1}-(5,6,7,8-tetrahydroquinolin-8-yl)butane-1,4-diamine (29):



A microwave vessel was charged with 13 mg (0.03 mmol) of intermediate **28** dissolved in 2 mL EtOH. To this was added 20 µL of hydrazine (~80% in H_2O), and the reaction was heated in a microwave for 1 hour at 80 °C. The solvents were evaporated *in vacuo* and the product was purified by column chromatography using 8% 7N NH_3 in MeOH in DCM as eluent, yielding a brown solid. Yield: 8 mg (0.02 mmol, 84%). LC-MS; *m*/*z*: 350.3 $[M+H]^+$. ^{1}H NMR (400 MHz, $CDCl_3$) δ 8.61 (d, *J* = 8.0 Hz, CH_{Ar}, 1H), 7.61 (dd, *J* = 6.0 Hz, *J* = 3.3 Hz, CH_{Ar}, 2H), 7.44 (d, *J* = 7.6 Hz, CH_{Ar}, 1H), 7.21 (dd, *J* = 6.0 Hz, *J* = 3.2 Hz, CH_{Ar}, 2H), 7.16 (dd, *J* = 7.7 Hz, *J* = 4.8 Hz, CH_{Ar}, 1H), 4.16 – 3.98 (m, CH_2, 3H), 2.96 – 2.81 (m, CH, 1H), 2.81 – 2.66 (m, CH_2, 2H), 2.66 – 2.49 (m, CH_2, 3H), 2.30 – 2.17 (m, CH_2, 1H), 2.14 – 2.01 (m, CH_2, 1H), 1.93 (tdd, *J* = 12.8 Hz, *J* = 10.0 Hz, *J* = 2.8 Hz, CH_2, 1H), 1.81 – 1.64 (m, CH_2, 1H), 1.57 – 1.32 (m, CH_2, 4H). ^{13}C NMR (101 MHz, $CDCl_3$) δ 157.61, 156.52, 146.81, 137.46, 134.75, 122.28, 121.68, 61.89, 53.56, 50.62, 49.62, 41.78, 31.01, 29.37, 26.04, 23.49, 21.53.

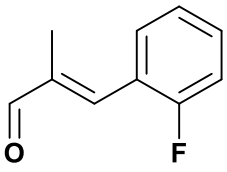
(*S*,*E*)-*N*-(4-(((1*H*-benzo[*d*]imidazol-2-yl)methyl)(5,6,7,8-tetrahydroquinolin-8-yl)amino)butyl)-6-(2-(4-(2-(5,5-difluoro-7-(thiophen-2-yl)-5*H*-4λ^4,5λ^4-dipyrrolo[1,2-c:2',1'-*f*][1,3,2]diazaborinin-3-yl)vinyl)phenoxy)acetamido)hexanamide (30):



BODIPY 630/650-X succinimide ester (1.2 mg, 1.8 pmol) was dissolved in 1 mL MeCN, and to it were added compound **29** (1.0 mg, 1.6 eq.) and DIPEA (2 µL, 4 eq.). This mixture was left to stir in an amber vial at room temperature overnight. LCMS showed complete conversion of the BODIPY dye to product (mass found: 895.4; M+H), so solvents were evaporated *in vacuo* after which the crude was purified by preparative RP-HPLC (5-95% solvent B, 30 min). Yield: 0.9 mg (53%). Purity of the compound was confirmed to be >95% by LC-MS using a long method run. HRMS calculated for $C_{50}H_{53}BF_2N_8O_3S$: 895.4101 found: 895.4036 $[M+H]^+$.

7.3.4 Synthesis of fluorescent ACKR3 probes

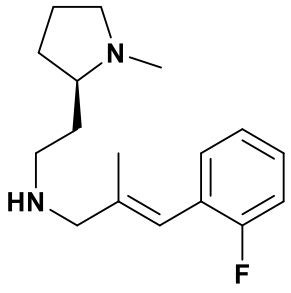
(*E*)-3-(2-fluorophenyl)-2-methylacrylaldehyde (31):



2-fluorobenzaldehyde (3 mL, 28 mmol) was taken up in a 50 mL mixture of EtOH and H_2O (95:5), and to was added KOH (156 mg, 10 mol%). This solution was cooled to -17 °C using a salt/ice bath, before dropwise addition of 2.32 mL (1.15 eq.) of propionaldehyde. The reaction was allowed to slowly reach room temperature at which it was maintained for 24 hours. Upon completion of the reaction the solvents were evaporated *in vacuo*, and the crude was purified by column chromatography using 5% EtOAc in hexane as eluent, yielding a colourless oil. Yield: 3.68g (25.2 mmol, 90%). ^{1}H NMR (400 MHz, $CDCl_3$) δ 9.54 (s, CHO, 1H), 7.47 (t, *J* = 7.6 Hz, CH_{Ar}, 1H), 7.34 – 7.29 (m, CH, CH_{Ar}, 2H), 7.16 (t, *J* = 7.6 Hz, CH_{Ar}, 1H),

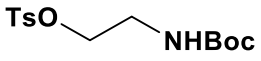
7.07 (t, *J* = 9.7 Hz, *J* = 8.4 Hz, CH_{Ar}, 1H), 1.95 (s, CH_3, 3H). ^{13}C NMR (101 MHz, $CDCl_3$) δ 194.90, 161.59, 159.09, 141.14, 141.09, 140.01, 131.35, 131.26, 130.20, 130.17, 124.10, 124.07, 123.07, 122.95, 115.88, 115.66, 10.90, 10.88.

(*R*,*E*)-3-(2-fluorophenyl)-2-methyl-*N*-(2-(1-methylpyrrolidin-2-yl)ethyl)prop-2-en-1-amine (32):



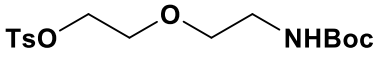
A roundbottom flask containing 10 mL MeOH was charged with (*R*)-2-(1-Methylpyrrolidin-2-yl)ethanamine dihydrochloride (0.5 g, 2.49 mmol) and TEA (0.7 mL, 2 eq.). This mixture was stirred at room temperature for 30 minutes before addition of 2.5 mL glacial AcOH and MeOH, reaching a final volume of 25 mL. Aldehyde fragment **31** (0.408g, 1 eq.) and Na_2SO_4 (150 mg, 1.0 mmol) were added and the mixture was left to stir at room temperature overnight. Finally, 2-Picoline borane complex (0.266g, 1 eq.) was added and the reaction was left to stir until completion (24 hours). The reaction mixture was concentrated *in vacuo* and the residue was taken up in H_2O. The aqueous was washed with DCM (3x 100 mL), after which it was basified to pH 14.0 using concentrated NaOH. This was then extracted with DCM (5x 100 mL), the organics combined, dried over $MgSO_4$ and concentrated *in vacuo*. Column purification using 2.5-7% 7N NH_3 in MeOH in DCM yielded the desired fragment as a colourless oil. Yield: 0.435g (1.57 mmol, 63%). LC-MS; 277.2 $[M+H]^+$. ^1H NMR (400 MHz, $CDCl_3$) δ 7.16 (t, *J* = 7.6 Hz, CH_{Ar}, 1H), 7.12 – 7.02 (m, CH_{Ar}, 1H), 7.01 – 6.86 (m, CH_{Ar}, 2H), 6.32 (s, CH, 1H), 3.24 (s, CH_2, 2H), 2.95 (ddd, *J* = 9.6 Hz, *J* = 7.8 Hz, *J* = 2.1 Hz, CH_2, 1H), 2.70 – 2.47 (m, CH_2, 2H), 2.22 (s, CH_3, 3H), 2.07 – 1.95 (m, CH_2, 2H), 1.90 – 1.75 (m, CH_2, 2H), 1.71 (s, CH_3, 3H), 1.67 – 1.49 (m, CH_2, 2H), 1.48 – 1.30 (m, CH_2, 2H). ^{13}C NMR (101 MHz, $CDCl_3$) δ 161.25, 158.80, 139.47, 130.61, 130.58, 127.91, 127.83, 125.65, 125.51, 123.37, 123.34, 118.05, 118.03, 115.26, 115.04, 64.54, 57.75, 57.14, 57.12, 46.50, 40.39, 40.37, 33.92, 30.61, 21.90, 16.59, 16.57. For storage purposes, the fragment was kept as a diHCl salt by stirring the freebase in diethylether, triturating the solution with concentrated HCl in IPA and filtering off the white precipitates.

2-((*tert*-butoxycarbonyl)amino)ethyl 4-methylbenzenesulfonate (33a):



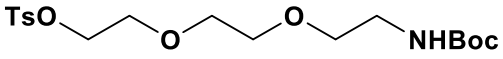
N-Boc-ethanolamine (1 mL, 6.46 mmol) was taken up in 20 mL DCM, and to it was added 1.8 mL (2 eq.) TEA. This mixture was stirred for 5 minutes at room temperature, after which it was cooled to 0 °C. Tosyl chloride (1.23g, 1 eq.) was dissolved in 10 mL DCM and added to the reaction mixture in a dropwise fashion. When the addition was completed the reaction mixture was allowed to slowly reach room temperature, at which it was maintained overnight. Upon completion (TLC), the solvents were evaporated *in vacuo* and the product was purified by column chromatography using 20-100% EtOAc in hexane as eluent. The product was isolated as an off white solid. Yield: 0.8g (2.5 mmol, 40%). LC-MS: *m*/*z*: 316.1 $[M+H]^+$. ^{1}H NMR (400 MHz, $CDCl_3$) δ 7.78 (d, *J* = 8.0 Hz, CH_{Ar}, 2H), 7.35 (d, *J* = 8.0 Hz, CH_{Ar}, 2H), 4.93 (s, NH, 1H), 4.06 (t, *J* = 5.2 Hz, CH_2, 2H), 3.37 (q, *J* = 5.2 Hz, CH_2, 2H), 2.44 (s, CH_3, 3H), 1.40 (s, Boc, 9H). ^{13}C NMR (101 MHz, $CDCl_3$) δ 155.62, 145.02, 132.64, 129.95, 127.91, 79.73, 69.44, 39.73, 28.28, 21.63.

2-(2-((*tert*-butoxycarbonyl)amino)ethoxy)ethyl 4-methylbenzenesulfonate (33b):



This compound has been prepared previously in-house.

2,2-dimethyl-4-oxo-3,8,11-trioxa-5-azatridecan-13-yl 4-methylbenzenesulfonate (33c):

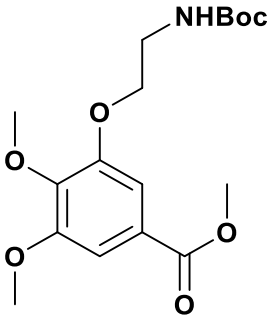


Tert-butyl (2-(2-(2-hydroxyethoxy) ethoxy)ethyl)carbamate (0.25g, 1.0 mmol) was taken up in 15 mL DCM, and to it was added 0.28 mL (2 eq.) TEA. This mixture was stirred for 10 minutes at room temperature, after which it was cooled to 0 °C. Tosyl chloride (0.191g, 1 eq.) was dissolved in 10 mL DCM and added to the reaction mixture in a dropwise fashion. When the addition was completed the reaction mixture was allowed to slowly reach room temperature, at which it was maintained overnight. Upon completion (TLC),

the solvents were evaporated *in vacuo* and the product was purified by column chromatography using 50% EtOAc in hexane as eluent. The product was isolated as a colourless oil. Yield: 0.146g (0.36 mmol, 36%). LC-MS; *m*/*z*: 404.2 $[M+H]^+$. ^{1}H NMR (400 MHz, $CDCl_3$) δ 7.78 (d, *J* = 8.0 Hz, CH_{Ar}, 2H), 7.33 (d, *J* = 8.1 Hz, CH_{Ar}, 2H), 4.98 (s, NH, 1H), 4.22 – 4.10 (m, CH_2, 2H), 3.68 (dd, *J* = 5.7 Hz, *J* = 4.0 Hz, CH_2, 2H), 3.62 – 3.51 (m, CH_2, 4H), 3.49 (t, *J* = 5.2 Hz, CH_2, 2H), 3.27 (q, *J* = 5.4 Hz, CH_2, 2H), 2.43 (s, CH_3, 3H), 1.42 (s, Boc, 9H). ^{13}C NMR (101 MHz, $CDCl_3$) δ 155.94, 144.84, 132.95, 129.82, 127.93, 79.16, 70.66, 70.23, 69.20, 68.68, 40.31, 28.39, 21.62.

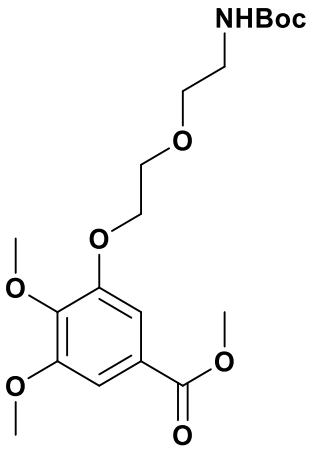
General procedures for the *O*-alkylation of 4,5-dimethyoxy-3-hydroxybenzoate (compounds 34a-c): To a roundbottom flask containing 15 mL DMF were added 4,5-dimethyoxy-3-hydroxybenzoate (1 eq.), the appropriate tosylated alcohol (1 eq.), and $CsCO_3$ (3 eq.). The reaction was carried out at 60 °C until LCMS indicated completion. The reaction mixture was then poured onto brine and extracted with EtOAc (3x 50mL). The organics were combined, dried over $NaSO_4$ and concentrated *in vacuo*. The products were purified by column chromatography using 50% EtOAc in hexane as eluent.

Methyl 3-(2-((tert-butoxycarbonyl)amino)ethoxy)-4,5-dimethoxybenzoate (34a):



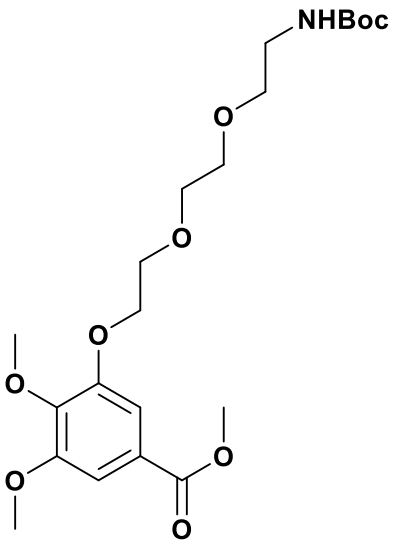
Prepared using 0.343g (1.09 mmol) 2-((*tert*-butoxy carbonyl)amino)ethyl 4-methylbenzenesulfonate (**33a**). Yield: 0.244g (0.69 mmol, 63%, colourless oil). LC-MS; *m*/*z*: 356.1 $[M+H]^+$. ^{1}H NMR (400 MHz, $CDCl_3$) δ 7.30 – 7.21 (m, CH_{Ar}, 2H), 5.15 (br s, NH, 1H), 4.07 (t, *J* = 5.2 Hz, CH_2, 2H), 3.86 (s, $2CH_3$, 6H), 3.86 (s, CH_3, 3H), 3.52 (q, *J* = 5.5 Hz, CH_2, 2H), 1.40 (s, Boc, 9H). ^{13}C NMR (101 MHz, $CDCl_3$) δ 166.45, 155.87, 153.03, 151.86, 142.69, 125.15, 108.77, 107.17, 79.37, 68.81, 60.89, 56.16, 52.15, 40.07, 28.33.

Methyl 3-(2-(2-((tert-butoxycarbonyl)amino)ethoxy)ethoxy)-4,5-dimethoxy benzoate (34b):



Prepared using 0.12g (0.33 mmol) 2-(2-((*tert*-butoxycarbonyl)amino)ethoxy)ethyl 4-methylbenzene sulfonate (**33b**). Yield: 0.104g (0.26 mmol, 80%, colourless oil). LC-MS; *m*/*z*: 400.4 $[M+H]^+$. ^{1}H NMR (400 MHz, $CDCl_3$) δ 7.31 (dd, *J* = 15.0 Hz, *J* = 1.9 Hz, CH_{Ar}, 2H), 5.02 (br s, NH, 1H), 4.27 – 4.16 (m, CH_2, 2H), 3.91 (s, CH_3, 3H), 3.89 (s, $2CH_3$, 6H), 3.86 – 3.78 (m, CH_2, 2H), 3.60 (t, *J* = 5.1 Hz, CH_2, 2H), 3.32 (q, *J* = 5.4 Hz, CH_2, 2H), 1.41 (s, Boc, 9H). ^{13}C NMR (101 MHz, $CDCl_3$) δ 166.60, 155.95, 153.02, 152.07, 142.72, 124.98, 109.99, 108.71, 107.04, 79.15, 70.35, 69.43, 68.76, 60.86, 56.22, 52.19, 40.42, 28.36.

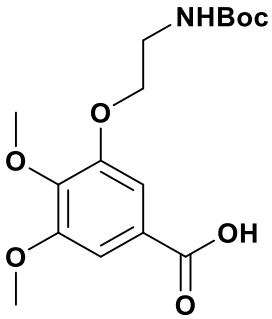
Methyl 3-((2,2-dimethyl-4-oxo-3,8,11-trioxa-5-azatridecan-13-yl)oxy)-4,5-dimethoxybenzoate (34c):



Prepared using 0.146g (0.36 mmol) 2,2-dimethyl-4-oxo-3,8,11-trioxa-5-azatridecan-13-yl 4-methylbenzenesulfonate (**33c**). Yield: 0.133g (0.3 mmol, 83%, colourless oil). LC-MS; *m*/*z*: 444.2 $[M+H]^+$. ^{1}H NMR (400 MHz, $CDCl_3$) δ 7.30 (dd, *J* = 10.1 Hz, *J* = 6.5 Hz, CH_{Ar}, 2H), 5.05 (br s, NH, 1H), 4.22 (t, *J* = 5.6 Hz, CH_2, 2H), 3.94 – 3.86 (m, $3CH_3$, CH_2, 11H), 3.77 – 3.68 (m, CH_2, 2H), 3.67 – 3.58 (m, CH_2, 2H), 3.54 (t, *J* = 5.2 Hz, CH_2, 2H), 3.30 (q, *J* = 5.4 Hz, CH_2, 2H), 1.42 (s, Boc, 9H). ^{13}C NMR (101 MHz, $CDCl_3$) δ 166.59, 155.96, 153.00, 152.06, 142.74, 124.99, 108.69, 107.01, 79.11, 70.75, 70.31, 70.27, 69.60, 68.81, 60.86, 56.22, 52.18, 40.36, 28.38.

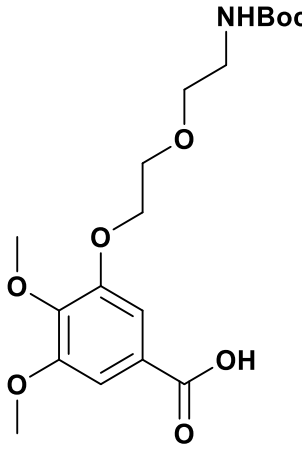
General procedure for the ester hydrolysis of methyl esters 34a-c: To a roundbottom flask containing a mixture of THF and H2O (1:1) were added the appropriate methyl ester intermediate (1 eq.) and lithium hydroxide monohydrate (3 eq.). This solution was stirred at room temperature until LCMS and TLC indicated full conversion. The THF was removed *in vacuo* and H_2O was added to dilute the reaction mixture. This was then washed with EtOAc (2x 20mL), after which the aqueous was acidified using 2N aq. HCl. The product was extracted with EtOAc (3x 30mL), the organics were combined and dried over $MgSO_4$.

3-(2-((*tert*-butoxycarbonyl)amino)ethoxy)-4,5-dimethoxybenzoic acid (35a):



Prepared using 0.1g (0.28 mmol) of methyl ester **34a**. Yield: 95 mg (0.28 mmol, quant., colourless oil). LC-MS; *m*/*z*: 342.1 $[M+H]^+$. ^{1}H NMR (400 MHz, $CDCl_3$) δ 10.56 (br s, OH, 1H), 7.37 (s, CH_{Ar}, 2H), 5.18 (br s, NH, 1H), 4.13 (t, *J* = 5.2 Hz, CH_2, 2H), 4.03 – 3.79 (m, $2CH_3$, 6H), 3.59 (q, *J* = 5.5 Hz, CH_2, 2H), 1.46 (s, Boc, 9H). ^{13}C NMR (101 MHz, $CDCl_3$) δ 170.76, 156.06, 153.08, 151.91, 143.30, 124.57, 109.37, 107.74, 79.71, 68.90, 60.99, 56.22, 40.12, 28.38.

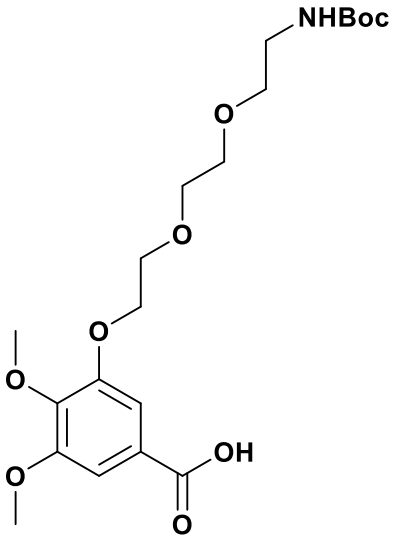
3-(2-(2-((*tert*-butoxycarbonyl)amino)ethoxy)ethoxy)-4,5-dimethoxybenzoic acid (35b):



Prepared using 0.104g (0.26 mmol) of methyl ester **34b**. Yield: 0.1 g (0.26 mmol, quant., brownish oil). LC-MS; *m*/*z*: 386.4 $[M+H]^+$. ^{1}H NMR (400 MHz, $CDCl_3$) δ 10.19 (br s, OH, 1H), 7.37 (d, *J* = 15.2 Hz, CH_{Ar}, 2H), 5.11 (br s, NH, 1H), 4.22 (t, *J* = 4.5 Hz, CH_2, 2H), 4.05 – 3.82 (m, $2CH_3$, CH_2, 8H), 3.63 (t, *J* = 5.1 Hz, CH_2, 2H), 3.35 (q, *J* = 5.4 Hz, CH_2, 2H), 1.43 (s, Boc, 9H). ^{13}C NMR (101 MHz, $CDCl_3$) δ

170.77, 156.14, 153.02, 152.06, 143.27, 124.37, 109.21, 107.56, 79.34, 70.35, 69.44, 68.74, 60.90, 56.23, 40.42, 28.37.

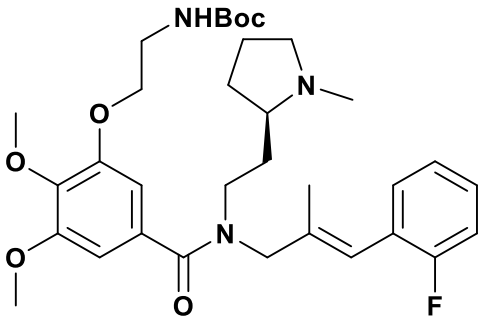
3-((2,2-dimethyl-4-oxo-3,8,11-trioxa-5-azatridecan-13-yl)oxy)-4,5-dimethoxybenzoic acid (35c):



Prepared using 0.133g (0.3 mmol) of methyl ester **34c**. Yield: 0.124 g (0.3 mmol, quant., colourless oil). LC-MS; *m/z*: 430.1 $[M+H]^+$. ^1H NMR (400 MHz, $CDCl_3$) δ 10.24 (br s, OH, 1H), 7.36 (dd, *J* = 14.4 Hz, *J* = 1.8 Hz, 2H), 5.13 (br s, NH, 1H), 4.24 (t, *J* = 4.8 Hz, CH_2, 2H), 3.92 (d, *J* = 9.9 Hz, $2CH_3$, CH_2, 8H), 3.74 (dd, *J* = 5.8 Hz, *J* = 3.4 Hz, CH_2, 2H), 3.65 (dd, *J* = 5.8 Hz, *J* = 3.4 Hz, CH_2, 2H), 3.56 (t, *J* = 5.2 Hz, CH_2, 2H), 3.32 (q, *J* = 5.5 Hz, CH_2, 2H), 1.43 (s, Boc, 9H). ^{13}C NMR (101 MHz, $CDCl_3$) δ 177.06, 156.17, 153.01, 152.08, 143.34, 124.25, 109.29, 107.51, 79.35, 70.74, 70.28, 69.65, 68.85, 60.91, 56.23, 40.35, 28.38, 14.17.

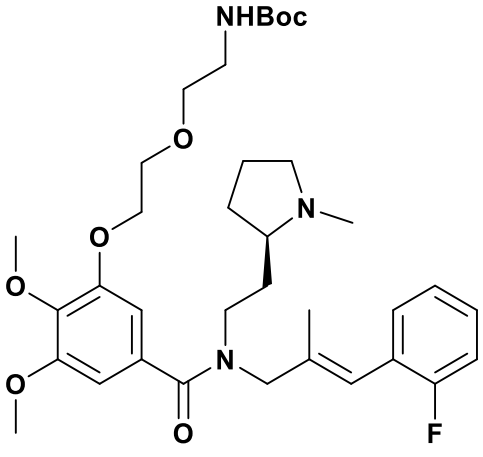
General procedure for the peptide coupling between amine fragment 32 and compounds 35a-c: To a roundbottom flask containing DMF were added **32** (1 eq.), corresponding benzoic acid (1 eq.), HATU (1 eq.), and DIPEA (2 eq.). This mixture was stirred at room temperature for 2 hours, or until completion (LCMS). The solvent was evaporated *in vacuo* and the crude was purified by column chromatography using 4% 7N NH_3 in MeOH in DCM as eluent.

***Tert*-butyl (*R*,*E*)-(2-(5-((3-(2-fluorophenyl)-2-methylallyl)(2-(1-methylpyrrolidin-2-yl)ethyl)carbamoyl)-2,3-dimethoxyphenoxy)ethyl)carbamate (36a):**



Prepared using 40 mg (0.11 mmol) of amine fragment **32**. Yield: 48 mg (0.08 mmol, 72%, brownish solid). LC-MS; *m*/*z*: 600.5 $[M+H]^+$. ^{1}H NMR (400 MHz, $CDCl_3$) δ 7.28 – 7.21 (m, CH_{Ar}, 2H), 7.13 (td, *J* = 7.5 Hz, *J* = 1.2 Hz, CH_{Ar}, 1H), 7.07 (t, *J* = 10.1 Hz, *J* = 8.2 Hz, CH_{Ar}, 1H), 6.83 – 6.62 (m, CH_{Ar}, 2H), 6.45 (s, CH, 1H), 5.09 (br s, NH, 1H), 4.13 – 3.92 (m, CH_2, 4H), 3.86 (s, $2CH_3$, 6H), 3.59 – 3.47 (m, CH_2, 2H), 3.16 – 2.92 (m, CH, 1H), 2.37 (s, CH_2, 2H), 2.27 – 1.92 (m, CH_2, 6H), 1.90 – 1.52 (m, CH_3, CH_2, 6H), 1.45 (s, Boc, CH_2, 11H). ^{13}C NMR (101 MHz, $CDCl_3$) δ 171.43, 161.31, 158.86, 155.85, 153.46, 152.17, 139.63, 136.19, 131.86, 130.47, 128.68, 123.72, 119.37, 115.58, 115.36, 105.80, 104.41, 79.46, 68.89, 64.21, 60.96, 57.14, 56.19, 40.50, 40.06, 38.60, 30.94, 30.55, 28.38, 21.98, 16.05.

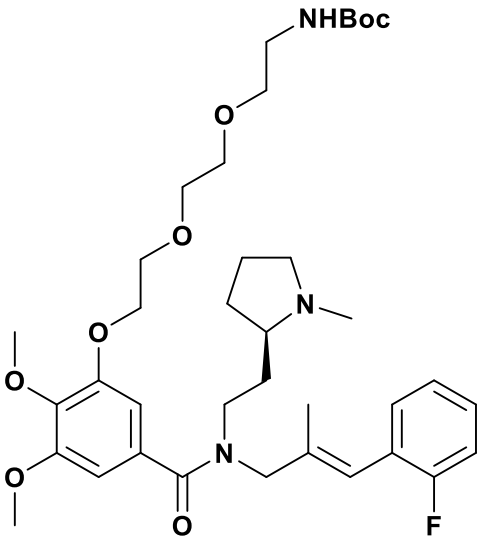
***Tert*-butyl (*R*,*E*)-(2-(2-(5-((3-(2-fluorophenyl)-2-methylallyl)(2-(1-methylpyrrolidin-2-yl)ethyl)carbamoyl)-2,3-dimethoxyphenoxy)ethoxy)ethyl)carbamate (36b):**



Prepared using 40 mg (0.11 mmol) of amine fragment **32**. Yield: 54 mg (0.08 mmol, 72%, brownish solid). LC-MS; *m*/*z*: 644.6 $[M+H]^+$. ^{1}H NMR (400 MHz, $CDCl_3$) δ 7.26 – 7.21 (m, CH_{Ar}, 2H), 7.13 (t, *J* = 7.5 Hz, CH_{Ar}, 1H), 7.07 (t, *J* = 8.2 Hz, CH_{Ar}, 1H), 6.76 – 6.62 (m, CH_{Ar}, 2H), 6.45 (s, CH, 1H), 5.04 (br s, NH, 1H), 4.39-4.25 (m, CH, 1H), 4.12 (s, CH_2, 2H), 4.04-3.96 (m, CH_2, 1H), 3.89-3.76 (m, $2CH_3$, CH_2, 8H), 3.59 (q, *J* = 5.5 Hz, CH_2, 2H), 3.31 (q, *J* = 5.4 Hz, CH_2, 2H), 3.09-3.00 (m, CH_2, 1H), 2.35-1.95 (m, CH_2, 7H), 1.84-1.58 (m, CH_3, CH_2, 7H), 1.49-1.42 (m, Boc, CH_2, 11H). ^{13}C NMR (101 MHz, $CDCl_3$) δ 171.53, 162.49, 161.31, 158.85,

155.96, 153.34, 152.32, 139.58, 136.21, 130.46, 130.43, 128.68, 123.70, 115.55, 115.33, 105.61, 104.17, 79.15, 70.35, 69.35, 64.15, 60.84, 57.16, 56.19, 53.43, 42.91, 40.41, 38.59, 36.45, 28.39, 21.99, 16.06.

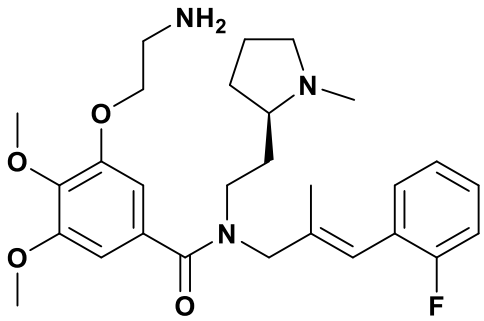
***Tert*-butyl (*R*,*E*)-(2-(2-(2-(5-((3-(2-fluorophenyl)-2-methylallyl)(2-(1-methylpyrrolidin-2-yl)ethyl)carbamoyl)-2,3-dimethoxyphenoxy)ethoxy)ethoxy)ethyl)-carbamate (36c):**



Prepared using 30 mg (0.11 mmol) of amine fragment **32**. Yield: 58 mg (0.08 mmol, 77%, colourless oil). LC-MS; *m*/*z*: 688.4 $[M+H]^+$. ^{1}H NMR (400 MHz, $CDCl_3$) δ 7.39 – 7.17 (m, CH_{Ar}, 2H), 7.11 (td, *J* = 7.5 Hz, *J* = 1.2 Hz, CH_{Ar}, 1H), 7.08 – 7.00 (m, CH_{Ar}, 1H), 6.75 – 6.61 (m, CH_{Ar}, 2H), 6.44 (s, CH, 1H), 5.06 (br s, NH, 1H), 4.47 – 4.21 (m, CH_2, 4H), 4.22 – 4.09 (m, CH_2, 2H), 4.06 – 3.93 (m, CH_2, 1H), 3.93 – 3.77 (m, $2CH_3$, CH_2, 8H), 3.69 (t, *J* = 4.6 Hz, CH_2, 2H), 3.61 (dd, *J* = 5.8 Hz, *J* = 3.5 Hz, CH_2, 2H), 3.52 (t, *J* = 5.2 Hz, CH_2, 2H), 3.47 – 3.35 (m, CH, 1H), 3.33 – 3.25 (m, CH_2, 2H), 3.12 – 2.91 (m, CH_2, 1H), 2.47 – 2.25 (m, CH_2, 2H), 2.25 – 1.91 (m, CH_2, 2H), 1.88-1.55 (m, CH_3, CH_2, 8H), 1.42 (s, Boc, 9H). ^{13}C NMR (101 MHz, $CDCl_3$) δ 171.53, 161.30, 158.85, 155.97, 153.35, 152.41, 139.58, 136.21, 130.46, 128.67, 123.70, 119.35, 115.54, 115.33, 105.62, 104.15, 79.11, 70.72, 70.32, 70.27, 69.60, 68.82, 60.83, 57.15, 56.26, 56.18, 40.36, 28.40, 21.98, 16.04.

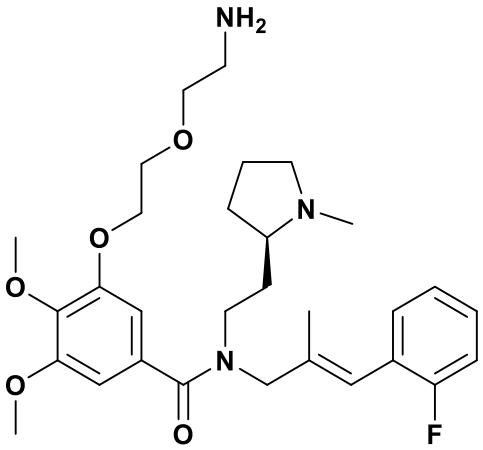
General procedure for the *N*-Boc deprotection of intermediates 36a-c: The appropriate Boc-protected intermediate was taken up in a 4:1 mixture of DCM and TFA, and was stirred at room temperature until completion (LCMS). The reaction mixture was concentrated *in vacuo* and residual TFA was removed by co-evaporation with toluene. The residue was then taken up in H_2O and washed with EtOAc (2x 20 mL), after which the aqueous was basified to pH 14.0 using concentrated aq. NaOH. The product was then extracted using DCM (5x 20 mL), the combined organics dried over Na_2SO_4, and finally the solvents were removed *in vacuo* to afford the desired congeners as a freebase. For storage purposes these compounds were kept as diHCl salts, by stirring the compounds in 4N HCl in dioxane for 5 minutes, and evaporation of the solvents.

(*R*,*E*)-3-(2-aminoethoxy)-*N*-(3-(2-fluorophenyl)-2-methylallyl)-4,5-dimethoxy-*N*-(2-(1-methylpyrrolidin-2-yl)ethyl)benzamide (37a):



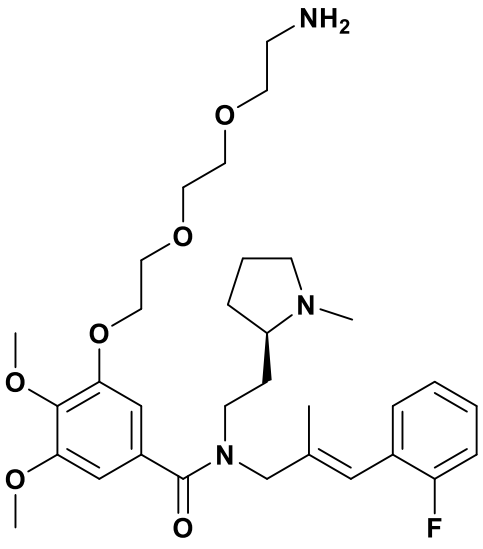
Prepared using 46 mg (0.08 mmol) compound **36a**. Yield: 38 mg (0.08 mmol, quant., colourless oil). LC-MS; *m*/*z*: 500.3 $[M+H]^+$. ^{1}H NMR (400 MHz, DMSO-d_6) δ 11.04 (s, NH^+, 1H), 8.39 (s, NH_3^+, 3H), 7.46 – 7.29 (m, CH_{Ar}, 2H), 7.28 – 7.16 (m, CH_{Ar}, 2H), 6.91 – 6.71 (m, CH_{Ar}, 2H), 6.56 – 6.32 (m, CH, 1H), 4.21-4.09 (m, CH_2, 2H), 4.08-3.92 (m, CH_2, 2H), 3.87-3.82 (m, CH, 1H), 3.75 (s, $2CH_3$, 6H), 3.55-3.44 (m, CH_2, 1H), 3.33-3.12 (m, CH_2, 3H), 3.08-3.03 (m, CH_2, 1H), 2.80-2.71 (m, CH_3, CH_2, 5H), 2.02-1.70 (m, CH_2, 5H), 1.65 (s, CH_3, 3H). ^{13}C NMR (101 MHz, DMSO-d_6) δ 170.87, 161.08, 158.65, 153.32, 151.80, 137.28, 131.19, 131.16, 129.43, 124.64, 118.77, 115.93, 115.72, 106.96, 105.14, 66.48, 65.38, 60.94, 56.40, 55.23, 29.66, 27.89, 21.51, 16.33, 15.64.

(*R*,*E*)-3-(2-(2-aminoethoxy)ethoxy)-*N*-(3-(2-fluorophenyl)-2-methylallyl)-4,5-dimethoxy-*N*-(2-(1-methylpyrrolidin-2-yl)ethyl)benzamide (37b):



Prepared using 54 mg (0.08 mmol) compound **36b**. Yield: 46 mg (0.08 mmol, quant., brownish oil). LC-MS; *m*/*z*: 544.3 $[M+H]^+$. ^{1}H NMR (400 MHz, DMSO-d_6) δ 11.51 – 11.05 (m, NH^+, 1H), 8.58 – 8.02 (m, NH_3^+, 3H), 7.47 – 7.29 (m, CH_{Ar}, 2H), 7.23 (dt, *J* = 10.4 Hz, *J* = 6.8 Hz, CH_{Ar}, 2H), 6.95 – 6.55 (m, CH_{Ar}, 2H), 6.53 – 6.34 (m, CH, 1H), 4.41 – 4.07 (m, CH_2, 3H), 3.75 (m, $2CH_3$, CH_2, 10H), 3.53-3.50 (m, CH_2, CH, 3H), 3.28-3.24 (m, CH_2, 1H), 2.97 (q, *J* = 5.5 Hz, CH_2, 2H), 2.79-2.70 (m, CH_2, 3H), 2.32 (d, *J* = 10.4 Hz, CH_2, 1H), 1.99 (s, CH_3, 3H), 1.88 – 1.72 (m, CH_2, 3H), 1.66 (s, CH_3, 3H). ^{13}C NMR (101 MHz, DMSO-d_6) δ 161.08, 158.65, 153.19, 152.31, 137.40, 131.18, 131.14, 129.41, 124.66, 115.93, 115.71, 105.79, 104.53, 69.31, 68.65, 67.15, 66.26, 60.62, 56.36, 55.21, 49.03, 42.78, 29.69, 27.90, 21.51, 16.35, 14.55.

(*R*,*E*)-3-(2-(2-(2-aminoethoxy)ethoxy)ethoxy)-*N*-(3-(2-fluorophenyl)-2-methylallyl)-4,5-dimethoxy-*N*-(2-(1-methylpyrrolidin-2-yl)ethyl)benzamide (37c):

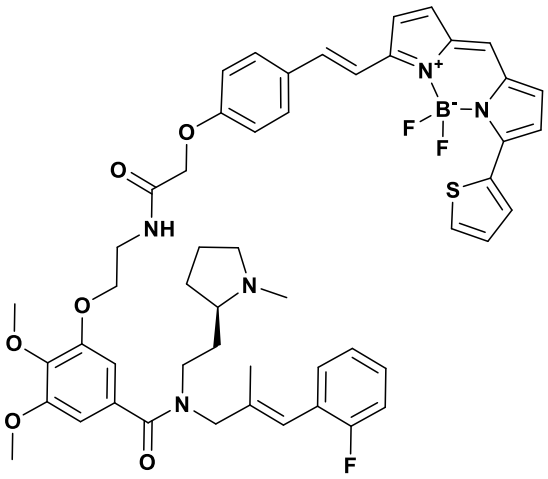


Prepared using 58 mg (0.085 mmol) compound **36c**. Yield: 50 mg (0.085 mmol, quant., colourless oil). LC-MS; *m*/*z*: 588.3 $[M+H]^+$. ^{1}H NMR (400 MHz, DMSO-d_6) δ 11.61 – 10.84 (m, NH^+, 1H), 8.15 (s, NH_3^+, 3H), 7.42 – 7.32 (m, CH_{Ar}, 2H), 7.30 – 7.16 (m, CH_{Ar}, 2H), 6.85 – 6.65 (m, CH_{Ar}, 2H), 6.53 – 6.30 (m, CH, 1H), 4.23 – 4.00 (m, CH_2, 3H), 3.90 – 3.69 (m, $2CH_3$, CH_3, 10H), 3.69 – 3.42 (m, CH_2, CH, 7H), 3.34 – 3.17

(m, CH_2, 1H), 3.08-2.88 (m, CH_2, 3H), 2.87 – 2.64 (m, CH_2, 4H), 2.41 – 2.22 (m, CH_2, 2H), 2.12 – 1.55 (m, CH_2, CH_3, 6H). ^{13}C NMR (101 MHz, DMSO-d_6) δ 171.02, 161.08, 158.65, 153.19, 152.35, 137.43, 131.18, 129.41, 124.67, 124.63, 118.43, 115.93, 115.71, 105.72, 104.53, 70.22, 70.14, 69.38, 68.76, 67.10, 66.28, 65.38, 60.56, 56.36, 56.03, 55.23, 42.81, 29.67, 27.92, 21.52, 16.36, 15.64.

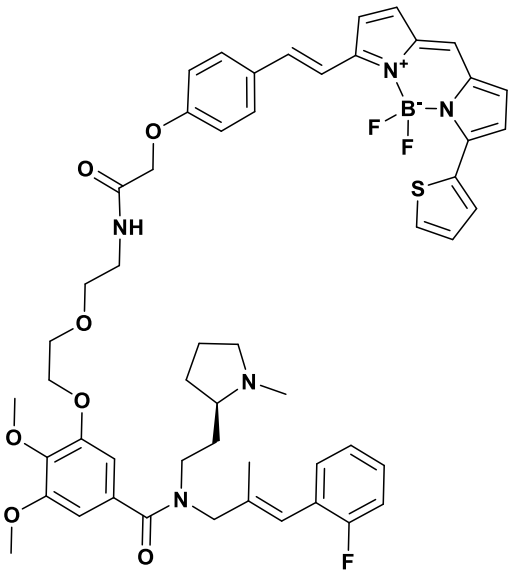
General procedure for the peptide coupling between congeners 37a-c and BODIPY 630/650: To a small roundbottom flask was added 1 mL DMF, (*E*)-2-(4-(2-(5,5-difluoro-7-(thiophen-2-yl)-5*H*-4λ^4,5λ^4-dipyrrolo[1,2-*c*:2',1'-*f*][1,3,2]diazaborinin-3-yl)vinyl)phenoxy)acetic acid (2 eq.), HATU (1 eq.), *N*-hydroxysuccinimide (1.3 eq.), and DIPEA (6 eq.). This mixture was stirred in the dark at room temperature for 1 hour, after which the corresponding congener (1 eq.) was added. This final reaction mixture was left to stir in the dark until completion, after which the reaction mixture was concentrated *in vacuo*, and the crude purified by RP-HPLC (5-95% solvent B, 30 min).

3-(2-(2-(4-((*E*)-2-(5,5-difluoro-7-(thiophen-2-yl)-5*H*-4λ^4,5λ^4-dipyrrolo[1,2-*c*:2',1'-*f*][1,3,2]diazaborinin-3-yl)vinyl)phenoxy)acetamido)ethoxy)-*N*-((E)-3-(2-fluorophenyl)-2-methylallyl)-4,5-dimethoxy-*N*-(2-((*R*)-1-methylpyrrolidin-2-yl)ethyl)benzamide (38a):



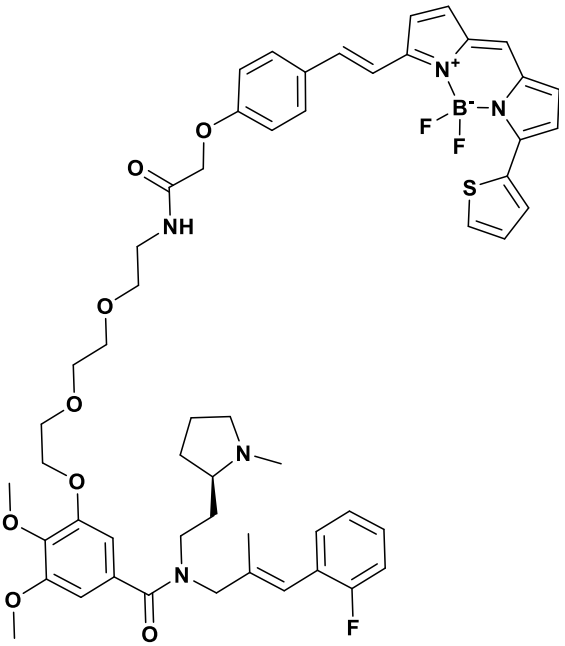
This probe was prepared using 1 mg (2 pmol) compound **37a**. LCMS showed complete conversion to the product after a reaction time of 1 hour (mass found: 932.4; M+H$^+$). Yield: 1.0 mg (54%). Purity of the compound was confirmed to be >95% by LC-MS using a long method run. HRMS calculated for $C_{51}H_{53}BF_3N_5O_6S$: 932.384 found: 932.3845 $[M+H]^+$.

3-(2-(2-(2-(4-((*E*)-2-(5,5-difluoro-7-(thiophen-2-yl)-5*H*-4λ^4,5λ^4-dipyrrolo[1,2-*c*:2',1'-*f*][1,3,2]diazaborinin-3-yl)vinyl)phenoxy)acetamido)ethoxy)ethoxy)-*N*-((*E*)-3-(2-fluorophenyl)-2-methylallyl)-4,5-dimethoxy-*N*-(2-((*R*)-1-methylpyrrolidin-2-yl)ethyl)benzamide (38b):



This probe was prepared using 1 mg (1.8 pmol) compound **37b**. LCMS showed complete conversion to the product after a reaction time of 1 hour (mass found: 976.4; M+H$^+$). Yield: 0.9 mg (50%). Purity of the compound was confirmed to be >95% by LC-MS using a long method run. HRMS calculated for $C_{53}H_{57}BF_3N_5O_7S$: 976.4100 found: 976.4168 $[M+H]^+$.

3-(2-(2-(2-(2-(4-((*E*)-2-(5,5-difluoro-7-(thiophen-2-yl)-5*H*-4λ^4,5λ^4-dipyrrolo[1,2-*c*:2',1'-*f*][1,3,2]diazaborinin-3-yl)vinyl)phenoxy)acetamido)ethoxy)ethoxy)ethoxy)-*N*-((*E*)-3-(2-fluorophenyl)-2-methylallyl)-4,5-dimethoxy-*N*-(2-((*R*)-1-methylpyrrolidin-2-yl)ethyl)benzamide (38c):

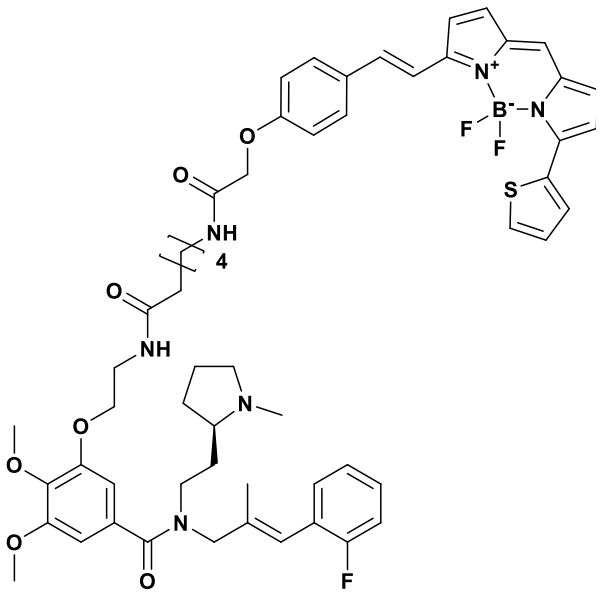


This probe was prepared using 1 mg (1.7 pmol) compound **37c**. LCMS showed complete conversion to the product after a reaction time of 1 hour (mass found: 1020.4; M+H$^+$). Yield: 1.0 mg (58%). Purity of the compound was confirmed to be >95% by LC-MS using a long method run. HRMS calculated for

$C_{55}H_{61}BF_3N_5O_8S$: 1020.4362 found: 1020.4379 $[M+H]^+$.

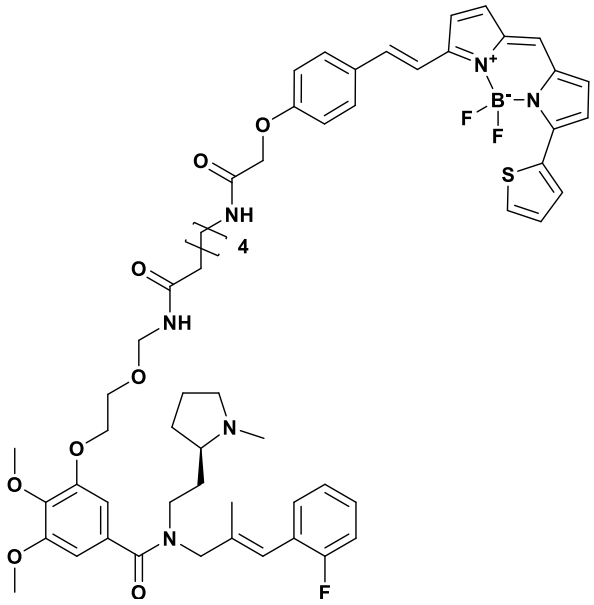
General procedure for the conjugation of congeners 37a-c to succinimidyl ester-protected BODIPY dyes: To a small vial were added 1 mL MeCN, the appropriate BODIPY dye (1 eq.), the appropriate congener (5 eq.), and TEA (50 eq.), and the mixture was stirred until completion at room temperature in the dark. Upon completion (LCMS), the solvents were removed *in vacuo* and the crude was purified by RP-HPLC (5-95% solvent B, 30 min).

3-(2-(6-(2-(4-((*E*)-2-(5,5-difluoro-7-(thiophen-2-yl)-5H-4λ^4,5λ^4-dipyrrolo[1,2-*c*:2',1'-*f*][1,3,2]diazaborinin-3-yl)vinyl)phenoxy)acetamido)hexanamido)ethoxy)-*N*-((E)-3-(2-fluorophenyl)-2-methylallyl)-4,5-dimethoxy-*N*-(2-((*R*)-1-methylpyrrolidin-2-yl)ethyl)benzamide (39a):



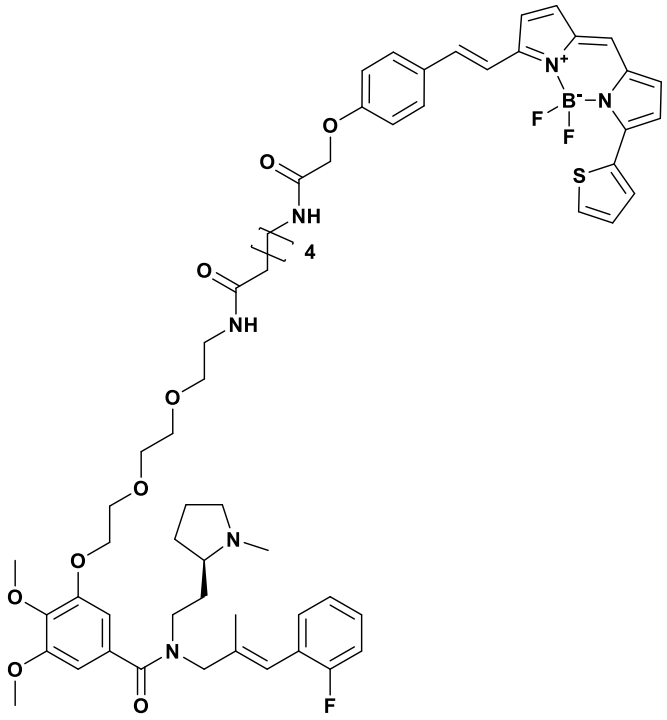
Prepared using BODIPY 630/650-X NHS ester (1 mg, 1.5 pmol) and compound **37a** (4 mg, 5 eq.). LC-MS showed complete conversion of the starting materials to the product after stirring overnight (*m*/*z*: 1045.5 $[M+H]^+$). Yield: 1.1 mg (70%). Purity of the compound was confirmed to be >95% by LC-MS using a long method run. HRMS calculated for $C_{57}H_{64}BF_3N_6O_7$: 1045.4678 found: 1045.4836 $[M+H]^+$.

3-(2-(2-(6-(2-(4-((*E*)-2-(5,5-difluoro-7-(thiophen-2-yl)-5*H*-4l4,5l4-dipyrrolo[1,2-*c*:2',1'-*f*][1,3,2]diazaborinin-3-yl)vinyl)phenoxy)acetamido)hexanamido) ethoxy)ethoxy)-*N*-((*E*)-3-(2-fluorophenyl)-2-methylallyl)-4,5-dimethoxy-*N*-(2-((*R*)-1-methylpyrrolidin-2-yl)ethyl)benzamide (39b):



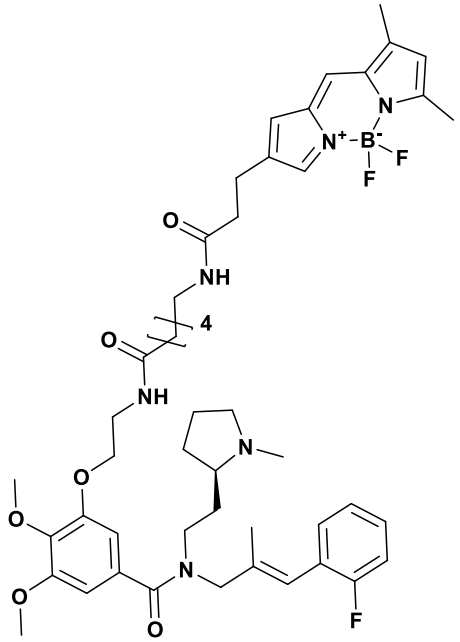
Prepared using BODIPY 630/650-X NHS ester (1 mg, 1.5 pmol) and compound **37b** (4 mg, 5 eq.). LC-MS showed complete conversion of the starting materials to the product after stirring overnight (*m*/*z*: 1089.5 $[M+H]^+$). Yield: 1.0 mg (61%). Purity of the compound was confirmed to be >95% by LC-MS using a long method run. HRMS calculated for $C_{59}H_{68}BF_3N_6O_8S$: 1089.494, found: 1089.4943 $[M+H]^+$.

3-((18-(4-((*E*)-2-(5,5-difluoro-7-(thiophen-2-yl)-5*H*-4λ^4,5λ^4-dipyrrolo[1,2-*c*:2',1'-*f*][1,3,2]diazaborinin-3-yl)vinyl)phenoxy)-10,17-dioxo-3,6-dioxa-9,16-diazaoctadecyl)oxy)-*N*-((*E*)-3-(2-fluorophenyl)-2-methylallyl)-4,5-dimethoxy-*N*-(2-((*R*)-1-methylpyrrolidin-2-yl)ethyl)benzamide (39c):



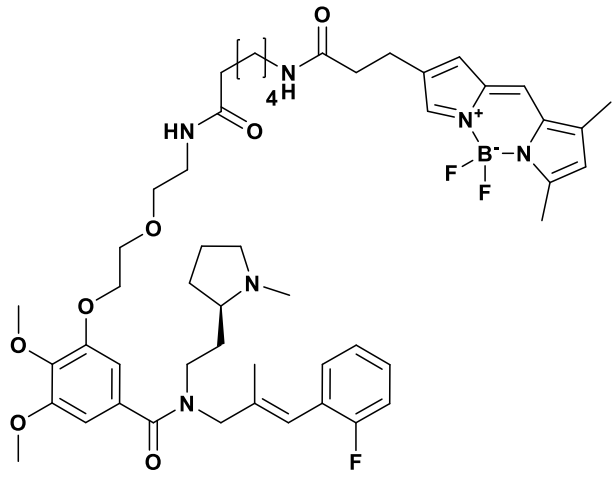
Prepared using BODIPY 630/650-X NHS ester (1 mg, 1.5 pmol) and compound **37c** (4 mg, 4.5 eq.). LC-MS showed complete conversion of the starting materials to the product after stirring overnight (*m*/*z*: 1133.5 $[M+H]^+$). Yield: 1.3 mg (76%). Purity of the compound was confirmed to be >95% by LC-MS using a long method run. HRMS calculated for $C_{61}H_{72}BF_3N_6O_9S$: 1133.5203 found: 1133.5326 $[M+H]^+$.

(*R*,*E*)-3-(2-(6-(3-(5,5-difluoro-7,9-dimethyl-5*H*-4λ^4,5λ^4-dipyrrolo[1,2-*c*:2',1'-*f*][1,3,2]diazaborinin-2-yl)propanamido)hexanamido)ethoxy)-*N*-(3-(2-fluorophenyl)-2-methylallyl)-4,5-dimethoxy-*N*-(2-(1-methylpyrrolidin-2-yl)ethyl)benzamide (40a):



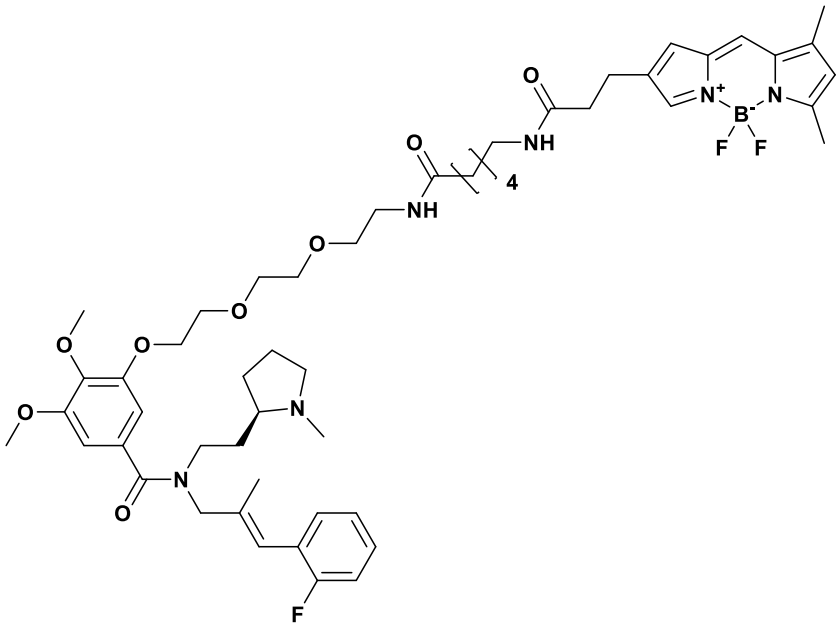
Prepared using BODIPY FL-X NHS ester (1 mg, 2.0 pmol) and compound **37a** (2 mg, 2 eq.). LC-MS showed complete conversion of the starting materials to the product after 5 hours (*m*/*z*: 887.5 $[M+H]^+$). Yield: 1.0 mg (56%). Purity of the compound was confirmed to be >95% by LC-MS using a long method run. HRMS calculated for $C_{48}H_{62}BF_3N_6O_6$: 887.4852 found: 887.4880 $[M+H]^+$.

(*R*,*E*)-3-(2-(2-(6-(3-(5,5-difluoro-7,9-dimethyl-5*H*-4l4,5l4-dipyrrolo[1,2-*c*:2',1'-*f*][1,3,2]diazaborinin-2-yl)propanamido)hexanamido)ethoxy)ethoxy)-*N*-(3-(2-fluorophenyl)-2-methylallyl)-4,5-dimethoxy-*N*-(2-(1-methylpyrrolidin-2-yl)ethyl)benzamide (40b):



Prepared using BODIPY FL-X NHS ester (1 mg, 2.0 pmol) and compound **37b** (2 mg, 2 eq.). LC-MS showed complete conversion of the starting materials to the product after stirring overnight (*m*/*z*: 931.5 $[M+H]^+$). Yield: 1.3 mg (70%). Purity of the compound was confirmed to be >95% by LC-MS using a long method run. HRMS calculated for $C_{50}H_{66}BF_3N_6O_7$: 931.5114 found: 931.5165 $[M+H]^+$.

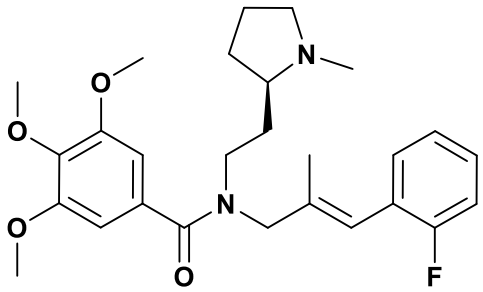
(*R*,*E*)-3-((19-(5,5-difluoro-7,9-dimethyl-5*H*-4λ^4,5λ^4-dipyrrolo[1,2-*c*:2',1'-*f*][1,3,2] diazaborinin-2-yl)-10,17-dioxo-3,6-dioxa-9,16-diazanonadecyl)oxy)-*N*-(3-(2-fluorophenyl)-2-methylallyl)-4,5-dimethoxy-*N*-(2-(1-methylpyrrolidin-2-yl)ethyl) benzamide (40c):



Prepared using BODIPY FL-X NHS ester (1 mg, 2.0 pmol) and compound **37c** (2 mg, 2 eq.). LC-MS showed complete conversion of the starting materials to the product after stirring overnight (*m*/*z*: 975.5 $[M+H]^+$). Yield: 1.5 mg (77%). Purity of the compound was confirmed to be >95% by LC-MS using a long method run. HRMS calculated for $C_{52}H_{70}BF_3N_6O_8$: 975.5376, found: 975.5498 $[M+H]^+$.

Synthesis of reference compound SD02-17-1 (GD301):

(*R*,*E*)-*N*-(3-(2-fluorophenyl)-2-methylallyl)-3,4,5-trimethoxy-*N*-(2-(1-methylpyrrolidin-2-yl)ethyl)benzamide:



Styrene intermediate **32** (30 mg, 0.11 mmol) was taken up in 4 mL DMF, and to it were added 3,4,5-trimethoxybenzoic acid (23 mg, 1 eq.), HBTU (42 mg, 1 eq.), and DIPEA (38 µL, 2 eq.). This was stirred at room temperature for 2.5 hours, after which LC-MS showed complete conversion (*m*/*z*: 471.3 $[M+H]^+$). The solvents were evaporated *in vacuo*, and the crude product was purified by preparative RP-HPLC (5-95% solvent B, 30 min). Yield: 47 mg (0.1 mmol, 91%, colourless oil). ^{1}H NMR (400 MHz, DMSO-d_6) δ 10.27-9.88 (m, NH^+, 1H), 7.38-7.31 (m, CH_{Ar}, 2H), 7.24 – 7.20 (m, CH_{Ar}, 2H), 6.74 (s, CH_{Ar}, 2H), 6.48 – 6.39 (m, CH, 1H), 4.36-4.17 (m, CH, 1H), 4.04 (s, CH_2, 2H), 3.83-3.69 (m, $3OCH_3$, 9H), 3.58-3.48 (m, CH_2, 2H), 3.28 (br s, CH_2, 2H), 3.12-2.98 (m, CH_2, 1H), 2.90-2.75 (m, CH_2, 2H), 2.38-2.24 (m, CH_2, 1H), 2.09-1.66 (m, CH_2, CH_3, 8H). ^{13}C NMR (101 MHz, DMSO-d_6) δ 171.15, 161.11, 159.33, 159.00, 158.67, 158.33, 153.18, 138.87, 137.42, 131.09, 129.49, 124.66, 118.44, 115.94, 115.51, 104.41, 66.70, 60.55, 56.45, 55.54, 42.76, 29.37, 28.17, 21.45, 16.32. Purity of the compound was confirmed to be >95% by LC-MS using a long method run.

7.4 Pharmacology

7.4.1 Cell culture

All cell lines were cultured in Dulbecco's modified Eagle's medium (DMEM), supplemented with 10% foetal bovine serum (FBS). Cells were grown in T75 tissue culture flasks (75 cm^2) at 37°C, in 95% O_2 and 5% CO_2. Cells were left to grow up to 80% confluency prior to passaging to prevent loss of protein expression and cell detachment. The protocol used for splitting cells is as follows: Growth medium (DMEM) was aspirated using a Pasteur pipette, after which the cells were gently washed with 5 mL of PBS (Phosphate Buffered Saline). After aspiration of the PBS Trypsin (1 mL) was added to the cells and was left to incubate for 5 minutes. The cells were then taken up in 10 mL growth medium and centrifuged to remove the trypsin. The cells were gently resuspended in 10 mL growth medium and transferred to new T75 flasks at appropriate dilutions. Typically cells were diluted to a ratio 1:5-1:20.

7.4.2 Membrane preparation

For the preparation of HEK293-NLuc-CXCR4 and HEK293-Nluc-ACKR3 membranes, cells were cultured in 500 cm^2 trays and left to grow to 90% confluency. The growth medium was removed and the cells were gently washed with 10 mL of PBS to remove any residual medium. This was then removed, 20 mL of fresh PBS was added and the cells were removed using a plastic scraper. The cells were transferred into a falcon tube and spun down for 10 minutes at 4 °C and 1500 rpm in an Eppendorf centrifuge. The supernatant was discarded and the cells were resuspended in 15 mL PBS. Using a Dounce homogeniser, the cells were lysed for ten 2 second bursts. These were then centrifuged for 20 minutes at 4 °C and 1500 g to remove any unbroken cells. The supernatant was transferred to high speed centrifuge tubes and centrifuged for 30 minutes at 4 °C and maximum speed in an ultra-centrifuge. Quantification of the protein content of the membranes was performed using a Pierce™ BCA Protein Assay Kit (ThermoFisher Scientific).

7.4.3 Transient transfection of HEK293 cells

For the generation of a HEK293-SNAP-ACKR3 cell line cDNA encoding a SNAP-ACKR3 construct had already been prepared by fellow PhD student Birgit Caspar. Clear, 8-well glass plates (Nunc Lab-Tek, Thermo-Fisher Scientific, UK) were first coated with

poly-D-lysine (10 µg mL^{-1} in PBS; filter sterilised using a 0.2µm filter), to allow for cell-adherence. HEK293 cells were then seeded at a density of 30 000 cells per well and left to grow for 24 hours. The next day a mixture was prepared of 0.020 µg/µL DNA solution in OptiMEM to which was added 5.9 µl of FuGENE® HD reagent to achieve a reagent:DNA mixture of 3:1. This was gently pipetted up- and down 5 times after which it was left to incubate at room temperature for 20 minutes and finally added to the cells, adding 0.23 µg DNA to each well. The cells were left to incubate for 24 hours after which they were ready to be used.

7.4.4 NanoBRET™ saturation binding experiments using membranes

In non-treated white clear-bottom 96-well plates membranes expressing Nluc-CXCR4 or NLuc-ACKR3 were diluted to a concentration of 10,000 ng in 20 µL in HEPES-Buffered Saline Solution containing 0.2% BSA (HBSS; 147 mmol/L NaCL, 24 mmol/L KCl, 1.3 mmol/L $CaCl_2$, 1 mmol/L $MgSO_4$, 10 mmol/L HEPES, 2 mmol/L sodium pyruvate, 1.43 mmol/L $NaHCO_3$, 4.5 mmol/L D-glucose, pH 7.2–7.45). To the membranes were added 10 µL HBSS, competing ligand (AMD3100 for CXCR4, SD02-17-1 for ACKR3, both at a final concentration of 10 µM), and 20 µL of relevant fluorescent ligand. The concentration of ligand ranged between 0-1000 nM; using a serial dilution of 8 steps. The plates were incubated in the dark for 1 hour at 37°C without CO_2. The Nanoluc® substrate furimazine (Promega) was then added (5 µL per well, 10µM final concentration) and the plates were immediately read using the PHERAstar FS plate reader (BMG Labtech, UK) at room temperature. For the red-fluorescing ligands module 610-LP 460-80 was used, and for the green-fluorescing ligands module 1108A1 was used. The filtered light from each well was simultaneously measured using 460 nm (80-nm band-pass) and >610 nm longpass filters for BODIPY 630/650-X coupled ligands, and 475 nm (30-nm band-pass) and 535 nm (30 nm bandpass) filters for BODIPY FL-X coupled ligands. The resulting raw BRET ratio was calculated by dividing the fluorescence by the luminescence.

7.4.5 NanoBRET™ saturation binding experiments using whole cells

HEK293 cells stably expressing NLuc-ACKR3 were seeded on white clear-bottom 96-well plates pre-treated with poly-D-lysine lysine (10 µg mL^{-1} in PBS; filter sterilised using a 0.2µm filter), at a density of 30 000 cells per well. The cells were left to grow

for 24 hours prior to being used. The medium in each well was removed and replaced with HBSS containing 0.2% BSA and the required concentration of the fluorescent ligand (final concentration ranging 0-1000 nM) with or without the competing ligand SD02-17-1 (final concentration of 10 µM). Upon the addition of the fluorescent ligand, the plates were incubated in the dark for 1 hour at 37°C without CO_2. The Nanoluc® substrate furimazine (Promega) was then added (5 µL per well, 10µM final concentration) and the plates were immediately read using the PHERAstar FS plate reader (BMG Labtech, UK) at 37 °C. Module 610-LP 460-80 was used, and the filtered light from each well was simultaneously measured using 460 nm (80-nm band-pass) and >610 nm longpass filters. The resulting raw BRET ratio was calculated by dividing the fluorescence by the luminescence.

7.4.6 NanoBRET™ competition binding experiments using membranes

In non-treated white clear-bottom 96-well plates membranes expressing Nluc-CXCR4 were diluted to a concentration of 10,000 ng in 20 µL HBSS containing 0.2% BSA. To the membranes were added 10 µL of either compound **9** or compound **23** (in HBSS, final concentration of 100 nM and 250nM, respectively), and 20 µL HBSS containing increasing concentrations of CXCL12 and small molecules AMD3100 and IT1t. For CXCL12 a concentration range of 0-1.0 µmol/L was used, using a serial dilution of 6 steps. For the small molecules a concentration range of 0-10.0 µmol/L was used, using a serial dilution of 7 steps. After addition of all components, the cells were incubated in the dark for 2 hours at 37 °C (no CO_2). The Nanoluc® substrate furimazine (Promega) was then added (5 µL per well, 10µM final concentration) and the plates were immediately read using the PHERAstar FS plate reader (BMG Labtech, UK) at room temperature. For the red-fluorescing ligands module 610-LP 460-80 was used, and for the green-fluorescing ligands module 1108A1 was used. The filtered light from each well was simultaneously measured using 460 nm (80-nm band-pass) and >610 nm longpass filters for BODIPY 630/650-X coupled ligands, and 475 nm (30-nm band-pass) and 535 nm (30 nm bandpass) filters for BODIPY FL-X coupled ligands. The resulting raw BRET ratio was calculated by dividing the fluorescence by the luminescence.

7.4.7 NanoBRET™ competition binding experiments using whole cells

HEK293 cells stably expressing NLuc-ACKR3 were seeded on white clear-bottom 96-well plates pre-treated with poly-D-lysine lysine (10 µg mL^{-1} in PBS; filter sterilised using a 0.2µm filter), at a density of 30 000 cells per well. The cells were left to grow for 24 hours prior to being used. The medium in each well was removed and replaced with 25 µL HBSS containing 0.2% BSA and the appropriate fluorescent ligand. For compound **39c** a final concentration was used of 750 nM, while for compound **40a** a final concentration was used of 100 nM. To the cells was furthermore added 25 µL HBSS containing increasing concentrations of CXCL12 and SD02-17-1. For CXCL12 a concentration range of 0-1.0 µmol/L was used, using a serial dilution of 6 steps. For the small molecules a concentration range of 0-10.0 µmol/L was used, using a serial dilution of 7 steps. After addition, the cells were incubated in the dark for 2 hours at 37 °C (no CO_2). The Nanoluc® substrate furimazine (Promega) was then added (5 µL per well, 10µM final concentration) and the plates were immediately read using the PHERAstar FS plate reader (BMG Labtech, UK) at 37 °C. For the red-fluorescing ligands module 610-LP 460-80 was used, and for the green-fluorescing ligands module 1108A1 was used. The filtered light from each well was simultaneously measured using 460 nm (80-nm band-pass) and >610 nm longpass filters for BODIPY 630/650-X coupled ligands, and 475 nm (30-nm band-pass) and 535 nm (30 nm bandpass) filters for BODIPY FL-X coupled ligands. The resulting raw BRET ratio was calculated by dividing the fluorescence by the luminescence.

7.4.8 GloSensor™ cAMP assay

For this assay a HEK293 Glosensor™ cell line stably expressing CXCR4 containing an N-terminal SNAP tag was used. This cell line has been previously developed in-house. Cells were removed from the -80 °C freezer and allowed to defrost at room temperature. Once defrosted, cells were transferred to a 30 mL universal tube, suspended in growth media and centrifuged at room temperature for 5 minutes at 1500 rpm. The supernatant was poured off, the cell pellet was resuspended medium and added to a T75 flask in the presence of 200 ug/mL Hygromycin B. After having split the cells two times, they were seeded onto clear-bottomed 96-well plates that have been pre-coated with poly-D-lysine. Cells from a single T75 flask with cells at

90% confluency were used to plate two plates. After leaving the cells to grow for 24 hours the medium was removed and replaced by 100 µL HBSS containing cAMP reagent (final concentration per well of 1 mg/mL).

For the experiments using the fluorescent ligands as antagonists, the plates were covered and left to incubate for 1 hour at 37 °C without CO_2. After 1 hour the relevant fluorescent ligands were added to achieve a final concentration of 1 µM after which the plates were covered and left to incubate for another hour at 37 °C without CO_2. After a total incubation period of 2 hours, basal luminescence was measured on a PHERAstar FS plate reader (BMG Labtech, UK) at 37 °C. Finally, increasing concentrations of CXCL12 ranging 0-100nM were added in the presence of Forskolin (FSK, final concentration of 30 µM), and the plates were immediately read over a duration of 1 hour at 37 °C.

For the experiments using the fluorescent ligands as agonists, cAMP reagent was added to the cells which were then left to incubate in the dark for 2 hours at 37 °C without CO_2. Basal luminescence was measured on a PHERAstar FS plate reader at 37 °C, after which were added Forskolin (final concentration 30 µM) and the fluorescent ligands (final concentrations ranging 0-10 µM). The plates were immediately read over a duration of 1 hour at 37 °C.

7.4.9 Confocal microscopy

7.4.9.1 CXCR4 imaging

The same HEK293-SNAP-CXCR4 cell line used for the GloSensor™ cAMP assay was used for confocal microscopy experiments. Cells were seeded on poly-D-lysine coated 8 well clear plates (Nunc Lab-Tek, Thermo-Fisher Scientific, UK) at a density of 30 000 cells per well. The next day, cells were treated with 0.5mM membrane impermeable HaloTag Alexa Fluor 488 dye (Promega Corporation, USA) in growth medium for 30 min at 37°C. Cells were then carefully washed three times with HBSS, and prior to imaging incubated for 30 minutes with the fluorescent ligands. In the experiments looking at localisation of the ligands, a final concentration was used of 100 nM. In the experiments investigating the nonspecific binding, final concentrations were used of 50 nM. Here, after having obtained images showing

binding of the ligands, AMD3100 was added at a final concentration of 10 µM and was left to equilibrate for 30 minutes before images were obtained. The experiments were performed on a LSM710 confocal microscope fitted with a 40x Pan Apochromat water objective (1.2NA) using Argon488 and Argon 546 laser excitation (3% power), a long pass 540 filter and a pin hole diameter of 1 Airy unit. The stage was warmed to 37 °C throughout the experiments. All images were taken as single equatorial slices with 8 averages. For the experiment investigating nonspecific binding subsequent images were obtained using identical settings for laser power, detector offset and gain.

7.4.9.2 ACKR3 imaging

HEK293 cells transiently expressing SNAP-ACKR3 were treated with 0.5mM membrane impermeable HaloTag Alexa Fluor 647 dye (Promega Corporation, USA) in growth medium for 30 min at 37°C. Cells were then carefully washed three times with HBSS before being used for experiments. Confocal imaging was again performed on a LSM710 confocal microscope fitted with a 40x Pan Apochromat water objective (1.2NA) using Argon488 and Argon 546 laser excitation (3% power), and a pin hole diameter of 1 Airy unit. The stage was warmed to 37 °C throughout the experiments. For the imaging, cells were treated with 50 nM of fluorescent ligand, after which images were obtained as single equatorial slices with 8 averages after 1, 5, and 30 minutes. To the cells was then added SD02-17-1 at a final concentration of 10 µM, and images were obtained after 15 and 25 minutes. Identical settings for laser power, detector offset and gain were used throughout the experiment.

7.5 Data analysis

All of the data generated has been analyzed using Prism 7 software (GraphPad).

Saturation-binding curves were simultaneously fitted to obtain the total and nonspecific components using the following equation:

$$= \frac{B_{max}\ x\ [B]}{[B] + K_{\mathrm{d}}} + ((M\ x\ [B]) + C)$$

where B_{max} is the maximal level of specific binding, [B] is the concentration of the fluorescent ligand in nM, K_d is the equilibrium dissociation constant in nM, M is the slope of the linear nonspecific binding component, and C is the y-axis intercept. Competition NanoBRET™ data were fitted using a one-site sigmoidal response curve given by the following equation:

$$\%\ uninhibited\ binding = 100 - \frac{(100\ x\ [A^n])}{([A^n] + IC_{50}^n)} + NS$$

where [A] is the concentration of competing drug, NS is the nonspecific binding, n is the Hill coefficient, and IC_{50} is the concentration of ligand required to inhibit 50% of the specific binding of the fluorescent ligand. The IC_{50} values from competition-binding curves were used to calculate the K_i of the unlabeled ligands using the Cheng–Prusoff equation:

$$K_i = \frac{IC_{50}}{1 + \frac{[L]}{K_{\mathrm{d}}}}$$

where [L] is the concentration of fluorescent ligand in nM, and K_d is the dissociation constant of the fluorescent ligand in nM. The K_d values used were obtained from the saturation binding experiments.

Functional experiments using the GloSensor™ cAMP assay yielded one-site concentration-response curves. Sigmoidal agonist concentration-response curves were fitted to the data by nonlinear regression using:

$$Response = \frac{E_{\max} \times [\mathrm{A}]}{\mathrm{EC}_{50} + [\mathrm{A}]}$$

where E_{max} is the maximal response, [A] is the agonist concentration, and EC_{50} is the concentration of agonist that produces 50% of the maximal response. Antagonist K_b values were calculated as the shift of the agonist concentration-response curve in the presence of a fixed concentration of the antagonist, using the following concentration:

$$DR = 1 + \frac{[B]}{K_b}$$

Where DR (dose ratio) is the ratio of the [agonist] required to stimulate an identical response in the presence and absence of a fixed concentration of antagonist [B].

8 References

1. Sokol, C. L.; Luster, A. D. The Chemokine System in Innate Immunity. *Cold Spring Harbor Perspectives in Biology* **2015,** 7, a016303.
2. Zlotnik, A.; Yoshie, O. Chemokines: a new classification system and their role in immunity. *Immunity* **2000,** 12, 121-7.
3. Wu, V.-Y.; Walz, D. A.; McCoy, L. E. Purification and Characterization of Human and Bovine Platelet Factor 4. *Preparative Biochemistry* **1977,** 7, 479-493.
4. Allen, S. J.; Crown, S. E.; Handel, T. M. Chemokine:Receptor Structure, Interactions, and Antagonism. *Annual Review of Immunology* **2007,** 25, 787-820.
5. Rollins, B. J. Chemokines. *Blood* **1997,** 90, 909-928.
6. Bachelerie, F.; Ben-Baruch, A.; Burkhardt, A. M.; Combadiere, C.; Farber, J. M.; Graham, G. J.; Horuk, R.; Sparre-Ulrich, A. H.; Locati, M.; Luster, A. D.; Mantovani, A.; Matsushima, K.; Murphy, P. M.; Nibbs, R.; Nomiyama, H.; Power, C. A.; Proudfoot, A. E.; Rosenkilde, M. M.; Rot, A.; Sozzani, S.; Thelen, M.; Yoshie, O.; Zlotnik, A. International Union of Basic and Clinical Pharmacology. [corrected]. LXXXIX. Update on the extended family of chemokine receptors and introducing a new nomenclature for atypical chemokine receptors. *Pharmacological Reviews* **2014,** 66, 1-79.
7. Murdoch, C.; Finn, A. Chemokine receptors and their role in inflammation and infectious diseases. *Blood* **2000,** 95, 3032-3043.
8. Balkwill, F. The significance of cancer cell expression of the chemokine receptor CXCR4. *Seminars in Cancer Biology* **2004,** 14, 171-9.
9. Chou, C. C.; Fine, J. S.; Pugliese-Sivo, C.; Gonsiorek, W.; Davies, L.; Deno, G.; Petro, M.; Schwarz, M.; Zavodny, P. J.; Hipkin, R. W. Pharmacological characterization of the chemokine receptor, hCCR1 in a stable transfectant and differentiated HL-60 cells: antagonism of hCCR1 activation by MIP-1beta. *British Journal of Pharmacology* **2002,** 137, 663-75.
10. Bachelerie, F.; Graham, G. J.; Locati, M.; Mantovani, A.; Murphy, P. M.; Nibbs, R.; Rot, A.; Sozzani, S.; Thelen, M. An atypical addition to the chemokine receptor nomenclature: IUPHAR Review 15. *British Journal of Pharmacology* **2015,** 172, 3945-3949.
11. Liekens, S.; Schols, D.; Hatse, S. CXCL12-CXCR4 axis in angiogenesis, metastasis and stem cell mobilization. *Current Pharmaceutical Design* **2010,** 16, 3903-20.
12. Nagasawa, T.; Hirota, S.; Tachibana, K.; Takakura, N.; Nishikawa, S.-i.; Kitamura, Y.; Yoshida, N.; Kikutani, H.; Kishimoto, T. Defects of B-cell lymphopoiesis and bone-marrow myelopoiesis in mice lacking the CXC chemokine PBSF/SDF-1. *Nature* **1996,** 382, 635-638.
13. Zou, Y.-R.; Kottmann, A. H.; Kuroda, M.; Taniuchi, I.; Littman, D. R. Function of the chemokine receptor CXCR4 in haematopoiesis and in cerebellar development. *Nature* **1998,** 393, 595-599.
14. Busillo, J. M.; Benovic, J. L. Regulation of CXCR4 signaling. *Biochimica et Biophysica Acta (BBA) - Biomembranes* **2007,** 1768, 952-963.
15. Vila-Coro, A. J.; Rodriguez-Frade, J. M.; Martin De Ana, A.; Moreno-Ortiz, M. C.; Martinez, A. C.; Mellado, M. The chemokine SDF-1alpha triggers CXCR4 receptor dimerization and activates the JAK/STAT pathway. *FASEB Journal* **1999,** 13, 1699-710.

16. Cheng, Z.-J.; Zhao, J.; Sun, Y.; Hu, W.; Wu, Y.-L.; Cen, B.; Wu, G.-X.; Pei, G. β-Arrestin Differentially Regulates the Chemokine Receptor CXCR4-mediated Signaling and Receptor Internalisation, and This Implicates Multiple Interaction Sites between β-Arrestin and CXCR4. *Journal of Biological Chemistry* **2000,** 275, 2479-2485.
17. Sun, Y.; Cheng, Z.; Ma, L.; Pei, G. β-Arrestin2 Is Critically Involved in CXCR4-mediated Chemotaxis, and This Is Mediated by Its Enhancement of p38 MAPK Activation. *Journal of Biological Chemistry* **2002,** 277, 49212-49219.
18. Busillo, J. M.; Benovic, J. L. Regulation of CXCR4 Signaling. *Biochimica et biophysica acta* **2007,** 1768, 952-963.
19. Feng, Y.; Broder, C. C.; Kennedy, P. E.; Berger, E. A. HIV-1 entry cofactor: functional cDNA cloning of a seven-transmembrane, G protein-coupled receptor. *Science* **1996,** 272, 872-7.
20. Hernandez, P. A.; Gorlin, R. J.; Lukens, J. N.; Taniuchi, S.; Bohinjec, J.; Francois, F.; Klotman, M. E.; Diaz, G. A. Mutations in the chemokine receptor gene CXCR4 are associated with WHIM syndrome, a combined immunodeficiency disease. *Nature Genetics* **2003,** 34, 70-4.
21. Libert, F.; Parmentier, M.; Lefort, A.; Dinsart, C.; Van Sande, J.; Maenhaut, C.; Simons, M. J.; Dumont, J. E.; Vassart, G. Selective amplification and cloning of four new members of the G protein-coupled receptor family. *Science* **1989,** 244, 569-72.
22. Gerrits, H.; van Ingen Schenau, D. S.; Bakker, N. E.; van Disseldorp, A. J.; Strik, A.; Hermens, L. S.; Koenen, T. B.; Krajnc-Franken, M. A.; Gossen, J. A. Early postnatal lethality and cardiovascular defects in CXCR7-deficient mice. *Genesis* **2008,** 46, 235-45.
23. Kapas, S.; Clark, A. J. Identification of an orphan receptor gene as a type 1 calcitonin gene-related peptide receptor. *Biochemical and Biophysical Research Communications* **1995,** 217, 832-8.
24. Sreedharan, S. P.; Robichon, A.; Peterson, K. E.; Goetzl, E. J. Cloning and expression of the human vasoactive intestinal peptide receptor. *Proceedings of the National Academy of Sciences of the United States of America* **1991,** 88, 4986-4990.
25. Cook Jonathan, S.; Wolsing Dana, H.; Lameh, J.; Olson Christy, A.; Correa Paul, E.; Sadee, W.; Blumenthal Edward, M.; Rosenbaum Jan, S. Characterization of the RDC1 gene which encodes the canine omolog of a proposed human VIP receptor Expression does not correlate with an increase in VIP binding sites. *FEBS Letters* **1992,** 300, 149-152.
26. Sánchez-Martín, L.; Sánchez-Mateos, P.; Cabañas, C. CXCR7 impact on CXCL12 biology and disease. *Trends in Molecular Medicine* **2013,** 19, 12-22.
27. Balabanian, K.; Lagane, B.; Infantino, S.; Chow, K. Y.; Harriague, J.; Moepps, B.; Arenzana-Seisdedos, F.; Thelen, M.; Bachelerie, F. The chemokine SDF-1/CXCL12 binds to and signals through the orphan receptor RDC1 in T lymphocytes. *Journal of Biological Chemistry* **2005,** 280, 35760-6.
28. Burns, J. M.; Summers, B. C.; Wang, Y.; Melikian, A.; Berahovich, R.; Miao, Z.; Penfold, M. E.; Sunshine, M. J.; Littman, D. R.; Kuo, C. J.; Wei, K.; McMaster, B. E.; Wright, K.; Howard, M. C.; Schall, T. J. A novel chemokine receptor for SDF-1 and I-TAC involved in cell survival, cell adhesion, and tumor development. *Journal of Experimental Medicine* **2006,** 203, 2201-13.

29. Naumann, U.; Cameroni, E.; Pruenster, M.; Mahabaleshwar, H.; Raz, E.; Zerwes, H. G.; Rot, A.; Thelen, M. CXCR7 functions as a scavenger for CXCL12 and CXCL11. *PLoS One* **2010,** 5, e9175.
30. Luker, K. E.; Steele, J. M.; Mihalko, L. A.; Ray, P.; Luker, G. D. Constitutive and chemokine-dependent internalisation and recycling of CXCR7 in breast cancer cells to degrade chemokine ligands. *Oncogene* **2010,** 29, 4599-610.
31. Rajagopal, S.; Kim, J.; Ahn, S.; Craig, S.; Lam, C. M.; Gerard, N. P.; Gerard, C.; Lefkowitz, R. J. Beta-arrestin- but not G protein-mediated signaling by the "decoy" receptor CXCR7. *Proceedings of the National Academy of Sciences of the United States of America* **2010,** 107, 628-32.
32. Valentin, G.; Haas, P.; Gilmour, D. The chemokine SDF1a coordinates tissue migration through the spatially restricted activation of Cxcr7 and Cxcr4b. *Current Biology* **2007,** 17, 1026-31.
33. Graham, G. J.; Locati, M.; Mantovani, A.; Rot, A.; Thelen, M. The biochemistry and biology of the atypical chemokine receptors. *Immunological Letters* **2012,** 145, 30-8.
34. Cruz-Orengo, L.; Holman, D. W.; Dorsey, D.; Zhou, L.; Zhang, P.; Wright, M.; McCandless, E. E.; Patel, J. R.; Luker, G. D.; Littman, D. R.; Russell, J. H.; Klein, R. S. CXCR7 influences leukocyte entry into the CNS parenchyma by controlling abluminal CXCL12 abundance during autoimmunity. *Journal of Experimental Medicine* **2011,** 208, 327-39.
35. Wang, Y.; Li, G.; Stanco, A.; Long, J. E.; Crawford, D.; Potter, G. B.; Pleasure, S. J.; Behrens, T.; Rubenstein, J. L. CXCR4 and CXCR7 have distinct functions in regulating interneuron migration. *Neuron* **2011,** 69, 61-76.
36. Sanchez-Alcaniz, J. A.; Haege, S.; Mueller, W.; Pla, R.; Mackay, F.; Schulz, S.; Lopez-Bendito, G.; Stumm, R.; Marin, O. Cxcr7 controls neuronal migration by regulating chemokine responsiveness. *Neuron* **2011,** 69, 77-90.
37. Guo, Q.; Gao, B. L.; Zhang, X. J.; Liu, G. C.; Xu, F.; Fan, Q. Y.; Zhang, S. J.; Yang, B.; Wu, X. H. CXCL12-CXCR4 Axis Promotes Proliferation, Migration, Invasion, and Metastasis of Ovarian Cancer. *Oncological Research* **2014,** 22, 247-58.
38. Kakinuma, T.; Hwang, S. T. Chemokines, chemokine receptors, and cancer metastasis. *Journal of Leukocyte Biology* **2006,** 79, 639-651.
39. Lazennec, G.; Richmond, A. Chemokines and chemokine receptors: new insights into cancer-related inflammation. *Trends in Molecular Medicine* **2010,** 16, 133-144.
40. Hadi, R.; Reza, S.; D., M. T.; Najmaldin, S. Role of chemokines in metastatic niche: new insights along with a diagnostic and prognostic approach. *APMIS* **2018,** 126, 359-370.
41. Owen, J. D.; Strieter, R.; Burdick, M.; Haghnegahdar, H.; Nanney, L.; Shattuck-Brandt, R.; Richmond, A. Enhanced tumor-forming capacity for immortalized melanocytes expressing melanoma growth stimulatory activity/growth-regulated cytokine beta and gamma proteins. *International Journal of Cancer* **1997,** 73, 94-103.
42. Ben-Baruch, A. Organ selectivity in metastasis: regulation by chemokines and their receptors. *Clinical & Experimental Metastasis* **2008,** 25, 345-56.
43. Sehgal, A.; Keener, C.; Boynton, A. L.; Warrick, J.; Murphy, G. P. CXCR-4, a chemokine receptor, is overexpressed in and required for proliferation of glioblastoma tumor cells. *Journal of Surgical Oncology* **1998,** 69, 99-104.

44. Koshiba, T.; Hosotani, R.; Miyamoto, Y.; Ida, J.; Tsuji, S.; Nakajima, S.; Kawaguchi, M.; Kobayashi, H.; Doi, R.; Hori, T.; Fujii, N.; Imamura, M. Expression of Stromal Cell-derived Factor 1 and CXCR4 Ligand Receptor System in Pancreatic Cancer: A Possible Role for Tumor Progression. *American Association for Cancer Research* **2000,** 6, 3530-3535.
45. Lee, Y. T. Breast carcinoma: pattern of metastasis at autopsy. *Journal of Surgical Oncology* **1983,** 23, 175-80.
46. Muller, A.; Homey, B.; Soto, H.; Ge, N.; Catron, D.; Buchanan, M. E.; McClanahan, T.; Murphy, E.; Yuan, W.; Wagner, S. N.; Barrera, J. L.; Mohar, A.; Verastegui, E.; Zlotnik, A. Involvement of chemokine receptors in breast cancer metastasis. *Nature* **2001,** 410, 50-6.
47. Alsayed, Y.; Ngo, H.; Runnels, J.; Leleu, X.; Singha, U. K.; Pitsillides, C. M.; Spencer, J. A.; Kimlinger, T.; Ghobrial, J. M.; Jia, X.; Lu, G.; Timm, M.; Kumar, A.; Cote, D.; Veilleux, I.; Hedin, K. E.; Roodman, G. D.; Witzig, T. E.; Kung, A. L.; Hideshima, T.; Anderson, K. C.; Lin, C. P.; Ghobrial, I. M. Mechanisms of regulation of CXCR4/SDF-1 (CXCL12)-dependent migration and homing in multiple myeloma. *Blood* **2007,** 109, 2708-17.
48. Greim, H.; Kaden, D. A.; Larson, R. A.; Palermo, C. M.; Rice, J. M.; Ross, D.; Snyder, R. The bone marrow niche, stem cells, and leukemia: impact of drugs, chemicals, and the environment. *Annals of the New York Academy of Sciences* **2014,** 1310, 7-31.
49. Chemdiv. *CXCR4-Targeted Library*. http://www.chemdiv.com/cxcr4-targeted-libraries.
50. Burger, J. A.; Kipps, T. J. CXCR4: a key receptor in the crosstalk between tumor cells and their microenvironment. *Blood* **2006,** 107, 1761-7.
51. Orimo, A.; Gupta, P. B.; Sgroi, D. C.; Arenzana-Seisdedos, F.; Delaunay, T.; Naeem, R.; Carey, V. J.; Richardson, A. L.; Weinberg, R. A. Stromal fibroblasts present in invasive human breast carcinomas promote tumor growth and angiogenesis through elevated SDF-1/CXCL12 secretion. *Cell* **2005,** 121, 335-48.
52. Ao, M.; Franco, O. E.; Park, D.; Raman, D.; Williams, K.; Hayward, S. W. Cross-talk between paracrine-acting cytokine and chemokine pathways promotes malignancy in benign human prostatic epithelium. *Cancer Research* **2007,** 67, 4244-53.
53. Sun, X.; Cheng, G.; Hao, M.; Zheng, J.; Zhou, X.; Zhang, J.; Taichman, R. S.; Pienta, K. J.; Wang, J. CXCL12 / CXCR4 / CXCR7 chemokine axis and cancer progression. *Cancer Metastasis Reviews* **2010,** 29, 709-22.
54. Calatozzolo, C.; Canazza, A.; Pollo, B.; Di Pierro, E.; Ciusani, E.; Maderna, E.; Salce, E.; Sponza, V.; Frigerio, S.; Di Meco, F.; Schinelli, S.; Salmaggi, A. Expression of the new CXCL12 receptor, CXCR7, in gliomas. *Cancer Biology & Therapy* **2011,** 11, 242-53.
55. Levoye, A.; Balabanian, K.; Baleux, F.; Bachelerie, F.; Lagane, B. CXCR7 heterodimerizes with CXCR4 and regulates CXCL12-mediated G protein signaling. *Blood* **2009,** 113, 6085-93.
56. Decaillot, F. M.; Kazmi, M. A.; Lin, Y.; Ray-Saha, S.; Sakmar, T. P.; Sachdev, P. CXCR7/CXCR4 heterodimer constitutively recruits beta-arrestin to enhance cell migration. *Journal of Biological Chemistry* **2011,** 286, 32188-97.

57. Drury, L. J.; Ziarek, J. J.; Gravel, S.; Veldkamp, C. T.; Takekoshi, T.; Hwang, S. T.; Heveker, N.; Volkman, B. F.; Dwinell, M. B. Monomeric and dimeric CXCL12 inhibit metastasis through distinct CXCR4 interactions and signaling pathways. *Proceedings of the National Academy of Sciences of the United States of America* **2011,** 108, 17655-60.
58. Domanska, U. M.; Kruizinga, R. C.; Nagengast, W. B.; Timmer-Bosscha, H.; Huls, G.; de Vries, E. G. E.; Walenkamp, A. M. E. A review on CXCR4/CXCL12 axis in oncology: No place to hide. *European Journal of Cancer* **2013,** 49, 219-230.
59. Ramsey, D. M.; McAlpine, S. R. Halting metastasis through CXCR4 inhibition. *Bioorganic & Medicinal Chemistry Letters* **2013,** 23, 20-25.
60. "Mozobil approved for non-Hodgkin's lymphoma and multiple myeloma". In www.empr.com, 2008.
61. Peled, A.; Abraham, M.; Avivi, I.; Rowe, J. M.; Beider, K.; Wald, H.; Tiomkin, L.; Ribakovsky, L.; Riback, Y.; Ramati, Y.; Aviel, S.; Galun, E.; Shaw, H. L.; Eizenberg, O.; Hardan, I.; Shimoni, A.; Nagler, A. The high-affinity CXCR4 antagonist BKT140 is safe and induces a robust mobilization of human CD34+ cells in patients with multiple myeloma. *Clinical cancer research : an official journal of the American Association for Cancer Research* **2014,** 20, 469-479.
62. Beider, K.; Ribakovsky, E.; Abraham, M.; Wald, H.; Weiss, L.; Rosenberg, E.; Galun, E.; Avigdor, A.; Eizenberg, O.; Peled, A.; Nagler, A. Targeting the CD20 and CXCR4 pathways in non-hodgkin lymphoma with rituximab and high-affinity CXCR4 antagonist BKT140. *Clinical cancer research : an official journal of the American Association for Cancer Research* **2013,** 19, 3495-3507.
63. Hotte, S.; Hirte, H.; Iacobucci, A.; Wong, D.; Cantin, L.; Korz, W.; Miller, W. Phase I/II study of CTCE-9908, a novel anticancer agent that inhibits CXCR4, in patients with advanced solid cancers. *Molecular Cancer Therapeutics* **2007,** 6, A153.
64. Wong, D.; Korz, W. Translating an Antagonist of Chemokine Receptor CXCR4: From Bench to Bedside. *Clinical Cancer Research* **2008,** 14, 7975.
65. Setia, G.; Hagog, N.; Jalilizeinali, B.; Funkhouser, S.; Pierzchanowski, L.; Lan, F.; Gabig, T. G.; Kiner-Strachan, B.; Kelleher, K.; Hsu, M.-C.; Chang, L.-W.; Schuster, M. W. A Phase II, Open-Label Pilot Study to Evaluate the Hematopoietic Stem Cell Mobilization of TG-0054 Combined with G-CSF in 12 Patients with Multiple Myeloma, Non-Hodgkin Lymphoma or Hodgkin Lymphoma - an Interim Analysis. *Blood* **2015,** 126, 515.
66. Pernas, S.; Martin, M.; Kaufman, P. A.; Gil-Martin, M.; Gomez Pardo, P.; Lopez-Tarruella, S.; Manso, L.; Ciruelos, E.; Perez-Fidalgo, J. A.; Hernando, C.; Ademuyiwa, F. O.; Weilbaecher, K.; Mayer, I.; Pluard, T. J.; Martinez Garcia, M.; Vahdat, L.; Perez-Garcia, J.; Wach, A.; Barker, D.; Fung, S.; Romagnoli, B.; Cortes, J. Balixafortide plus eribulin in HER2-negative metastatic breast cancer: a phase 1, single-arm, dose-escalation trial. *Lancet Oncology* **2018,** 19, 812-824.
67. Xue, L.-J.; Mao, X.-B.; Ren, L.-L.; Chu, X.-Y. Inhibition of CXCL12/CXCR4 axis as a potential targeted therapy of advanced gastric carcinoma. *Cancer Medicine* **2017,** 6, 1424-1436.
68. Kashyap, M. K.; Kumar, D.; Jones, H.; Amaya-Chanaga, C. I.; Choi, M. Y.; Melo-Cardenas, J.; Ale-Ali, A.; Kuhne, M. R.; Sabbatini, P.; Cohen, L. J.; Shelat, S. G.; Rassenti, L. Z.; Kipps, T. J.; Cardarelli, P. M.; Castro, J. E. Ulocuplumab (BMS-936564 / MDX1338): a fully human anti-CXCR4 antibody induces cell death in chronic

lymphocytic leukemia mediated through a reactive oxygen species-dependent pathway. *Oncotarget* **2016,** 7, 2809-2822.
69. Wang, C.; Chen, W.; Shen, J. CXCR7 Targeting and Its Major Disease Relevance. *Frontiers in Pharmacology* **2018,** 9, 641.
70. Debnath, B.; Xu, S.; Grande, F.; Garofalo, A.; Neamati, N. Small Molecule Inhibitors of CXCR4. *Theranostics* **2013,** 3, 47-75.
71. Seibert, C.; Sakmar, T. P. Small-molecule antagonists of CCR5 and CXCR4: a promising new class of anti-HIV-1 drugs. *Current Pharmaceutical Design* **2004,** 10, 2041-62.
72. Khan, A.; Greenman, J.; Archibald, S. J. Small molecule CXCR4 chemokine receptor antagonists: developing drug candidates. *Current Medicinal Chemistry* **2007,** 14, 2257-77.
73. Barbieri, F.; Bajetto, A.; Thellung, S.; Würth, R.; Florio, T. Drug design strategies focusing on the CXCR4/CXCR7/CXCL12 pathway in leukemia and lymphoma. *Expert Opinion on Drug Discovery* **2016,** 11, 1093-1109.
74. Gerlach, L. O.; Jakobsen, J. S.; Jensen, K. P.; Rosenkilde, M. R.; Skerlj, R. T.; Ryde, U.; Bridger, G. J.; Schwartz, T. W. Metal ion enhanced binding of AMD3100 to Asp262 in the CXCR4 receptor. *Biochemistry* **2003,** 42, 710-7.
75. Jacobson, O.; Weiss, I. D.; Szajek, L.; Farber, J. M.; Kiesewetter, D. O. 64Cu-AMD3100--a novel imaging agent for targeting chemokine receptor CXCR4. *Bioorganic & Medicinal Chemistry* **2009,** 17, 1486-93.
76. Mosi, R. M.; Anastassova, V.; Cox, J.; Darkes, M. C.; Idzan, S. R.; Labrecque, J.; Lau, G.; Nelson, K. L.; Patel, K.; Santucci, Z.; Wong, R. S. Y.; Skerlj, R. T.; Bridger, G. J.; Huskens, D.; Schols, D.; Fricker, S. P. The molecular pharmacology of AMD11070: An orally bioavailable CXCR4 HIV entry inhibitor. *Biochemical Pharmacology* **2012,** 83, 472-479.
77. Moyle, G.; DeJesus, E.; Boffito, M.; Wong, R. S.; Gibney, C.; Badel, K.; MacFarland, R.; Calandra, G.; Bridger, G.; Becker, S.; Team, X. A. C. T. S. Proof of Activity with AMD11070, an Orally Bioavailable Inhibitor of CXCR4-Tropic HIV Type 1. *Clinical Infectious Diseases* **2009,** 48, 798-805.
78. O'Boyle, G.; Swidenbank, I.; Marshall, H.; Barker, C. E.; Armstrong, J.; White, S. A.; Fricker, S. P.; Plummer, R.; Wright, M.; Lovat, P. E. Inhibition of CXCR4-CXCL12 chemotaxis in melanoma by AMD11070. *British Journal of Cancer* **2013,** 108, 1634-40.
79. Parameswaran, R.; Yu, M.; Lim, M.; Groffen, J.; Heisterkamp, N. Combination of drug therapy in acute lymphoblastic leukemia with a CXCR4 antagonist. *Leukemia* **2011,** 25, 1314-23.
80. Das, D.; Maeda, K.; Hayashi, Y.; Gavande, N.; Desai, D. V.; Chang, S. B.; Ghosh, A. K.; Mitsuya, H. Insights into the Mechanism of Inhibition of CXCR4: Identification of Piperidinylethanamine Analogs as Anti-HIV-1 Inhibitors. *Antimicrobial Agents and Chemotherapy* **2015,** 59, 1895-1904.
81. Arimont, M.; Sun, S.-L.; Leurs, R.; Smit, M.; de Esch, I. J. P.; de Graaf, C. Structural Analysis of Chemokine Receptor–Ligand Interactions. *Journal of Medicinal Chemistry* **2017**.
82. Liang, Z.; Zhan, W.; Zhu, A.; Yoon, Y.; Lin, S.; Sasaki, M.; Klapproth, J. M.; Yang, H.; Grossniklaus, H. E.; Xu, J.; Rojas, M.; Voll, R. J.; Goodman, M. M.; Arrendale, R. F.;

Liu, J.; Yun, C. C.; Snyder, J. P.; Liotta, D. C.; Shim, H. Development of a unique small molecule modulator of CXCR4. *PLoS One* **2012,** 7, e34038.
83. Thoma, G.; Streiff, M. B.; Kovarik, J.; Glickman, F.; Wagner, T.; Beerli, C.; Zerwes, H. G. Orally bioavailable isothioureas block function of the chemokine receptor CXCR4 in vitro and in vivo. *Journal of Medicinal Chemistry* **2008,** 51, 7915-20.
84. Wu, B.; Chien, E. Y.; Mol, C. D.; Fenalti, G.; Liu, W.; Katritch, V.; Abagyan, R.; Brooun, A.; Wells, P.; Bi, F. C.; Hamel, D. J.; Kuhn, P.; Handel, T. M.; Cherezov, V.; Stevens, R. C. Structures of the CXCR4 chemokine GPCR with small-molecule and cyclic peptide antagonists. *Science* **2010,** 330, 1066-71.
85. Nguyen, H. H.; Kim, M. B.; Wilson, R. J.; Butch, C.; Kuo, K. M.; Miller, E. J.; Tahirovic, Y. A.; Jecs, E.; Truax, V. M.; Wang, T.; Sum, C.; Cvijic, M. E.; Schroeder, G. M.; Wilson, L. J.; Liotta, D. C. Design, Synthesis, and Pharmacological Evaluation of Second-Generation Tetrahydroisoquinoline-Based CXCR4 Antagonists with Favorable ADME Properties. *Journal of Medicinal Chemistry* **2018**.
86. Jecs, E.; Miller, E. J.; Wilson, R. J.; Nguyen, H. H.; Tahirovic, Y. A.; Katzman, B. M.; Truax, V. M.; Kim, M. B.; Kuo, K. M.; Wang, T.; Sum, C. S.; Cvijic, M. E.; Schroeder, G. M.; Wilson, L. J.; Liotta, D. C. Synthesis of Novel Tetrahydroisoquinoline CXCR4 Antagonists with Rigidified Side-Chains. *ACS Medicinal Chemistry Letters* **2018,** 9, 89-93.
87. Murakami, T.; Kumakura, S.; Yamazaki, T.; Tanaka, R.; Hamatake, M.; Okuma, K.; Huang, W.; Toma, J.; Komano, J.; Yanaka, M.; Tanaka, Y.; Yamamoto, N. The Novel CXCR4 Antagonist KRH-3955 Is an Orally Bioavailable and Extremely Potent Inhibitor of Human Immunodeficiency Virus Type 1 Infection: Comparative Studies with AMD3100. *Antimicrobial Agents and Chemotherapy* **2009,** 53, 2940-2948.
88. Kalatskaya, I.; Berchiche, Y. A.; Gravel, S.; Limberg, B. J.; Rosenbaum, J. S.; Heveker, N. AMD3100 Is a CXCR7 Ligand with Allosteric Agonist Properties. *Molecular Pharmacology* **2009,** 75, 1240.
89. Wijtmans, M.; Maussang, D.; Sirci, F.; Scholten, D. J.; Canals, M.; Mujić-Delić, A.; Chong, M.; Chatalic, K. L. S.; Custers, H.; Janssen, E.; de Graaf, C.; Smit, M. J.; de Esch, I. J. P.; Leurs, R. Synthesis, modeling and functional activity of substituted styrene-amides as small-molecule CXCR7 agonists. *European Journal of Medicinal Chemistry* **2012,** 51, 184-192.
90. Novack, A.; Wright, J. J.; Kraskinski, A.; Hu, C. Substituted quinolones and methods of use. 2009.
91. Pennell, A. M. K.; Leleti, M. R.; Thomas, W. D; Zhang, P. Tricyclic, heteroaromatic compounds modulating CXCR4 and/or CXCR7. 2010.
92. Zhang, X.; Fan, P.; Gleason, M. M.; Jaen, J. C.; Li, L.; McMahon, J. P.; Powers, J.; Zheng, Y. Modulators of CXCR7. 2012.
93. Zabel, B. A.; Wang, Y.; Lewen, S.; Berahovich, R. D.; Penfold, M. E.; Zhang, P.; Powers, J.; Summers, B. C.; Miao, Z.; Zhao, B.; Jalili, A.; Janowska-Wieczorek, A.; Jaen, J. C.; Schall, T. J. Elucidation of CXCR7-mediated signaling events and inhibition of CXCR4-mediated tumor cell transendothelial migration by CXCR7 ligands. *Journal of Immunology* **2009,** 183, 3204-11.
94. Qian, T.; Liu, Y.; Dong, Y.; Zhang, L.; Dong, Y.; Sun, Y.; Sun, D. CXCR7 regulates breast tumor metastasis and angiogenesis in vivo and in vitro. *Molecular Medicine Reports* **2018,** 17, 3633-3639.

95. Tamamura, H.; Xu, Y.; Hattori, T.; Zhang, X.; Arakaki, R.; Kanbara, K.; Omagari, A.; Otaka, A.; Ibuka, T.; Yamamoto, N.; Nakashima, H.; Fujii, N. A Low-Molecular-Weight Inhibitor against the Chemokine Receptor CXCR4: A Strong Anti-HIV Peptide T140. *Biochemical and Biophysical Research Communications* **1998,** 253, 877-882.
96. Tamamura, H.; Fujisawa, M.; Hiramatsu, K.; Mizumoto, M.; Nakashima, H.; Yamamoto, N.; Otaka, A.; Fujii, N. Identification of a CXCR4 antagonist, a T140 analog, as an anti-rheumatoid arthritis agent. *FEBS Letters* **2004,** 569, 99-104.
97. Wire, B. BioLineRx Announces Positive Clinical Results from First Part of Phase 2 Trial in r/r AML. In *Data strongly suggest BL-8040 has potent anti-leukemic activity in combination with Ara-C in AML*, Business Wire: 2015.
98. Faber, A.; Roderburg, C.; Wein, F.; Saffrich, R.; Seckinger, A.; Horsch, K.; Diehlmann, A.; Wong, D.; Bridger, G.; Eckstein, V.; Ho, A. D.; Wagner, W. The Many Facets of SDF-1α, CXCR4 Agonists and Antagonists on Hematopoietic Progenitor Cells. *Journal of Biomedicine and Biotechnology* **2007,** 2007, 10.
99. Robinson, J. A.; DeMarco, S.; Gombert, F.; Moehle, K.; Obrecht, D. The design, structures and therapeutic potential of protein epitope mimetics. *Drug Discovery Today* **2008,** 13, 944-951.
100. Peng, S. B.; Zhang, X.; Paul, D.; Kays, L. M.; Gough, W.; Stewart, J.; Uhlik, M. T.; Chen, Q.; Hui, Y. H.; Zamek-Gliszczynski, M. J.; Wijsman, J. A.; Credille, K. M.; Yan, L. Z. Identification of LY2510924, a novel cyclic peptide CXCR4 antagonist that exhibits antitumor activities in solid tumor and breast cancer metastatic models. *Molecular Cancer Therapeutics* **2015,** 14, 480-90.
101. Cho, B.-S.; Zeng, Z.; Mu, H.; Wang, Z.; Konoplev, S.; McQueen, T.; Protopopova, M.; Cortes, J.; Marszalek, J. R.; Peng, S.-B.; Ma, W.; Davis, R. E.; Thornton, D. E.; Andreeff, M.; Konopleva, M. Antileukemia activity of the novel peptidic CXCR4 antagonist LY2510924 as monotherapy and in combination with chemotherapy. *Blood* **2015,** 126, 222.
102. Tamamura, H.; Omagari, A.; Hiramatsu, K.; Gotoh, K.; Kanamoto, T.; Xu, Y.; Kodama, E.; Matsuoka, M.; Hattori, T.; Yamamoto, N.; Nakashima, H.; Otaka, A.; Fujii, N. Development of specific CXCR4 inhibitors possessing high selectivity indexes as well as complete stability in serum based on an anti-HIV peptide T140. *Bioorganic & Medicinal Chemistry Letters* **2001,** 11, 1897-902.
103. Gravel, S.; Malouf, C.; Boulais, P. E.; Berchiche, Y. A.; Oishi, S.; Fujii, N.; Leduc, R.; Sinnett, D.; Heveker, N. The peptidomimetic CXCR4 antagonist TC14012 recruits beta-arrestin to CXCR7: roles of receptor domains. *Journal of Biological Chemistry* **2010,** 285, 37939-43.
104. Oishi, S.; Kuroyanagi, T.; Kubo, T.; Montpas, N.; Yoshikawa, Y.; Misu, R.; Kobayashi, Y.; Ohno, H.; Heveker, N.; Furuya, T.; Fujii, N. Development of Novel CXC Chemokine Receptor 7 (CXCR7) Ligands: Selectivity Switch from CXCR4 Antagonists with a Cyclic Pentapeptide Scaffold. *Journal of Medicinal Chemistry* **2015,** 58, 5218-5225.
105. Jähnichen, S.; Blanchetot, C.; Maussang, D.; Gonzalez-Pajuelo, M.; Chow, K. Y.; Bosch, L.; De Vrieze, S.; Serruys, B.; Ulrichts, H.; Vandevelde, W.; Saunders, M.; De Haard, H. J.; Schols, D.; Leurs, R.; Vanlandschoot, P.; Verrips, T.; Smit, M. J. CXCR4 nanobodies (VHH-based single variable domains) potently inhibit chemotaxis and HIV-1 replication and mobilize stem cells. *Proceedings of the National Academy of Sciences* **2010,** 107, 20565-20570.

106. Maussang, D.; Mujic-Delic, A.; Descamps, F. J.; Stortelers, C.; Vanlandschoot, P.; Stigter-van Walsum, M.; Vischer, H. F.; van Roy, M.; Vosjan, M.; Gonzalez-Pajuelo, M.; van Dongen, G. A.; Merchiers, P.; van Rompaey, P.; Smit, M. J. Llama-derived single variable domains (nanobodies) directed against chemokine receptor CXCR7 reduce head and neck cancer cell growth in vivo. *Journal of Biological Chemistry* **2013,** 288, 29562-72.
107. Briddon, S. J.; Kellam, B.; Hill, S. J. Design and use of fluorescent ligands to study ligand-receptor interactions in single living cells. *Methods in Molecular Biology* **2011,** 746, 211-36.
108. Yang, Y.; Zhang, Q.; Gao, M.; Yang, X.; Huang, Z.; An, J. A Novel CXCR4-Selective High-Affinity Fluorescent Probe and Its Application in Competitive Binding Assays. *Biochemistry* **2014,** 53, 4881-4883.
109. Eichel, K.; von Zastrow, M. Subcellular Organization of GPCR Signaling. *Trends in Pharmacological Sciences* **2018,** 39, 200-208.
110. Luker, G. D.; Luker, K. E. Optical Imaging: Current Applications and Future Directions. *Journal of Nuclear Medicine* **2008,** 49, 1-4.
111. Baran, J.; Pituch-Noworolska, A.; Krzeszowiak, A.; Wieckiewicz, J.; Stachura, J.; Pryjma, J.; Popiela, T.; Szczepanik, A.; Zembala, M. Detection of cancer cells in the blood by FACS sorting of CD45- cells. *International Journal of Molecular Medicine* **1998,** 1, 573-8.
112. Hall, M. P.; Unch, J.; Binkowski, B. F.; Valley, M. P.; Butler, B. L.; Wood, M. G.; Otto, P.; Zimmerman, K.; Vidugiris, G.; Machleidt, T.; Robers, M. B.; Benink, H. A.; Eggers, C. T.; Slater, M. R.; Meisenheimer, P. L.; Klaubert, D. H.; Fan, F.; Encell, L. P.; Wood, K. V. Engineered Luciferase Reporter from a Deep Sea Shrimp Utilizing a Novel Imidazopyrazinone Substrate. *ACS Chemical Biology* **2012,** 7, 1848-1857.
113. Stoddart, L. A.; Kilpatrick, L. E.; Hill, S. J. NanoBRET Approaches to Study Ligand Binding to GPCRs and RTKs. *Trends in Pharmacological Sciences* **2018,** 39, 136-147.
114. Hanaoka, H.; Mukai, T.; Tamamura, H.; Mori, T.; Ishino, S.; Ogawa, K.; Iida, Y.; Doi, R.; Fujii, N.; Saji, H. Development of a 111In-labeled peptide derivative targeting a chemokine receptor, CXCR4, for imaging tumors. *Nuclear Medicine and Biology* **2006,** 33, 489-94.
115. Nomura, W.; Tanabe, Y.; Tsutsumi, H.; Tanaka, T.; Ohba, K.; Yamamoto, N.; Tamamura, H. Fluorophore labeling enables imaging and evaluation of specific CXCR4-ligand interaction at the cell membrane for fluorescence-based screening. *Bioconjugate Chemistry* **2008,** 19, 1917-20.
116. Kuil, J.; Buckle, T.; Yuan, H.; van den Berg, N. S.; Oishi, S.; Fujii, N.; Josephson, L.; van Leeuwen, F. W. Synthesis and evaluation of a bimodal CXCR4 antagonistic peptide. *Bioconjugate Chemistry* **2011,** 22, 859-64.
117. Zhou, N.; Luo, Z.; Luo, J.; Fan, X.; Cayabyab, M.; Hiraoka, M.; Liu, D.; Han, X.; Pesavento, J.; Dong, C. Z.; Wang, Y.; An, J.; Kaji, H.; Sodroski, J. G.; Huang, Z. Exploring the stereochemistry of CXCR4-peptide recognition and inhibiting HIV-1 entry with D-peptides derived from chemokines. *Journal of Biological Chemistry* **2002,** 277, 17476-85.
118. Nimmagadda, S.; Pullambhatla, M.; Stone, K.; Green, G.; Bhujwalla, Z. M.; Pomper, M. G. Molecular imaging of CXCR4 receptor expression in human cancer

xenografts with [64Cu]AMD3100 positron emission tomography. *Cancer Research* **2010,** 70, 3935-44.
119. Poty, S.; Gourni, E.; Desogere, P.; Boschetti, F.; Goze, C.; Maecke, H. R.; Denat, F. AMD3100: A Versatile Platform for CXCR4 Targeting (68)Ga-Based Radiopharmaceuticals. *Bioconjugate Chemistry* **2016,** 27, 752-61.
120. Khan, A.; Silversides, J. D.; Madden, L.; Greenman, J.; Archibald, S. J. Fluorescent CXCR4 chemokine receptor antagonists: metal activated binding. *Chemical Communications* **2007**, 416-418.
121. Knight, J. C.; Hallett, A. J.; Brancale, A.; Paisey, S. J.; Clarkson, R. W.; Edwards, P. G. Evaluation of a fluorescent derivative of AMD3100 and its interaction with the CXCR4 chemokine receptor. *Chembiochem* **2011,** 12, 2692-8.
122. Poty, S.; Desogere, P.; Goze, C.; Boschetti, F.; D'Huys, T.; Schols, D.; Cawthorne, C.; Archibald, S. J.; Maecke, H. R.; Denat, F. New AMD3100 derivatives for CXCR4 chemokine receptor targeted molecular imaging studies: synthesis, anti-HIV-1 evaluation and binding affinities. *Dalton Transactions* **2015,** 44, 5004-5016.
123. Wiederschain, G. Y. The Molecular Probes handbook. A guide to fluorescent probes and labeling technologies. *Biochemistry (Moscow)* **2011,** 76, 1276-1276.
124. Mason, J. S.; Bortolato, A.; Congreve, M.; Marshall, F. H. New insights from structural biology into the druggability of G protein-coupled receptors. *Trends in Pharmacological Sciences* **2012,** 33, 249-60.
125. Xu, L.; Li, Y.; Sun, H.; Li, D.; Hou, T. Structural basis of the interactions between CXCR4 and CXCL12/SDF-1 revealed by theoretical approaches. *Molecular Biosystems* **2013,** 9, 2107-17.
126. Magnani, J. S., Arun. Glycomimetic-peptidomimetic inhibitors of e-selectins and cxcr4 chemokine receptors. WO/2012/061662, 10.05.2012, 2012.
127. Zhang, C.; Du, C.; Feng, Z.; Zhu, J.; Li, Y. Hologram Quantitative Structure Activity Relationship, Docking, and Molecular Dynamics Studies of Inhibitors for CXCR4. *Chemical Biology & Drug Design* **2015,** 85, 119-136.
128. Schrödinger. *Glide, Small-Molecule Drug Discovery Suite 2018-3*, 2018.
129. Catalano, J. G.; Gudmundsson, K. S.; Svolto, A.; Boggs, S. D.; Miller, J. F.; Spaltenstein, A.; Thomson, M.; Wheelan, P.; Minick, D. J.; Phelps, D. P.; Jenkinson, S. Synthesis of a novel tricyclic 1,2,3,4,4a,5,6,10b-octahydro-1,10-phenanthroline ring system and CXCR4 antagonists with potent activity against HIV-1. *Bioorganic & Medicinal Chemistry Letters* **2010,** 20, 2186-90.
130. Gudmundsson, K. S.; Boggs, S. D.; Catalano, J. G.; Svolto, A.; Spaltenstein, A.; Thomson, M.; Wheelan, P.; Jenkinson, S. Imidazopyridine-5,6,7,8-tetrahydro-8-quinolinamine derivatives with potent activity against HIV-1. *Bioorganic & Medicinal Chemistry Letters* **2009,** 19, 6399-403.
131. Miller, J. F.; Gudmundsson, K. S.; Richardson, L. D. A.; Jenkinson, S.; Spaltenstein, A.; Thomson, M.; Wheelan, P. Synthesis and SAR of novel isoquinoline CXCR4 antagonists with potent anti-HIV activity. *Bioorganic & Medicinal Chemistry Letters* **2010,** 20, 3026-3030.
132. Pyarasani, R. D.; John, A.; Santos, L. S. Recent developments of chiral induction in the syntheses of biologically important alkaloids. *Current Topics in Medicinal Chemistry* **2013,** 13, 2184-99.

133. Boggs, S.; Elitzin, V. I.; Gudmundsson, K.; Martin, M. T.; Sharp, M. J. Kilogram-Scale Synthesis of the CXCR4 Antagonist GSK812397. *Organic Process Research & Development* **2009,** 13, 781-785.
134. Miyaura, N.; Ishiyama, T.; Sasaki, H.; Ishikawa, M.; Sato, M.; Suzuki, A. Palladium-catalyzed inter- and intramolecular cross-coupling reactions of B-alkyl-9-borabicyclo[3.3.1]nonane derivatives with 1-halo-1-alkenes or haloarenes. Syntheses of functionalized alkenes, arenes, and cycloalkenes via a hydroboration-coupling sequence. *Journal of the American Chemical Society* **1989,** 111, 314-321.
135. Crawford, J. B.; Chen, G.; Gauthier, D.; Wilson, T.; Carpenter, B.; Baird, I. R.; McEachern, E.; Kaller, A.; Harwig, C.; Atsma, B.; Skerlj, R. T.; Bridger, G. J. AMD070, a CXCR4 Chemokine Receptor Antagonist: Practical Large-Scale Laboratory Synthesis. *Organic Process Research & Development* **2008,** 12, 823-830.
136. Pfleger, K. D.; Seeber, R. M.; Eidne, K. A. Bioluminescence resonance energy transfer (BRET) for the real-time detection of protein-protein interactions. *Nature Protocols* **2006,** 1, 337-45.
137. Sun, S.; Yang, X.; Wang, Y.; Shen, X. In Vivo Analysis of Protein-Protein Interactions with Bioluminescence Resonance Energy Transfer (BRET): Progress and Prospects. *International Journal of Molecular Sciences* **2016,** 17.
138. England, C. G.; Ehlerding, E. B.; Cai, W. Nanoluc®: A Small Luciferase Is Brightening Up the Field of Bioluminescence. *Bioconjugate Chemistry* **2016,** 27, 1175-1187.
139. Kufareva, I.; Salanga, C. L.; Handel, T. M. Chemokine and chemokine receptor structure and interactions: implications for therapeutic strategies. *Immunology Cell Biology* **2015,** 93, 372-83.
140. Binkowski, B.; Fan, F.; Wood, K. Engineered luciferases for molecular sensing in living cells. *Current Opinion in Biotechnology* **2009,** 20, 14-8.
141. Mona, C. E.; Besserer-Offroy, É.; Cabana, J.; Leduc, R.; Lavigne, P.; Heveker, N.; Marsault, É.; Escher, E. Design, synthesis, and biological evaluation of CXCR4 ligands. *Organic & Biomolecular Chemistry* **2016,** 14, 10298-10311.
142. Pike, J. A.; Styles, I. B.; Rappoport, J. Z.; Heath, J. K. Quantifying receptor trafficking and colocalization with confocal microscopy. *Methods* **2017,** 115, 42-54.
143. Prlj, A.; Vannay, L.; Corminboeuf, C. Fluorescence Quenching in BODIPY Dyes: The Role of Intramolecular Interactions and Charge Transfer. *Helvetica Chimica Acta* **2017,** 100, e1700093.
144. Vernall, A. J.; Stoddart, L. A.; Briddon, S. J.; Ng, H. W.; Laughton, C. A.; Doughty, S. W.; Hill, S. J.; Kellam, B. Conversion of a non-selective adenosine receptor antagonist into A3-selective high affinity fluorescent probes using peptide-based linkers. *Organic & Biomolecular Chemistry* **2013,** 11, 5673-82.
145. Luker, K. E.; Lewin, S. A.; Mihalko, L. A.; Schmidt, B. T.; Winkler, J. S.; Coggins, N. L.; Thomas, D. G.; Luker, G. D. Scavenging of CXCL12 by CXCR7 Promotes Tumor Growth and Metastasis of CXCR4-positive Breast Cancer Cells. *Oncogene* **2012,** 31, 4750-4758.
146. Tripathi, A.; Gaponenko, V.; Majetschak, M. Commercially available antibodies directed against alpha-adrenergic receptor subtypes and other G protein-coupled receptors with acceptable selectivity in flow cytometry experiments. *Naunyn Schmiedebergs Arch Pharmacol* **2016,** 389, 243-8.

147. Williams, J. L.; Patel, J. R.; Daniels, B. P.; Klein, R. S. Targeting CXCR7/ACKR3 as a therapeutic strategy to promote remyelination in the adult central nervous system. *The Journal of Experimental Medicine* **2014,** 211, 791.
148. Cruz-Orengo, L.; Holman, D. W.; Dorsey, D.; Zhou, L.; Zhang, P.; Wright, M.; McCandless, E. E.; Patel, J. R.; Luker, G. D.; Littman, D. R.; Russell, J. H.; Klein, R. S. CXCR7 influences leukocyte entry into the CNS parenchyma by controlling abluminal CXCL12 abundance during autoimmunity. *The Journal of Experimental Medicine* **2011,** 208, 327.
149. Montpas, N.; Cabana, J.; St-Onge, G.; Gravel, S.; Morin, G.; Kuroyanagi, T.; Lavigne, P.; Fujii, N.; Oishi, S.; Heveker, N. Mode of Binding of the Cyclic Agonist Peptide TC14012 to CXCR7: Identification of Receptor and Compound Determinants. *Biochemistry* **2015,** 54, 1505-1515.
150. Sato, S.; Sakamoto, T.; Miyazawa, E.; Kikugawa, Y. One-pot reductive amination of aldehydes and ketones with α-picoline-borane in methanol, in water, and in neat conditions. *Tetrahedron* **2004,** 60, 7899-7906.
151. Arnott, J. A.; Planey, S. L. The influence of lipophilicity in drug discovery and design. *Expert Opinions in Drug Discovery* **2012,** 7, 863-75.
152. Crump, M. P.; Gong, J. H.; Loetscher, P.; Rajarathnam, K.; Amara, A.; Arenzana-Seisdedos, F.; Virelizier, J. L.; Baggiolini, M.; Sykes, B. D.; Clark-Lewis, I. Solution structure and basis for functional activity of stromal cell-derived factor-1; dissociation of CXCR4 activation from binding and inhibition of HIV-1. *The EMBO Journal* **1997,** 16, 6996-7007.
153. Stoddart, L. A.; Johnstone, E. K. M.; Wheal, A. J.; Goulding, J.; Robers, M. B.; Machleidt, T.; Wood, K. V.; Hill, S. J.; Pfleger, K. D. G. Application of BRET to monitor ligand binding to GPCRs. *Nature methods* **2015,** 12, 661-663.
154. Keppler, A.; Kindermann, M.; Gendreizig, S.; Pick, H.; Vogel, H.; Johnsson, K. Labeling of fusion proteins of O6-alkylguanine-DNA alkyltransferase with small molecules in vivo and in vitro. *Methods* **2004,** 32, 437-44.
155. Kim, T. K.; Eberwine, J. H. Mammalian cell transfection: the present and the future. *Analytical and Bioanalytical Chemistry* **2010,** 397, 3173-3178.
156. Stoddart, L. A.; Vernall, A. J.; Briddon, S. J.; Kellam, B.; Hill, S. J. Direct visualisation of internalisation of the adenosine A3 receptor and localization with arrestin3 using a fluorescent agonist. *Neuropharmacology* **2015,** 98, 68-77.
157. Schembri, L. S.; Stoddart, L. A.; Briddon, S. J.; Kellam, B.; Canals, M.; Graham, B.; Scammells, P. J. Synthesis, Biological Evaluation, and Utility of Fluorescent Ligands Targeting the μ-Opioid Receptor. *Journal of Medicinal Chemistry* **2015,** 58, 9754-9767.
158. Conroy, S.; Kindon, N. D.; Glenn, J.; Stoddart, L. A.; Lewis, R. J.; Hill, S. J.; Kellam, B.; Stocks, M. J. Synthesis and Evaluation of the First Fluorescent Antagonists of the Human P2Y2 Receptor Based on AR-C118925. *Journal of Medicinal Chemistry* **2018,** 61, 3089-3113.
159. Zhang, R.; Xie, X. Tools for GPCR drug discovery. *Acta Pharmacologica Sinica* **2012,** 33, 372-384.
160. Thomsen, W.; Frazer, J.; Unett, D. Functional assays for screening GPCR targets. *Current Opinion in Biotechnology* **2005,** 16, 655-665.

161. Kauk, M.; Hoffmann, C. Intramolecular and Intermolecular FRET Sensors for GPCRs – Monitoring Conformational Changes and Beyond. *Trends in Pharmacological Sciences* **2018,** 39, 123-135.
162. Tao Wang, Z. L., Mary Ellen Cvijic, Carol Krause, Litao Zhang, and Chi Shing Sum. Measurement of β-Arrestin Recruitment for GPCR Targets. *Assay Guidance Manual [Internet]* **2017**.
163. Picot, J.; Guerin, C. L.; Le Van Kim, C.; Boulanger, C. M. Flow cytometry: retrospective, fundamentals and recent instrumentation. *Cytotechnology* **2012,** 64, 109-30.
164. Givan, A. L. Flow Cytometry: An Introduction. In *Flow Cytometry Protocols*, Hawley, T. S.; Hawley, R. G., Eds. Humana Press: Totowa, NJ, 2011; pp 1-29.
165. Leers, M. P. G.; Schoffelen, R. H. M. G.; Hoop, J. G. M.; Theunissen, P. H. M. H.; Oosterhuis, J. W. A.; vd Bijl, H.; Rahmy, A.; Tan, W.; Nap, M. Multiparameter flow cytometry as a tool for the detection of micrometastatic tumour cells in the sentinel lymph node procedure of patients with breast cancer. *Journal of Clinical Pathology* **2002,** 55, 359-366.